# Dynamics and Control for Vibration Isolation Design

Dino Sciulli

Dissertation submitted to the faculty of the Virginia Polytechnic Institute and State Universityin partial fulfillment of the requirements for the degree of

Doctor of Philosophy
in
Engineering Mechanics

Daniel J. Inman, Chairman
Harley H. Cudney
Robert A. Heller
Scott L. Hendricks
Dean T. Mook

April, 1997
Blacksburg, Virginia

Keywords: Vibration Isolation, Active Isolation, Passive Isolation, Visualization

# Dynamics and Control for Vibration Isolation Design

Dino Sciulli

## (ABSTRACT)

The single-degree-of-freedom (SDOF) system is the most widely used model for vibration isolation systems. The SDOF system is a simple but worthy model because it quantifies many results of an isolation system. For instance, a SDOF model predicts that the high frequency transmissibility increases when the isolator has passive damping although this does not occur for an isolator implementing active damping. A severe limitation of this system is that it cannot be used when the base and/or equipment are flexible.

System flexibility has been considered in previous literature but the flexibility has always been approximated which leads to truncation errors. The analysis used in this work is more sophisticated in that it can model the system flexibility without the use of any approximations. Therefore, the true effects of system flexibility can be analyzed analytically.

Current literature has not fully explored the choice of mount frequency or actuator placement for flexible systems either. It is commonly suggested that isolators should be designed with a low-frequency mount. That is, the isolator frequency should be much lower than any of the system frequencies. It is shown that these isolators tend to perform best in an overall sense; however, mount frequencies designed between system modes tend to have a coupling effect. That is, the lower frequencies have such a strong interaction between each other that when isolator damping is present, multiple system modes are attenuated. Also, when the base and equipment are flexible, isolator placement becomes a critical issue. For low-frequency mount designs, the first natural frequency can shift as much as 15.6% for various isolator placements. For a mid-frequency mount design, the shift of the first three modes can be as high as 34.9%, 26.6% and 11.3%, respectively, for varying isolator placements.

# Dedication

I dedicate this dissertation to my parents, Diodato and Antonia Sciulli. At an early age they embedded the idea that with hard work nothing was beyond my grasp. Also, as a child they were my role models because they came to America knowing little English and having little money and yet was able to raise and educate a family of four. Through the years they made sacrifices so their children could lead a better life and their sacrifices are reflected in this work.

# Acknowledgements

I wish to first thank my family and relatives for all their support through the many years of education that I have gone through. This includes, my mom and dad, my brothers Carlo and Tony, my sister Rosa, and my extended family through marriages which include Carlo's wife Beth and their children Jennifer and AJ, as well as Rosa's husband Shawn. Thanks for everything.

I would like to give special thanks to Dr. Inman for all his help during my three years at Virginia Tech. I could not have asked for a better advisor to guide me through my doctoral studies.

I would like to also thank a few friends from my Stanford days who made school a lot more enjoyable by their friendships: Dr. Robert Braun, John Cancian and Jim Hu.

Last but certainly not least, I would like to thank all the members in the MSL group for their friendships. I would like to give special thanks to the following members: Eric and his family for their support and friendship these past three years. Jens and Melissa for their friendship over the past few years as well; I want an invitation when you decide to make it official. Greg for his help on being a sounding board for my ideas and giving me other possible solutions that may have slipped by me. Debbie for helping me understand that you a need a sound body to match a sound mind. Clay for all the times I poked fun at him for reloading Windows NT software on his machine; I guess I have to find another person to have the great MAC-PC debate. And the Brazilian branch of MSL: Mauro and Sergio. Especially Mauro for his friendship and hospitality while I visited in Brazil. Also, I would like to thank him for helping me work out the initial bugs in my code and giving me insight into possible extensions for my dissertation.

The work in this dissertation was funded by the United States Air Force Palace Knight program.

# Contents

# List of Figures

# List of Tables

# Chapter 1

# Introduction

The idea of suppressing unwanted vibrations with the use of vibration isolators has been around for five decades. Isolation devices are currently used in a wide range of applications: automobiles, buildings, aerospace structures such as helicopters and satellites, and machinery such as precision tools and hand tools. When analyzing isolation systems, a question that arises is "What are the isolation criteria or what are the criteria that defines isolation?" A general answer to this question would be that vibration isolation is the means to mitigate unwanted oscillating disturbances or forces. This can be a result in reducing forces or vibrations emanating from a foundation to a piece of equipment or it can be a result of reducing forces or vibrations emanating from the equipment to its foundation.

This chapter will discuss vibration isolation concepts such as defining isolation performance in terms of transmissibility and discussing the use of active and passive isolators. Another method of suppressing vibrations is to use a vibration absorber. The vibration absorber, at first glance, seems very similar to an isolator; therefore, a discussion of the similarities and differences between the two will be made. A literature review of current and past publications on vibration isolation is discussed as well. The last sections in this chapter states the objectives and gives a brief review of this dissertation.

## 1.1 Vibration Isolation Concepts

The simplest model for a vibration isolation system is the single-degree-of-freedom system shown in Figure 1.1. The equipment and foundation are assumed rigid and the foundation mass is considered negligible with respect to the equipment mass. For design purposes, the isolator is massless and is modeled as a viscous damper with a damping coefficient $c$ and a spring with a stiffness $k$. The spring stiffness and damping coefficient are also assumed to be constant in the frequency range of interest. The values for the isolator's spring and damper are chosen to reduce as much vibration in the system as possible.

When subjected to steady-state sinusoidal vibrations, the isolator's performance can be

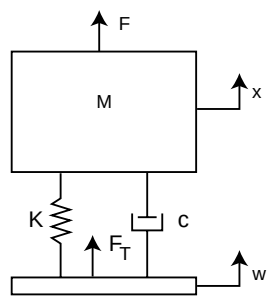


Figure 1.1: Single-Degree-of-Freedom Vibration Isolator

measured by three different ratios: the absolute transmissibility, the relative transmissibility and the motion response of the system [1]. The absolute transmissibility measures how well the isolator has reduced the transmitted force to the foundation or the reduction in the equipment displacement. The absolute transmissibility is defined as the ratio of the equipment's vibration level or magnitude to the excitation vibration level ($TR_a = x/w$) or the ratio of the force transmitted at the foundation to the excitation force ($TR_a = F_t/F$). These magnitude ratios are equivalent if the system is linear and uniaxial [2]. The relative transmissibility is a measure of the clearance required in an isolator. It is defined as the ratio of the relative displacement between the equipment and foundation to the displacement of foundation, $TR_r = (x - w)/w$. As noted in [1], the relative transmissibility is significant only when the isolator is used to reduce the equipment's vibration that emanate from the foundation. The motion response is defined as the ratio of the equipment's displacement to the excitation force on the equipment, $TR_m = x/F$. This ratio will give the equipment's displacement when an excitation force is subjected directly on the equipment. Therefore, the isolator will be packaged to account for the equipment motion.

## 1.2 Passive and Active Isolation

The first isolators were designed using only passive elements, that is, no power source was required to store or dissipate energy. The passive isolators exhibit some stiffness and/or damping which are critical in constructing an effective isolator. One key parameter of the isolator, the stiffness, is used to determine the corner frequency or mount frequency ($\omega_o$) of the isolator, which is normally where the the isolator starts to isolate disturbances. The corner frequency also becomes important when analyzing the absolute transmissibility of a system. For disturbances at frequencies above $\sqrt{2}\omega_o$, the absolute transmissibility is less than unity and vibration isolation occurs. When the disturbance frequency is less than $\sqrt{2}\omega_o$, vibration amplification occurs (see Section 1.4 or Section 2.1). For disturbance frequencies much lower than the corner frequency, the absolute transmissibility is unity. When

the disturbance frequency approaches the natural frequency of the system, a resonant condition occurs and the transmissibility is unbounded if no damping is present in the isolator. Since the isolator performs best when the disturbance frequency is greater than $\sqrt{2}w_o$, the corner frequency of the isolator should be minimized as much as possible. However, there is a limit on the value of the corner frequency and the limit is determined by the static sag of the isolator when the system is subjected to a static loading. Therefore, the isolator must support the equipment under static loading and must also be compliant so that disturbances are not transmitted to the equipment. Figure 1.2 is an idealized depiction of the isolator stiffness across the frequency range of interest.

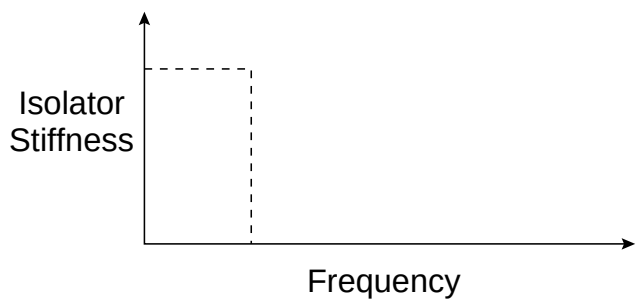


Figure 1.2: Ideal Isolator Stiffness as a Function of Frequency

Another design constraint for the isolator is the amount of damping present in the isolator. If damping is not present, the absolute transmissibility will be theoretically unbounded when the disturbance frequency approaches the system's natural frequency. If damping is present, the absolute transmissibility will no longer approach infinity at the resonant condition but will be finite. However, the transmissibility at disturbance frequencies greater than $\sqrt{2}\omega_o$ will be amplified (see Section 1.4 or Section 2.1) due to isolator damping.

As mentioned previously, passive techniques have no active power source; therefore, there is no chance of instability. However, when greater performance is required and passive techniques alone cannot perform adequately, active techniques may be used in conjunction with the passive ones. Adding an active system to the isolator makes the system more complex and the number of issues that need to be addressed are increased. Some issues that arise due to the addition of the active system are the selection of actuators and sensors, weight constraints, power requirements, stability, closed-loop performance and analyzing situations when the active system fails.

With the addition of an active isolator, the low frequency performance is improved by effectively decoupling the isolator frequency from static sag. The isolator can also add internal damping to reduce the absolute transmissibility at resonance without degrading the high frequency attenuation. An active isolator can also be designed to achieve narrowband isolation. This is a very attractive option when a known high-energy disturbance is present

in the system. Also, by using adaptive control techniques, an active isolator can "actively" change to meet new and unforeseen demands on the system.

## 1.3 Modeling Issues

Modeling of isolation systems makes use of two major assumptions: the system has only uni-axial motion, that is, a single-degree-of-freedom (SDOF) system and the foundation and equipment are rigid. Even though the SDOF model is a very simple model, a wealth of information about vibration isolation may be obtained. However, it has been proposed by various authors [3–5] that a two-degree-of-freedom (2DOF) model should replace the SDOF model since the 2DOF model is a step closer to a more accurate or realistic system. Historically, the drawback with the 2DOF model is that it is more complex to analyze. However, today's computational ability and analysis tools are fully capable of treating multiple-degree-of-freedom models, including the analysis of fully flexible systems.

The assumption that both the equipment and foundation are rigid will be valid if the equipment frequencies are much higher than the corner frequency of the isolator. However, in most aerospace structures this assumption is usually not valid because aerospace structures tend to be lightweight and very flexible. The flexibility in the system needs to be represented; otherwise, it will affect the transmissibility of the system or it can affect the stability of an active controller.

## 1.4 Isolators versus Absorbers

Vibration isolators are not the only way to reduce vibrations to some sensitive piece of equipment. Another implementation to reduce vibrations is to use a vibration absorber [1, 6, 7]. These two devices seem similar but are quite different in the way they reduce vibrations. Therefore, a brief summary is discussed about the isolator and absorber and then their differences are discussed.

The isolator in Figure 1.1 offers damping and stiffness to a system. In this figure, the isolator consists of a spring of stiffness $k$ and a viscous damper with a damping coefficient $c$. Common isolators are rubber mounts for isolating machinery and shock absorbers for improving ride comfort in an automobile. An isolator can also contain an active element such as a piezoceramic stack actuator.

The absorber shown in Figure 1.3 is an auxiliary mass ($m_a$) attached to a piece of equipment by some sort of stiffening material, in this case a spring of stiffness $K_a$. The absorber can be classified into two categories: dynamic absorber or damped vibration absorber [1]. If the auxiliary mass has little damping it is classified as a dynamic absorber and if the auxiliary mass is used to provide damping to the system it is known as a damped vibration absorber.

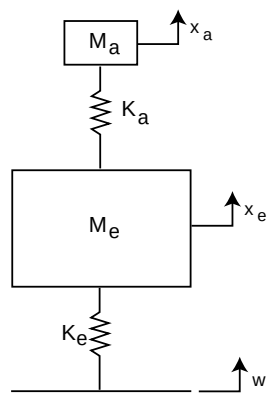


Figure 1.3: Vibration Absorber

A significant differences between an isolator and absorber is their location. The isolator has to be in the transmission path between the disturbance source and the equipment that will be isolated. On the other hand, the absorber is placed at the equipment's highest acceleration point. Another difference is that the absorber reduces vibrations by absorbing the vibrational energy through its mass deflection. The absorber spring must be able to withstand this force and its corresponding deflection; this places a geometric limitation on the design of the absorber. The isolator filters unwanted vibrations above some certain frequency with a specific choice of the isolator stiffness. The isolator is also limited by space constraints.

Absorbers work best when tuned to the exact disturbance frequency. At this tuning, there is no deflection of the primary mass. If the driving frequency changes, the absorber can still mitigate vibrations but at a reduced efficiency. There is also a limited range in which the driving frequency can change for the absorber to perform adequately. Figure 1.4 [7] is a plot of the vibration amplitude of the equipment mass to a force disturbance on the equipment. The shaded area in Figure 1.4 represents the acceptable range in which the driving frequency of the disturbance can change. Within this area ($0.897\omega_a < \omega_{dr} < 1.103\omega_a$), the vibrations of the primary mass will be reduced compared to a system that does not have an absorber.

Isolators work best when the isolator's natural frequency is small compared to the disturbance frequency. Vibrations are present in the system but at a reduced level. Figure 1.5 is a graphical representation of these statements and the nondimensional frequency is defined as the ratio of the driving frequency to the isolator's corner frequency ($\omega_{nd} = \omega_{dr}/\omega_o$). As seen from this figure, if the driving frequency increases with respect to the corner frequency, the isolator's performance increases. However, if the driving frequency decreases, the isolator performance is degraded until the point where the nondimensional frequency is $\sqrt{2}$. Below this point, the isolator no longer performs isolation but amplifies the motion

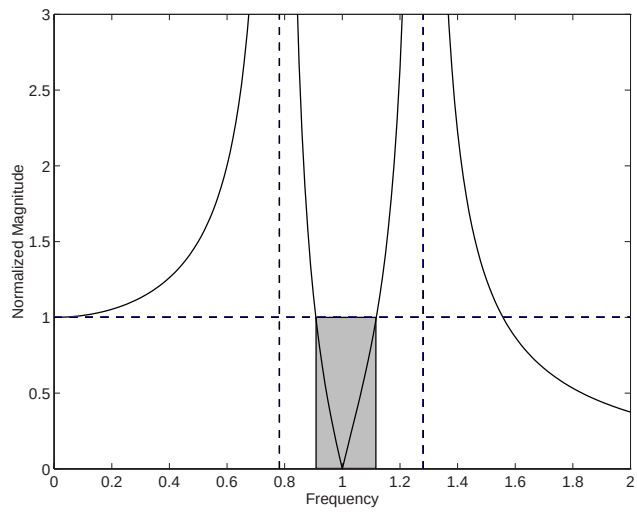


Figure 1.4: Absolute Magnitude for a Vibration Absorber

of the equipment.

The last difference between the two systems is the amount of damping present in an absorber and an isolator. Damping defeats the purpose of the absorber; the absorber can no longer have zero deflection at the attachment point because damping couples the equations of motion for the primary mass and the absorber mass. On the other hand, damping in an isolator is important in minimizing the vibration levels at the resonant frequency. However, passive damping causes the high frequency transmissibility to increase compared to an undamped system.

## 1.5 Literature Review

Currently there are over 3500 articles that discuss the use of vibration isolators to mitigate unwanted vibrations. These papers discuss the use of vibration isolators in a wide range of applications which can be divided into four major categories: machinery isolation [8–12], building or seismic isolation [4, 13], automotive isolation [13–16], and isolation of aerospace structures [17–19]. An isolator design in one field can usually be applied in any of the other fields.

### 1.5.1 Basic Concepts

There are numerous articles that review the basic concepts of vibration isolation but Harris [1], Nelson [3], Karnopp [13] and von Flotow [20] each give a different perspective

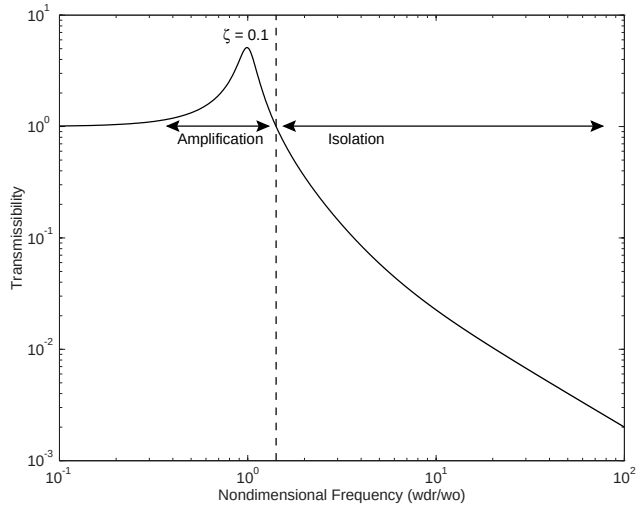


Figure 1.5: Absolute Magnitude for a Vibration Isolator

or insight into the vibration isolation concepts. These references cover basic vibration isolation ideas and concepts using both passive and active techniques.

The handbook by Harris dedicates five chapters on vibration isolation, ranging from theory to application. Basic concepts such as single-degree-of-freedom (SDOF) modeling and transmissibility are discussed as well as discussing isolation design for multiple-degree-of-freedom (MDOF) systems. Active and passive approaches to vibration isolation design are discussed as well.

Karnopp reviews the historical development of vibration isolation and also indicates how control theory or active control started to mark its influence in the 1960's. Like the other authors, he reviews the basic vibration isolation concepts and explains why no parameter set (stiffness or damping) for a passive system can result in an optimal state while an active system can achieve an optimal state. He also applies the concepts of vibration isolation to seismic platforms and automotive suspension systems.

Nelson reviews the basic vibration isolation problem for sinusoidal as well as random vibrations. His paper is somewhat different than the others because he stresses that only a few systems are dominated by a single-degree-of-freedom motion. Therefore, the classical single-degree-of-freedom model that is used in vibration isolation design should be replaced with a model that accounts for more degrees of freedom.

The paper by von Flotow reviews the concepts of using active or combined active/passive approaches in vibration isolators. He discusses the deficiencies of passive techniques and how active isolators can be used to overcome these problems. Concepts such as actuator placement and potential types of active control techniques are also discussed.

### 1.5.2 Active Control Concepts

There have been a large number of papers published in the area of active vibration isolation [8, 11, 14, 15, 17, 19–32]. The types of control architectures implemented in these papers are classical control concepts such as velocity feedback, optimal control concepts such as linear quadratic regulator (LQR) and linear quadratic gaussian (LQG) [21–23, 28], and adaptive control concepts such as the least mean squares (LMS) algorithm [11, 27, 30]. The control concepts used in active isolators are not limited to these control laws but are the most common. For example, Spanos *et al.* [17] used a loop shaping technique in the frequency domain to synthesize the control system. The loop shaping resulted in an $18^{th}$-order design consisting of a second-order low-pass filter, a fourth-order lead and lag filter, and four second-order notch filters.

Many of the implemented control architectures are designed to work at a specific disturbance frequency. These narrowband controllers [17, 21, 23, 24] provide compensator gains at the desired frequency to attenuate vibrations. The controllers will act rigid at all frequencies except at or very near the disturbance frequency. On the opposite extreme are the broadband controllers [17, 21, 22] which are designed to attenuate the transmissibility at all possible frequencies. They will attenuate vibrations at the disturbance frequency as well but usually not as well as the narrow-band controllers.

The most common types of narrowband controllers are the LQR and LQG controllers. Sievers and von Flotow [23] use the LQR and LQG controllers to make the closed-loop response act as a notch filter centered at the disturbance frequency. They also make use of frequency shaped cost functionals because this can lead to a more optimal controller. Hyde and Crawley [21] also used frequency shaped cost functionals so the transmissibility would have a second-order roll-off near the resonant condition. With a basic LQG controller, the closed-loop transmissibility decreases at a rate of 20 db/decade after reaching the closed-loop resonance. Nagaya and Kanai [22] use an optimal regulator with a disturbance cancellation method to obtain reductions in the transmissibility. In this case, the regulator is used to decrease the transmissibility at the resonant peak because the disturbance cancellation method cannot adequately cancel this part of the transmissibility.

There have also been numerous articles that use adaptive control schemes for control of active isolators [11, 26, 27, 30]. Chen and Lewis [30] used the LMS algorithm to create an adaptive narrowband controller. This algorithm provided more force attenuation and generally was more stable than other experiments that used force attenuation. Jenkins *et al.* [11] implemented a multi-channel version of the LMS algorithm on two different experiments. They showed that a combined active and passive mount are better equipped to handle low frequency vibrations than a passive system alone. Sommerfeldt and Tichy [27] used a modified LMS algorithm which was designed to account for transport delays in the systems so the new algorithm would remain stable. However, the new algorithm converged slower than the conventional LMS algorithm but if the error estimates were

made available, the modified algorithm converged as fast as the LMS algorithm.

It has been shown by Sievers and von Flotow [25] and MacMartin [26] that the LMS and LQG designs are equivalent in the steady state if the disturbance are harmonic in a narrowband frequency. This implies that the compensators are equivalent and their performance and robustness properties are identical. Therefore, choosing one approach over the other is irrelevant. However, if the narrowband disturbance frequencies vary greatly or if there is a broadband disturbance, these system will no longer be equivalent. MacMartin discusses the fact that even though these two architectures are implemented differently, one approach may give more insight into the isolation problem than the other. For example, the adaptive feedforward approach is more explicit in determining sensor locations. LQG or feedback controllers are easier to determine the effect of compensator closed-loop dynamics.

### 1.5.3 Methods to Determine Transmissibility for Flexible Structures

The benefit of assuming that the foundation and equipment are rigid is the simplicity in determining the transmissibility. Once the rigid assumptions are no longer valid, the task of deriving the transmissibility becomes more difficult. There are many different techniques to solve the isolation problem for continuous, i.e., flexible or distributed systems. However, all the techniques in the past use an approximation to the solution of the governing partial differential equation. Some of these techniques include using normalized modes [33], the assumed modes method [6], impedance methods [34–36], and the finite element method [37].

As mentioned in Section 1.3, not all systems have the base or equipment modeled as a rigid member. It has been shown by Blackwood and von Flotow [31] that base or equipment flexibility will make an isolator less effective. Therefore, the issues of base or equipment flexibility should be included in the isolator design.

The transmissibility due to a flexible foundation or equipment can be derived using approximate techniques mentioned above or using a formulation derived by Yang and Tan [38]. They derived a procedure that can find the exact closed-form solution of distributed parameter systems by use of a state-space technique. This formulation is valid for self-adjoint and nonself-adjoint systems with inhomogeneous boundary conditions. Yang improved on this procedure to determine the solution for any generic complex distributed parameter systems [39]. This new method can be used to evaluate many complex systems such as a system with lumped masses elastically connected to a beam, beams having point and distributed constraints, and rigid bodies elastically connected to a beam. This synthesis does not make use of approximations or series truncations and it can be used to determine the exact values for the eigenvalues, eigenfunctions and the forced responses of a complex distributed parameter system. Therefore, it is an ideal procedure to analyze complex vibration isolation systems.

### 1.5.4 Passive and Active Isolators for Flexible Structures

The use of passive isolators to isolate rigid equipment from a flexible base has been investigated by several authors. Sykes [36] used a mechanical impedance method to calculate the effectiveness of an isolator. He approximated the flexible foundation by assuming simple mechanical analogies: a mass, a damper, a spring, and a single resonator as well as using a general impedance for the foundation. Snowdon [40] also analyzed systems with flexible foundations and he used normalized modes to solve the isolation problem. Glauser and Ahmadi [18] analyzed isolating a launch vehicle payload and its sensitive subsystem. The payload was modeled as a nonuniform shear beam and the subsystem was modeled as a single-degree-of-freedom system. They analyzed the problem by solving the governing partial differential equations with normalized modes. Soliman and Hallam [41] took a general approach and studied the issue of vibration isolation between flexible foundations and flexible machines with the use of an impedance or mobility method. The drawback with their approach is determining the mobility functions. These functions become quite difficult to determine for complex isolation systems and experimentally measured quantities have to be used.

Several authors have investigated using active isolation between a rigid equipment and a flexible foundation. Watters *et al.* [8] published one of the first papers to consider foundation flexibility when using active isolation. This paper showed that the base dynamics were nearly decoupled from the force measurement, yet base acceleration exhibited strong interaction with the base modes. Sievers *et al.* [24] also looked at isolating machines from a flexible base. The analysis was done assuming a very limited knowledge of the plant dynamics and it was shown that active control is optimized if the structure has high modal overlap. Spanos *et al.* [17] used active control in conjunction with a passive mount to isolate equipment vibrations from a flexible structure. The active stage reduced the transmissibility above and below the corner frequency which was accomplished by using broadband force feedback control and narrowband control.

## 1.6 Objectives

The objective is to analyze a complex isolation system using a more sophisticated analysis than currently available in the literature that will avoid standard truncation errors. Both passive and active methods are examined in two complex scenarios: a flexible base and rigid equipment system and a flexible base and flexible equipment system. The purpose of the analysis is to provide new isolation criteria based on improved modeling and analysis. For each complex isolation model the objectives are similar.

One of the main objectives of this dissertation is to quantify what type of effect flexibility will have in the isolation design. For a SDOF model, the mount or corner frequency of the isolator is designed at the lowest possible frequency. Therefore, when flexibility is included

in the model, the effectiveness of the mount design will be thoroughly analyzed. Since the base will be modeled as a flexible system, it is worthwhile to determine what effect, if any, the placement of the isolator will have on the overall isolator performance.

The influence of isolator damping is an important consideration as well. For a SDOF model, the inclusion of damping increases the transmissibility at high frequencies; therefore, a determination of the influence of isolator damping in a system that has a flexible member will also be analyzed. Finally for the passive system, a discussion of isolator performance for varying parameters such as mount frequency, isolator location, and mass ratio will be analyzed. This analysis will simultaneously analyze all three parameters and a determination of the ideal values for these parameters will be made. Performance increases using dual isolators will also be discussed for each system.

The final objective is to determine how the modeling of flexibility will affect an isolation system that implements an active controller. This includes the best placement of the feedback sensor and determining isolator performance with various control methodologies. The control laws that will be considered are the proportional-plus-integral-plus-derivative ($\mathcal{PID}$) controller, the positive position feedback (PPF) controller, and the linear quadratic Gaussian (LQG) regulator.

## 1.7 Thesis Description

The single-degree-of-freedom model is extensively reviewed in Chapter 2. A review on the inherent features of the SDOF model using passive and active isolators are also made. A discussion on active controllers such as $\mathcal{PID}$ and LQG are fully considered and a comparison between the two control methodologies are made.

Chapter 3 uses a two-degree-of-freedom (2DOF) system to model the isolation system. This chapter discusses the limitation of the SDOF model and why a 2DOF model may be more accurate. By increasing the complexity of the model, the complexity of analyzing the transmissibility is increased. Therefore, a novel visualization approach was used to minimize the complexity in determining the transmissibility. Similar to the SDOF chapter, the use of active isolation is also considered. For this system, the effectiveness of a $\mathcal{PID}$ or $\mathcal{PD}$ controller and an LQG regulator is discussed.

Chapter 4 is a detailed analysis of Yang's method to find exact solutions to complex distributed systems. This includes a detailed review of his method and a discussion how the flexible base, rigid equipment and flexible base, flexible equipment systems should be analyzed in this method. A cantilever beam experiment is also discussed to verify the transfer function obtained by Yang's method.

The flexible base, rigid equipment system is discussed in Chapter 5 and the flexible base, flexible equipment is discussed in Chapter 6. Both chapters discuss the influence of the corner or mount frequency with and without damping. They also look at the influence

of isolator placement and mass ratios as well as determining performance increases with a dual isolator system. These chapters determine the ideal placement for the feedback sensor as well as using three different types of active controllers. A summary with conclusions, contributions and future work for this dissertation is provided in Chapter 7.

# Chapter 2

# Single-Degree-of-Freedom System

There are numerous applications where it is desirable to isolate the vibration of a given structure from the foundation on which it is mounted. For example, it is desirable to have passengers in a car feel little or no movement when traversing over a rough road. This chapter analyzes a single-degree-of-freedom (SDOF) system as a model for the vibration isolation system. The isolation may take the form of isolating a piece of equipment from disturbances on the foundation or isolating the foundation from vibrations emanating from the equipment. Either way, the goal is to minimize the vibration levels imparted to some part of the system.

The system under study is a second-order mass-spring-damper system as shown in Figure 2.1 where $w$ is a base excitation and $F$ is a force excitation. Both passive and active isolation will be considered and discussed. The control architecture that will be implemented are a proportional-plus-derivative ($\mathcal{PD}$) controller, a proportional-plus-integral-plus-derivative ($\mathcal{PID}$) controller, and a linear quadratic Gaussian (LQG) regulator. The effectiveness of active isolation and passive isolation will be determined through the system's absolute transmissibility.

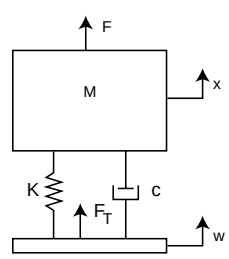


Figure 2.1: Second-Order Mass-Spring-Damper System

## 2.1 Passive Isolation

Assuming only a base excitation $w$, the equation of motion for the SDOF system is

$$m\ddot{x} + c(\dot{x} - \dot{w}) + k(x - w) = 0. \tag{2.1}$$

Letting $c/m = 2\zeta\omega_n,\ \omega_n = \sqrt{k/m}$ and dividing equation (2.1) through by the mass, the new governing equation becomes

$$\ddot{x} + 2\zeta\omega_n\dot{x} + \omega_n^2 x = 2\zeta\omega_n\dot{w} + \omega_n^2 w. \tag{2.2}$$

As mentioned in the introduction, the absolute transmissibility will be used as an indicator for acceptable isolator design. The absolute transmissibility may be formulated by taking the Laplace Transform of equation (2.2).

$$TR = \frac{X(s)}{W(s)} = \frac{2\zeta\omega_n s + \omega_n^2}{s^2 + 2\zeta\omega_n s + \omega_n^2} \tag{2.3}$$

Normalizing the frequency by S=s/$\omega_n$, equation (2.3) can be cast into the following nondimensional form.

$$TR = \frac{X(S)}{W(S)} = \frac{2\zeta S + 1}{S^2 + 2\zeta S + 1} \tag{2.4}$$

A plot of the absolute transmissibility versus the If there is no damping present in the isolator, the transmissibility is theoretically unbounded at the system's natural frequency. Increasing the amount of damping in the system will decrease the transmissibility at the resonant frequency; however, the high frequency transmissibility will be increased. On the other hand, active control can be used to mitigate the amplification of the high frequency transmissibility while attenuating the transmissibility at the resonant mode.

It is worthwhile to note that if the system was excited by an external force $F$ on the equipment, the absolute transmissibility would be defined as the ratio $F_T/F$, where $F_T$ is the force transmitted to the base. This absolute transmissibility is equivalent to equation (2.4) if the system is linear and uni-axial [2].

## 2.2 Active Isolation

As shown in section 2.1, passive isolator damping causes amplification of the system's transmissibility at high frequencies. To alleviate this problem, some type of active control should be used. There are numerous control strategies to choose from [20, 23], but this report will consider only classical control theory [42, 43] and optimal control theory [44–47].

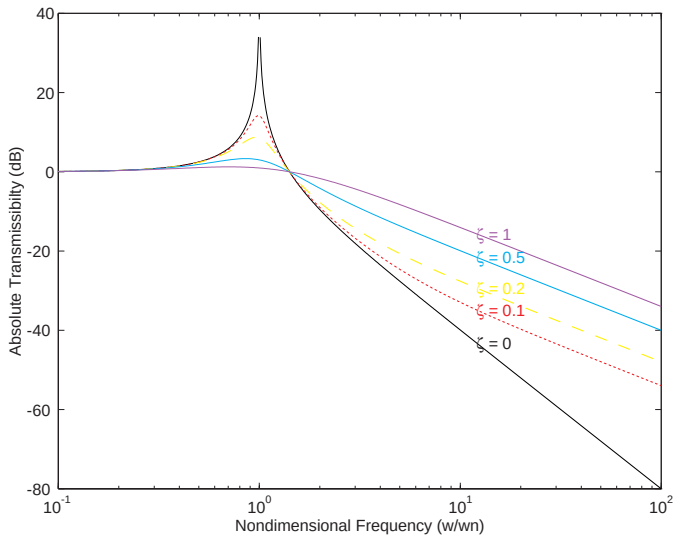


Figure 2.2: Absolute Transmissibility Plots for SDOF System

To implement an active control design, the isolator shown in Figure 2.1 needs to be redesigned. The passive damper will be replaced by an active force element ($F_c$ in Figure 2.3), i.e., an actuator. The actuator will implement an active control strategy that will add damping to the system. It is assumed that the absolute position, velocity, and acceleration $(x, \dot{x}, \ddot{x})$ of the equipment are readily available for input to the controller. It is also assumed that the control strategies will be implemented either by analog components or a digital computer.

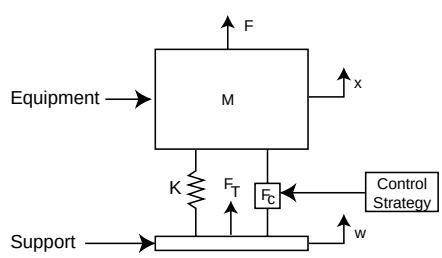


Figure 2.3: Second-Order System with Active Element

The block diagram for this new system is shown in Figure 2.4. The base excitation $w$ is the disturbance to the plant G(S). The gain H(S) for the disturbance is unity since there is no passive isolator damping present and D(S) is the transfer function for the compensator. The overall transfer function from the equipment displacement to a base disturbance is

$$\frac{X(S)}{W(S)} = \frac{G(S)H(S)}{1 + G(S)D(S)} \ , \tag{2.5}$$

where $G(S) = \frac{1}{S^2+1}$, $H(S) = 1$, and $r = 0$. Note that the plant has no damping and is

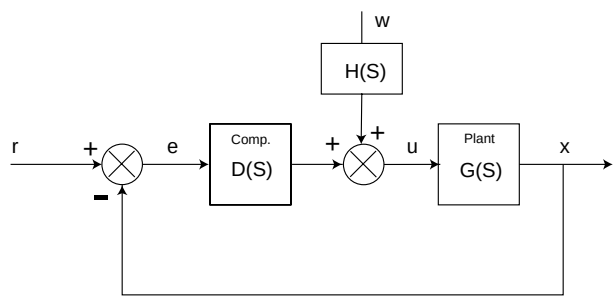


Figure 2.4: Block Diagram of Feedback Control Law Implementation

unstable at the resonant condition. Therefore, it is necessary that the active control law supply some sort of damping to the system through the actuator.

### 2.2.1 Classical Control

Classical control consists of designing a control architecture in the time or frequency domain for a single-input-single-output system (SISO). This can be accomplished by two methods: the root-locus design (time domain) method or the frequency response design (frequency domain) method. The frequency domain method was chosen since the transmissibility is easier to quantify in the frequency domain.

Two types of control laws are implemented for this system: a proportional-plus-integral-plus-derivative ($\mathcal{PID}$) controller, and a proportional-plus-derivative ($\mathcal{PD}$) controller. Both controllers were designed to decrease the transmissibility at the resonant condition. A secondary performance criteria used for adequate isolation design were the time responses, i.e., each system must have good rise times and settling times.

#### 2.2.1.1 $\mathcal{PD}$ Control

The transfer function for $\mathcal{PD}$ control as a function of the nondimensional frequency is

$$D(S) = K_D S + K_P \ , \tag{2.6}$$

where $K_D$ is the derivative gain and $K_P$ is the proportional gain. The value of $K_D$ is similar to a viscous damping coefficient term and the value of $K_P$ is similar to a stiffness term. For this problem, $K_D = 0.4$ and $K_P = 0.01$ was assigned. These values for the $\mathcal{PD}$ controller are similar to adding a passive damper with a damping ratio of $\zeta = 0.2$, and increasing the stiffness by a small margin. The small value for the proportional gain was chosen such that the natural frequency would not be significantly altered. Note that there

will be a tendency for the system to increase the natural frequency for values of $K_P > 0$ and to decrease the natural frequency for values of $K_P < 0$.

The frequency responses using passive isolation and $\mathcal{PD}$ control are shown in Figure 2.5. As seen from this figure, the transmissibility for $\mathcal{PD}$ control has characteristics similar the passive isolator; the transmissibility of the $\mathcal{PD}$ controller and the passive isolator are equivalent up to the resonant condition. However, active control outperforms the passive system in the higher frequency ranges. With active isolation, the high frequency transmissibility is comparable to an undamped system.

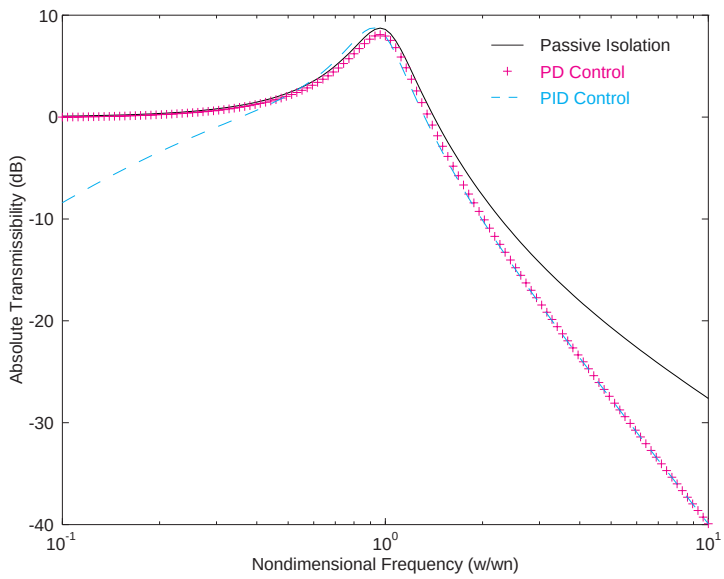


Figure 2.5: Absolute Transmissibility Plots for the Closed-Loop System

Figure 2.2 shows that a passive system with low damping will decrease the transmissibility at a rate of 40 dB/decade for frequencies greater than the corner frequency, i.e., $\omega/\omega_d > \sqrt{2}$. When damping starts to become large ($\zeta \gtrsim 0.1$) in the passive isolator, the transmissibility decreases at a slower rate. This decrease at high frequencies does not occur when an active isolator is used. The high frequency transmissibility for an active isolator decreases at a rate of 40 dB/decade which is comparable to an undamped isolator. Therefore, active isolation allows the attenuation of the transmissibility at the natural frequency without increasing the high frequency transmissibility.

The responses of each (passive and active) system to a step input are identical in Figure 2.6 since the passive and active systems are nearly identical in their transfer functions. The only difference is that the numerator in the passive system has an extra derivative term in it. This extra term will cause the high frequency transmissibility to increase compared to an undamped system.

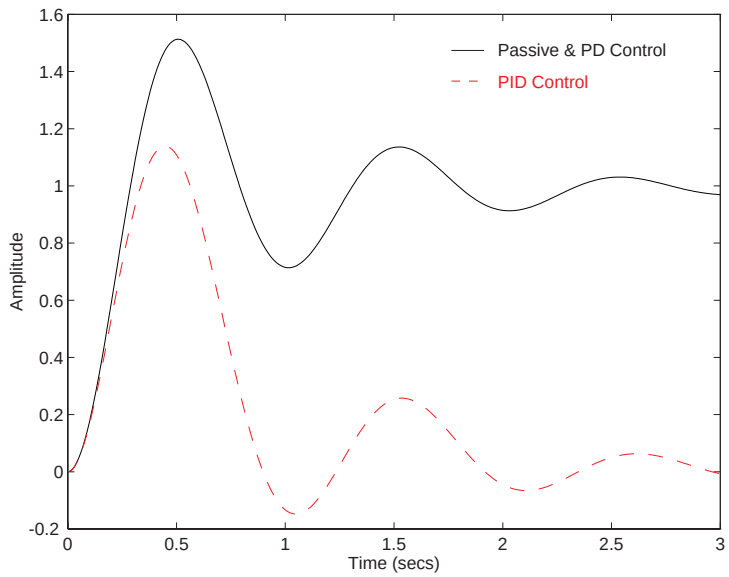


Figure 2.6: Step Response for Absolute Transmissibility Problem

#### 2.2.1.2 $\mathcal{PID}$ Control

The transfer function for the $\mathcal{PID}$ controller as a function of the nondimensional frequency is

$$D(S) = K_D S + K_P + K_I/S \ , \tag{2.7}$$

where $K_I$ is the integral gain, $K_D$ is the derivative gain, and $K_P$ is the proportional gain. Similar to the section on $\mathcal{PD}$ control, the proportional gain was chosen so that the natural frequency of the system would not be altered significantly and its final value was chosen at $K_P = 0.01$. The values of $K_D = 0.65$ and $K_I = 0.25$ were chosen such that this system would have the same amount of damping as the passive system or an active system using a $\mathcal{PD}$ controller. The integral gain was adjusted to make sure the transient response would quickly decay to its original position.

The frequency responses using a $\mathcal{PID}$ controller, a $\mathcal{PD}$ controller, and a passive isolator are shown in Figure 2.5. As seen from this figure, $\mathcal{PID}$ control is very similar to $\mathcal{PD}$ control except for a slight change in the natural frequency. The low frequency transmissibility for the $\mathcal{PID}$ controller is also significantly lower than a $\mathcal{PD}$ controller. The significance of using $\mathcal{PID}$ control is shown through the step responses in Figure 2.6. Unlike $\mathcal{PD}$ control or a passive isolator, the response of the $\mathcal{PID}$ system deviates and oscillates around its initial position which is attributable to the integrator. The integrator is used to cancel any constant disturbance inputs to the system. Since the damping of all three systems are nearly equivalent, the settling time for each system are also equivalent.

### 2.2.2 Linear Optimal Control

This section looks at designing an optimal controller for a single-input-single-output (SISO) linear system. The state-space representation for this system is

$$\begin{aligned} \dot{\vec{\mathbf{x}}} &= \underline{\underline{\mathbf{A}}}\vec{\mathbf{x}} + \vec{\mathbf{B}}u \\ y &= \vec{\mathbf{C}}\vec{\mathbf{x}} + Du \\ z &= \vec{\mathbf{C}}_z\vec{\mathbf{x}} \ , \end{aligned} \tag{2.8}$$

where $y$ is the output of the system and $z$ is the performance metric.

The optimal control $u$ is a control history that minimizes the cost over all admissible control histories where the optimal cost is given below.

$$\mathcal{J} = \int_0^\infty (\vec{\mathbf{x}}^T\underline{\underline{\mathbf{Q}}}\vec{\mathbf{x}} + u^T\underline{\underline{\mathbf{R}}}u)dt \tag{2.9}$$

The state penalty is $\underline{\underline{\mathbf{Q}}} = \vec{\mathbf{C}}_z^T\vec{\mathbf{C}}_z$ and is a positive semi-definite matrix. The control penalty $\underline{\underline{\mathbf{R}}}$, on the other hand, is a positive definite matrix. The cost function is quadratic and penalizes the states of the system and the input of the system. This penalty is very flexible because it can penalize the system states or the system inputs more heavily by changing the state penalty or control penalty, respectively.

If the states of the system are known, the minimization of equation (2.9) leads to an optimal gain for the controller. This procedure is referred as the linear quadratic regulator (LQR) problem. If the states are not all known, an estimator must be designed to estimate the states of the system. The optimal solution for the estimator problem is known as a Kalman-Bucy filter. The combination of the optimal estimator and controller is referred to as the linear quadratic gaussian (LQG) regulator problem. A detailed discussion can be found in Anderson [45], Kwakernaak [46] or Siouris [47].

#### 2.2.2.1 Linear Quadratic Regulator

The linear optimal regulator is designed by the minimization of the cost function in equation (2.9). For a time invariant system, this minimization leads to the optimal state feedback control given in equation (2.10).

$$\begin{aligned} u(t) &= \vec{\mathbf{K}}_r\vec{\mathbf{x}}(t) \\ \vec{\mathbf{K}}_r &= -\underline{\underline{\mathbf{R}}}^{-1}\vec{\mathbf{B}}^T\underline{\underline{\mathbf{P}}}(t) \end{aligned} \tag{2.10}$$

$\underline{\underline{\mathbf{P}}}(t)$ is determined by the Algebraic Riccati Equation given in equation (2.11).

$$\dot{\underline{\underline{\mathbf{P}}}} = \underline{\underline{\mathbf{Q}}} - \underline{\underline{\mathbf{PBR}}}^{-1}\underline{\underline{\mathbf{B}}}^T\underline{\underline{\mathbf{P}}} + \underline{\underline{\mathbf{PA}}} + \underline{\underline{\mathbf{A}}}^T\underline{\underline{\mathbf{P}}} \tag{2.11}$$

It should be noted that the optimal control is time varying since $\underline{\underline{\mathbf{P}}}(t)$ is time varying. A time invariant control may be implemented by solving the steady-state solution from equation (2.11), i.e., setting $\dot{\underline{\underline{\mathbf{P}}}}(t) = 0$ and solving for $\underline{\underline{\mathbf{P}}}(t)$. For the steady-state solution to exist, the following criteria must exist:

i. $\underline{\underline{\mathbf{Q}}}$ must be positive semi-definite

ii. $\underline{\underline{\mathbf{R}}}$ must be positive definite

iii. The system $(\underline{\underline{\mathbf{A}}}, \underline{\underline{\mathbf{B}}})$ must be controllable to ensure solvability

iv. The system $(\underline{\underline{\mathbf{A}}}, \vec{\mathbf{C}}_z)$ must be observable to ensure stability.

#### 2.2.2.2 Linear Optimal Estimator

The LQR method is based on the fact that all states of the system are readily measurable; however, this is very difficult to attain in most applications. Therefore, some type of estimator is needed and an optimal estimator such as a Kalman-Bucy filter can be constructed.

Consider the following continuous-time stochastic linear system

$$\begin{aligned} \dot{\vec{\mathbf{x}}} &= \underline{\underline{\mathbf{A}}}\vec{\mathbf{x}} + \vec{\mathbf{B}}u + \vec{\mathbf{F}}\xi \\ y &= \vec{\mathbf{C}}\vec{\mathbf{x}} + \eta. \end{aligned} \tag{2.12}$$

The process noise $\xi$ and the measurement noise $\eta$ are assumed to be zero-mean, Gaussian white noise and are uncorrelated with each other. In other words,

$$\mathcal{E}[\xi(t)] = \mathcal{E}[\eta(t)] = 0 \tag{2.13a}$$

$$\mathcal{E}[\xi(t)\xi^T(\tau)] = Q_o(t)\delta(t-\tau) \tag{2.13b}$$

$$\mathcal{E}[\eta(t)\eta^T(\tau)] = R_f\delta(t-\tau) \tag{2.13c}$$

$$\mathcal{E}[\xi(t)\eta^T(\tau)] = 0 \tag{2.13d}$$

where $\mathcal{E}$ denotes the expected value. The estimator takes on the form

$$\begin{aligned} \dot{\hat{\vec{\mathbf{x}}}} &= \underline{\underline{\mathbf{A}}}\hat{\vec{\mathbf{x}}} + \vec{\mathbf{B}}u + \vec{\mathbf{K}}_f[y - \hat{y}] \\ \hat{y} &= \vec{\mathbf{C}}\hat{\vec{\mathbf{x}}} \end{aligned} \tag{2.14}$$

where $\hat{\vec{\mathbf{x}}}$ are the estimates of the states $\vec{\mathbf{x}}$ and the estimator minimizes the mean-square error. This minimization leads to the filter gain

$$\vec{\mathbf{K}}_f = \underline{\underline{\mathbf{P}}}\vec{\mathbf{C}}^T R^{-1}. \tag{2.15}$$

$\underline{\underline{\mathbf{P}}}$(t) is derived by the steady-state solution to the filtering Riccati equation:

$$\dot{\underline{\underline{\mathbf{P}}}} = \underline{\underline{\mathbf{0}}} = \underline{\underline{\mathbf{AP}}} + \underline{\underline{\mathbf{PA}}}^T + \vec{\mathbf{K}}_f Q_o \vec{\mathbf{K}}_f^T - \underline{\underline{\mathbf{P}}}\vec{\mathbf{C}}^T R_f^{-1} \vec{\mathbf{C}}\underline{\underline{\mathbf{P}}}. \tag{2.16}$$

For this steady-state solution to exist, the following must hold true:

i. $\vec{\mathbf{K}}_f Q_o \vec{\mathbf{K}}_f^T$ must be positive definite

ii. $R_f$ must be positive definite

iii. The system ($\underline{\underline{\mathbf{A}}}$,$\vec{\mathbf{C}}$) must be detectable

iv. The system ($\underline{\underline{\mathbf{A}}}$,$\vec{\mathbf{F}}$) must be stabilizable

#### 2.2.2.3 Disturbance Modeling

In the previous section it was assumed that the noise was a zero-mean, Gaussian process known as white noise. White noise implies that its power-density spectrum is uniform over the entire frequency range and that it has an infinite average power. An infinite average power is physically impossible; however, most random processes can be approximated with white noise because most noise processes have a flat power spectrum at much larger frequencies than which a system can respond.

If the system is driven by colored noise, the concept of a shaping filter may be employed. The shaping filter allows a system that is driven by colored noise to be replaced by an augmented system that is driven by white noise. This is fully discussed in Siouris [47] and only the discussion of the how the shaping filter changes the plant is discussed. Assume that the plant can be modeled as in equation (2.12) but now $\xi$ is a nonwhite, i.e., time-correlated, Gaussian noise process. Also, assume that $\xi$ is generated by the following shaping filter

$$\begin{aligned} \dot{\vec{\mathbf{x}}}_f &= \underline{\underline{\mathbf{A}}}_d \vec{\mathbf{x}}_f + \vec{\mathbf{B}}_d v \\ \xi &= \vec{\mathbf{C}}_d \vec{\mathbf{x}}_f \end{aligned} \tag{2.17}$$

where $v$ is a white-noise process. Augmenting the new state vector as

$$\vec{\boldsymbol{\zeta}} = \begin{Bmatrix} \vec{\mathbf{x}} \\ \vec{\mathbf{x}}_f \end{Bmatrix} , \tag{2.18}$$

the new augmented plant driven by white noise is

$$\begin{aligned} \frac{\mathrm{d}}{\mathrm{d}t} \begin{Bmatrix} \vec{\mathbf{x}} \\ \vec{\mathbf{x}}_f \end{Bmatrix} &= \begin{bmatrix} \underline{\underline{\mathbf{A}}} & \vec{\mathbf{F}}\vec{\mathbf{C}}_d \\ \underline{\underline{\mathbf{0}}} & \underline{\underline{\mathbf{A}}}_d \end{bmatrix} \begin{Bmatrix} \vec{\mathbf{x}} \\ \vec{\mathbf{x}}_f \end{Bmatrix} + \begin{Bmatrix} \vec{\mathbf{B}} \\ \vec{\mathbf{0}} \end{Bmatrix} u + \begin{Bmatrix} \vec{\mathbf{0}} \\ \vec{\mathbf{B}}_d \end{Bmatrix} v \\ y &= \begin{Bmatrix} \vec{\mathbf{C}} & \vec{\mathbf{0}} \end{Bmatrix} \begin{Bmatrix} \vec{\mathbf{x}} \\ \vec{\mathbf{x}}_f \end{Bmatrix} + \eta \ . \end{aligned} \tag{2.19}$$

Due to the addition of the shaping filter, the cost function in equation (2.9) will change and the new cost function will be

$$\mathcal{J} = \int_0^\infty \left( \left\{ \vec{\mathbf{x}}^T \quad \vec{\mathbf{x}}_f^T \right\} \begin{bmatrix} \underline{\underline{\mathbf{Q}}} & \underline{\underline{\mathbf{0}}} \\ \underline{\underline{\mathbf{0}}} & \underline{\underline{\mathbf{0}}} \end{bmatrix} \begin{Bmatrix} \vec{\mathbf{x}} \\ \vec{\mathbf{x}}_f \end{Bmatrix} + u^T \underline{\underline{\mathbf{R}}} u \right) \mathrm{d}t \ . \tag{2.20}$$

#### 2.2.2.4 Linear Quadratic Gaussian Regulator

The deterministic LQR problem can be combined with the stochastic estimation problem to form the Linear Quadratic Gaussian (LQG) regulator. The block diagram for this system is shown in Figure 2.7 which includes a shaping filter. The calculation for the estimates $\hat{\vec{\mathbf{x}}}$ of the states and the control law gain $K_r$ can be done independently of each other due to the Separation Theorem also known as the Certainty Equivalence Principle [45]. This theorem states that the closed-loop poles of the overall LQG formulation are the closed-loop poles due to the LQR formulation and the closed-loop poles of the estimator formulation.

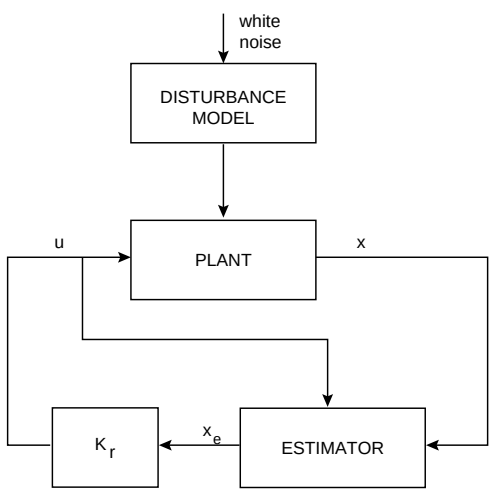


Figure 2.7: Block Diagram Representation of LQG Formulation

The combination of the regulator and estimator problem will change the state-space representation of our system. The new state-space representation to find the frequency response is

$$\begin{aligned} \frac{\mathrm{d}}{\mathrm{d}t} \begin{Bmatrix} \vec{\mathbf{x}} \\ \hat{\vec{\boldsymbol{\zeta}}} \end{Bmatrix} &= \begin{bmatrix} \underline{\underline{\mathbf{A}}} & -\vec{\mathbf{B}}\vec{\mathbf{K}}_r \\ \vec{\mathbf{K}}_f\vec{\mathbf{C}} & \underline{\underline{\mathbf{A}}}_a - \vec{\mathbf{B}}_a\vec{\mathbf{K}}_r - \vec{\mathbf{K}}_f\vec{\mathbf{C}}_a \end{bmatrix} \begin{Bmatrix} \vec{\mathbf{x}} \\ \hat{\vec{\boldsymbol{\zeta}}} \end{Bmatrix} + \begin{Bmatrix} \vec{\mathbf{F}} \\ \vec{\mathbf{0}} \end{Bmatrix} \xi + \begin{Bmatrix} \vec{\mathbf{0}} \\ \vec{\mathbf{K}}_f \end{Bmatrix} \eta \\ y &= \left\{ \vec{\mathbf{C}} \quad \vec{\mathbf{0}} \right\} \begin{Bmatrix} \vec{\mathbf{x}} \\ \hat{\vec{\boldsymbol{\zeta}}} \end{Bmatrix} + \eta \ . \end{aligned} \tag{2.21}$$

For simulation purposes in the time domain, the state-space representation should be

$$\begin{aligned}\frac{\mathrm{d}}{\mathrm{d}t}\begin{Bmatrix}\vec{\boldsymbol{\zeta}}\\ \hat{\vec{\boldsymbol{\zeta}}}\end{Bmatrix} &= \begin{bmatrix}\underline{\underline{\mathbf{A}}}_a & -\vec{\mathbf{B}}_a\vec{\mathbf{K}}_r\\ \vec{\mathbf{K}}_f\vec{\mathbf{C}}_a & \underline{\underline{\mathbf{A}}}_a - \vec{\mathbf{B}}_a\vec{\mathbf{K}}_r - \vec{\mathbf{K}}_f\vec{\mathbf{C}}_a\end{bmatrix}\begin{Bmatrix}\vec{\boldsymbol{\zeta}}\\ \hat{\vec{\boldsymbol{\zeta}}}\end{Bmatrix} + \begin{Bmatrix}\vec{\mathbf{F}}_a\\ \vec{\mathbf{0}}\end{Bmatrix} v + \begin{Bmatrix}\vec{\mathbf{0}}\\ \vec{\mathbf{K}}_f\end{Bmatrix}\eta\\ y &= \begin{Bmatrix}\vec{\mathbf{C}} & \vec{\mathbf{0}}\end{Bmatrix}\begin{Bmatrix}\vec{\mathbf{x}}\\ \hat{\vec{\boldsymbol{\zeta}}}\end{Bmatrix} + \eta\ .\end{aligned} \tag{2.22}$$

#### 2.2.2.5 Linear Quadratic Gaussian Results

When using classical controllers, the dynamics of the isolation system and compensator were given as transfer functions. Since the LQG regulator is designed using state-space methods, the transfer function in equation (2.4) can be recast into the state space similar to equation (2.12). If the states are given as

$$\vec{\mathbf{x}} = \begin{Bmatrix}x\\ \dot{x}\end{Bmatrix} \tag{2.23}$$

and viscous damping is neglected, the state-space matrices for the SDOF system are

$$\underline{\underline{\mathbf{A}}} = \begin{bmatrix}0 & 1\\ -1 & 0\end{bmatrix},\quad \vec{\mathbf{B}} = \begin{Bmatrix}0\\ -1\end{Bmatrix},\quad \vec{\mathbf{F}} = \begin{Bmatrix}0\\ 1\end{Bmatrix},\quad \vec{\mathbf{C}} = \begin{Bmatrix}1 & 0\end{Bmatrix}\ . \tag{2.24}$$

The disturbance is modeled as a sinusoid at the system's natural frequency and the state-space matrices in equation (2.17) are

$$\underline{\underline{\mathbf{A}}}_d = \begin{bmatrix}0 & 1\\ -1 & 0\end{bmatrix},\quad \vec{\mathbf{B}}_d = \begin{Bmatrix}0\\ 1\end{Bmatrix},\quad \vec{\mathbf{C}}_d = \begin{Bmatrix}1 & 0\end{Bmatrix}\ . \tag{2.25}$$

The following values were used for the penalties of the LQG regulator:

$$z = 1\text{x}10^3\begin{bmatrix}-1\text{x}10^{-3} & -1\text{x}10^{-1}\end{bmatrix},\quad R = 1,\quad Q_o = 1\text{x}10^{-6},\quad R_f = 1\ . \tag{2.26}$$

As mentioned in Section 2.2.2.4, equation (2.21) must be used when looking at the frequency response. Figure 2.8 is a comparison between passive isolation and active isolation using a LQG control architecture where two main features are prominent. The first feature is that the LQG controller acts as a notch filter at the system's natural frequency. Secondly, some broadband attenuation of the transmissibility is obtained around the natural frequency of the system.

As in classical controls, a time response should be done to get a better indication of performance and equation (2.22) should be used for these calculations. Unlike the classical controls section, a step input will not be used but a time response due to initial conditions. It is assumed that the mass is displaced by a value of 1 and let go from rest.

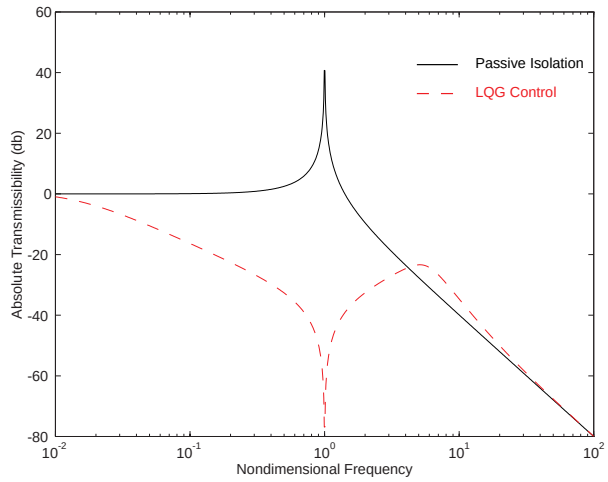


Figure 2.8: Absolute Transmissibility using LQG

The response of the undamped isolator, a $\mathcal{PID}$ or $\mathcal{PD}$ controller, and a LQG controller are shown in Figure 2.9. For the undamped system, the response of the equipment will oscillate indefinitely at its natural frequency. $\mathcal{PID}$ and $\mathcal{PD}$ control are equivalent and it takes a few seconds for the response to reach a steady-state solution. For the LQG controller, the system reaches a steady-state solution in 0.5 seconds.

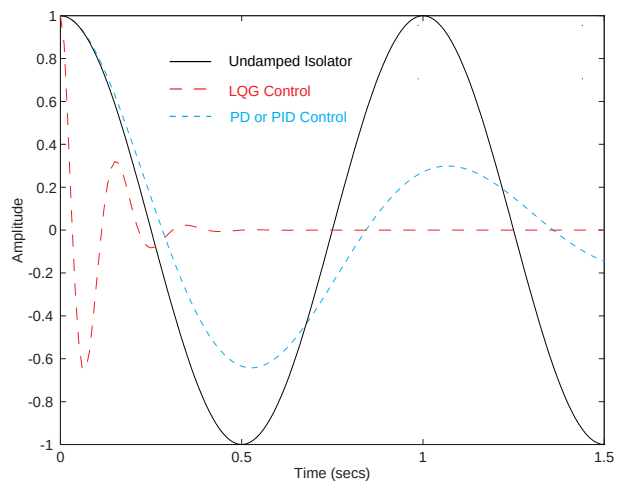


Figure 2.9: Time Response using LQG Due to Initial Conditions

## 2.3 Summary

This chapter addresses the issue whether passive isolator damping is sufficient to attenuate the transmissibility of a single-degree-of-freedom system. Passive damping is needed to attenuate the transmissibility at the resonant condition; however, it amplifies the high frequency transmissibility which is not desirable.

Active control, on the other hand, can still attenuate the transmissibility at the resonant condition but it does not amplify the high frequency transmissibility. Three types of active control laws were discussed: a $\mathcal{PD}$ controller, a $\mathcal{PID}$ controller, and an LQG regulator. $\mathcal{PD}$ control was similar to the passive isolator but it does not amplify the high frequency transmissibility. The $\mathcal{PID}$ compensator is similar to $\mathcal{PD}$ control except it decreases the low frequency transmissibility. The $\mathcal{PID}$ controller will also force the system back to its initial position when subjected to a step input.

The LQG controller is much better in attenuating the system transmissibility compared to either $\mathcal{PD}$ or $\mathcal{PID}$. The LQG controller not only attenuates the transmissibility at the natural frequency but decreases the transmissibility around the natural frequency as well. The LQG controller also outperforms $\mathcal{PID}$ and $\mathcal{PD}$ control in the time response when subjected to initial conditions.

# Chapter 3

# Two-Degree-of-Freedom System

There have been thousands of publications written about vibration isolation designs. Many of these articles have looked at the mass-spring-damper system as a model [3, 14, 15] and this model has been thoroughly discussed in Chapter 2. However, it has been stated by Nelson [48] and Macinante [4] that the single-degree-of-freedom (SDOF) model is not the ideal design model for the vibration isolation problem. There are numerous limitations with the SDOF model and a two-degree-of-freedom (2DOF) model should be used in the vibration isolation design.

This chapter will discuss the SDOF model's limitations and explain the need for a higher-order model such as the 2DOF model. The analysis of the 2DOF model includes describing the transmissibility of the 2DOF model, as well as describing a novel approach in viewing the transmissibility. This novel approach significantly decreases the number of plots needed to view the transmissibility compared to conventional approaches. The final section will determine how an active controller for the 2DOF model can be used to suppress vibrations. Three control methodologies will be implemented: a proportional-plus-derivative ($\mathcal{PD}$) controller, a proportional-plus-integral-plus-derivative ($\mathcal{PID}$) controller, and a linear quadratic Gaussian (LQG) regulator.

## 3.1 Single-Degree-of-Freedom Limitations

For a SDOF model, the equipment is modeled as a rigid mass and the isolator is modeled as a massless spring and damper. This model design is adequate if the isolator is used to minimize the equipment's vibration levels from a disturbance input to the base [4]. However, this is a poor model when some sensitive part of the equipment has to be isolated from the whole equipment itself. The SDOF model would no longer be a valid assumption since the equipment could no longer be modeled as a rigid member.

Another limitation is that the foundation is considered rigid not flexible. This means that vibrations cannot be transmitted to the equipment unless the whole base vibrates as a

rigid body. Therefore, this model would be inadequate to represent a piece of equipment on a suspended flexible floor. Also, the support is assumed to be massless and this assumption is not valid if the dynamics of the foundation alters the disturbance force imparted to it.

Even with these limitations, the SDOF model can still be used in certain circumstances. If a particular part of the equipment has stiff supports, the SDOF system may then be an accurate model. The force imparted to the equipment would be equivalent to the force imparted to a particular piece of equipment with rigid supports. The massless support assumption can also be valid in certain circumstances. If the disturbance to the equipment is accurately known, this assumption would hold true. This also assumes that the disturbance has a already accounted for the dynamics of the support.

## 3.2 Two-Degree-of-Freedom Model

The limitations described in Section 3.1 are alleviated by increasing the complexity of the system, i.e., adding more degrees of freedom. For example, the rigid foundation can be replaced by a mass-spring-damper system which will represent the base flexibility. Even though this system may be a more accurate model of the actual system, the two-degree-of-freedom (2DOF) has similar limitations to the SDOF. Therefore, the question arises to how many simplifications should be made to accurately model the system; too many simplifications can create an inaccurate model but not enough simplifications increases the complexity of the model. For example, the SDOF model has three independent parameters: the equipment mass, the isolator stiffness, and isolator damping. For the 2DOF model, the mass, stiffness, and damping of the structure supporting the equipment are independent parameters; in addition, the equipment's mass and the isolator's stiffness and damping are independent parameters. The number or parameters have doubled for the 2DOF model compared to the SDOF model. After nondimensionalizing the transmissibility for the SDOF model, the lone independent variable left is the damping ratio. It will be shown for a 2DOF model that there are five independent parameters that are significant to calculate the transmissibility: the nondimensional frequency, the mass ratio, the frequency ratio, the overall damping ratio, and the damping ratio. The complexity in analyzing the transmissibility for the 2DOF model has increased significantly; however, this increase in complexity is minimal compared to the increase of accuracy in modeling the system.

### 3.2.1 Transmissibility Overview

A 2DOF system can be modeled by interconnecting two mass-spring-damper systems as shown in Figure 3.1. This model can simulate a piece of equipment on a floor where $m_1$ represents the mass of the equipment and $k_1$ and $c_1$ are the stiffness and the damping of the isolator, respectively. The flexible foundation can be modeled as a mass-spring-damper system with a mass $m_2$, stiffness $k_2$, and damping coefficient $c_2$.

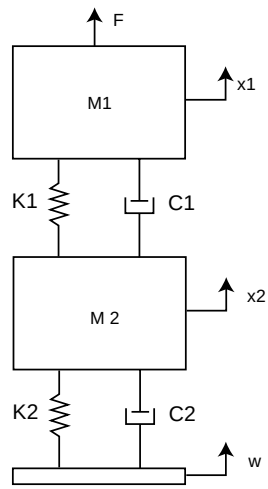


Figure 3.1: Two-Degree-of-Freedom Model

From the free body diagram in Figure 3.2, the governing equations of motion can be derived. Notice that the forces on the free body diagram are defined as

$$F_{k1} = \parallel k_1(x_1 - x_2) \parallel \qquad F_{k2} = \parallel k_2(x_2 - w) \parallel$$
$$F_{c1} = \parallel c_1(\dot{x}_1 - \dot{x}_2) \parallel \qquad F_{c2} = \parallel c_2(\dot{x}_2 - \dot{w}) \parallel .$$

By summing forces on each mass, the governing equations of motion are

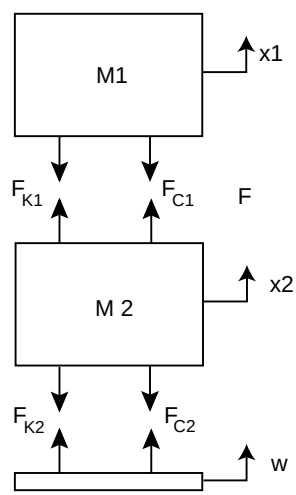


Figure 3.2: Free body Diagram of Two-Degree-of-Freedom Model

$$m_1\ddot{x}_1 + c_1\dot{x}_1 + k_1x_1 = c_1\dot{x}_2 + k_1x_2 \tag{3.1a}$$

$$m_2\ddot{x}_2 + (c_1 + c_2)\dot{x}_2 + (k_1 + k_2)x_2 = c_1\dot{x}_1 + k_1x_1 + c_2\dot{w} + k_2w \ . \tag{3.1b}$$

These equations can be rewritten as

$$\ddot{x}_1 + 2\zeta_1\omega_{n_1}\dot{x}_1 + \omega_{n_1}^2x_1 = 2\zeta_1\omega_{n_1}\dot{x}_2 + \omega_{n_1}^2x_2 \tag{3.2a}$$

$$\begin{aligned}\ddot{x}_2 + 2(\zeta_2\omega_{n_2} + \zeta_1\omega_{n_1}\rho)\dot{x}_2 + (\omega_{n_2}^2 + \rho\omega_{n_1}^2)x_2 = \\ 2\rho\zeta_1\omega_{n_1}\dot{x}_1 + \rho\omega_{n_1}^2x_1 + \omega_{n_2}^2w + 2\zeta_2\omega_{n_2}\dot{w} \ ,\end{aligned} \tag{3.2b}$$

where the following simplifications have been made

$$\begin{aligned} c_1/m_1 &= 2\zeta_1\omega_{n_1} \\ c_2/m_2 &= 2\zeta_2\omega_{n_2} \\ \omega_{n_1} &= \sqrt{k_1/m_1} \\ \omega_{n_2} &= \sqrt{k_2/m_2} \\ \rho &= m_1/m_2 \ . \end{aligned}$$

The Laplace transform of equation (3.2) leads to the transmissibility ratio

$$\frac{X_1(s)}{W(s)} = \frac{(2\zeta_2\omega_{n_2}s + \omega_{n_2}^2)\ (2\zeta_1\omega_{n_1}s + \omega_{n_1}^2)}{D} \tag{3.3}$$

where

$$D = [s^2 + (2\zeta_2\omega_{n_2} + \rho 2\zeta_1\omega_{n_1})s + (\omega_{n_2}^2 + \rho\omega_{n_1}^2)][s^2 + 2\zeta_1\omega_{n_1}s + \omega_{n_1}^2] - \rho(2\zeta_1\omega_{n_1}s + \omega_{n_1}^2)^2 \ .$$

Using the following substitutions

$$\begin{aligned} \gamma &= \frac{\omega_{n_2}}{\omega_{n_1}} = \text{frequency ratio} \\ \beta &= \frac{c_1}{c_2} = \text{viscous damping ratio} \\ S &= \frac{s}{\omega_{n_1}} = \text{nondimensional frequency} \\ \alpha &= \frac{\zeta_1}{\zeta_2} = \frac{\beta}{\gamma\rho} = \text{overall damping ratio} \end{aligned}$$

and placing them into equation (3.3), results in the following nondimensional transmissibility ratio:

$$TR = \frac{\gamma\ (2\zeta_2S + \gamma)(2\alpha\zeta_2S + 1)}{[S^2 + 2\zeta_2(\gamma + \rho\alpha)S + (\gamma^2 + \rho)][S^2 + 2\alpha\zeta_2S + 1] - \rho(2\alpha\zeta_2S + 1)^2}. \tag{3.4}$$

A comparison of the transmissibility between the SDOF system and the 2DOF system is shown in Figure 3.3. Values for the frequency ratio, overall damping ratio, mass ratio, and damping ratio were $\gamma = 1,\ \alpha = 1,\ \rho = 1,$ and $\zeta_2 = 0$, respectively. For the 2DOF model, there are two modes corresponding to each degree of freedom. At high frequencies, the SDOF transmissibility decreases at a rate of 40 dB/decade while the 2DOF transmissibility decreases at a rate of 80 dB/decade.

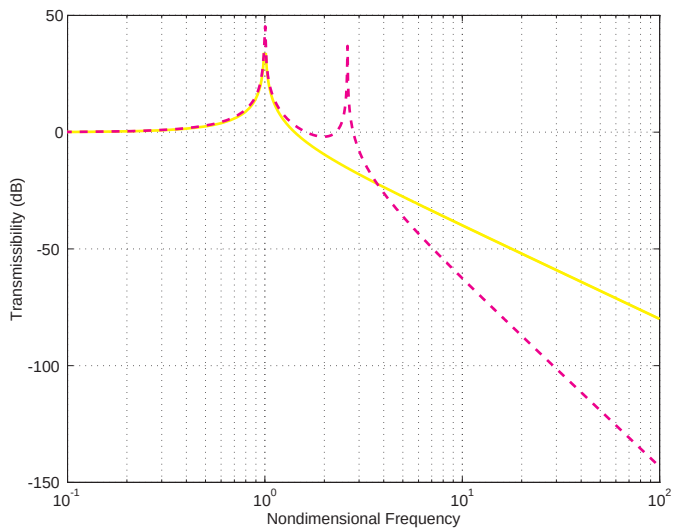


Figure 3.3: Transmissibility Comparison for SDOF model and Two-DOF Model

### 3.2.2 Two-Degree-of-Freedom Visualization

The transmissibility ratio in equation (3.4) is a function of five independent variables: the nondimensional frequency ($S$), the mass ratio ($\rho$), the frequency ratio ($\gamma$), the overall damping ratio ($\alpha$), and the damping ratio of the isolator ($\zeta_2$). Viewing the effects of each variable using a two-dimensional transmissibility plot can become very cumbersome. In Figure 3.3, for example, the transmissibility was plotted versus the nondimensional frequency while keeping the mass ratio, frequency ratio, overall damping ratio, and damping ratio fixed to certain values. For other values of these ratios, the transmissibility must be recalculated and replotted. With this type of procedure, numerous plots need to be drawn in order to see the effect of these ratios on the transmissibility.

To alleviate this problem, various authors tend to make surface plots of the transmissibility versus two nondimensional parameters while keeping the values of the other ratios fixed. The novel approach produced in the next section reduces the total number of plots to be calculated compared to other approaches. The approach is unique in that it finds the

root mean square (RMS) level of the transmissibility using four of the five nondimensional parameters. Therefore, one plot is drawn for each value of the lone independent nondimensional variable. The RMS level of the transmissibility is used because it is an overall indication of how well the system can be isolated over the frequency range of interest. The RMS levels are color coded for each value of mass, frequency, overall damping ratio, and a given damping ratio for the foundation and then the RMS levels are plotted versus these ratios. The RMS transmissibility levels are shown in two ways. First, the plots of the RMS levels are shown via planes (mass and frequency ratio varying) with constant overall damping ratios. By looking at these planes, the designer can make a judgment of which mass, frequency, and overall damping ratios would be tolerable in their design. The other plots show all values of the RMS levels in a rectangular volume for varying mass, frequency, and overall damping ratios.

#### 3.2.2.1 Visualization Techniques

The transmissibility values used in the visualization software were obtained from equation (3.4). A value for the damping ratio ($\zeta_2$) was arbitrarily chosen while the other ratios were varied. The nondimensional frequency range of interest was from 0.0001 to 100, while the mass ratio and frequency ratio were each varied from 0.01 to 100. The overall damping ratio ($\alpha$) is dependent on the value of the damping ratio ($\zeta_2$).

i. For $\zeta_2 = 0.0001$, the overall damping ratio ranged from 0.0001 to 10,000

ii. For $\zeta_2 = 0.001$, the overall damping ratio ranged from 0.001 to 1,000

iii. For $\zeta_2 = 0.01$, the overall damping ratio ranged from 0.01 to 100

For each of these ratios, the RMS level of the transmissibility was obtained by the following equation [6]:

$$RMS = \sqrt{\int_w |G(w)|^2 S_f(w)\ \mathrm{d}w}\ , \tag{3.5}$$

where $S_f(\omega) = 1$. The RMS level of the transmissibility for the 2DOF problem is

$$\begin{aligned} RMS_{tdof} &= \sqrt{\int_S \left| \frac{\gamma\ (2\zeta_2 S + \gamma)(2\alpha\zeta_2 S + 1)}{\mathrm{D(S)}} \right|^2\ \mathrm{d}S} \\ \mathrm{D(S)} &= [S^2 + 2\zeta_2(\gamma + \rho\alpha)S + (\gamma^2 + \rho)][S^2 + 2\alpha\zeta_2 S + 1] - \rho(2\alpha\zeta_2 S + 1)^2\ . \end{aligned} \tag{3.6}$$

The RMS level of the transmissibility ($RMS_{tdof}$) was then scaled with respect to a 2DOF system when mass 1 is rigidly attached to mass 2 as shown in Figure 3.4. It is assumed that

the stiffness and damping ratio of this new system are equivalent to the stiffness $k_2$ and the damping ratio $\zeta_2$ of the 2DOF foundation, respectively. With this scaling, a designer can determine whether it would be better to attach the isolated equipment in a rigid manner or use some sort of elastic damping connection between the masses.

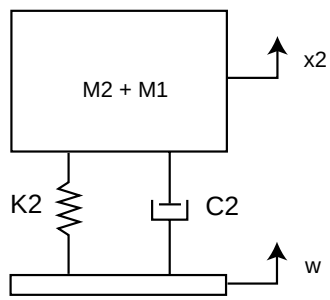


Figure 3.4: 2DOF System with Mass 1 Rigidly Attached to Mass 2

The transmissibility ratio for this new system is similar to equation (2.3), except $w_n^2 = w_{n_2}^2(\frac{1}{1+\rho})$, $\zeta = \zeta_2$, and $S = s/w_{n_1}$.

$$TR = \frac{2\zeta_2\gamma\sqrt{\frac{1}{1+\rho}}S + \frac{1}{1+\rho}}{\gamma^2 S^2 + 2\zeta_2\gamma\sqrt{\frac{1}{1+\rho}}S + \frac{1}{1+\rho}} \tag{3.7}$$

The RMS level for this new SDOF system is obtained by replacing $G(w)$ in equation (3.5) with equation (3.7):

$$RMS_{sdof} = \sqrt{\int_S \left| \frac{2\zeta_2\gamma\sqrt{\frac{1}{1+\rho}}S + \frac{1}{1+\rho}}{\gamma^2 S^2 + 2\zeta_2\gamma\sqrt{\frac{1}{1+\rho}}S + \frac{1}{1+\rho}} \right|^2 \mathrm{d}S} \ . \tag{3.8}$$

The new scaled RMS transmissibility will be

$$RMS_{scaled} = \frac{RMS_{tdof}}{RMS_{sdof}} \ . \tag{3.9}$$

The scaled transmissibility ratio is then formatted for input to the Application Visualization System (AVS) [49] software where the data will be plotted. This format includes finding the RMS levels in decibels before they are placed in the data file. The AVS software plotted the RMS levels as colors for the following nondimensional parameters: mass ratio, frequency ratio, and overall damping ratio. The lowest level of the transmissibility is assigned the color blue (white for greyscale output). The highest RMS transmissibility level

was assigned the color red (black for greyscale output). For intermediate RMS values, a colormap generated colors between blue and red for the colored output and between black and white for the greyscale output.

#### 3.2.2.2 2DOF Visualization via Sliced Planes and Volumes

The scaled transmissibility for the 2DOF system was obtained for three different values of the damping ratio ($\zeta_2$) : 0.01, 0.001, and 0.0001. Two plots were then formed for each value of the damping ratio. One plot shows the RMS scaled transmissibility data in sliced planes. The planes, mass ratio $\rho$ versus frequency ratio $\gamma$, are plotted versus different values of the overall damping ratio $\alpha$. The second plot shows the data in a rectangular volume format. The face shown in these plots is a section of the mass ratio versus the frequency ratio at the lowest overall damping ratio. Note the mass ratio and overall damping ratio increase from right to left and the frequency ratio increase from bottom to top.

As stated earlier, the data were converted to decibels and the critical value for the scaled transmissibility occurs at zero decibels. At this point, the transmissibility of the 2DOF system ($RMS_{sdof}$) with a rigid connection between the two masses is equivalent to the 2DOF system ($RMS_{tdof}$) for some particular value of the isolator stiffness and damping. Therefore, from a designer's viewpoint, a rigid connection would be a better design anytime the scaled transmissibility is greater than zero decibels. An elastically damped connection between the two masses would be a better design anytime the scaled transmissibility is less than zero decibels.

Plots for $\zeta_2 = 0.01$ are shown in Figure 3.7 and Figure 3.8. The best design points for this system are at low frequencies and mass ratios for an isolated system with little damping. Actually, most of the mass ratios where the frequency ratio is less than one is a good design area. This is expected since at low frequency ratios the isolated mass is not significantly influenced by the other mass. However, there are some bands in this area (high mass ratios) that are not good design points and should not be taken into consideration. Designs can still accomplished at these high mass ratios but with caution.

Similar results were obtained for $\zeta_2 = 0.001$ (Figure 3.7 and Figure 3.8) and for $\zeta_2 = 0.0001$ (Figure 3.9 and Figure 3.10). Unlike the figures for $\zeta_2 = 0.01$, the possible (good) design points has been reduced. However, designs can still be accomplished in similar regions for the 2DOF system when $\zeta_2 = 0.01$.

### 3.2.3 Active Control

Section 2.2 indicates why some sort of active control should be used in a vibration isolation design for a single-degree-of-freedom model (SDOF). Therefore, a comparison between active and passive isolators will be discussed for the two-degree-of-freedom (2DOF) model as well. Passive damping will be incorporated in the isolator by a viscous damper

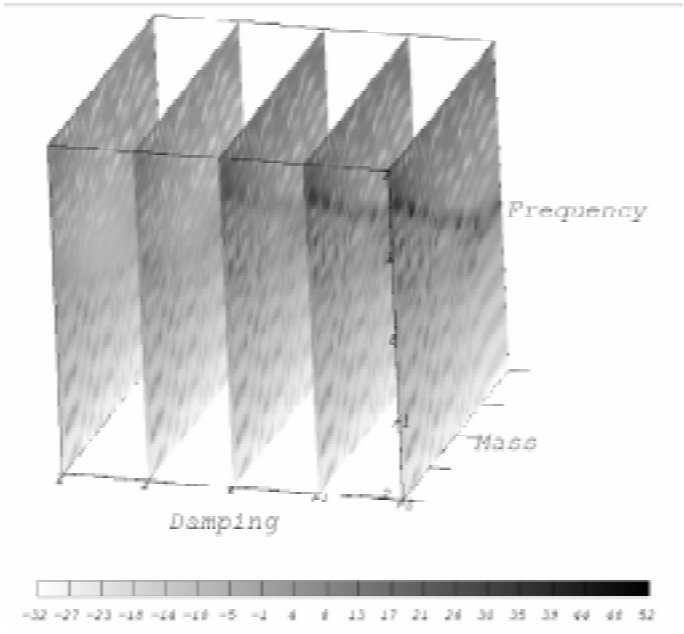


Figure 3.5: RMS Transmissibility for $\zeta_2 = .01$

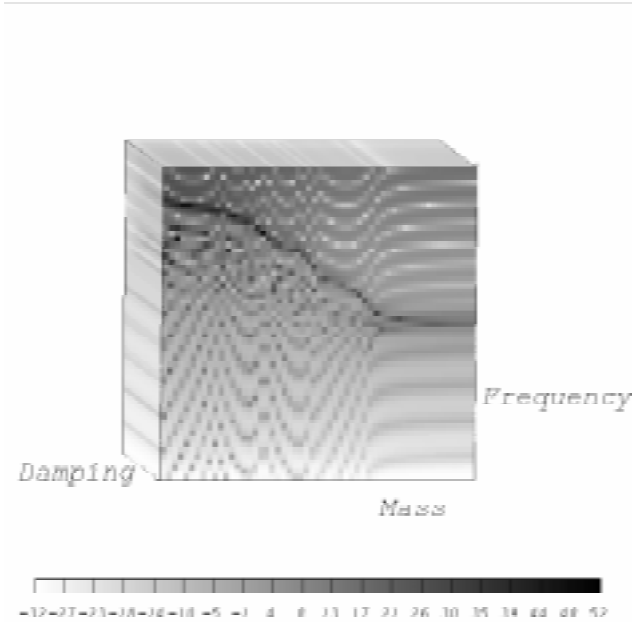


Figure 3.6: RMS Transmissibility for $\zeta_2 = .01$

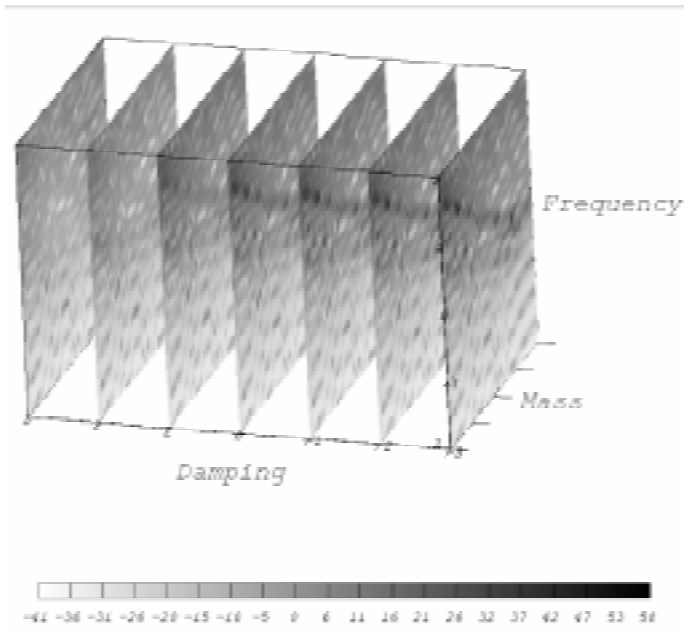


Figure 3.7: RMS Transmissibility for $\zeta_2 = .001$

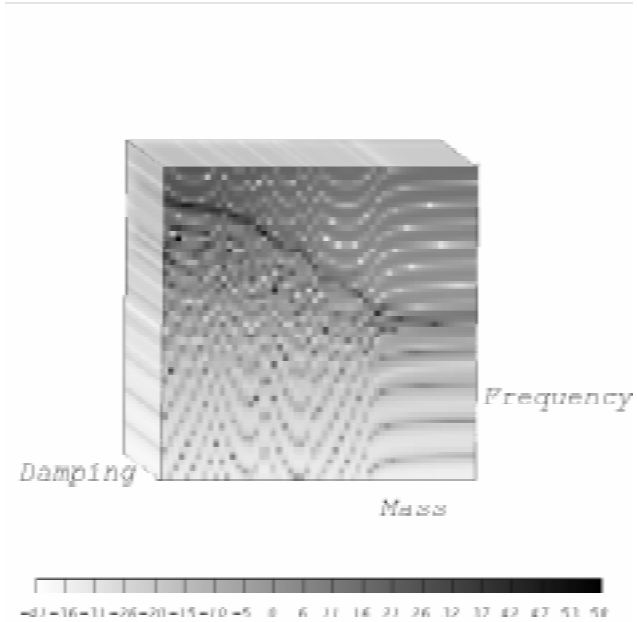


Figure 3.8: RMS Transmissibility for $\zeta_2 = .001$

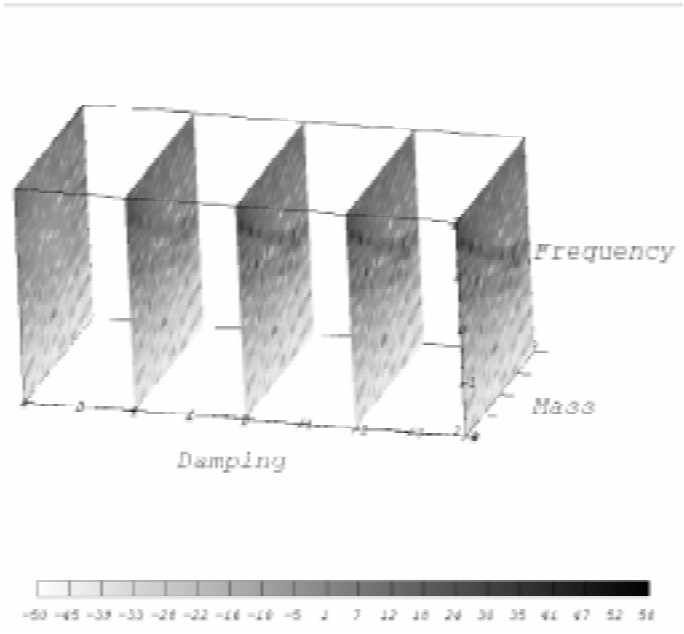


Figure 3.9: RMS Transmissibility for $\zeta_2 = .0001$

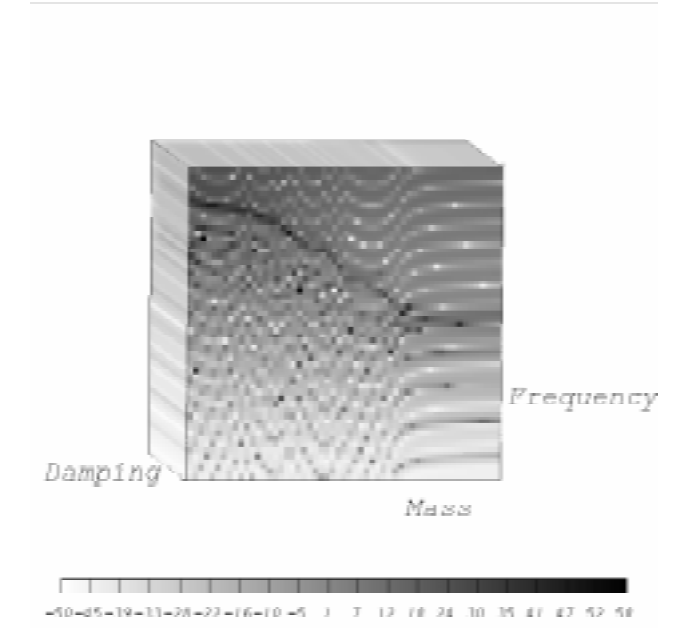


Figure 3.10: RMS Transmissibility for $\zeta_2 = .0001$

and active damping will be accomplished by an actuator placed between the equipment and the base. The active isolator or actuator will implement three different control strategies: a proportional-plus-derivative ($\mathcal{PD}$) controller, a proportional-plus-integral-plus-derivative ($\mathcal{PID}$) controller, and a linear quadratic Gaussian (LQG) regulator. Performance of each controller will be measured by each system's frequency response and their time responses due to a step input on the base.

#### 3.2.3.1 Active and Passive Damping Comparison for the 2DOF Model

For the SDOF model, when viscous damping is used to model the isolator damping, the transmissibility at high frequencies is increased compared to an undamped system. A similar situation occurs for the 2DOF model as shown in Figure 3.11. When the isolator includes passive damping, the first mode is attenuated but the transmissibility at frequencies greater than the first mode is increased with respect to an undamped system. This high frequency transmissibility amplification does not occur for a system using an active isolator. The active isolator, in this instance, will use velocity feedback from the equipment as the control law and the transmissibility for this system is shown in Figure 3.11. The first mode is damped similar to the system using a damped passive isolator. Unlike the passive isolator, the system using an active isolator does not increase the transmissibility in the higher frequency ranges. Actually, after the first mode, the active system's transmissibility is equivalent to a passive system with no isolator damping. Notice that the active isolator does not attenuate or damp the second mode of the system.

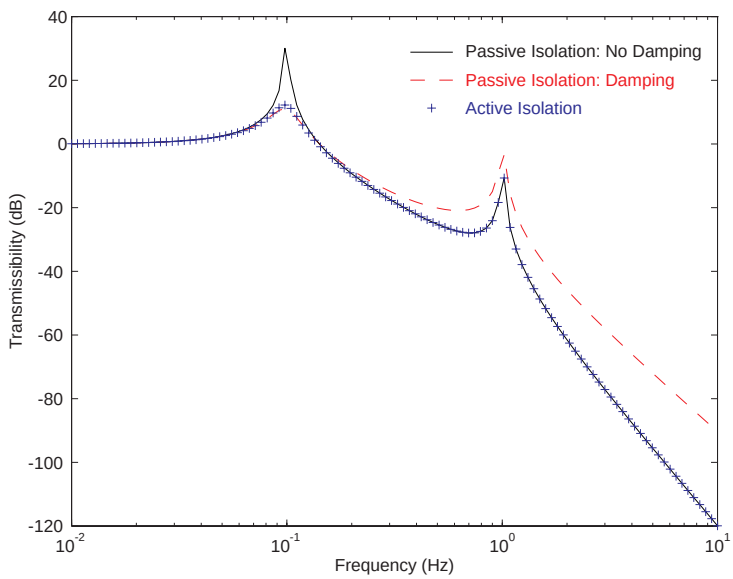


Figure 3.11: Comparison of Active and Passive Damping for a 2DOF Model

### 3.2.4 $\mathcal{PD}$ and $\mathcal{PID}$ Control

This section considers two classical control techniques: the proportional-plus-derivative ($\mathcal{PD}$) controller, and the proportional-plus-integral-plus-derivative ($\mathcal{PID}$) controller. The form of these controllers in terms of a transfer function is

$$D(s) = K_p + K_d s + K_i/s \ , \tag{3.10}$$

where $K_p$, $K_d$, and $K_i$ are the proportional, derivative and integral gains, respectively. The implementation of this controller is similar to the one described in Section 2.2 with the transfer function of the plant $G(s)$ given by equation (3.3). The plant is assumed to have no damping and the first two natural frequencies occur at $\omega_{n_1} = 0.1$ Hz and $\omega_{n_2} = 1$ Hz. It is also assumed that the mass ratio is unity and the response of the equipment will be used as the isolation criteria.

The proportional gain was set to a very small value since this term tends to change the natural frequency of the system. The gains for the derivative and integral gain were chosen so that good transient responses would occur, i.e., adequate rise times and settling times. The frequency responses for no control, $\mathcal{PD}$ control and $\mathcal{PID}$ control are shown in Figure 3.12. As seen from this figure, $\mathcal{PD}$ control damps the first mode but has no effect on the second mode. $\mathcal{PID}$ control is very similar to $\mathcal{PD}$ control except that $\mathcal{PID}$ control will attenuate the low frequency transmissibility.

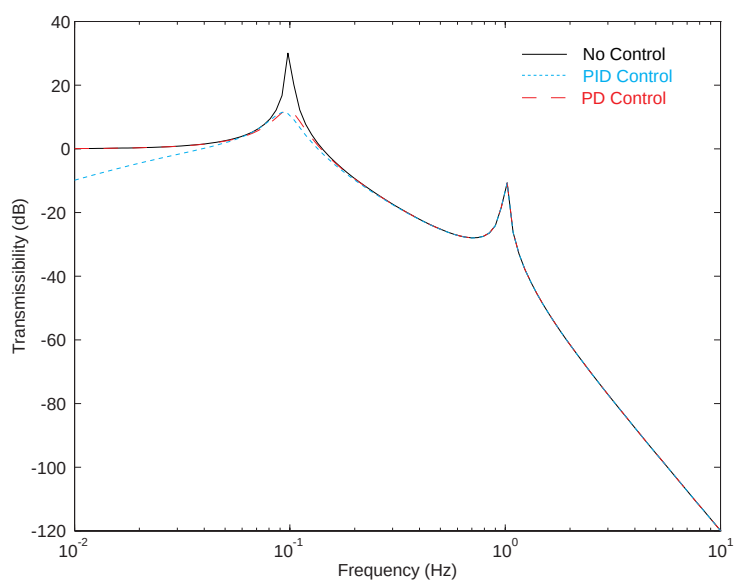


Figure 3.12: Frequency Response of 2DOF Model using $\mathcal{PID}$ and $\mathcal{PD}$ Control

The time responses for an undamped system and an active system using $\mathcal{PD}$ and $\mathcal{PID}$ control are shown in Figure 3.13. The response of the system is measured by the displacement of the equipment due to a step input at the base. For the undamped system,

the equipment will oscillate indefinitely, neither increasing or decreasing. An active isolator using $\mathcal{PD}$ control can add damping to the system as shown in Figure 3.13. After a specific amount of time, the system response using $\mathcal{PD}$ control will eventually settle to a steady-state solution. $\mathcal{PID}$ control is very similar to $\mathcal{PD}$ control; it adds damping to the system and the displacement eventually settles to a steady-state solution. The main difference between the two is that $\mathcal{PID}$ control will force the system to settle around its initial position. This is a salient feature of $\mathcal{PID}$ control; it is able to cancel any constant disturbance imparted to the system.

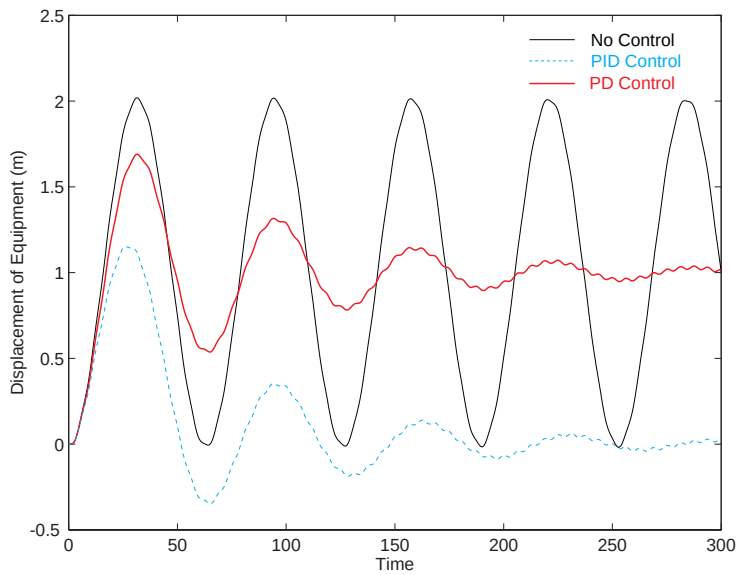


Figure 3.13: Time Response of 2DOF Model using $\mathcal{PID}$ and $\mathcal{PD}$ Control

#### 3.2.4.1 Linear Quadratic Gaussian Control

A detailed discussion of the LQG controller is not done since a thorough discussion has been made in Chapter 2. The concepts used in Chapter 2 are exactly the same used here except for the differences in the state-space description of the isolator model. It is assumed that every state of the system is not directly measurable; therefore, a Kalman-Bucy estimator is used. It is also assumed that the disturbance is known and can be modeled with a shaping filter.

The LQG controller is implemented in the state space; therefore, the 2DOF isolation system has to be defined in the state space. Assuming that any damping in the isolator will be solely due to the control implementation, the state-space representation of the 2DOF

model is

$$\begin{aligned} \dot{\vec{\mathbf{z}}} &= \underline{\underline{\mathbf{A}}}\vec{\mathbf{z}} + \vec{\mathbf{B}}u + \vec{\mathbf{F}}w \\ y &= \vec{\mathbf{C}}\vec{\mathbf{z}} \ , \end{aligned} \tag{3.11}$$

where

$$\underline{\underline{\mathbf{A}}} = \begin{bmatrix} 0 & 1 & 0 & 0 \\ -\omega_{n_1}^2 & 0 & \omega_{n_1}^2 & 0 \\ 0 & 0 & 0 & 1 \\ \rho\omega_{n_1}^2 & 0 & -\omega_{n_2}^2 - \rho\omega_{n_1}^2 & 0 \end{bmatrix}, \quad \vec{\mathbf{B}} = \begin{Bmatrix} 0 \\ 1 \\ 0 \\ -\rho \end{Bmatrix}, \quad \vec{\mathbf{F}} = \begin{Bmatrix} 0 \\ 0 \\ 0 \\ \omega_{n_2}^2 \end{Bmatrix}$$

$$\vec{\mathbf{C}} = \begin{Bmatrix} 1 & 0 & 0 & 0 \end{Bmatrix}^T, \quad \vec{\mathbf{z}} = \begin{Bmatrix} \vec{\mathbf{x}}_1 \\ \dot{\vec{\mathbf{x}}}_1 \\ \vec{\mathbf{x}}_2 \\ \dot{\vec{\mathbf{x}}}_2 \end{Bmatrix}.$$

Note that the input $u$ is $F_{act}/m_1$ where $F_{act}$ is the force due to the actuator and $m_1$ is the mass of the equipment.

The frequency responses for the undamped open-loop system and the closed-loop system using an LQG regulator are shown in Figure 3.14. Similar to the SDOF model, there is significant attenuation at the first mode shown by the formation of a notch. There is also some attenuation at frequencies above and below the first mode as well but there is no attenuation at the second mode. The performance of the LQG controller can be increased by adjusting the performance index of the controller. For this system, the performance index penalized the position of the equipment much heavier than the velocity of the equipment.

Another indicator to determine how well the LQG controller is performing is to look at the time responses. The time responses for the undamped system and the controlled system are shown in Figure 3.15. For the undamped system, the response of the equipment will be an indefinite oscillation in which the equipment displacement will never settle to a steady-state solution. On the other hand, when LQG is applied to the system, the response eventually settles to a steady-state solution. The LQG controller has a similar response as the $\mathcal{PD}$ controller shown in Figure 3.13 but the LQG controller can have a similar response as the $\mathcal{PID}$ controller as well. This can be accomplished by adjusting the performance index and the penalties for the LQG controller.

## 3.3 Summary

This chapter analyzes the two-degree-of-freedom (2DOF) system as a model for the vibration isolation design. The transmissibility for the 2DOF system is determined and a

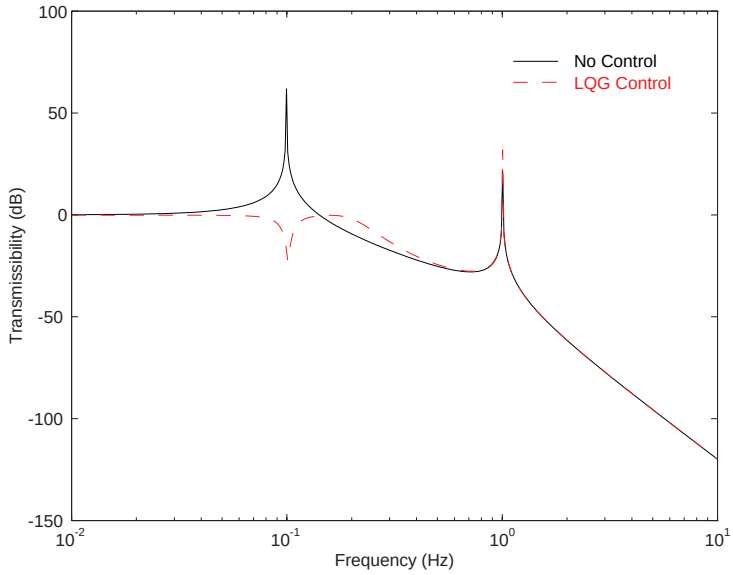


Figure 3.14: Frequency Response of 2DOF Model using LQG Control

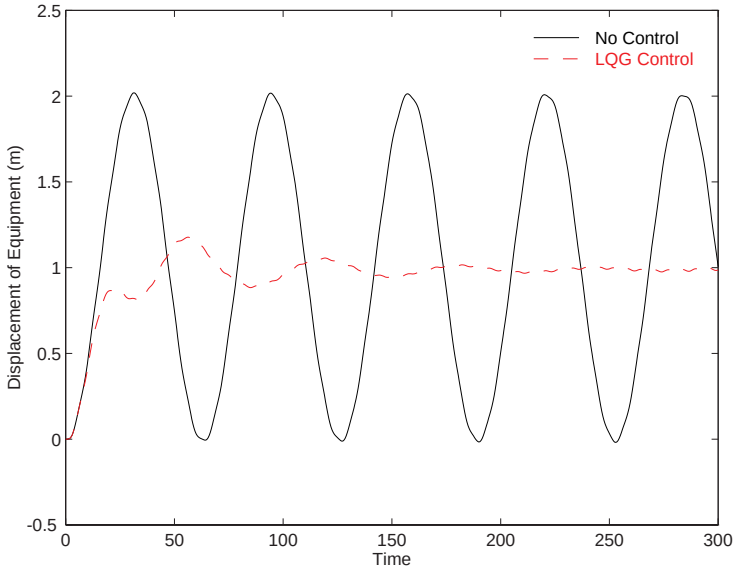


Figure 3.15: Time Response of 2DOF Model using LQG Control

comparison is made with respect to the SDOF model. Since the transmissibility is more complex to analyze in the 2DOF model, a novel approach is used to reduce the complexity of this analysis. This approach significantly reduces the number of plots needed to fully understand the 2DOF model. Similar to the SDOF system, it was shown that passive damping will decrease the first mode but increase the high frequency transmissibility of the system compared to an undamped system.

It was also shown that an active isolator does not increase the high frequency transmissibility; however, it does damp or attenuate the first mode. Therefore, the use of active isolation on the 2DOF model is fully discussed in this chapter as well. Three different control methodologies were discussed: a proportional-plus-derivative ($\mathcal{PD}$) controller, a proportional-plus-integral-plus-derivative ($\mathcal{PID}$) controller, and a linear quadratic Gaussian (LQG) regulator. All three were shown to be effective in attenuating the transmissibility at the first mode of the system. A comparison between each controller was made and it was discussed how the performance of the LQG controller can be modified to mimic either the $\mathcal{PD}$ or the $\mathcal{PID}$ performance by adjusting the performance index.

# Chapter 4

# Modeling of Distributed Systems

There are many methods that can model distributed systems using approximate methods such as the finite element method, impedance methods, mobility methods and the assumed modes method. However, Yang developed a transfer function synthesis (TFS) method that can analytically analyze any complex one-dimensional system [39]. The complex system can consist of distributed systems and lumped systems with any type of constraints. The constraints can take on the form of boundary conditions, point constraints, and distributed constraints.

For many of these approximate methods, system flexibility can be modeled with eigenvalues and eigenfunctions. Note that the eigensolutions are heavily dependent on the system boundary conditions. In contrast, Yang's method uses no knowledge of the eigensolutions. In fact, the TFS method is used to find the eigensolutions of the complex system for arbitrary boundary conditions. The frequency response functions obtained from the TFS method can also be used to predict system stability.

The first three sections in this chapter are a derivation of the TFS method. The fourth section discusses how the TFS method is modified when multiple distributed parameters are present such as longitudinal and transverse vibrations. The fifth section gives a brief overview how the TFS method can be used to find eigenvalues, eigenfunctions, frequency response functions and time responses. Section six analyzes some common lumped parameter systems used in vibration isolation designs and discusses how their inclusion into the isolator design will affect the TFS method. Section seven discusses the use of active controls such as a proportional-plus-integral-plus-derivative ($\mathcal{PID}$) controller, a positive position feedback (PPF) controller, and a linear quadratic Gaussian (LQG) regulator. The final section verifies the TFS method with a simple cantilever beam experiment.

## 4.1 Transfer Function Synthesis

An n$^{\text{th}}$-order, linear distributed parameter system response $W(x,t)$ can be described by the following equation which is nondimensional in the spatial variable.

$$\left\{A\frac{\partial^2}{\partial t^2}+B\frac{\partial}{\partial t}+C\right\}W(x,t)=f(x,t), \qquad x\in(0,1), \qquad t>0 \tag{4.1}$$

The system has inhomogeneous boundary conditions represented by

$$M_jW(x,t)|_{x=0}+N_jW(x,t)|_{x=1}=\gamma_j(t), \qquad t\geq 0, \qquad j=1,2,\ldots,n\ . \tag{4.2}$$

$A$, $B$, and $C$ in equation (4.1) are spatial differential operators that are equal to

$$A=\sum_{k=0}^{n}a_k\frac{\partial^k}{\partial x^k}\ , \qquad B=\sum_{k=0}^{n}b_k\frac{\partial^k}{\partial x^k}\ , \qquad C=\sum_{k=0}^{n}c_k\frac{\partial^k}{\partial x^k}\ , \tag{4.3}$$

where $a_k$, $b_k$, $c_k$ are constants which can represent inertia, damping, distributed constraints, coriolis acceleration, axial loads, mass transport, centrifugal forces, and circulatory effects. $M_j$ and $N_j$ are linear, temporal, spatial, differential operators; $\gamma_j(t)$ are known functions representing the external disturbances at the boundaries, and $f(x,t)$ is the external disturbance. The initial conditions of the distributed parameter system are

$$W(x,t)|_{t=0}=u_o(x) \qquad \frac{\partial W(x,t)}{\partial t}|_{t=0}=v_o(x), \qquad x\in(0,1)\ . \tag{4.4}$$

The Laplace transform of equation (4.1) with respect to time is

$$\left\{s^2A+sB+C\right\}\overline{W}(x,s)=\overline{f}(x,s)+(sA+B)u_o(x)+Av_o(x)=\overline{f}_{el}(x,s)\ , \tag{4.5}$$

where $\overline{()}$ represents a Laplace transformation. The boundary conditions in the Laplace domain are

$$\overline{M}_j\overline{W}(x,s)|_{x=0}+\overline{N}_j\overline{W}(x,s)|_{x=1}=\overline{\gamma}(s)=\overline{\gamma}_j(s)+\overline{\gamma}_{Ij}(s) \qquad j=1,2,\ldots,n\ . \tag{4.6}$$

$\overline{\gamma}_{Ij}$ is a polynomial in $s$ representing the initial conditions at the boundaries. Equation (4.5) can be recast into a state-space form as

$$\frac{\partial}{\partial x}\vec{\boldsymbol{\eta}}(x,s)=\underline{\underline{\mathbf{F}}}(s)\vec{\boldsymbol{\eta}}(x,s)+\vec{\mathbf{f}}(x,s) \tag{4.7a}$$

$$\underline{\underline{\mathbf{M}}}(s)\vec{\boldsymbol{\eta}}(0,s)+\underline{\underline{\mathbf{N}}}(s)\vec{\boldsymbol{\eta}}(1,s)=\vec{\boldsymbol{\gamma}}(s)\ , \tag{4.7b}$$

where

$$\vec{\boldsymbol{\eta}}(x,s) = \begin{Bmatrix} \overline{W}(x,s) \\ \frac{\partial \overline{W}(x,s)}{\partial x} \\ \vdots \\ \frac{\partial^{n-1}\overline{W}(x,s)}{\partial x^{n-1}} \end{Bmatrix}, \qquad \vec{\mathbf{f}}(x,s) = \begin{Bmatrix} 0 \\ 0 \\ \vdots \\ \frac{\overline{f}_{el}(x,s)}{a_n s^2 + b_n s + c_n} \end{Bmatrix}, \qquad \vec{\boldsymbol{\gamma}}(s) = \begin{Bmatrix} \overline{\gamma}_1(s) \\ \overline{\gamma}_2(s) \\ \vdots \\ \overline{\gamma}_n(s) \end{Bmatrix} .$$

$\underline{\underline{\mathbf{F}}}(s)$ is defined as

$$\underline{\underline{\mathbf{F}}}(s) = \begin{bmatrix} 0 & 1 & & & \\ 0 & 0 & 1 & & \\ & \ddots & \ddots & \ddots & \\ & & & 0 & 1 \\ d_o(s) & d_1(s) & \cdots & \cdots & d_k(s) \end{bmatrix} , \tag{4.8}$$

and the coefficients of the matrix $\underline{\underline{\mathbf{F}}}(s)$ are

$$d_k(s) = -\frac{a_k s^2 + b_k s + c_k}{a_n s^2 + b_n s + c_n}, \qquad k = 0, 1, \ldots, n-1 \ . \tag{4.9}$$

The solution to equation (4.7a) given the boundary conditions in equation (4.7b) are

$$\vec{\boldsymbol{\eta}}(x,s) = \int_0^1 \underline{\underline{\mathbf{G}}}(x,\xi,s)\vec{\mathbf{f}}(\xi,s)\mathrm{d}\xi + \underline{\underline{\mathbf{H}}}(x,s)\vec{\boldsymbol{\gamma}}(s), \qquad x \in (0,1) \tag{4.10}$$

where

$$\underline{\underline{\mathbf{G}}}(x,\xi,s) = \begin{cases} e^{\underline{\underline{\mathbf{F}}}(s)x}\left[\underline{\underline{\mathbf{M}}}(s) + \underline{\underline{\mathbf{N}}}(s)e^{\underline{\underline{\mathbf{F}}}(s)}\right]^{-1}\underline{\underline{\mathbf{M}}}(s)e^{-\underline{\underline{\mathbf{F}}}(s)\xi} & \xi < x \\ -e^{\underline{\underline{\mathbf{F}}}(s)x}\left[\underline{\underline{\mathbf{M}}}(s) + \underline{\underline{\mathbf{N}}}(s)e^{\underline{\underline{\mathbf{F}}}(s)}\right]^{-1}\underline{\underline{\mathbf{N}}}(s)e^{\underline{\underline{\mathbf{F}}}(s)(1-\xi)} & \xi > x \end{cases} \tag{4.11a}$$

$$\underline{\underline{\mathbf{H}}}(x,s) = e^{\underline{\underline{\mathbf{F}}}(s)x}\left[\underline{\underline{\mathbf{M}}}(s) + \underline{\underline{\mathbf{N}}}(s)e^{\underline{\underline{\mathbf{F}}}(s)}\right]^{-1}. \tag{4.11b}$$

## 4.2 Modification to Transfer Function Synthesis

The transfer function synthesis is based on the assumption that the spatial operator for the beam is nondimensional. That is, the position on the beam ranges between the values of zero and one not between zero and the length of the beam. Therefore, to use this method for a physical system, the governing equations of a beam in transverse or axial vibrations need to be recast into nondimensional form. This can be accomplished by dividing the spatial variable $x$ by the length. The nondimensional spatial variable and its derivatives are

$$x^\dagger = x/L, \qquad \frac{1}{L^n}\frac{\partial^n}{\partial x^{\dagger n}} = \frac{\partial^n}{\partial x^n} \ .$$

The system in the state space is

$$\frac{\partial \vec{\boldsymbol{\eta}}^{\dagger}(x^{\dagger}, s)}{\partial x^{\dagger}} = \underline{\underline{\mathbf{F}}}^{\dagger}(s)\vec{\boldsymbol{\eta}}(x^{\dagger}, s) + \vec{\mathbf{f}}^{\dagger}(x^{\dagger}, s) \ ,$$

where $\underline{\underline{\mathbf{F}}}^{\dagger}(s) = L\underline{\underline{\mathbf{F}}}(s)$, $\vec{\mathbf{f}}^{\dagger}(x^{\dagger}, s) = L\vec{\mathbf{f}}(x, s)$ and

$$\vec{\boldsymbol{\eta}}^{\dagger}(x^{\dagger}, s) = \left\{ \overline{W}(x^{\dagger}, s) \quad 1/L\frac{\partial \overline{W}(x^{\dagger}, s)}{\partial x^{\dagger}} \quad \ldots \quad 1/L^{n-1}\frac{\partial \overline{W}(x^{\dagger}, s)}{\partial x^{\dagger}} \right\}^{T} .$$

In the next sections, the $()^{\dagger}$ and $\overline{()}$ will be dropped from all variables.

## 4.3 Transfer Function Synthesis for Complex System

The procedure outlined in Section 4.1 was formulated only for a single distributed system. However, it can be used for a complex distributed system by dividing the complex distributed system into a smaller number of single distributed systems, i.e., subsystems. The overall system response can be assembled from the response of each individual subsystem. This is accomplished by imposing force balance as well as displacement compatibility at the nodes where the subsystems are interconnected.

### 4.3.1 Subsystem Response

For each subsystem, define the displacement and strain vectors as

$$\vec{\boldsymbol{\alpha}}(x, s) = \begin{Bmatrix} W(x, s) \\ \frac{\partial W(x,s)}{\partial x} \\ \vdots \\ \frac{\partial^{n/2-1} W(x,s)}{\partial x^{n/2-1}} \end{Bmatrix} \qquad \vec{\boldsymbol{\epsilon}}(x, s) = \begin{Bmatrix} \frac{\partial^{n/2} W(x,s)}{\partial x^{n/2}} \\ \frac{\partial^{n/2+1} W(x,s)}{\partial x^{n/2+1}} \\ \vdots \\ \frac{\partial^{n-1} W(x,s)}{\partial x^{n-1}} \end{Bmatrix} , \tag{4.12}$$

where $\vec{\boldsymbol{\eta}} = \left\{\vec{\boldsymbol{\alpha}}^{T}(x, s) \ \vec{\boldsymbol{\epsilon}}^{T}(x, s)\right\}^{T}$. The internal force vector $\vec{\mathbf{P}}(x, s)$ is described by

$$\vec{\mathbf{P}}(x, s) = \underline{\underline{\mathbf{E}}}(s)\vec{\boldsymbol{\epsilon}}(x, s) \ , \tag{4.13}$$

where $\underline{\underline{\mathbf{E}}}(s)$ is a constitutive matrix. If $\vec{\boldsymbol{\gamma}}(s)$, $\underline{\underline{\mathbf{M}}}(s)$, and $\underline{\underline{\mathbf{N}}}(s)$ are defined as

$$\vec{\boldsymbol{\gamma}}(s) = \begin{Bmatrix} \vec{\boldsymbol{\alpha}}_0(s) = \vec{\boldsymbol{\alpha}}(0, s) \\ \vec{\boldsymbol{\alpha}}_1(s) = \vec{\boldsymbol{\alpha}}(1, s) \end{Bmatrix}, \qquad \underline{\underline{\mathbf{M}}}(s) = \begin{bmatrix} \underline{\underline{\mathbf{I}}}_{n/2} & \underline{\underline{\mathbf{0}}} \\ \underline{\underline{\mathbf{0}}} & \underline{\underline{\mathbf{0}}} \end{bmatrix}, \qquad \underline{\underline{\mathbf{N}}}(s) = \begin{bmatrix} \underline{\underline{\mathbf{0}}} & \underline{\underline{\mathbf{0}}} \\ \underline{\underline{\mathbf{I}}}_{n/2} & \underline{\underline{\mathbf{0}}} \end{bmatrix} ,$$

the solution of each subsystem becomes

$$\vec{\boldsymbol{\alpha}}(x,s) = \int_0^1 \underline{\underline{\mathbf{G}}}_{\alpha}(x,\xi,s)\vec{\mathbf{f}}(\xi,s)\mathrm{d}\xi + \underline{\underline{\mathbf{H}}}_{\alpha 0}(x,s)\vec{\boldsymbol{\alpha}}_0(s) + \underline{\underline{\mathbf{H}}}_{\alpha 1}(x,s)\vec{\boldsymbol{\alpha}}_1(s) \tag{4.14a}$$

$$\vec{\mathbf{P}}(x,s) = \underline{\underline{\mathbf{E}}}(s)\left\{\int_0^1 \underline{\underline{\mathbf{G}}}_{\epsilon}(x,\xi,s)\vec{\mathbf{f}}(\xi,s)\mathrm{d}\xi + \underline{\underline{\mathbf{H}}}_{\epsilon 0}(x,s)\vec{\boldsymbol{\alpha}}_0(s) + \underline{\underline{\mathbf{H}}}_{\epsilon 1}(x,s)\vec{\boldsymbol{\alpha}}_1(s)\right\} . \tag{4.14b}$$

The values of $\underline{\underline{\mathbf{G}}}_{\alpha}$, $\underline{\underline{\mathbf{G}}}_{\epsilon}$, $\underline{\underline{\mathbf{H}}}_{\alpha 0}$, $\underline{\underline{\mathbf{H}}}_{\alpha 1}$, $\underline{\underline{\mathbf{H}}}_{\epsilon 0}$, and $\underline{\underline{\mathbf{H}}}_{\epsilon 1}$ are partitioned matrices calculated from equation (4.11).

### 4.3.2 Subsystem Assembly

Suppose there are $N$ nodes where $Z$ subsystems are interconnected and define the global displacements at each node by $\vec{\mathbf{u}}_k$. The global nodal force of each subsystem is designated by $\vec{\mathbf{Q}}_k^{\delta}$, where $k$ is a particular node and $\delta$ is a given subsystem. At each node there can be constraint forces and external disturbances designated by $\underline{\underline{\mathbf{C}}}_k$ and $\vec{\mathbf{p}}_k$, respectively. The constraint matrix $\underline{\underline{\mathbf{C}}}_k$ is valid only for connection of lumped systems or distributed systems at a single point. The force balance of the $Z$ subsystems at node $l$ is

$$\vec{\mathbf{Q}}_l^A(s) + \vec{\mathbf{Q}}_l^B(s) + \vec{\mathbf{Q}}_l^C(s) + \cdots + \vec{\mathbf{Q}}_l^Z(s) - \underline{\underline{\mathbf{C}}}_l(s)\vec{\mathbf{u}}_l(s) + \vec{\mathbf{p}}_l(s) = \vec{\mathbf{0}} . \tag{4.15}$$

Note that subsystem $\delta$ exerts a force $-\vec{\mathbf{P}}^{\delta}(x_l,s)$ at node $l$; therefore, the subsystem global force at node $l$ is

$$\vec{\mathbf{Q}}_l^{\delta}(s) = -\underline{\underline{\mathbf{R}}}^{\delta}\vec{\mathbf{P}}^{\delta}(x_l,s) , \tag{4.16}$$

where $\underline{\underline{\mathbf{R}}}^{\delta}$ is the transformation matrix of the local forces to global forces for subsystem $\delta$. However, the local forces $\vec{\mathbf{P}}^{\delta}(x_l,s)$ are defined in local coordinates and these coordinates need to be transformed as well. The transformations of the local displacements to global displacements are accomplished with the transformation matrix $\underline{\underline{\mathbf{S}}}^{\delta}$ and $\underline{\underline{\mathbf{T}}}^{\delta}$ which are defined at either end of subsystem $\delta$.

$$\vec{\boldsymbol{\alpha}}^{\delta}(x_l,s) = \underline{\underline{\mathbf{S}}}^{\delta}\vec{\mathbf{u}}_l(s) \qquad \vec{\boldsymbol{\alpha}}^{\delta}(x_i,s) = \underline{\underline{\mathbf{T}}}^{\delta}\vec{\mathbf{u}}_i(s) \tag{4.17}$$

Placing equation (4.14b) and equation (4.17) into equation (4.16) gives the global force in terms of global coordinates.

$$\vec{\mathbf{Q}}_l^{\delta}(s) = -\underline{\underline{\mathbf{K}}}_{ll}^{\delta}(s)\vec{\mathbf{u}}_l(s) - \underline{\underline{\mathbf{K}}}_{li}^{\delta}\vec{\mathbf{u}}_i(s) - \vec{\mathbf{f}}_l^{\delta}(s) \tag{4.18}$$

This equation assumes that $x_i < x_l$; otherwise, the equation needs to be redefined. The matrices in equation (4.18) are

$$\underline{\underline{\mathbf{K}}}_{li}^{\delta}(s) = \underline{\underline{\mathbf{R}}}^{\delta}\underline{\underline{\mathbf{H}}}_{\epsilon 0}(x_l,s)\underline{\underline{\mathbf{T}}}^{\delta}, \quad \underline{\underline{\mathbf{K}}}_{ll}^{\delta}(s) = \underline{\underline{\mathbf{R}}}^{\delta}\underline{\underline{\mathbf{H}}}_{\epsilon 1}(x_l,s)\underline{\underline{\mathbf{S}}}^{\delta},$$
$$\vec{\mathbf{f}}_l^{\delta}(s) = \underline{\underline{\mathbf{R}}}^{\delta}\underline{\underline{\mathbf{E}}}^{\delta}(s)\int_0^1 \underline{\underline{\mathbf{G}}}_{\epsilon}^{\delta}(x_l,\xi,s)\vec{\mathbf{f}}^{\delta}(\xi,s)\mathrm{d}\xi . \tag{4.19}$$

With this result, the global forces of each subsystem connected at node $l$ are

$$\begin{aligned}
\vec{\mathbf{Q}}_l^A(s) &= -\underline{\underline{\mathbf{K}}}_{ll}^A(s)\vec{\mathbf{u}}_l(s) - \underline{\underline{\mathbf{K}}}_{li}^A(s)\vec{\mathbf{u}}_i(s) - \vec{\mathbf{f}}_l^A(s) \\
\vec{\mathbf{Q}}_l^B(s) &= -\underline{\underline{\mathbf{K}}}_{ll}^B(s)\vec{\mathbf{u}}_l(s) - \underline{\underline{\mathbf{K}}}_{lj}^B(s)\vec{\mathbf{u}}_j(s) - \vec{\mathbf{f}}_l^B(s) \\
&\vdots \\
\vec{\mathbf{Q}}_l^Z(s) &= -\underline{\underline{\mathbf{K}}}_{ll}^Z(s)\vec{\mathbf{u}}_l(s) - \underline{\underline{\mathbf{K}}}_{lm}^Z(s)\vec{\mathbf{u}}_m(s) - \vec{\mathbf{f}}_l^Z(s) \ .
\end{aligned} \tag{4.20}$$

Note that these equations automatically satisfy displacement compatibilities at node $l$. Placing equation (4.20) into equation (4.15) yields

$$\underline{\underline{\mathbf{K}}}_{ll}(s)\vec{\mathbf{u}}_l(s) + \underline{\underline{\mathbf{K}}}_{li}(s)\vec{\mathbf{u}}_i(s) + \underline{\underline{\mathbf{K}}}_{lj}(s)\vec{\mathbf{u}}_j(s) + \cdots + \underline{\underline{\mathbf{K}}}_{lm}(s)\vec{\mathbf{u}}_m(s) = \vec{\mathbf{q}}_l(s) \tag{4.21}$$

where

$$\begin{gathered}
\underline{\underline{\mathbf{K}}}_{ll}(s) = \underline{\underline{\mathbf{C}}}_l(s) + \underline{\underline{\mathbf{K}}}_{ll}^A(s) + \underline{\underline{\mathbf{K}}}_{ll}^B(s) + \cdots + \underline{\underline{\mathbf{K}}}_{ll}^Z(s) \\
\underline{\underline{\mathbf{K}}}_{li}(s) = \underline{\underline{\mathbf{K}}}_{li}^A(s), \quad \underline{\underline{\mathbf{K}}}_{lj}(s) = \underline{\underline{\mathbf{K}}}_{lj}^B(s), \quad \ldots, \quad \underline{\underline{\mathbf{K}}}_{lm}(s) = \underline{\underline{\mathbf{K}}}_{lm}^Z(s) \\
\vec{\mathbf{q}}_l(s) = \vec{\mathbf{p}}_l(s) - \vec{\mathbf{f}}_l^A(s) - \vec{\mathbf{f}}_l^B(s) - \cdots - \vec{\mathbf{f}}_l^Z(s) \ .
\end{gathered} \tag{4.22}$$

If force balance is imposed at each and every node, a matrix equilibrium equation can be formulated as

$$\underline{\underline{\mathbf{K}}}(s)\vec{\mathbf{u}}(s) = \vec{\mathbf{q}}(s), \tag{4.23}$$

where $\vec{\mathbf{u}}(s) = \{\vec{\mathbf{u}}_1^T(s) \ldots \vec{\mathbf{u}}_N^T(s)\}^T$, $\vec{\mathbf{q}}(s) = \{\vec{\mathbf{q}}_1^T(s) \ldots \vec{\mathbf{q}}_N^T(s)\}^T$, and $\underline{\underline{\mathbf{K}}}(s) = \underline{\underline{\mathbf{K}}}_{jk}(s)$. Note that $\underline{\underline{\mathbf{K}}}(s)$, $\vec{\mathbf{u}}(s)$, and $\vec{\mathbf{q}}(s)$ are the global stiffness matrix, the global nodal displacement vector, and the global force vector, respectively.

### 4.3.3 Imposing Boundary Conditions

Suppose a subsystem is attached at node $l$ and has the following prescribed boundary conditions at a point $x_i$ along the subsystem where $x_i < x_l$:

$$\underline{\underline{\mathbf{B}}}(s)\vec{\boldsymbol{\eta}}(x_i, s) = \vec{\boldsymbol{\kappa}}(s), \qquad \underline{\underline{\mathbf{B}}}(s) \in C^{n/2\text{x}n}, \qquad \vec{\boldsymbol{\kappa}}(s) \in C^{n/2\text{x}1} \ . \tag{4.24}$$

By setting $\vec{\boldsymbol{\gamma}}(s)$, $\underline{\underline{\mathbf{M}}}(s)$, and $\underline{\underline{\mathbf{N}}}(s)$ as

$$\vec{\boldsymbol{\gamma}}(s) = \begin{Bmatrix} \vec{\boldsymbol{\kappa}}(s) \\ \vec{\boldsymbol{\alpha}}(x_l, s) \end{Bmatrix}, \qquad \underline{\underline{\mathbf{M}}}(s) = \begin{bmatrix} \underline{\underline{\mathbf{B}}}(s) \\ \underline{\underline{\mathbf{0}}} \end{bmatrix}, \qquad \underline{\underline{\mathbf{N}}}(s) = \begin{bmatrix} \underline{\underline{\mathbf{0}}} & \underline{\underline{\mathbf{0}}} \\ \underline{\underline{\mathbf{I}}}_{n/2} & \underline{\underline{\mathbf{0}}} \end{bmatrix} \ , \tag{4.25}$$

the system response for each individual subsystem with the above boundary conditions is

$$\vec{\boldsymbol{\alpha}}(x,s) = \int_0^1 \underline{\underline{\mathbf{G}}}_{\alpha}(x,\xi,s)\vec{\mathbf{f}}(\xi,s)\mathrm{d}\xi + \underline{\underline{\mathbf{H}}}_{\alpha 0}(x,s)\vec{\boldsymbol{\kappa}}(s) + \underline{\underline{\mathbf{H}}}_{\alpha 1}(x,s)\vec{\boldsymbol{\alpha}}(x_l,s) \tag{4.26a}$$

$$\vec{\mathbf{P}}(x,s) = \underline{\underline{\mathbf{E}}}(s)\left\{\int_0^1 \underline{\underline{\mathbf{G}}}_{\epsilon}(x,\xi,s)\vec{\mathbf{f}}(\xi,s)\mathrm{d}\xi + \underline{\underline{\mathbf{H}}}_{\epsilon 0}(x,s)\vec{\boldsymbol{\kappa}}(s) + \underline{\underline{\mathbf{H}}}_{\epsilon 1}(x,s)\vec{\boldsymbol{\alpha}}(x_l,s)\right\} . \tag{4.26b}$$

If $x_i > x_l$, the system response is the same except $\underline{\underline{\mathbf{M}}}(s)$ and $\underline{\underline{\mathbf{N}}}(s)$ are now defined by

$$\underline{\underline{\mathbf{N}}}(s) = \begin{bmatrix} \underline{\underline{\mathbf{B}}}(s) \\ \underline{\underline{\mathbf{0}}} \end{bmatrix}, \qquad \underline{\underline{\mathbf{M}}}(s) = \begin{bmatrix} \underline{\underline{\mathbf{0}}} & \underline{\underline{\mathbf{0}}} \\ \underline{\underline{\mathbf{I}}}_{n/2} & \underline{\underline{\mathbf{0}}} \end{bmatrix} . \tag{4.27}$$

## 4.4 Formulation for Transverse and Axial Vibrations

The above procedure was designed only for the single distributed parameter $W(x,t)$. However, in many cases, the subsystems may have multiple distributed parameters. For example, consider an L-shaped beam that has two subsystems perpendicular to each other. With this system, there will be a deflection in the transverse and longitudinal direction for each subsystem. Therefore, the effects of longitudinal vibrations and transverse vibrations must be included in the transfer function synthesis analysis and this procedure is described below.

### 4.4.1 Multiple Distributed Parameters

The two main distributed parameters used in this dissertation are longitudinal vibrations denoted by $u(x,t)$ and transverse vibrations denoted by $w(x,t)$. The governing equation for a beam in longitudinal or axial vibration is a second-order linear partial differential equation given by

$$\frac{\partial}{\partial x}\left(EA(x)\frac{\partial u(x,t)}{\partial x}\right) + f_u(x,t) = \rho(x)\frac{\partial^2 u(x,t)}{\partial t^2} , \tag{4.28}$$

where $\rho(x)$ is the mass per unit length, $E$ is the modulus of elasticity, $A(x)$ is the area, and $f_u(x,t)$ are the external longitudinal forces. The governing equation for a beam due to transverse vibrations is a fourth-order linear partial differential equation given by

$$-\frac{\partial^2}{\partial x^2}\left(EI(x)\frac{\partial^2 w(x,t)}{\partial x^2}\right) + f_w(x,t) = \rho(x)\frac{\partial^2 w(x,t)}{\partial t^2} , \tag{4.29}$$

where $f_w$ are transverse forces and $I(x)$ is the moment of inertia.

By defining $W(x,t) = \{u(x,t)\ w(x,t)\}^T$, the transfer function synthesis method described in the previous sections can be used with some slight modifications. Assign $n_1$ as the order of the beam due to axial vibrations and $n_2$ as the order of the beam under transverse vibrations; the total order of the combined system is $n = n_1 + n_2$. The parameters given in equation (4.7a) can be recast into state space as

$$\vec{\boldsymbol{\eta}}(x,s) = \begin{Bmatrix} \alpha_1(x,s) \\ \epsilon_1(x,s) \\ \vec{\boldsymbol{\alpha}}_2(x,s) \\ \vec{\boldsymbol{\epsilon}}_2(x,s) \end{Bmatrix} = \begin{Bmatrix} u(x,s) \\ u'(x,s) \\ w(x,s) \\ w'(x,s) \\ w''(x,s) \\ w'''(x,s) \end{Bmatrix}, \quad \vec{\mathbf{f}}(x,s) = L \begin{Bmatrix} 0 \\ \frac{\overline{f}^u(x,s)}{EA} \\ 0 \\ 0 \\ 0 \\ \frac{\overline{f}^w(x,s)}{EI} \end{Bmatrix},$$

$$\underline{\underline{\mathbf{F}}}(s) = L \begin{bmatrix} 0 & 1 & 0 & 0 & 0 & 0 \\ \rho s^2/EA & 0 & 0 & 0 & 0 & 0 \\ 0 & 0 & 0 & 1 & 0 & 0 \\ 0 & 0 & 0 & 0 & 1 & 0 \\ 0 & 0 & 0 & 0 & 0 & 1 \\ 0 & 0 & -\rho s^2/EI & 0 & 0 & 0 \end{bmatrix}.$$

The displacement and strain vectors are defined as

$$\vec{\boldsymbol{\alpha}}(x,s) = \begin{pmatrix} \alpha_1(x,s) \\ \vec{\boldsymbol{\alpha}}_2(x,s) \end{pmatrix} = \begin{pmatrix} u(x,s) \\ w(x,s) \\ w'(x,s) \end{pmatrix}, \quad \vec{\boldsymbol{\epsilon}}(x,s) = \begin{pmatrix} \epsilon_1(x,s) \\ \vec{\boldsymbol{\epsilon}}_2(x,s) \end{pmatrix} = \begin{pmatrix} u'(x,s) \\ w''(x,s) \\ w'''(x,s) \end{pmatrix}. \tag{4.30}$$

By setting the parameters $\vec{\boldsymbol{\gamma}}(s)$, $\underline{\underline{\mathbf{M}}}(s)$, and $\underline{\underline{\mathbf{N}}}(s)$ for the boundary condition as

$$\vec{\gamma}(s) = \begin{Bmatrix} \vec{\boldsymbol{\alpha}}_0(s) \\ \vec{\boldsymbol{\alpha}}_1(s) \end{Bmatrix} = \begin{Bmatrix} \alpha_1(0,s) \\ \alpha_2(0,s) \\ \alpha_1(1,s) \\ \alpha_2(1,s) \end{Bmatrix}, \tag{4.31}$$

$$\underline{\underline{\mathbf{M}}}(s) = \begin{bmatrix} 1 & 0 & 0 & 0 & 0 & 0 \\ 0 & 0 & 1 & 0 & 0 & 0 \\ 0 & 0 & 0 & 1 & 0 & 0 \\ 0 & 0 & 0 & 0 & 0 & 0 \\ 0 & 0 & 0 & 0 & 0 & 0 \\ 0 & 0 & 0 & 0 & 0 & 0 \end{bmatrix}, \ \underline{\underline{\mathbf{N}}}(s) = \begin{bmatrix} 0 & 0 & 0 & 0 & 0 & 0 \\ 0 & 0 & 0 & 0 & 0 & 0 \\ 0 & 0 & 0 & 0 & 0 & 0 \\ 1 & 0 & 0 & 0 & 0 & 0 \\ 0 & 0 & 1 & 0 & 0 & 0 \\ 0 & 0 & 0 & 1 & 0 & 0 \end{bmatrix}, \tag{4.32}$$

the solution for the combined system will be given by equation (4.14b). The partitioned values for $\underline{\underline{\mathbf{G}}}$ and $\underline{\underline{\mathbf{H}}}$, specifically $\underline{\underline{\mathbf{G}}}_\alpha$, $\underline{\underline{\mathbf{G}}}_\epsilon$, $\underline{\underline{\mathbf{H}}}_{\alpha 0}$, $\underline{\underline{\mathbf{H}}}_{\alpha 1}$, $\underline{\underline{\mathbf{H}}}_{\epsilon 0}$, $\underline{\underline{\mathbf{H}}}_{\epsilon 1}$ are formulated by the following

equations.

$$\underline{\underline{\mathbf{G}}}_{\alpha}(x,\xi,s)\vec{\mathbf{f}}(\xi,s) = \begin{Bmatrix} G_{1:\frac{n_1}{2},n_1} \\ G_{n_1+1:n_1+\frac{n_2}{2},n_1} \end{Bmatrix} \frac{\overline{f}^u(x,s)L}{EA} + \begin{Bmatrix} G_{1:\frac{n_1}{2},n} \\ G_{n_1+1:n_1+\frac{n_2}{2},n} \end{Bmatrix} \frac{\overline{f}^w(x,s)L}{EI} \tag{4.33a}$$

$$\underline{\underline{\mathbf{G}}}_{\epsilon}(x,\xi,s)\vec{\mathbf{f}}(\xi,s) = \begin{Bmatrix} G_{\frac{n_1}{2}+1:n_1,n_1} \\ G_{n_1+\frac{n_2}{2}+1:n,n_1} \end{Bmatrix} \frac{\overline{f}^u(x,s)L}{EA} + \begin{Bmatrix} G_{\frac{n_1}{2}+1:n_1,n} \\ G_{n_1+\frac{n_2}{2}+1:n,n} \end{Bmatrix} \frac{\overline{f}^w(x,s)L}{EI} \tag{4.33b}$$

$$\underline{\underline{\mathbf{H}}}_{\alpha 0} = \begin{bmatrix} H(1:\frac{n_1}{2},1:\frac{n}{2}) \\ H(n_1+1:n_1+\frac{n_2}{2},1:\frac{n}{2}) \end{bmatrix} \quad \underline{\underline{\mathbf{H}}}_{\alpha 1} = \begin{bmatrix} H(1:\frac{n_1}{2},\frac{n}{2}+1:n) \\ H(n_1+1:n_1+\frac{n_2}{2},\frac{n}{2}+1:n) \end{bmatrix} \tag{4.34a}$$

$$\underline{\underline{\mathbf{H}}}_{\epsilon 0} = \begin{bmatrix} H(\frac{n_1}{2}+1:n_1,1:\frac{n}{2}) \\ H(n_1+\frac{n_2}{2}+1:n,1:\frac{n}{2}) \end{bmatrix} \quad \underline{\underline{\mathbf{H}}}_{\epsilon 1} = \begin{bmatrix} H(\frac{n_1}{2}+1:n_1,\frac{n}{2}+1:n) \\ H(n_1+\frac{n_2}{2}+1:n,\frac{n}{2}+1:n) \end{bmatrix} \tag{4.34b}$$

### 4.4.2 Rotation Matrices

When a subsystem is rotated by an angle $\psi$ with respect to another subsystem as shown in Figure 4.1, the rotation matrices to transfer parameters from global to local frames have to be determined. The two subsystems in this figure are connected at node $l$ where $F_x$, $F_y$, $M$, $u$, $w$, $\theta$ are the forces/moments and displacements in the local frame and $Fg_x$, $Fg_y$, $Mg$, $u_g$, $w_g$, $\theta_g$ are the forces/moments and displacements in the global frame.

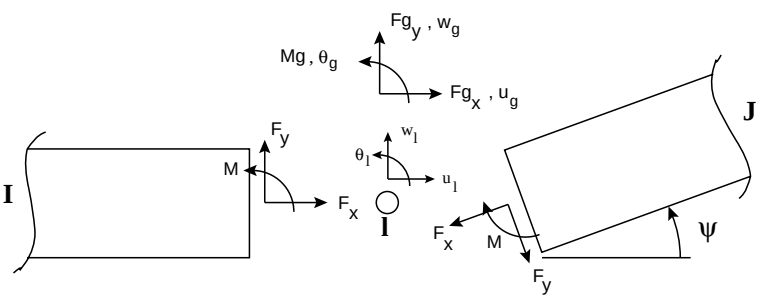


Figure 4.1: Rotation of Local Coordinates and Forces

The transformation of forces between the global and local frames at nodes $l$ and $j$ is

$$\vec{\mathbf{F}}_{g_j} = \underline{\underline{\mathbf{R}}}_j \vec{\mathbf{F}}_j, \quad \vec{\mathbf{F}}_{g_l} = \underline{\underline{\mathbf{R}}}_l \vec{\mathbf{F}}_l \ . \tag{4.35}$$

$\vec{\mathbf{F}}_{g_l}$ and $\vec{\mathbf{F}}_{g_j}$ are the global forces at nodes $l$ and $j$, respectively; $\vec{\mathbf{F}}_l$ and $\vec{\mathbf{F}}_j$ are the local forces at nodes $l$ and $j$, respectively. The force vectors (local and global) and rotation

matrices for a system having longitudinal and transverse vibrations are represented by

$$\vec{\mathbf{F}}_{g_j} = \vec{\mathbf{F}}_{g_l} = \begin{Bmatrix} Fg_x \\ Mg \\ Fg_y \end{Bmatrix}, \quad \vec{\mathbf{F}}_j = \begin{Bmatrix} F_{xj} \\ M_j \\ F_{yj} \end{Bmatrix}, \quad \vec{\mathbf{F}}_l = \begin{Bmatrix} F_{xl} \\ M_l \\ F_{yl} \end{Bmatrix} , \tag{4.36a}$$

$$\underline{\underline{\mathbf{R}}}_j = \begin{bmatrix} \cos(\psi) & 0 & -\sin(\psi) \\ 0 & 1 & 0 \\ \sin(\psi) & 0 & \cos(\psi) \end{bmatrix}, \quad \underline{\underline{\mathbf{R}}}_l = \begin{bmatrix} -\cos(\psi) & 0 & \sin(\psi) \\ 0 & -1 & 0 \\ -\sin(\psi) & 0 & -\cos(\psi) \end{bmatrix} . \tag{4.36b}$$

Similar to the forces, the transformation between global and local displacements at each node have to be formulated. The equations describing the rotation of the displacements from local to global coordinates are given by

$$\vec{\mathbf{u}}_{g_j} = \underline{\underline{\mathbf{S}}}_j \vec{\boldsymbol{\alpha}}_j, \quad \vec{\mathbf{u}}_{g_l} = \underline{\underline{\mathbf{S}}}_l \vec{\boldsymbol{\alpha}}_l , \tag{4.37}$$

where $\vec{\mathbf{u}}_{g_l}$ and $\vec{\mathbf{u}}_{g_j}$ are the global displacements at nodes $l$ and $j$, respectively; $\vec{\boldsymbol{\alpha}}_l$ and $\vec{\boldsymbol{\alpha}}_j$ are the local displacements at nodes $l$ and $j$, respectively. The displacement and rotation matrices for a system that can vibrate in a longitudinal and transverse directions are represented by the following equations.

$$\vec{\mathbf{u}}_{g_j} = \vec{\mathbf{u}}_{g_l} = \begin{Bmatrix} u_g \\ w_g \\ \theta_g \end{Bmatrix}, \quad \vec{\boldsymbol{\alpha}}_j = \begin{Bmatrix} u_j \\ w_j \\ \theta_j \end{Bmatrix}, \quad \vec{\boldsymbol{\alpha}}_l = \begin{Bmatrix} u_l \\ w_l \\ \theta_l \end{Bmatrix}, \tag{4.38a}$$

$$\underline{\underline{\mathbf{S}}}_j = \begin{bmatrix} \cos(\psi) & -\sin(\psi) & 0 \\ \sin(\psi) & \cos(\psi) & 0 \\ 0 & 0 & 1 \end{bmatrix}, \quad \underline{\underline{\mathbf{S}}}_l = \begin{bmatrix} \cos(\psi) & -\sin(\psi) & 0 \\ \sin(\psi) & \cos(\psi) & 0 \\ 0 & 0 & 1 \end{bmatrix} . \tag{4.38b}$$

## 4.5 Analysis of Complex Distributed System

After assembling the global dynamic stiffness matrix $\underline{\underline{\mathbf{K}}}(s)$, the complex distributed system can be analyzed. This analysis can determine the following quantities for the complex distributed system: eigenvalues and eigenfunctions of the system, transfer functions or frequency response functions (FRFs) between any two points on the system, and time responses to any type of disturbance input.

### 4.5.1 Eigenvalue Problem

To solve the eigenvalue problem, all external disturbances are set to zero, i.e., $\vec{\mathbf{q}}(s)$ in equation (4.23) is set to $\vec{\mathbf{0}}$. Therefore, the characteristic equation of the complex distributed system is

$$\det[\underline{\underline{\mathbf{K}}}(s)] = 0 . \tag{4.39}$$

Note that the characteristic equation is nonlinear and has an infinite number of solutions. The eigenvalues $\lambda_k$ are determined by letting $s = j\omega$ where $j = \sqrt{-1}$ and solving for the value of $\omega$ that satisfies the above characteristic equation.

The eigenfunctions are determined in two steps after the eigenvalues are found. The first step is to find the nontrivial solution $\vec{\mathbf{u}}(\lambda_k)$ from $\underline{\underline{\mathbf{K}}}(\lambda_k)\vec{\mathbf{u}}(\lambda_k) = \vec{\mathbf{0}}$ for each individual eigenvalue. Determining the solution is equivalent to finding the nullspace of the global stiffness matrix evaluated at the eigenvalue $\lambda_k$. The global nodal displacement vector $\vec{\mathbf{u}}(\lambda_k)$ is then transformed into local coordinates by equation (4.37) and substituted into equation (4.14a) or equation (4.26a) depending whether the subsystem has boundary conditions or not. The evaluation of the displacement vector $\vec{\boldsymbol{\alpha}}(x, s)$ along the subsystem is the mode shape for that individual subsystem. The overall mode shape of the complex distributed system is determined by interconnecting the mode shapes of each individual subsystem.

### 4.5.2 Transfer Function

The transfer function of the complex distributed system can be determined between any two points if the system is excited by a harmonic external disturbance. Once the input/output pair for the transfer function is chosen, the output of the system can be determined by finding the displacement $\vec{\mathbf{u}}(i\omega)$ at the sensor location within a desired frequency range. The displacement at each frequency is determined by $\vec{\mathbf{u}}(i\omega) = \underline{\underline{\mathbf{K}}}^{-1}(i\omega)\vec{\mathbf{q}}(i\omega)$ and the global displacement vector is transformed to local coordinates through equation (4.37). The resulting local displacement vectors will give the transfer function for the input/output pair that was chosen.

### 4.5.3 Time Response

The time response of the complex distributed system can be determined through modal superposition. The excitation of the system can take the form of initial conditions, external disturbances, or both. This section will briefly describe how the time response should be calculated for a system undergoing a transverse vibration $w(x, t)$. It should be noted that modal superposition is an approximate technique to the solution of the time response. However, since this the transfer function synthesis (TFS) method calculates exact eigenfunctions, the number of terms used in the expansion will be minimized.

Assuming proportional damping as the model for the system structural damping, the governing partial differential equation of the system is

$$-EI\frac{\partial^4 w(x,t)}{\partial x^4} - \left[\rho\gamma + \beta EI\frac{\partial^4}{\partial x^4}\right]\frac{\partial w(x,t)}{\partial t} + f_{w'}(x,t) = \rho\frac{\partial^2 w(x,t)}{\partial t^2} \ . \tag{4.40}$$

The solution of equation (4.40) will have the form

$$w(x,t) = \sum_{r=1}^{\infty} W_r(x) q_r(t) \tag{4.41}$$

where $W_r(x)$ are the eigenfunctions of the system. Inserting equation (4.41) into equation (4.40) leads to the following equation.

$$-\sum_{r=1}^{\infty} q_r(t) EI \frac{\mathrm{d}^4 W_r(x)}{\mathrm{d}x^4} - \sum_{r=1}^{\infty} \dot{q}_r(t) \left[ \gamma\rho W_r(x) + \beta EI \frac{\mathrm{d}^4 W_r(x)}{\mathrm{d}x^4} \right] + f_{w'}(x,t) = \sum_{r=1}^{\infty} \ddot{q}_r(t) \rho(x) W_r(x) \qquad 0 < x < 1 \tag{4.42}$$

Multiplying equation (4.42) by $W_s(x)$ and integrating over the domain, $\mathcal{D} : 0 < x < 1$, results in a coupled set of ordinary differential equations which can be written as

$$\underline{\underline{\mathbf{M}}}\ddot{\vec{\mathbf{x}}} + \underline{\underline{\mathbf{C}}}\dot{\vec{\mathbf{x}}} + \underline{\underline{\mathbf{K}}}\vec{\mathbf{x}} = \vec{\mathbf{Q}} \ . \tag{4.43}$$

Note that this equation assumes the expansion of $w(x,t)$ is finite. One method to solve the response for this system is to recast equation (4.43) into state space and then solving a set of first-order ordinary differential equations.

## 4.6 Constraints of Lumped and Distributed Systems

The term $-\underline{\underline{\mathbf{C}}}_l(s)\vec{\mathbf{u}}_l(s)$ in equation (4.15) is valid only for a lumped system connected to a distributed system at a single point. However, there are several types of point constraints or combined lumped parameter dynamic subsystems that are commonly used in vibration isolation designs. The following sections will describe these constraints and formulate the constraint matrix.

### 4.6.1 Point Masses

A lumped mass $M$ can be attached to a distributed system at location $x_i$ as shown in Figure 4.2. This mass can model a sensor such as an accelerometer. Under transverse or longitudinal vibrations, the mass produces a force $f_c(x_i,t)$ on the system. Under transverse vibrations, the force is given by $f_c(x_i,t) = -M\ddot{w}(x_i,t)$; transformed in the Laplace domain, the force becomes $F_c(x_i,s) = -Ms^2 w(x_i,s)$. For a beam under transverse vibration, the global displacement vector at node $i$ is $\vec{\mathbf{u}}_i(s) = \{w(x_i,s)\ \frac{\partial w(x_i,s)}{\partial x}\}^T$ where the global force

vector is $\vec{\mathbf{f}}(s) = \{M_m(x_i, s)\ F(x_i, s)\}^T$; the term $M_m$ is the moment at the point $x_i$. With these definitions the constraint matrix $\underline{\underline{\mathbf{C}}}_i(s)$ is

$$\underline{\underline{\mathbf{C}}}_i(s) = \begin{bmatrix} 0 & 0 \\ Ms^2 & 0 \end{bmatrix} . \tag{4.44}$$

For a beam under longitudinal vibration, where $u_l = u(x_i, s)$ and $f(s) = F(x_i, s)$, the constraint matrix is $C_i(s) = Ms^2$.

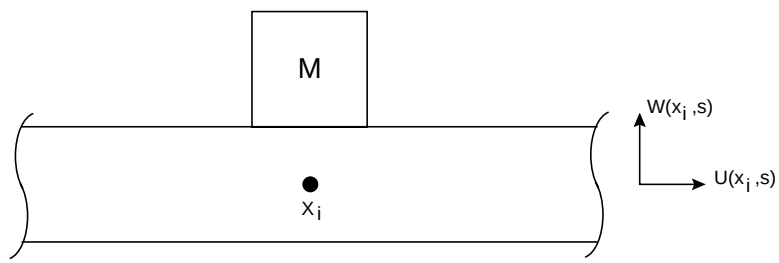


Figure 4.2: Lumped Mass in Transverse or Longitudinal Vibration

If the distributed system is under transverse vibration and the lumped mass has rotary inertia, a moment will be produced. The moment is $M_c(x_i, t) = -I_r \frac{\partial \ddot{w}(x_i,t)}{\partial x}$ and in the Laplace domain this will be $M_c(x_i, s) = -I_r s^2 \frac{\partial w(x_i,s)}{\partial x}$. Under transverse vibration, where $\vec{\mathbf{u}}_i(s) = \{w(x_i, s)\ \frac{\partial w(x_i,s)}{\partial x}\}^T$ and $\vec{\mathbf{f}}(s) = \{M_m(x_i, s)\ F(x_i, s)\}^T$, the constraint matrix $\underline{\underline{\mathbf{C}}}_i(s)$ is

$$\underline{\underline{\mathbf{C}}}_i(s) = \begin{bmatrix} 0 & I_r s^2 \\ Ms^2 & 0 \end{bmatrix} . \tag{4.45}$$

### 4.6.2 Mass-Spring-Damper Systems

A rigid body of mass $M$ can be elastically connected to a distributed system at location $x_i$ as shown in Figure 4.3. The elastic support has a stiffness $k_p$, viscous damping coefficient $c_p$, and the support is assumed massless.

The equation of motion for the rigid body is

$$m\ddot{y}(t) = -c_p\{\dot{y}(t) - \dot{w}(x_i, t)\} - k_p\{y(t) - w(x_i, t)\} + F_m(t) .$$

By taking the Laplace transform and solving for $y$, the equation becomes

$$y(s) = \frac{(c_p s + k_p)}{ms^2 + c_p s + k_p} w(x_i, s) + \frac{F_m(s)}{ms^2 + c_p s + k_p} . \tag{4.46}$$

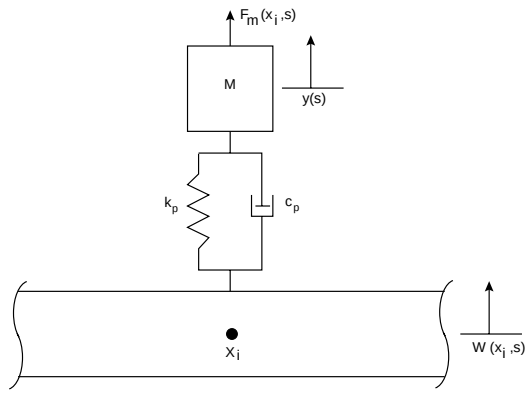


Figure 4.3: Spring-Mass-Damper System in Transverse or Longitudinal Vibration

The rigid body exerts a force $f_c(x_i, t)$ on the distributed system which is described by

$$f_c(x_i, t) = c_p\{\dot{y}(t) - \dot{w}(x_i, t)\} + k_p\{y(t) - w(x_i, t)\} \ .$$

In the Laplace domain this equation becomes

$$f_c(x_i, s) = (c_p s + k_p)\{y(s) - w(x_i, s)\} \ . \tag{4.47}$$

Placing equation (4.46) into equation (4.47) results in the following force on the system.

$$f_c(x_i, s) = \frac{-ms^2(c_p s + k_p)}{ms^2 + c_p s + k_p} w(x_i, s) + \frac{(c_p s + k_p)}{ms^2 + c_p s + k_p} F_m(s) \tag{4.48}$$

For a beam under transverse vibration, the displacement is $\vec{\mathbf{u}}_i(s) = \{w(x_i, s) \ \frac{\partial w(x_i,s)}{\partial x}\}^T$ and the force is $\vec{\mathbf{f}}(s) = \{M_m(x_i, s) \ F(x_i, s)\}^T$; therefore, the term $\underline{\underline{\mathbf{C}}}_i(s)$ is

$$\underline{\underline{\mathbf{C}}}_i(s) = \begin{bmatrix} 0 & 0 \\ \frac{ms^2(c_p s + k_p)}{ms^2 + c_p s + k_p} & 0 \end{bmatrix} \ . \tag{4.49}$$

Note that an additional forcing term is added at node $i$, namely $\left\{0 \ \ \frac{-(c_p s + k_p)}{ms^2 + c_p s + k_p} F_m(s)\right\}^T$ which should be added to the external force vector $\vec{\mathbf{q}}_i(s)$.

### 4.6.3 Point Connection of Subsystems

Figure 4.4 shows a situation where two subsystems are connected to each other at a single point by a mechanism $C$. This mechanism can be a spring, a viscous damper, an

actuator, etc. The forces $\vec{\mathbf{Q}}_{cj}(s)$ and $\vec{\mathbf{Q}}_{cl}(s)$ for this type of system are related to the nodal displacements by

$$\begin{Bmatrix} \vec{\mathbf{Q}}_{cj}(s) \\ \vec{\mathbf{Q}}_{cl}(s) \end{Bmatrix} = - \begin{bmatrix} \underline{\underline{\mathbf{C}}}_{jj}(s) & \underline{\underline{\mathbf{C}}}_{jl}(s) \\ \underline{\underline{\mathbf{C}}}_{lj}(s) & \underline{\underline{\mathbf{C}}}_{ll}(s) \end{bmatrix} \begin{Bmatrix} \vec{\mathbf{u}}_j(s) \\ \vec{\mathbf{u}}_l(s) \end{Bmatrix} . \tag{4.50}$$

The $\underline{\underline{\mathbf{C}}}$ matrices are the transfer functions describing the mechanism at each connection point. To include the forces $\vec{\mathbf{Q}}_{cl}$ and $\vec{\mathbf{Q}}_{cj}$ in each subsystem's force balance, equation (4.15) will have to be modified. The force $\vec{\mathbf{Q}}_{cj}$ will now have an effect on node $j$ as well as node $l$; the same holds true for the force $\vec{\mathbf{Q}}_{cl}$. Therefore, the force balance at node $j$ will have components from the forces $\vec{\mathbf{Q}}_{cj}$ and $\vec{\mathbf{Q}}_{cl}$, i.e. $\underline{\underline{\mathbf{C}}}_{lj}$ and $\underline{\underline{\mathbf{C}}}_{jl}$, respectively. The force balance at node $l$ will have components $\underline{\underline{\mathbf{C}}}_{jl}$ and $\underline{\underline{\mathbf{C}}}_{ll}$ in its force balance.

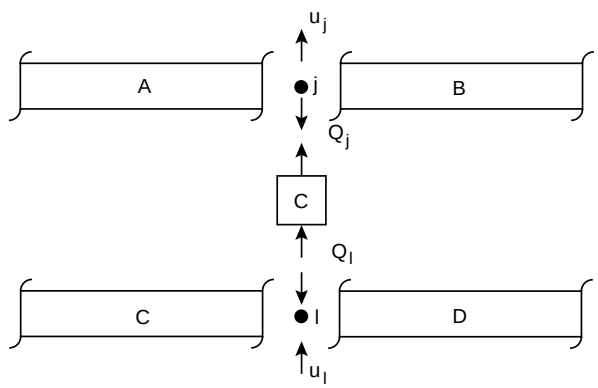


Figure 4.4: Point Connections of Distributed Systems

## 4.7 Active Isolation for FBRE System

The flexible base, rigid equipment system is depicted by Figure 4.3. The equipment is assumed rigid with a mass $m_e$ and the base is assumed flexible with a mass per unit length $\rho$. The frequency and time responses for the flexible base, rigid equipment (FBRE) system using active isolators are implemented quite easily using the transfer function synthesis method. For the frequency response, control laws are implemented as constraints on the distributed system, while the time response is determined by modal superposition. Passive isolation is discussed first since the implementation of an active isolator is quite similar to a passive isolator. For active isolation systems, it is assumed that the actuator is placed in parallel with the passive isolator. Three different control methodologies will be discussed: a proportional-plus-integral-plus-derivative ($\mathcal{PID}$) controller, a linear quadratic Gaussian (LQG) regulator, and a positive position feedback (PPF) controller.

### 4.7.1 Passive Isolation

As stated previously, the FBRE system can be modeled by a beam and a mass-spring-damper system as shown in Figure 4.3. For this system, a general approach for the frequency response functions and time response are taken. That is, boundary conditions are arbitrary and the base is assumed to have a length $L$. The isolator is placed at a distance $x_i$ from the left end of the base and consists of a massless spring and damper with a spring stiffness $k_p$ and damping coefficient $c_p$.

#### 4.7.1.1 Frequency Response for Passive Isolator

The frequency response for any system is outlined in Section 4.5.2 and will not be discussed here. However, a discussion how the mass-spring-damper affects the TFS methods will be addressed. The influence of the mass-spring-damper system was discussed in Section 4.6.2 and the results are briefly discussed here. The addition of the mass-spring-damper system on the beam will influence the constraint matrix and the external force vector in equation (4.15). The constraint matrix $\underline{\underline{\mathbf{C}}}_l(s)$ for this system is

$$\underline{\underline{\mathbf{C}}}_l(s) = \begin{bmatrix} 0 & 0 \\ \frac{ms^2(c_p s + k_p)}{ms^2 + c_p s + k_p} & 0 \end{bmatrix} .$$

and the additional term added to the global force vector is

$$\vec{\mathbf{q}}_l(s) = \begin{Bmatrix} 0 \\ \frac{-(c_p s + k_p)}{ms^2 + c_p s + k_p} F_m(s) \end{Bmatrix} .$$

Once these matrices are determined, the frequency response for the FBRE system can be formulated.

#### 4.7.1.2 Time Response for Passive Isolator

Given the FBRE system in Figure 4.3, the equations of motion for the base and the equipment are given in equation (4.51a) and equation (4.51b), respectively. It is assumed that the structural damping is modeled as a proportional damped beam where $\gamma$ and $\beta$ are the significant parameters.

$$\begin{aligned} -EI\frac{\partial^4 w(x,t)}{\partial x^4} + f(x,t) + k_p\left\{y(t) - w(x,t)\right\}\delta(x - x_i) - \rho\gamma\frac{\partial w(x,t)}{\partial t} \\ -\beta EI\frac{\partial^5 w(x,t)}{\partial x^4 \partial t} + c_p[\dot{y}(t) - \dot{w}(x,t)]\delta(x - x_i) = \rho\frac{\partial^2 w(x,t)}{\partial t^2} \end{aligned} \tag{4.51a}$$

$$m_e\ddot{y}(t) + c_p\dot{y}(t) + k_p y(t) = k_p w(x,t) + c_p\dot{w}(x,t) + F_y(t) \tag{4.51b}$$

Equation (4.51a) is valid over the domain, $\mathcal{D} : 0 < x < 1$, while equation (4.51b) is valid at the isolator attachment point on the base, $x = x_i$. The base displacement for the combined system can be written as

$$w(x,t) = \sum_{r=1}^{\infty} V_r(x) q_r(t) \approx \sum_{r=1}^{\infty} \Phi_r(x) q_r(t) \ ,$$

where $V_r(x)$ are the actual eigenfunctions of the FBRE system. Since the eigenfunctions are piecewise continuous at the isolator location, the higher derivatives of the eigenfunctions will be discontinuous. Therefore, the true eigenfunctions $V_r(x)$ are approximated by the continuous functions $\Phi_r(x)$. By using this substitution, the governing equations of motion are

$$\begin{aligned} &- EIq_r(t)\frac{\mathrm{d}^4\Phi_r(x)}{\mathrm{d}x^4} + f(x,t) - \dot{q}_r(t)[\rho\gamma + \beta EI\frac{\mathrm{d}^4}{\mathrm{d}x^4}]\Phi_r(x) + k_p y(t)\delta(x-x_i) \\ &- k_p q_r(t)\Phi_r(x)\delta(x-x_i) + c_p\dot{y}(t)\delta(x-x_i) - c_p\dot{q}_r(t)\Phi_r(x)\delta(x-x_i) = \rho\Phi_r(x)\ddot{q}_r(t) \end{aligned} \tag{4.52a}$$

$$m_e\ddot{y}(t) + c_p\dot{y}(t) + k_p y(t) = k_p\Phi_r(x_i)q_r(t) + c_p\Phi_r(x_i)\dot{q}_r(t) + F_y(t) \tag{4.52b}$$

where the repeated indices imply a summation and $r = 1, 2, \ldots \infty$. Multiplying equation (4.52a) by $\Phi_s(x)$ and integrating over the domain results in the following change.

$$\begin{aligned} &- q_r(t)\int_0^1 \Phi_s(x)EI\frac{\mathrm{d}^4\Phi_r(x)}{\mathrm{d}x^4}\mathrm{d}x + \int_0^1 \Phi_s(x)f(x,t)\mathrm{d}x - \dot{q}_r(t)\int_0^1 \rho\gamma\Phi_s(x)\Phi_r(x)\mathrm{d}x \\ &- \dot{q}_r(t)\int_0^1 \beta EI\Phi_s(x)\frac{\mathrm{d}^4\Phi_r(x)}{\mathrm{d}x^4}\mathrm{d}x + k_p y(t)\int_0^1 \Phi_s(x)\delta(x-x_i)\mathrm{d}x \\ &- k_p q_r(t)\int_0^1 \Phi_s(x)\Phi_r(x)\delta(x-x_i)\mathrm{d}x + c_p\dot{y}(t)\int_0^1 \Phi_s(x)\delta(x-x_i)\mathrm{d}x \\ &- c_p\dot{q}_r(t)\int_0^1 \Phi_s(x)\Phi_r(x)\delta(x-x_i)\mathrm{d}x = \ddot{q}_r(t)\int_0^1 \Phi_s(x)\rho\Phi_r(x)\mathrm{d}x \qquad r,s = 1,2,\ldots \end{aligned} \tag{4.53}$$

When the number of modes $\Phi(x)$ are finite, say $r, s = 1, 2, \ldots, n$, equation (4.52b) and equation (4.53) can be recast into a system of matrix equations such as

$$\underline{\underline{\mathbf{M}}}\ddot{\vec{\mathbf{x}}}(t) + \underline{\underline{\mathbf{C}}}\dot{\vec{\mathbf{x}}}(t) + \underline{\underline{\mathbf{K}}}\vec{\mathbf{x}}(t) = \vec{\mathbf{Q}}(t) \ , \tag{4.54}$$

where

$$\vec{\mathbf{x}}(t) = \begin{Bmatrix} q_1(t) \\ q_2(t) \\ \vdots \\ q_n(t) \\ y(t) \end{Bmatrix} \qquad \underline{\underline{\mathbf{M}}} = \begin{bmatrix} M_{s,r} & M_{s,n+1} \\ M_{n+1,r} & M_{n+1,n+1} \end{bmatrix} \qquad \underline{\underline{\mathbf{C}}} = \begin{bmatrix} C_{s,r} & C_{s,n+1} \\ C_{n+1,r} & C_{n+1,n+1} \end{bmatrix}$$

$$\underline{\underline{\mathbf{K}}} = \begin{bmatrix} K_{s,r} & K_{s,n+1} \\ K_{n+1,r} & K_{n+1,n+1} \end{bmatrix} \qquad \vec{\mathbf{Q}} = \begin{Bmatrix} Q_1(t) \\ Q_2(t) \\ \vdots \\ Q_n(t) \\ F_y(t) \end{Bmatrix} .$$

The components of the mass matrix $\underline{\underline{\mathbf{M}}}$ are

$$\begin{aligned} M_{s,r} &= \int_0^1 \rho \Phi_s(x) \Phi_r(x) \mathrm{d}x \\ M_{s,n+1} = M_{n+1,s} &= \vec{\mathbf{0}} \qquad\qquad M_{n+1,n+1} = m_e \ . \end{aligned} \tag{4.55}$$

The components of the stiffness matrix $\underline{\underline{\mathbf{K}}}$ are

$$\begin{aligned} K_{s,r} &= \int_0^1 \Phi_s(x) EI \frac{\partial^4 \Phi_r(x)}{\partial x^4} \mathrm{d}x + k_p \Phi_s(x_i) \Phi_r(x_i) \\ K_{s,n+1} = K_{n+1,s} &= -k_p \Phi_s(x_i) \qquad\qquad K_{n+1,n+1} = k_p \ . \end{aligned} \tag{4.56}$$

The components of the damping matrix $\underline{\underline{\mathbf{C}}}$ are

$$\begin{aligned} C_{s,r} &= \int_0^1 \Phi_s(x) \beta EI \frac{\partial^4 \Phi_r(x)}{\partial x^4} \mathrm{d}x + \int_0^1 \rho \gamma \Phi_s(x) \Phi_r(x) \mathrm{d}x + c_p \Phi_s(x_i) \Phi_r(x_i) \\ C_{s,n+1} = C_{n+1,s} &= -c_p \Phi_s(x_i) \qquad\qquad C_{n+1,n+1} = c_p \ . \end{aligned} \tag{4.57}$$

The force vector $\vec{\mathbf{Q}}$ is determined by the following integral and $F_y(t)$ is the force applied on the equipment.

$$Q_s(t) = \int_0^1 \Phi_s(x) f(x,t) \mathrm{d}x$$

The solution to the system of matrix equations are readily solved in the state space. Recast into state space, the new equations are

$$\begin{aligned} \dot{\vec{\mathbf{z}}} &= \underline{\underline{\mathbf{A}}} \vec{\mathbf{z}} + \vec{\mathbf{B}} u \\ g &= \vec{\mathbf{C}}_{ss} \vec{\mathbf{z}} + D u \end{aligned} \tag{4.58}$$

where

$$\vec{\mathbf{z}} = \begin{Bmatrix} \vec{\mathbf{x}} \\ \dot{\vec{\mathbf{x}}} \end{Bmatrix} \qquad \underline{\underline{\mathbf{A}}} = \begin{bmatrix} \underline{\underline{\mathbf{0}}} & \underline{\underline{\mathbf{I}}} \\ -\underline{\underline{\mathbf{M}}}^{-1} \underline{\underline{\mathbf{K}}} & -\underline{\underline{\mathbf{M}}}^{-1} \underline{\underline{\mathbf{C}}} \end{bmatrix} \qquad \vec{\mathbf{B}} = \begin{Bmatrix} \vec{\mathbf{0}} \\ \underline{\underline{\mathbf{M}}}^{-1} \vec{\mathbf{Q}} \end{Bmatrix} \tag{4.59}$$

and $g$ is the output of the combined system which will represent the equipment displacement. Therefore, the vector $\vec{\mathbf{C}}_{ss}$ and D are

$$\vec{\mathbf{C}}_{ss} = \begin{Bmatrix} 0_1 & 0 & \dots & 0_n & \boxed{1} & 0_1 & 0 & \dots & 0_n & 0 \end{Bmatrix} \qquad D = 0 \ , \tag{4.60}$$

where the boxed quantity specifies the displacement $y$ of the equipment.

### 4.7.2 Classical Control Implementations

Classical control strategies such as proportional-plus-integral-plus-derivative control, and proportional-plus-derivative control are discussed. For the frequency response, only the implementation of the $\mathcal{PID}$ controller is formulated because $\mathcal{PD}$ control can be formulated by letting the appropriate integral gain go to zero. For the time response, both $\mathcal{PID}$ and $\mathcal{PD}$ controllers are discussed.

#### 4.7.2.1 Frequency Response

Similar to the passive system, an active controller will affect the constraint matrix and force vector in equation (4.15). The following paragraphs are a detailed discussion on the formulation of the constraint matrix and the additional forcing term that arises.

A free body diagram for the rigid equipment is shown in Figure 4.5. The force $F_p$ is the force exerted by the passive isolator and the force $F_a$ is the force exerted by the actuator. In general, the isolator will have some damping and stiffness given by $c_p$ and $k_p$, respectively. The actuator will implement a $\mathcal{PID}$ controller; therefore, the gains for proportional, derivative, and integral control are given by $K_P$, $K_D$, and $K_I$, respectively. Feedback will come from the flexible base or rigid equipment. The displacement of the equipment and base at the actuator attachment points are $y(t)$ and $w(x_i, t)$, respectively.

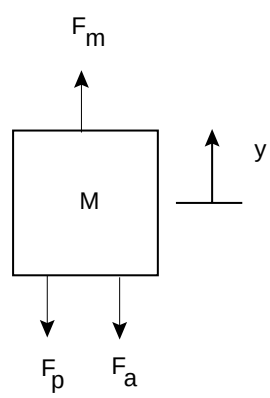


Figure 4.5: Free Body Diagram for Equipment in FBRE System

Assuming equipment feedback, the governing equation of motion for the rigid equipment in the Laplace domain is

$$\begin{aligned} ms^2Y(s) = -F_p(s) - F_a(s) + F_m(s) = &- (k_p + c_p s) * [Y(s) - W(x_i, s)] \\ &- (K_P + K_D s + K_I/s)Y(s) + F_m(s) \ . \end{aligned} \tag{4.61}$$

The displacement of the equipment is

$$\begin{aligned} Y(s) =& \frac{k_p + c_p s}{ms^2 + (c_p + K_D)s + K_P + k_p + K_I/s} W(x_i, s) \\ &+ \frac{F_m}{ms^2 + (c_p + K_D)s + K_P + k_p + K_I/s} \ . \end{aligned} \tag{4.62}$$

The constraint force on the flexible base due to the isolator and actuator in terms of the base displacement $W(x_i, s)$ is

$$\begin{aligned} f_c(s) = F_p(s) + F_a(s) =& \frac{-ms^2(k_p + c_p s)}{ms^2 + (c_p + K_D)s + K_P + k_p + K_I/s} W(x_i, s) \\ &+ \frac{(c_p + K_D)s + K_P + k_p + K_I/s}{ms^2 + (c_p + K_D)s + K_P + k_p + K_I/s} F_m(s) \ . \end{aligned} \tag{4.63}$$

In the term $-\underline{\underline{\mathbf{C}}}_l(s)\vec{\mathbf{u}}_l(s)$, the constraint matrix $\underline{\underline{\mathbf{C}}}_l(s)$ is

$$\underline{\underline{\mathbf{C}}}_l(s) = \begin{bmatrix} 0 & 0 \\ \frac{ms^2(c_p s + k_p)}{ms^2 + (c_p + K_D)s + K_P + k_p + K_I/s} & 0 \end{bmatrix} \ . \tag{4.64}$$

Note that an additional forcing term is added at node $l$ to $\vec{\mathbf{q}}_l(s)$ and this term is

$$\vec{\mathbf{q}}_l(s) = \begin{Bmatrix} 0 \\ \frac{(c_p + K_D)s + K_P + k_p + K_I/s}{ms^2 + (c_p + K_D)s + K_P + k_p + K_I/s} F_m(s) \end{Bmatrix} \ . \tag{4.65}$$

When base feedback is used, the governing equation of motion of the equipment is

$$\begin{aligned} ms^2 Y(s) = -F_p(s) - F_a(s) + F_m(s) =& -(k_p + c_p s) * [Y(s) - W(x_i, s)] \\ &+ (K_P + K_D s + K_I/s) W(x_i, s) + F_m(s) \ . \end{aligned} \tag{4.66}$$

The displacement of the equipment is

$$Y(s) = \frac{k_p + K_P + c_p s + K_D s + K_I/s}{ms^2 + c_p s + k_p} W(x_i, s) + \frac{F_m}{ms^2 + c_p s + k_p} \ , \tag{4.67}$$

and the constraint force on the flexible base due to the isolator and actuator in terms of base displacement $W(x_i, s)$ is

$$\begin{aligned} f_c(s) = F_p(s) + F_a(s) =& \frac{(-ms^2 + K_P + K_D s + K_I/s)(k_p + c_p s)}{ms^2 + c_p s + k_p} W(x_i, s) \\ &- (K_D s + K_P + K_I/s) W(x_i, s) + \frac{c_p s + k_p}{ms^2 + c_p s + k_p} F_m(s) \ . \end{aligned} \tag{4.68}$$

In the term $-\underline{\underline{\mathbf{C}}}_l(s)\vec{\mathbf{u}}_l(s)$, the constraint matrix $\underline{\underline{\mathbf{C}}}_l(s)$ is

$$\underline{\underline{\mathbf{C}}}_l(s) = \begin{bmatrix} 0 & 0 \\ \frac{(ms^2-K_P-K_Ds-K_I/s)(c_ps+k_p)}{ms^2+c_ps+k_p} + K_Ds + K_P + K_I/s & 0 \end{bmatrix} . \tag{4.69}$$

An additional forcing term is added at node $l$ to $\vec{\mathbf{q}}_l(s)$ and this term is

$$\vec{\mathbf{q}}_l(s) = \begin{Bmatrix} 0 \\ \frac{F_m(s)[c_ps+k_p]}{ms^2+c_ps+k_p} \end{Bmatrix} . \tag{4.70}$$

#### 4.7.2.2 Time Response

Results carried out in Section 4.7.1.2 for the passive system can be used when $\mathcal{PID}$ control the control law. The impact of $\mathcal{PID}$ control is divided into two different sections: one section describes the changes to the damping and stiffness matrices, $\underline{\underline{\mathbf{C}}}$ and $\underline{\underline{\mathbf{K}}}$, due to the $\mathcal{PD}$ control part and the other section describes the change to the state-space equations when integral control is added. Since the system is assumed linear, these two parts can be analyzed separately and then combined together to give the overall results for the $\mathcal{PID}$ controller.

$\mathcal{PD}$ control modifies the passive damping and stiffness matrices, $\underline{\underline{\mathbf{C}}}$ and $\underline{\underline{\mathbf{K}}}$, given in equation (4.56) and equation (4.57); $\mathcal{PD}$ control has no affect on the mass matrix $\underline{\underline{\mathbf{M}}}$. It is assumed that a sensor will be able to measure the displacement and velocity of the equipment and send the signal back to the actuator. The force of the actuator that implements $\mathcal{PD}$ control is

$$F_{act} = K_P\ y(t) + K_D\ \dot{y}(t)\ .$$

The proportional gain $K_P$ will affect the terms $K_{s,n+1}$ and $K_{n+1,n+1}$ in equation (4.56) and the new values are

$$K_{s,n+1} = -(K_P + k_p)\Phi_s(x_i) \qquad\qquad K_{n+1,n+1} = K_P + k_p\ .$$

The derivative gain $K_D$ will affect the terms $C_{s,n+1}$ and $C_{n+1,n+1}$ in equation (4.57) and the new values are

$$C_{s,n+1} = -(K_D + c_p)\Phi_s(x_i) \qquad\qquad C_{n+1,n+1} = K_D + c_p\ .$$

Unlike $\mathcal{PD}$ control, the integral part of $\mathcal{PID}$ control will not directly affect the damping and stiffness matrices but will change the form of the state-space equations. A new state for the integral control $\int y(t)\mathrm{d}t$ must be introduced into the system-state $z$. Therefore, the new states are represented by $\vec{\mathbf{v}}$ where

$$\vec{\mathbf{v}} = \begin{Bmatrix} \vec{\mathbf{z}} \\ \int y\mathrm{d}t \end{Bmatrix} = \begin{Bmatrix} \vec{\mathbf{x}} \\ \dot{\vec{\mathbf{x}}} \\ \int y\mathrm{d}t \end{Bmatrix} .$$

The new state-space equations are

$$\begin{aligned} \dot{\vec{\mathbf{v}}} &= \underline{\underline{\mathbf{A}}}_{cl}\vec{\mathbf{v}} + \vec{\mathbf{B}}_{cl}u \\ g &= \vec{\mathbf{C}}_{cl}\vec{\mathbf{v}} + D_{cl}u \ . \end{aligned} \tag{4.71}$$

The next issue that needs to be addressed is how integral feedback affects the base and equipment equations. Let's assume that the gain due to integral control is $K_I$ and the integrator will add a term $K_I \int y(t)\mathrm{d}t$ to equation (4.51a) and equation (4.51b). If the same procedure is used to get to the system matrix equations, the effect of integral control is to add a vector $\vec{\mathbf{T}}$ to the right hand side of equation (4.54) where $\vec{\mathbf{T}}$ is

$$\vec{\mathbf{T}} = K_I \begin{Bmatrix} \Phi_1(x_i) \\ \Phi_2(x_i) \\ \vdots \\ \Phi_n(x_i) \\ -1 \end{Bmatrix} \int y(t)\mathrm{d}t \ .$$

Therefore, the addition of integral control will have two major effects on the state-space equations in equation (4.58). First, it will add a new state $\int y(t)\mathrm{d}t$ resulting in the new states $\vec{\mathbf{v}}$. Second, integral control will also affect the matrices $\underline{\underline{\mathbf{A}}}, \vec{\mathbf{B}}, \vec{\mathbf{C}}_{ss}$, and $D$ in the state-space equations. The matrix $\underline{\underline{\mathbf{A}}}$ will be adjusted by the two vectors $\vec{\mathbf{T}}$ and $\vec{\mathbf{G}}$, where $\vec{\mathbf{T}}$ is given above and $\vec{\mathbf{G}}$ is

$$\vec{\mathbf{G}} = \begin{Bmatrix} 0_1 & 0 & 0 & \dots & 0_n & 1 \end{Bmatrix} \ .$$

The new closed-loop matrix $\underline{\underline{\mathbf{A}}}_{cl}$ is

$$\underline{\underline{\mathbf{A}}}_{cl} = \begin{bmatrix} \underline{\underline{\mathbf{0}}} & \underline{\underline{\mathbf{I}}} & \vec{\mathbf{0}} \\ -\underline{\underline{\mathbf{M}}}^{-1}\underline{\underline{\mathbf{K}}} & -\underline{\underline{\mathbf{M}}}^{-1}\underline{\underline{\mathbf{C}}} & \underline{\underline{\mathbf{M}}}^{-1}\vec{\mathbf{T}} \\ \vec{\mathbf{G}} & \vec{\mathbf{0}} & 0 \end{bmatrix}$$

where $\underline{\underline{\mathbf{K}}}$ and $\underline{\underline{\mathbf{C}}}$ incorporate the changes due to $\mathcal{PD}$ control. The vectors, $\vec{\mathbf{B}}_{cl}$ and $\vec{\mathbf{C}}_{cl}$, are

$$\vec{\mathbf{B}}_{cl} = \begin{Bmatrix} \vec{\mathbf{B}} \\ 0 \end{Bmatrix} = \begin{Bmatrix} \vec{\mathbf{0}} \\ \vec{\mathbf{Q}}_s \\ 0 \end{Bmatrix} \qquad \vec{\mathbf{C}}_{cl} = \begin{Bmatrix} \vec{\mathbf{C}}_{ss} & 0 \end{Bmatrix} \ ,$$

and the term $D_{cl}$ is equivalent to $D$, i.e., $D_{cl} = 0$.

### 4.7.3 Positive Position Feedback Control

Higher-order controllers such as a second-order controller are implemented easily in the transfer function synthesis as well. An example of a second-order controller is the positive position feedback (PPF) controller. The premise for this type of controller is to use a portion of the filter position coordinate ($g\omega^2\eta$) as feedback to the structure [50, 51]. The PPF compensator takes on the form

$$\ddot{\eta} + 2\zeta_f\omega_f\dot{\eta} + \omega_f^2\eta = \omega_f^2\xi$$

where $\xi$ is the modal coordinate, $\eta$ is the filter coordinate, $\omega_f$ is the filter frequency, and $\zeta_f$ is the filter damping ratio. For the FBRE system, it is assumed that the position of the rigid equipment will be sent to the compensator. Note that the modal coordinate will not be sent but the actual position of the equipment. This will not significantly affect the results as will be shown in Chapter 5.

#### 4.7.3.1 Frequency Response

The equations of motion for the equipment and active isolator using PPF control in the Laplace domain are

$$\begin{aligned} ms^2Y(s) &= -(k_p + c_ps)[Y(s) - W(x_i, s)] - g\omega^2\eta(s) + F_m(s) \\ \eta(s) &= \frac{\omega_f^2 Y(s)}{s^2 + 2\zeta_f\omega_f s + \omega_f^2} \ . \end{aligned}$$

Combining the above equations, the displacement of the equipment is

$$Y(s) = \frac{k_p + c_ps}{\text{den}}W(x_i, s) + \frac{F_m(s)}{D(s)} \tag{4.72a}$$

$$D(s) = ms^2 + c_ps + k_p + \frac{g\omega^2\omega_f^2}{s^2 + 2\zeta_f\omega_f s + \omega_f^2} \ . \tag{4.72b}$$

The force on the base due to the actuator is

$$f_c(s) = \frac{-ms^2(k_p + c_ps)}{D(s)}W(x_i, s) + \frac{k_p + c_ps + \frac{g\omega^2\omega_f^2}{s^2+2\zeta_f\omega_f s+\omega_f^2}}{D(s)}F_m(s) \tag{4.73}$$

and the constraint matrix $\underline{\underline{\mathbf{C}}}_l(s)$ is

$$\underline{\underline{\mathbf{C}}}_l(s) = \begin{bmatrix} 0 & 0 \\ \frac{ms^2(c_ps+k_p)}{D(s)} & 0 \end{bmatrix} \ . \tag{4.74}$$

The additional forcing term due to the controller is

$$\vec{\mathbf{q}}_l(s) = \left\{ \begin{array}{c} 0 \\ \frac{k_p + c_p s + \frac{g\omega^2\omega_f^2}{s^2+2\zeta_f\omega_f s+\omega_f^2}}{D(s)} F_m(s) \end{array} \right\} . \tag{4.75}$$

#### 4.7.3.2 Time Response

Like $\mathcal{PID}$ control, PPF control uses the results obtained in Section 4.7.1.2. The PPF filter will change the dynamic system matrices in equation (4.54) by adding a new state, the filter position $\eta$ to $\vec{\mathbf{x}}$. If equipment feedback is used, the new dynamic matrix equation is

$$\underline{\underline{\mathbf{M}}}_{ppf}\ddot{\vec{\mathbf{x}}}(t) + \underline{\underline{\mathbf{C}}}_{ppf}\dot{\vec{\mathbf{x}}}(t) + \underline{\underline{\mathbf{K}}}_{ppf}\vec{\mathbf{x}}(t) = \vec{\mathbf{Q}}_{ppf}(t) . \tag{4.76}$$

The values for each term in this equation are

$$\vec{\mathbf{x}}(t) = \left\{ \begin{array}{c} q_1(t) \\ q_2(t) \\ \vdots \\ q_n(t) \\ y(t) \\ \eta(t) \end{array} \right\} \qquad \underline{\underline{\mathbf{M}}}_{ppf} = \begin{bmatrix} M_{s,r} & M_{s,n+1} & \vec{\mathbf{0}} \\ M_{n+1,r} & M_{n+1,n+1} & 0 \\ \vec{\mathbf{0}} & 0 & 1 \end{bmatrix} \qquad \vec{\mathbf{Q}}_{ppf} = \left\{ \begin{array}{c} Q_1(t) \\ Q_2(t) \\ \vdots \\ Q_n(t) \\ F_y(t) \\ 0 \end{array} \right\}$$

$$\underline{\underline{\mathbf{C}}}_{ppf} = \begin{bmatrix} C_{s,r} & C_{s,n+1} & \vec{\mathbf{0}} \\ C_{n+1,r} & C_{n+1,n+1} & 0 \\ \vec{\mathbf{0}} & 0 & 2\zeta_f\omega_f \end{bmatrix} \qquad \underline{\underline{\mathbf{K}}}_{ppf} = \begin{bmatrix} K_{s,r} & K_{s,n+1} & -g\omega^2\Phi_s(x_i) \\ K_{n+1,r} & K_{n+1,n+1} & g\omega^2 \\ \vec{\mathbf{0}} & -\omega_f^2 & \omega_f^2 \end{bmatrix} .$$

The terms in $M_{ppf}$, $C_{ppf}$, and $K_{ppf}$ are given by equation (4.55), equation (4.57), and equation (4.56), respectively. Note that $\omega_f$ and $\zeta_f$ are the filter frequency and damping ratio, respectively. The solution for this equation is solved exactly like the passive system; the above equations are cast into the state space given by equation (4.58) and equation (4.59). The new vector $\vec{\mathbf{C}}_{ss}$ for PPF control is

$$\vec{\mathbf{C}}_{ss} = \left\{ 0_1 \quad \ldots \quad 0_n \quad 1 \quad \boxed{0} \quad 0_1 \quad \ldots \quad 0_n \quad 0 \quad \boxed{0} \right\}$$

where the boxed values are due to the addition of the new state $\eta$.

### 4.7.4 LQG Control

The previous paragraphs looked at very simple control methodologies, and this section will look at an optimal solution to the isolation problem for the flexible base, rigid

equipment system. Since it is quite difficult to measure every state of this system, an optimal (Kalman-Bucy) estimator will be designed. It is also assumed that a model of the disturbance source will be known so that a shaping filter will be used.

It should be noted that LQG control cannot be directly implemented in the TFS method. However, an accurate approximate system can be determined through modal expansion. Remember that the actual system eigenfunctions can be determined and will be used in the expansion.

#### 4.7.4.1 Frequency Response

The design methodology for LQG compensation is thoroughly discussed in Section 2.2.2. The development of the state-space matrices for the passive system is given in Section 4.7.1.2 and the $\underline{\underline{\mathbf{A}}}$, $\vec{\mathbf{B}}$, $\vec{\mathbf{C}}$, and $D$ matrices are used to build the optimal estimator and regulator. The number of modes to formulate these matrices are determined by making sure the natural frequencies of the first eight modes are within 0.1% of the actual values. Since the exact eigenfunctions of the FBRE system can be found, the number of modes needed for the given criteria should be only eight. For convenience, the state-space representation for the optimal control problem is

$$\begin{aligned}\dot{\vec{\mathbf{x}}} &= \underline{\underline{\mathbf{A}}}\vec{\mathbf{x}} + \vec{\mathbf{B}}u + \vec{\mathbf{F}}\xi \\ y &= \vec{\mathbf{C}}\vec{\mathbf{x}} + \eta \ ,\end{aligned}$$

where $\underline{\underline{\mathbf{A}}}$, $\vec{\mathbf{B}}$, and $\vec{\mathbf{C}}$ are defined in equation (4.59) and equation (4.60). Note that $\vec{\mathbf{B}}$ in equation (4.59) is actually $\vec{\mathbf{F}}$ in the above equation. $\vec{\mathbf{B}}$ is formulated by the following equation

$$\vec{\mathbf{B}} = \begin{Bmatrix} \vec{\mathbf{0}} \\ \underline{\underline{\mathbf{M}}}^{-1}\vec{\mathbf{R}} \end{Bmatrix} \tag{4.77}$$

where

$$\vec{\mathbf{R}} = \begin{Bmatrix} \Phi_1(x_i) & \cdots & \Phi_n(x_i) & -1 \end{Bmatrix}^T \ . \tag{4.78}$$

#### 4.7.4.2 Time Response

The transient response for the LQG control will be implemented by using the state-space design implemented above. By using the procedure as outlined in Section 2.2.2 and specifically equation (2.22), the transient response due to any input can be calculated.

## 4.8 Active Isolation for FBFE System

Section 4.6.3 describes the situation when two subsystems are connected at a single point by some mechanism. This mechanism can take the form of a passive or an active isolator. The next sections describe the mechanism terms in equation (4.50) for a passive isolator and several active isolation systems. The active isolator is placed parallel to the passive isolator; therefore, the passive isolation system will be described first. The active isolator system will implement the same control methodologies as described in Section 4.7 for the FBRE system, i.e., $\mathcal{PID}$ control, PPF control, and LQG control.

### 4.8.1 Passive Isolation, No Active Control

Figure 4.4 is a generic figure for two subsystems connected by some mechanism C. For passive isolation, the mechanism C will consist of a massless spring of stiffness $k_p$ and a damper with a damping coefficient $c_p$. The displacement of the equipment at node $j$ in local coordinates is $W_j(x_j, s)$ and the displacement of the base at node $l$ in local coordinates is $W_l(x_l, s)$.

#### 4.8.1.1 Frequency Response

As mentioned in the previous paragraph, the isolator consists of a massless spring and viscous damper. The forces on the equipment (top beam) at node $j$ and the base (bottom beam) at node $l$ are

$$\begin{aligned} Q_j(s) &= -(k_p + c_p s)[W_j(x_j, s) - W_l(x_l, s)] \\ Q_l(s) &= (k_p + c_p s)[W_j(x_j, s) - W_l(x_l, s)] \ . \end{aligned}$$

Realizing that the global nodal displacements are $\vec{\mathbf{u}}_k = \left\{ W_k(x_k, s) \quad \frac{\partial W_k(x_k,s)}{\partial x} \right\}^T$, the matrices in equation (4.50) are

$$\begin{aligned} \underline{\underline{\mathbf{C}}}_{jj} &= \underline{\underline{\mathbf{C}}}_{ll} = \begin{bmatrix} 0 & 0 \\ k_p + c_p s & 0 \end{bmatrix} \\ \underline{\underline{\mathbf{C}}}_{jl} &= \underline{\underline{\mathbf{C}}}_{lj} = \begin{bmatrix} 0 & 0 \\ -(k_p + c_p s) & 0 \end{bmatrix} \ . \end{aligned} \tag{4.79}$$

#### 4.8.1.2 Time Response

For the following time responses, there are no assumptions made on each distributed system such as boundary conditions, length of each subsystem, or material properties. The

only assumption for the beams is that the damping in each distributed system will be modeled as proportional damping. Therefore, the governing equations of motion are

$$\begin{aligned}-E^bI^b\frac{\partial^4 w(x_b,t)}{\partial {x_b}^4}+f^b(x_b,t)+k_p\left\{y(x,t)-w(x,t)\right\}\delta(x-x_i)-\rho^b\gamma^b\frac{\partial w(x_b,t)}{\partial t}\\ -\beta^bE^bI^b\frac{\partial^5 w(x_b,t)}{\partial x_b^4\partial t}+c_p[\dot{y}(x,t)-\dot{w}(x,t)]\delta(x-x_i)=\rho^b\frac{\partial^2 w(x_b,t)}{\partial t^2}\end{aligned} \tag{4.80a}$$

$$\begin{aligned}-E^eI^e\frac{\partial^4 y(x_e,t)}{\partial {x_e}^4}+f^e(x_e,t)-k_p\left\{y(x,t)-w(x,t)\right\}\delta(x-x_i)-\rho^e\gamma^e\frac{\partial y(x_e,t)}{\partial t}\\ -\beta^eE^eI^e\frac{\partial^5 y(x_e,t)}{\partial x_e^4\partial t}-c_p[\dot{y}(x,t)-\dot{w}(x,t)]\delta(x-x_i)=\rho^e\frac{\partial^2 y(x_e,t)}{\partial t^2}\end{aligned} \tag{4.80b}$$

where $w(x_b,t)$ is the deflection of the base at the location $x_b$ on the base and $y(x_e,t)$ is the deflection of the equipment at the location $x_e$ along the equipment. Equation (4.80a) is valid over the domain, $\mathcal{D}:0<x_b<1$, where $x_b$ is the position on the base and the length of the base is nondimensional. Equation (4.80b) is valid over the domain, $\mathcal{D}:0<x_e<1$, where $x_e$ is the position on the equipment and the length of the equipment is nondimensional. The base and equipment displacement can be expanded in modal form as

$$w(x_b,t)=\sum_{r=1}^{\infty}V_r^b(x_b)q_r^b(t)\approx\sum_{r=1}^{\infty}\Phi_r^b(x_b)q_r^b(t) \tag{4.81a}$$

$$y(x_e,t)=\sum_{t=1}^{\infty}V_t^e(x_e)q_t^e(t)\approx\sum_{t=1}^{\infty}\Phi_t^e(x_e)q_t^e(t)\ , \tag{4.81b}$$

respectively. $V_r^b(x_b)$ and $V_t^e(x_e)$ are the eigenfunctions for the base and equipment, respectively. Since the eigenfunctions are piecewise continuous at the isolator attachment point, the higher derivatives of the eigenfunctions are discontinuous. Therefore, the actual eigenfunctions are approximated by the continuous functions $\Phi_r^b(x_b)$ and $\Phi_t^e(x_e)$. Substituting equation (4.81a) and equation (4.81b) into equation (4.80a) and equation (4.80b) leads to the following equations where the repeated indices in $r$ and $t$ imply a summation.

$$\begin{aligned}&-E^bI^bq_r^b(t)\frac{\mathrm{d}^4\Phi_r^b(x_b)}{\mathrm{d}{x_b}^4}+f^b(x_b,t)-\dot{q}_r^b\left[\rho^b\gamma^b+\beta^bE^bI^b\frac{\mathrm{d}^4}{\mathrm{d}{x_b}^4}\right]\Phi_r^b(x_b)+k_p[q_t^e(t)\Phi_t^e(x_i)\\ &-q_r^b(t)\Phi_r^b(x_i)]+c_p\left[\dot{q}_t^e(t)\Phi_t^e(x_i)-\dot{q}_r^b(t)\Phi_r^b(x_i)\right]=\rho^b\Phi_r^b(x_b)\ddot{q}_r^b(t)\end{aligned} \tag{4.82a}$$

$$\begin{aligned}&-E^eI^eq_t^e(t)\frac{\mathrm{d}^4\Phi_t^e(x_e)}{\mathrm{d}{x_e}^4}+f^e(x_e,t)-\dot{q}_t^e\left[\rho^e\gamma^e+\beta^eE^eI^e\frac{\mathrm{d}^4}{\mathrm{d}{x_e}^4}\right]\Phi_t^e(x_e)-\\ &k_p[q_t^e(t)\Phi_t^e(x_i)-q_r^b(t)\Phi_r^b(x_i)]-c_p\left[\dot{q}_t^e(t)\Phi_t^e(x_i)-\dot{q}_r^b(t)\Phi_r^b(x_i)\right]=\rho^e\Phi_t^e(x_e)\ddot{q}_t^e(t)\end{aligned} \tag{4.82b}$$

Note that $x_i$ is the location of the isolator and is a fixed quantity while $x_e$ and $x_b$ are variables for the equipment and base, respectively. Multiply equation (4.82a) and equation (4.82b) by $\Phi_u^b(x_b)$ and $\Phi_v^e(x_e)$, respectively, and then integrate over the beam and equipment domains leads to the following equations.

$$\begin{aligned}
&- q_r^b(t)\int_0^1 \Phi_u^b(x_b)E^bI^b\frac{\mathrm{d}^4\Phi_r^b(x_b)}{\mathrm{d}{x_b}^4}\mathrm{d}x_b + \int_0^1 \Phi_u^b(x_b)f(x_b,t)\mathrm{d}x_b \\
&- \dot{q}_r^b(t)\int_0^1 \rho^b\gamma^b\Phi_u^b(x_b)\Phi_r^b(x_b)\mathrm{d}x_b - \dot{q}_r^b(t)\int_0^1 \beta^bE^bI^b\Phi_u^b(x_b)\frac{\mathrm{d}^4\Phi_r^b(x_b)}{\mathrm{d}{x_b}^4}\mathrm{d}x_b \\
&+ k_p\left[q_t^e(t)\Phi_u^b(x_i)\Phi_t^e(x_i) - q_r^b(t)\Phi_u^b(x_i)\Phi_r^b(x_i)\right] \\
&+ c_p\left[\dot{q}_t^e(t)\Phi_u^b(x_i)\Phi_t^e(x_i) - \dot{q}_r^b(t)\Phi_u^b(x_i)\Phi_r^b(x_i)\right] = \ddot{q}_r^b(t)\int_0^1 \rho^b\Phi_u^b(x_b)\Phi_r^b(x_b)\mathrm{d}x_b
\end{aligned} \tag{4.83a}$$

$$\begin{aligned}
&- q_t^e(t)\int_0^1 \Phi_v^e(x_e)E^eI^e\frac{\mathrm{d}^4\Phi_t^e(x_e)}{\mathrm{d}{x_e}^4}\mathrm{d}x_e + \int_0^1 \Phi_v^e(x_e)f(x_e,t)\mathrm{d}x_e \\
&- \dot{q}_t^e(t)\int_0^1 \rho^e\gamma^e\Phi_v^e(x_e)\Phi_t^e(x_e)\mathrm{d}x_e - \dot{q}_t^e(t)\int_0^1 \beta^eE^eI^e\Phi_v^e(x_e)\frac{\mathrm{d}^4\Phi_t^e(x_e)}{\mathrm{d}{x_e}^4}\mathrm{d}x_e \\
&- k_p\left[q_t^e(t)\Phi_v^e(x_i)\Phi_t^e(x_i) - q_r^b(t)\Phi_v^e(x_i)\Phi_r^b(x_i)\right] \\
&- c_p\left[\dot{q}_t^e(t)\Phi_v^e(x_i)\Phi_t^e(x_i) - \dot{q}_r^b(t)\Phi_v^e(x_i)\Phi_r^b(x_i)\right] = \ddot{q}_t^e(t)\int_0^1 \rho^e\Phi_v^e(x_e)\Phi_t^e(x_e)\mathrm{d}x_e
\end{aligned} \tag{4.83b}$$

If the number of modes are finite, that is $r, u = 1, 2, \ldots, m$ and $t, v = 1, 2, \ldots, n$, the above equations can be recast into a system of matrix equations:

$$\underline{\underline{\mathbf{M}}}\ddot{\vec{\mathbf{x}}}(t) + \underline{\underline{\mathbf{C}}}\dot{\vec{\mathbf{x}}}(t) + \underline{\underline{\mathbf{K}}}\vec{\mathbf{x}}(t) = \vec{\mathbf{Q}}(t)\ , \tag{4.84}$$

where

$$\vec{\mathbf{x}} = \begin{Bmatrix} q_1^b(t) \\ \vdots \\ q_m^b(t) \\ q_1^e(t) \\ \vdots \\ q_n^e(t) \end{Bmatrix} \qquad \underline{\underline{\mathbf{M}}} = \begin{bmatrix} M_{u,r} & \underline{\underline{\mathbf{0}}} \\ \underline{\underline{\mathbf{0}}} & M_{v,t} \end{bmatrix} \qquad \underline{\underline{\mathbf{C}}} = \begin{bmatrix} C_{u,r} & C_{u,t} \\ C_{v,r} & C_{v,t} \end{bmatrix} \tag{4.85}$$

$$\underline{\underline{\mathbf{K}}} = \begin{bmatrix} K_{u,r} & K_{u,t} \\ K_{v,r} & K_{v,t} \end{bmatrix} \qquad \vec{\mathbf{Q}} = \begin{Bmatrix} Q_1^b(t) & \cdots & Q_m^b(t) & Q_1^e(t) & \cdots & Q_n^e(t) \end{Bmatrix}^T . \tag{4.86}$$

The components of the mass matrix $\underline{\underline{\mathbf{M}}}$ are

$$
\begin{aligned}
M_{u,r} &= \int_0^1 \rho^b \Phi_r^b(x_b)\Phi_u^b(x_b)\mathrm{d}x_b \\
M_{v,t} &= \int_0^1 \rho^e \Phi_t^e(x_e)\Phi_v^e(x_e)\mathrm{d}x_e \ .
\end{aligned}
\tag{4.87}
$$

The components of the damping matrix $\underline{\underline{\mathbf{C}}}$ are

$$
\begin{aligned}
C_{u,r} &= \int_0^1 \left[\rho^b\gamma^b\Phi_u^b(x_b)\Phi_r^b(x_b) + \beta^b E^b I^b \Phi_u^b(x_b)\frac{\mathrm{d}^4\Phi_r^b(x_b)}{\mathrm{d}{x_b}^4}\right]\mathrm{d}x_b + c_p\Phi_u^b(x_i)\Phi_r^b(x_i) \\
C_{u,t} &= -c_p\Phi_u^b(x_i)\Phi_t^e(x_i) \\
C_{v,r} &= -c_p\Phi_v^e(x_i)\Phi_r^b(x_i) \\
C_{v,t} &= \int_0^1 \left[\rho^e\gamma^e\Phi_v^e(x_e)\Phi_t^e(x_e) + \beta^e E^e I^e \Phi_v^e(x_e)\frac{\mathrm{d}^4\Phi_t^e(x_e)}{\mathrm{d}{x_e}^4}\right]\mathrm{d}x_e + c_p\Phi_v^e(x_i)\Phi_t^e(x_i) \ .
\end{aligned}
\tag{4.88}
$$

The components of the stiffness matrix $\underline{\underline{\mathbf{K}}}$ are

$$
\begin{aligned}
K_{u,r} &= \int_0^1 E^b I^b \Phi_u^b(x_b)\frac{\mathrm{d}^4\Phi_r^b(x_b)}{\mathrm{d}{x_b}^4}\mathrm{d}x_b + k_p\Phi_u^b(x_i)\Phi_r^b(x_i) \\
K_{u,t} &= -k_p\Phi_u^b(x_i)\Phi_t^e(x_i) \\
K_{v,r} &= -k_p\Phi_v^e(x_i)\Phi_r^b(x_i) \\
K_{v,t} &= \int_0^1 E^e I^e \Phi_v^e(x_e)\frac{\mathrm{d}^4\Phi_t^e(x_e)}{\mathrm{d}{x_e}^4}\mathrm{d}x_e + k_p\Phi_v^e(x_i)\Phi_t^e(x_i) \ .
\end{aligned}
\tag{4.89}
$$

The components of the force vector $\vec{\mathbf{Q}}(t)$ are

$$
\begin{aligned}
Q_u^b &= \int_0^1 \Phi_u^b(x_b) f(x_b,t)\mathrm{d}x_b \\
Q_v^e &= \int_0^1 \Phi_v^e(x_e) f(x_e,t)\mathrm{d}x_e \ .
\end{aligned}
\tag{4.90}
$$

Similar to the FBRE system, the matrix equations can be recast into state space as given in equation (4.58) and equation (4.59).

### 4.8.2 Classical Control

This section will discuss the formulation of time and frequency responses using classical control techniques. The control law that will be discussed is a proportional-plus-integral-plus-derivative ($\mathcal{PID}$) controller. Proportional-plus-derivative ($\mathcal{PD}$) control has a similar implementation by setting the integral gain to zero.

#### 4.8.2.1 Frequency Response

Feedback for this system can occur at the base or the equipment. The forces on each subsystem using equipment feedback are

$$\begin{aligned} Q_j(s) &= -(k_p + c_p s)[W_j(x_j, s) - W_l(x_l, s)] - (K_P + K_D s + K_I/s)W_j(x_j, s) \\ Q_l(s) &= (k_p + c_p s)[W_j(x_j, s) - W_l(x_l, s)] + (K_P + K_D s + K_I/s)W_j(x_j, s) \ . \end{aligned}$$

Therefore, the $\underline{\underline{\mathbf{C}}}$ matrices for equipment feedback are

$$\begin{aligned} \underline{\underline{\mathbf{C}}}_{jj} &= \begin{bmatrix} 0 & 0 \\ k_p + c_p s + K_P + K_D s + K_I/s & 0 \end{bmatrix} & \underline{\underline{\mathbf{C}}}_{jl} &= \begin{bmatrix} 0 & 0 \\ -k_p - c_p s & 0 \end{bmatrix} \\ \underline{\underline{\mathbf{C}}}_{lj} &= \begin{bmatrix} 0 & 0 \\ -k_p - c_p s - K_P - K_D s - K_I/s & 0 \end{bmatrix} & \underline{\underline{\mathbf{C}}}_{ll} &= \begin{bmatrix} 0 & 0 \\ k_p + c_p s & 0 \end{bmatrix} \ . \end{aligned} \tag{4.91}$$

If feedback occurs from the base, the forces on each subsystem are

$$\begin{aligned} Q_j(s) &= -(k_p + c_p s)[W_j(x_j, s) - W_l(x_l, s)] + (K_P + K_D s + K_I/s)W_l(x_l, s) \\ Q_l(s) &= (k_p + c_p s)[W_j(x_j, s) - W_l(x_l, s)] - (K_P + K_D s + K_I/s)W_l(x_l, s) \ . \end{aligned}$$

From these equations, the $\underline{\underline{\mathbf{C}}}$ matrices are

$$\begin{aligned} \underline{\underline{\mathbf{C}}}_{jj} &= \begin{bmatrix} 0 & 0 \\ k_p + c_p s & 0 \end{bmatrix} & \underline{\underline{\mathbf{C}}}_{jl} &= \begin{bmatrix} 0 & 0 \\ -k_p - c_p s - K_P - K_D s - K_I/s & 0 \end{bmatrix} \\ \underline{\underline{\mathbf{C}}}_{lj} &= \begin{bmatrix} 0 & 0 \\ -k_p - c_p s & 0 \end{bmatrix} & \underline{\underline{\mathbf{C}}}_{ll} &= \begin{bmatrix} 0 & 0 \\ k_p + c_p s + K_P + K_D s + K_I/s & 0 \end{bmatrix} \ . \end{aligned} \tag{4.92}$$

#### 4.8.2.2 Time Response

The time response using $\mathcal{PID}$ control is similar to the one derived for the FBRE system. The $\mathcal{PD}$ part will affect the stiffness and damping matrix while the integral part will add more states to the system. Since the system is linear, the results of each individual part can be found separately and combined together.

For equipment feedback, the actuator force using $\mathcal{PD}$ control is

$$F_{act} = K_P y(x,t) + K_D y(x,t) \ .$$

The proportional gain $K_P$ will affect the terms $K_{u,t}$ and $K_{v,t}$ in the stiffness matrix. The new terms in equation (4.89) are

$$\begin{aligned} K_{u,t} &= -(K_P + k_p)\Phi_u^b(x_i)\Phi_t^e(x_i) \\ K_{v,t} &= (K_P + k_p)\Phi_v^e(x_i)\Phi_t^e(x_i) + \int_0^{L_e} EI^e \Phi_v^e(x_e) \frac{\mathrm{d}^4\Phi_t^e(x_e)}{\mathrm{d}{x_e}^4} \mathrm{d}x_e \ . \end{aligned} \tag{4.93}$$

The derivative gain $K_D$ will affect the terms $C_{u,t}$ and $C_{v,t}$ in the damping matrix. The terms in equation (4.88) are

$$\begin{aligned} C_{u,t} &= -(K_D + c_p)\Phi_u^b(x_i)\Phi_t^e(x_i) \\ C_{v,t} &= (K_D + c_p)\Phi_v^e(x_i)\Phi_t^e(x_i) \\ &\quad + \int_0^{L_e} \left[\rho^e\gamma^e\Phi_v^e(x_e)\Phi_t^e(x_e) + \beta^e EI^e\Phi_v^e(x_e)\frac{\mathrm{d}^4\Phi_t^e(x_e)}{\mathrm{d}{x_e}^4}\right]\mathrm{d}x_e \ . \end{aligned} \tag{4.94}$$

The integral part of $\mathcal{PID}$ control does not directly affect the dynamic matrix equation but adds integral states corresponding to the feedback location. The new states added to the FBFE system with equipment feedback are

$$K_I\delta(x_e - x_i)\int y(x_e,t)\mathrm{d}t = K_I\Phi_t^e(x_e)\delta(x_e - x_i)\int q_t^e(t)\mathrm{d}t \ , \tag{4.95}$$

where $K_I$ is the integral gain and $t = 1, 2, \ldots n$. The overall new states are

$$\vec{\mathbf{v}} = \begin{Bmatrix} \vec{\mathbf{z}} \\ \int q_t^e(t)\mathrm{d}t \end{Bmatrix} = \begin{Bmatrix} \vec{\mathbf{x}} \\ \dot{\vec{\mathbf{x}}} \\ \int q_t^e(t)\mathrm{d}t \end{Bmatrix} \tag{4.96}$$

with the new state-space equations given below.

$$\dot{\vec{\mathbf{v}}} = \underline{\underline{\mathbf{A}}}_{cl}\vec{\mathbf{v}} + \vec{\mathbf{B}}_{cl}u \tag{4.97}$$

$$g = \vec{\mathbf{C}}_{cl}\vec{\mathbf{v}} + D_{cl}u \tag{4.98}$$

The new closed-loop matrix is

$$\underline{\underline{\mathbf{A}}}_{cl} = \begin{bmatrix} \underline{\underline{\mathbf{0}}} & \underline{\underline{\mathbf{I}}} & \underline{\underline{\mathbf{0}}} \\ -\underline{\underline{\mathbf{M}}}^{-1}\underline{\underline{\mathbf{K}}} & -\underline{\underline{\mathbf{M}}}^{-1}\underline{\underline{\mathbf{C}}} & \underline{\underline{\mathbf{M}}}^{-1}\underline{\underline{\mathbf{T}}} \\ \underline{\underline{\mathbf{G}}} & \underline{\underline{\mathbf{0}}} & \underline{\underline{\mathbf{0}}} \end{bmatrix} \tag{4.99}$$

where $\underline{\underline{\mathbf{K}}}$ and $\underline{\underline{\mathbf{C}}}$ incorporate the changes due to $\mathcal{PD}$ control. The matrices $\underline{\underline{\mathbf{T}}}$ and $\underline{\underline{\mathbf{G}}}$ are

$$\underline{\underline{\mathbf{T}}} = K_I \begin{bmatrix} \Phi_1^b(x_i)\Phi_t^e(x_i) \\ \vdots \\ \Phi_m^b(x_i)\Phi_t^e(x_i) \\ -\Phi_1^e(x_i)\Phi_t^e(x_i) \\ \vdots \\ -\Phi_n^e(x_i)\Phi_t^e(x_i) \end{bmatrix} \tag{4.100}$$

and

$$\underline{\underline{\mathbf{G}}} = \begin{bmatrix} \underline{\underline{\mathbf{0}}} & \underline{\underline{\mathbf{I}}} \end{bmatrix} \ , \tag{4.101}$$

where $\underline{\underline{\mathbf{0}}}$ is an [n,m] matrix of zeros and $\underline{\underline{\mathbf{I}}}$ is an [n,n] identity matrix.

### 4.8.3 PPF Control

A higher-order controller such as the positive position feedback (PPF) controller can be used to attenuate the transmissibility at a specific mode. The premise of the PPF controller is to send a portion of the filter position coordinate, specifically $g\omega^2\eta$ to the structure [50, 51]. The PPF compensator takes on the form

$$\ddot{\eta} + 2\zeta_f\omega_f\dot{\eta} + \omega_f^2\eta = \omega_f^2\xi$$

where $\xi$ is the modal coordinate, $\eta$ is the filter coordinate, $\omega_f$ is the filter frequency and $\zeta_f$ is the filter damping ratio. For the FBFE system, it is assumed that the position of the equipment will be sent to the compensator. Note that the modal coordinate will not be sent but the actual position of the equipment and this will not significantly affect the results as shown in Chapter 6.

#### 4.8.3.1 Frequency Response

For PPF control, the forces on each subsystem which includes the forces from the passive isolator are

$$\begin{aligned} Q_j(s) &= -(k_p + c_p s)[W_j(x_j, s) - W_l(x_l, s)] - \frac{g\omega^2\omega_f^2}{s^2 + 2\zeta_f\omega_f s + \omega_f^2} W_j(x_j, s) \\ Q_l(s) &= (k_p + c_p s)[W_j(x_j, s) - W_l(x_l, s)] + \frac{g\omega^2\omega_f^2}{s^2 + 2\zeta_f\omega_f s + \omega_f^2} W_j(x_j, s) \ . \end{aligned}$$

Therefore, the elements of the $\underline{\underline{\mathbf{C}}}$ matrix are

$$\begin{aligned} \underline{\underline{\mathbf{C}}}_{jj} &= \begin{bmatrix} 0 & 0 \\ k_p + c_p s + \frac{g\omega^2\omega_f^2}{s^2+2\zeta_f\omega_f s+\omega_f^2} & 0 \end{bmatrix} & \underline{\underline{\mathbf{C}}}_{jl} &= \begin{bmatrix} 0 & 0 \\ -k_p - c_p s & 0 \end{bmatrix} \\ \underline{\underline{\mathbf{C}}}_{lj} &= \begin{bmatrix} 0 & 0 \\ -k_p - c_p s - \frac{g\omega^2\omega_f^2}{s^2+2\zeta_f\omega_f s+\omega_f^2} & 0 \end{bmatrix} & \underline{\underline{\mathbf{C}}}_{ll} &= \begin{bmatrix} 0 & 0 \\ k_p + c_p s & 0 \end{bmatrix} \ . \end{aligned} \tag{4.102}$$

#### 4.8.3.2 Time Response

The PPF time response uses the dynamic matrix equation obtained in Section 4.8.1.2. The PPF filter changes the matrix equation by adding a new state to the system, the filter position $\eta(t)$. The dynamic matrix equation is now

$$\underline{\underline{\mathbf{M}}}_{ppf}\ddot{\vec{\mathbf{x}}}(t) + \underline{\underline{\mathbf{C}}}_{ppf}\dot{\vec{\mathbf{x}}}(t) + \underline{\underline{\mathbf{K}}}_{ppf}\vec{\mathbf{x}}(t) = \vec{\mathbf{Q}}_{ppf}(t) \ , \tag{4.103}$$

where

$$\vec{\mathbf{x}}(t) = \begin{Bmatrix} q_1^b(t) \\ \vdots \\ q_m^b(t) \\ q_1^e(t) \\ \vdots \\ q_m^e(t) \\ \eta(t) \end{Bmatrix} \qquad \underline{\underline{\mathbf{M}}}_{ppf} = \begin{bmatrix} M_{u,r} & \underline{\underline{\mathbf{0}}} & \vec{\mathbf{0}} \\ \underline{\underline{\mathbf{0}}} & M_{v,t} & 0 \\ \vec{\mathbf{0}} & 0 & 1 \end{bmatrix} \qquad \vec{\mathbf{Q}}_{ppf} = \begin{Bmatrix} Q_1^b(t) \\ \vdots \\ Q_m^b(t) \\ Q_1^e(t) \\ \vdots \\ Q_n^e(t) \\ 0 \end{Bmatrix}$$

$$\underline{\underline{\mathbf{C}}}_{ppf} = \begin{bmatrix} C_{u,r} & C_{u,t} & \vec{\mathbf{0}} \\ C_{v,r} & C_{v,t} & \vec{\mathbf{0}} \\ \vec{\mathbf{0}} & \vec{\mathbf{0}} & 2\zeta_f\omega_f \end{bmatrix} \qquad \underline{\underline{\mathbf{K}}}_{ppf} = \begin{bmatrix} K_{u,r} & K_{u,t} & -g\omega^2\Phi_u^b(x_i) \\ K_{v,r} & K_{v,t} & g\omega^2\Phi_v^e(x_i) \\ \vec{\mathbf{0}} & -\omega_f^2\Phi_t^e(x_i) & \omega_f^2 \end{bmatrix} .$$

### 4.8.4 LQG Control

Unlike the previous control strategies, the linear quadratic Gaussian (LQG) regulator is a more complicated control architecture. This controller will implement an optimal regulator and Kalman-Bucy (optimal) filter. The estimator is necessary since all the states are not directly measurable. A detailed discussion of the LQG controller can be found in the references [45, 47].

#### 4.8.4.1 Frequency Response

The design methodology for LQG control is given in Section 2.2.2. To apply LQG control, the state-space matrices must be formed for the FBFE system. These matrices are derived in Section 4.8.1.2 and will be used to find the optimal gains for the regulator and the estimator. The number of modes to obtain these matrices will be determined by making sure the natural frequencies of the first eight modes are within 0.1% of the actual values. Similar to the FBRE system, the vector $\vec{\mathbf{B}}$ is actually $\vec{\mathbf{F}}$ and the vector $\vec{\mathbf{B}}$ is

$$\vec{\mathbf{B}} = \begin{Bmatrix} \vec{\mathbf{0}} \\ \underline{\underline{\mathbf{M}}}^{-1}\vec{\mathbf{R}} \end{Bmatrix} \tag{4.104}$$

where

$$\vec{\mathbf{R}} = \begin{Bmatrix} \Phi_1^b(x_i) & \cdots & \Phi_m^b(x_i) & \Phi_1^e(x_i) & \cdots & \Phi_n^e(x_i) \end{Bmatrix}^T. \tag{4.105}$$

#### 4.8.4.2 Time Response

The transient or time response will be determined by the state-space matrices that are formulated in the frequency response section. By using the procedure as outlined in Section 2.2.2 and specifically equation (2.22), the transient response due to any input can be calculated.

## 4.9 Experimental Verification

To verify the transfer function synthesis method, a cantilever beam experiment was conducted. An aluminum beam with clamped-free boundary conditions was attached to a shaker at the system's clamped end as shown in Figure 4.6. Two accelerometers were used to take data: one placed at the cantilevered end (input measurement) and the other placed a third of the distance along the beam from the cantilevered end (output measurement).

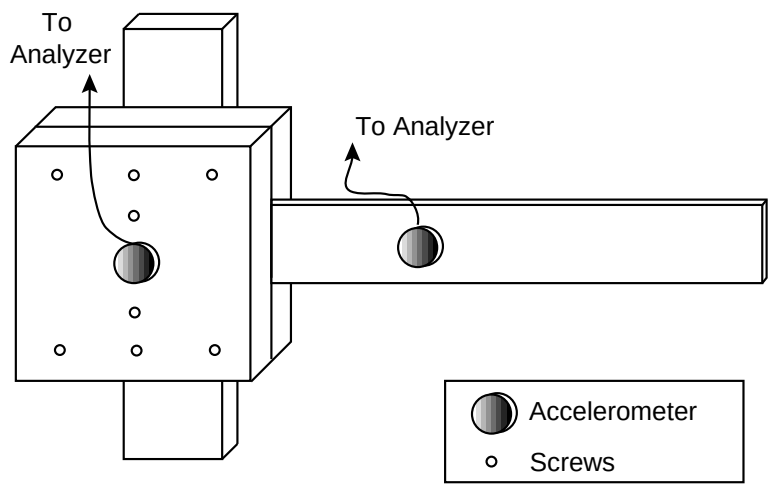


Figure 4.6: Experimental Setup

The dimensions and material properties for the aluminum beam are given in Table 4.1. The accelerometers were both manufactured by Kistler but different accelerometer models were used. The accelerometer on the beam had a higher sensitivity and could measure both transverse and rotational displacement. The pertinent parameters for the Kistler accelerometer attached to the beam are given in Table 4.2. Since the accelerometer wire was permanently attached to the accelerometer, the mass of the accelerometer could not be determined exactly. Also, only a portion of the accelerometer wire was attached along the beam and this mass has to be approximated.

Each experimental test used a 300 mV chirp signal as an input to the clamped end. A chirp signal was used over a random signal since the coherence was significantly better.

Table 4.1: Beam Parameters

| | |
|---|---|
| Modulus | 72x$10^9$ Pa |
| Density | 2800 kg/$m^3$ |
| thickness | .0625 in |
| width | 1.5 in |
| length | 10 in |

Table 4.2: Accelerometer Parameters

| | |
|---|---|
| mass of accel. | $\approx$ 11.798 gm |
| mass of wire | $\approx$ 2.0 gm |
| height | $0.41\overline{666}$ in |
| radius | $0.\overline{66666}$ in |
| MOI | 1.5403x$10^{-6}$ |

Fifty averages were taken over a frequency range of 10-1000 Hz and any data that caused an overload on the input or output was neglected.

### 4.9.1 Analytical Model without Damping

Three different models without damping using Yang's method were compared to the experimental transfer function. The first model does not account for the mass or inertia of the accelerometer, the second model accounts for the mass but not the inertia, and the third model accounts for both the mass and inertia of the accelerometer.

The comparison of analytical and experimental results for the first model are shown in Figure 4.7. As seen from this figure, the first mode from the analytical model is relatively close to the first mode from the experiment, approximately a 3% error. However, the next three frequencies from the analytical model have errors ranging from 10-20% compared to the frequencies obtained from the experiment.

Large errors in the higher modes of the first model occur because the mass of the accelerometer and the mass of the wire on the beam were neglected. These masses cannot be neglected since the mass of the accelerometer plus the wire is about one-fourth the mass of the beam. Therefore, the second model includes the mass of the accelerometer and wire. The mass of the wire that was actually attached to the beam was assumed to weigh about two grams. The results of this new model are shown in Figure 4.8 and this model matches the higher modes very closely. However, the fourth mode still shows significant errors. This can be attributed to the fact as the beam bends, the accelerometer is rotating. Therefore, the inertia of the accelerometer should be included in the model as well.

The third model includes the rotary inertia of the accelerometer. It was assumed that the accelerometer had the shape of a cylinder for the mass moment of inertia calculation. It is also assumed that the accelerometer center-of-gravity is placed at the midpoint. The results of this improved model are shown in Figure 4.9. The first four frequencies of the model are now within 2% of the experimental results.

The overall results for each model are tabulated in Table 4.3. Notice that in the last

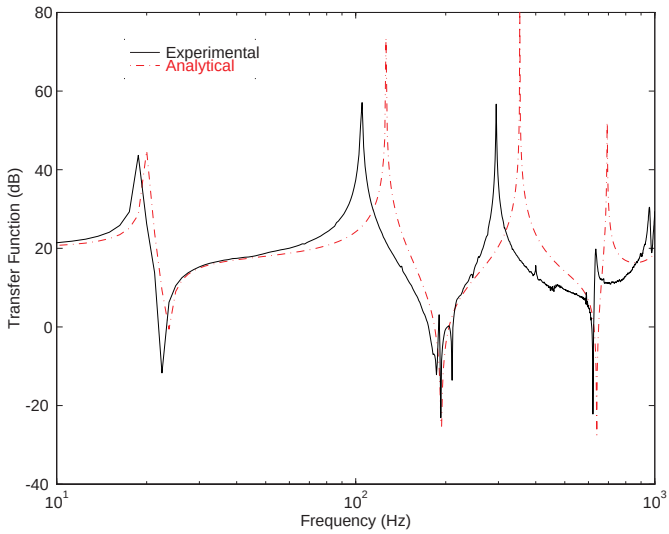


Figure 4.7: Model Without Accounting for Accelerometer Mass

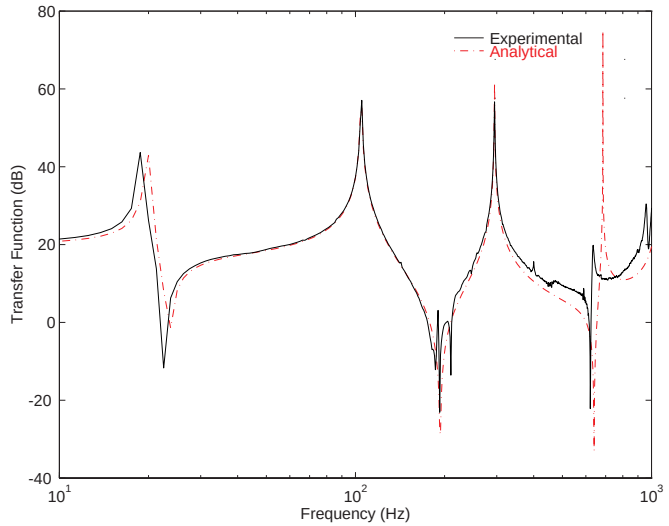


Figure 4.8: Model Accounting for Accelerometer Mass

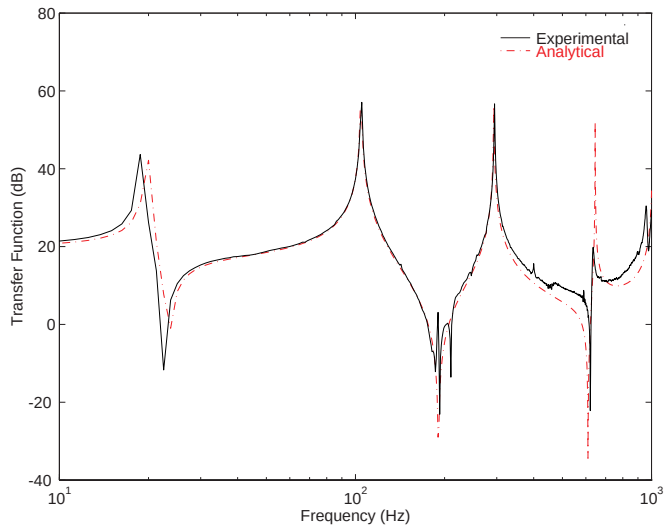


Figure 4.9: Model Accounting for Accelerometer Mass and Rotary Inertia

two models the frequencies are below the experimental results. There are several factors that can attribute to the lower frequencies in the analytical model. First, the accelerometer is not a point mass but is distributed over a finite portion of the beam. Second, the center-of-gravity of the accelerometer was not exactly known so the exact location of the accelerometer along the beam is not known exactly either. Also, the mass of the accelerometer and wire had to be approximated as well as the moment of inertia. Another reason that could result in lower frequencies was that the mass of the wire was distributed over a portion of the beam but was assumed to be a point mass at the accelerometer location. All of these factors are a cause for the slight differences in the analytical and experimental results.

Table 4.3: Natural Frequencies for Clamped Beam

| Natural Frequencies (Hz) | | | | |
|---|---|---|---|---|
| Mode | Experimental | Analytical | | |
| | | no mass | mass, no inertia | mass + inertia |
| 1 | 18.75 | 20.16 | 19.81 | 19.79 |
| 2 | 105.00 | 126.32 | 104.47 | 104.30 |
| 3 | 295.00 | 353.69 | 294.78 | 293.32 |
| 4 | 635.00 | 693.10 | 685.02 | 645.18 |

All three models do not include damping and the analytical peaks of each mode usually

do not correspond to the experimental peaks. This can be seen in Figure 4.7, Figure 4.8, and Figure 4.9 through the fourth mode. The next section modifies the transfer function synthesis to include damping in the beam.

### 4.9.2 Analytical Model with Damping

In Section 4.4, the analytical transfer function was formulated for a beam with no damping. The damping in the beam can be added to equation (4.29) by letting

$$f_w(x,t) = -F_c(x,t) + f_{w'}(x,t) \tag{4.106}$$

where $f_{w'}(x,t)$ are external forces that do not include damping forces. The damping force $F_c(x,t)$ is assumed to be proportional to the velocity and is

$$F_c(x,t) = \frac{\partial C' w(x,t)}{\partial t} \ , \tag{4.107}$$

where $C'$ is a linear homogeneous differential operator and is a part of the differential operator $B$ in equation (4.3).

In some special cases, the damping force is a linear combination of the spatial operators $A$ and $C$ in equation (4.3). In the case of proportional damping, the operator $C'$ is

$$C' = \gamma A + \beta C \ . \tag{4.108}$$

For the case of transverse vibration in this experiment, the spatial operators $A$ and $C$ are

$$A = \rho$$
$$C = EI\frac{\partial^4}{\partial x^4} \ ,$$

and the addition of proportional damping changes equation (4.29) to

$$-EI\frac{\partial^4 w(x,t)}{\partial x^4} - \left[\rho\gamma + \beta EI\frac{\partial^4}{\partial x^4}\right]\frac{\partial w(x,t)}{\partial t} = \rho\frac{\partial^2 w(x,t)}{\partial t^2} \ . \tag{4.109}$$

By taking the Laplace transform, this equation becomes

$$-EI(1+\beta s)\frac{\partial^4 W(x,s)}{\partial x^4} + F_{w'}(x,s) = \rho(s+\gamma)sW(x,s) \ . \tag{4.110}$$

This will change the matrix $\underline{\underline{\mathbf{F}}}(s)$ to

$$\underline{\underline{\mathbf{F}}}(s) = L\begin{bmatrix} 0 & 1 & 0 & 0 & 0 & 0 \\ \rho s^2/EA & 0 & 0 & 0 & 0 & 0 \\ 0 & 0 & 0 & 1 & 0 & 0 \\ 0 & 0 & 0 & 0 & 1 & 0 \\ 0 & 0 & 0 & 0 & 0 & 1 \\ 0 & 0 & \frac{-\rho(s+\gamma)s}{EI(1+\beta s)} & 0 & 0 & 0 \end{bmatrix} \ . \tag{4.111}$$

Experimental verification of $\gamma$ and $\beta$ was not performed since it is only necessary to verify that the model can incorporate damping properly. Therefore, the values for $\gamma$ and $\beta$ were taken from an identical experiment performed by Atalla [52]. The difference between this experiment and the one performed by Atalla is how tight the beam is connected to the shaker, which will affect the damping in the beam. The values for $\gamma$ and $\beta$ obtained by Atalla were 1.36 and 2.99x$10^{-6}$, respectively. The analytical transfer function that includes beam damping is shown in Figure 4.10. The resonant peak at the fourth mode has been significantly reduced compared to Figure 4.9. An exact match at the modes is not obtained since the values used for $\alpha$ and $\beta$ were taken from a previous experiment. Also, the proportional damping model used is only an approximation to the type of damping present in the system.

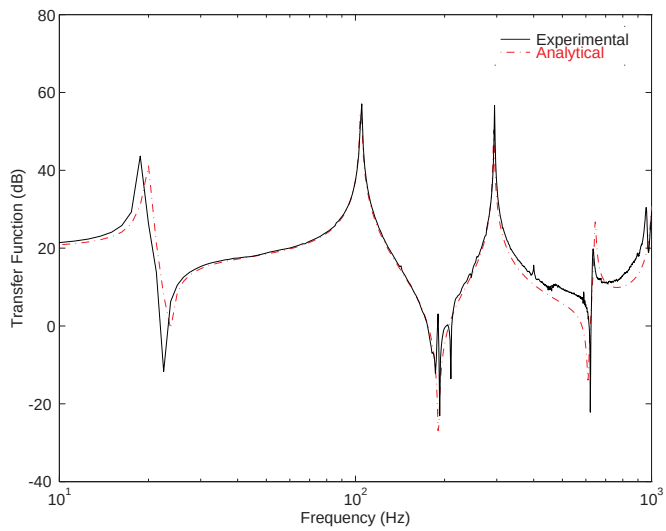


Figure 4.10: Continuous Beam with Proportional Damping

## 4.10 Summary

A transfer function method has been described to analyze any complex distributed parameter systems. These systems can consist of any combination of distributed systems, lumped systems, and varying types of constraint forces. This method is unique because it can obtain exact values for the eigenvalues, mode shapes (eigenfunction), and transfer functions for any complex distributed system. The TFS method can also determine the system's time responses but only approximately. However, with exact values of eigenvalues and eigenfunctions, the number of terms to obtain accurate results will be minimized.

It has also been shown how to implement active and passive control for two systems: the flexible base, rigid equipment (FBRE) system and the flexible base, flexible equipment

(FBFE) system. Three active control methodologies were discussed for each system; a proportional-plus-integral-plus-derivative controller, a positive position feedback controller, and a linear quadratic Gaussian regulator.

Lastly, an experiment was performed to validate the model using Yang's transfer function method. It has been shown that the transfer function method is in good agreement with experimental data and can be used to analyze vibration isolation systems that contain passive or active isolators.

# Chapter 5

# Flexible Base, Rigid Equipment

This chapter analyzes an isolation system that has a flexible base and a rigid equipment. The isolation analysis is comprised of two major sections: the first section analyzes passive isolators whereas the second section analyzes active isolators using various control methodologies

The section on passive isolation is divided into five major subsections. The first subsection determines the effectiveness of the mount frequency when base flexibility is assumed in the system. The second subsection determines the influence of isolator damping in the flexible base, rigid equipment (FBRE) system. The third section compares different damping types in the system and also compares how they will affect the FBRE system response. The fourth subsection analyzes the FBRE transmissibility for various values of the mount frequency, equipment mass, base mass, and isolator placement. The final subsection replaces the single isolator by a dual isolator and a comparison is made between each system.

Active isolation for the FBRE system is divided into two major subsections. The first part is a determination of the best sensor location. That is, should the sensor be placed on the equipment that is to be isolated or on the flexible base. The second part will implement three different control methodologies on the FBRE system. The control laws that will be used are classical control strategies such as the proportional-plus-derivative ($\mathcal{PD}$) and the proportional-plus-integral-plus-derivative ($\mathcal{PID}$) controller, the positive position feedback (PPF) controller, and the linear quadratic Gaussian (LQG) regulator.

## 5.1 Passive Isolation

From the SDOF model, the mount or corner frequency is designed to have the smallest possible value so that high frequency disturbances will be attenuated as quickly as possible. Therefore, it is desired to discover the effect of base flexibility for various values of isolator stiffness, i.e., mount frequencies. It has also been shown for the SDOF model that isolator damping will decrease the transmissibility at the resonant condition but will increase the

high frequency transmissibility. Similar results occur when the base is flexible; however, the choice of the mount frequency for the FBRE system will have a significant impact on the system transmissibility.

### 5.1.1 Mount Effectiveness

It has been shown that base flexibility has an adverse affect on vibration isolation designs [31] because an infinite number of modes will be present in the transmissibility. Therefore, the isolator mount should be designed such that it will attenuate the high frequency transmissibility as quickly as possible. When damping is present in the isolator, the isolator should also significantly decrease the transmissibility at one of the system's natural frequencies. With these conditions in mind, consider the base of the FBRE system as a pinned-pinned beam with its beam parameters given in Table 4.1. The base is modeled as a Bernoulli-Euler beam with no structural damping and the first seven frequencies of this base are given in column 2 (*No Mount*) of Table 5.1.

Table 5.1: Pinned-Pinned Beam Frequencies With and Without Mount

| Mode | No Mount | Mount Frequency (Hz) | | | |
|---|---|---|---|---|---|
| | | 7.1176 | 22.5079 | 71.1762 | 318.3099 |
| | | | | | |
| 1 | 56.5800 | 7.0177 | 19.6002 | 31.7227 | 34.0450 |
| 2 | 226.3200 | 57.3269 | 64.3001 | 113.2115 | 170.1849 |
| 3 | 509.2202 | 226.5334 | 228.4943 | 251.5864 | 503.1836 |
| 4 | 905.2822 | 509.2208 | 509.2386 | 509.4171 | 588.6136 |
| 5 | 1414.5090 | 905.3208 | 905.6690 | 909.2033 | 998.4023 |
| 6 | 2036.9077 | 1414.5467 | 1414.8861 | 1418.3245 | 1509.9098 |
| 7 | 2772.2491 | 2036.9095 | 2036.9256 | 2037.0881 | 2041.2554 |

Now consider a piece of equipment and isolator attached to the base at some arbitrary location. The equipment has a mass $m_e$ while the isolator consists of a massless spring and viscous damper. This new system will be referred as the the flexible base, rigid equipment (FBRE) system and this system is shown in Figure 5.1. The frequencies of this new system are dependent on the mount or corner frequency, $f_o = \sqrt{k/m_e}$, where $k$ is the isolator stiffness. If the mount frequency is much lower than the first mode of the base, the FBRE system will have natural frequencies corresponding to the concatenation of the mount frequency and the pinned-pinned beam frequencies. The mount frequency becomes the first FBRE mode, the first base mode is the second FBRE mode, the second base mode

is the third FBRE mode, etc. Note that the first mode of the FBRE system will be slightly smaller than the mount frequency for this low-frequency mount design. For example, the natural frequencies for the FBRE system with a mount frequency design at $f_o = 7.1176$ Hz are tabulated in column 3. The first mode for the FBRE system is very close to the mount frequency and modes 2-7 are nearly equivalent to modes 1-6 for the pinned-pinned beam.

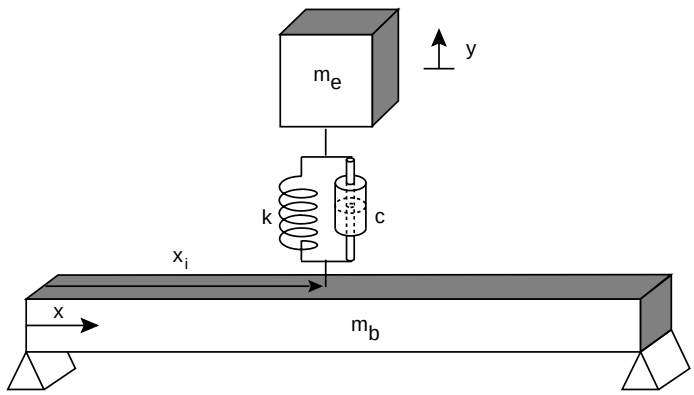


Figure 5.1: Rigid Equipment Mounted on Flexible Base via Isolator

As the mount frequency is designed closer to the first mode of the base, the modes of the FBRE system start to shift. Consider the case when the mount frequency is designed at $f_o = 22.5079$ Hz; the FBRE system will have a first mode that is 13% less than the mount frequency. The rest of the FBRE modes will be slightly higher than the base frequencies with the second mode shifting by 14%.

Somewhat different results are obtained when the mount frequency is designed between the base modes. For example, consider the case when the mount frequency is designed at $f_o = 71.1762$ Hz; the value of the mount frequency lies between the first two modes of the base. The new frequency that is added to the FBRE system due to the isolator mount is no longer near the mount frequency. In fact, the new mode of the FBRE system due to the isolator mount has a 59% shift in frequency. There has also been a dramatic shift of the base frequencies that are close to the mount frequency. The first mode of the FBRE system has shifted from the base frequency of 56.58 Hz to 31.72 Hz (44% shift) and the third mode of the FBRE system has shifted from 226.32 Hz to 251.59 Hz (11% shift). The significance of this interaction will be demonstrated when the isolator includes damping.

The above paragraphs describe what happens to the FBRE frequencies for different values of the mount frequency but the effect on the FBRE transmissibility has to be analyzed as well. The following frequency response functions (FRFs) will have a disturbance input at the pinned end of the base, i.e., at the location $x = 0$ m. The measured response of the equipment position is located at a distance $x_i = L/3.125 = 0.08128$ m from the left end. The first isolation design looks at a low-frequency mount design at $f_o = 7.1176$ Hz; the

mount frequency is much less than the first mode of the base. Figure 5.2 is a transmissibility comparison for a SDOF system, a FBRE system and a pinned-pinned beam. As seen from this figure, the transmissibility starts to decrease at a rate of 40 dB/decade after reaching the isolator mount frequency for either the SDOF system or the FBRE system. Note that the transmissibility for the SDOF system compares well to the FBRE system except for the infinite number of modes present in the FBRE system.

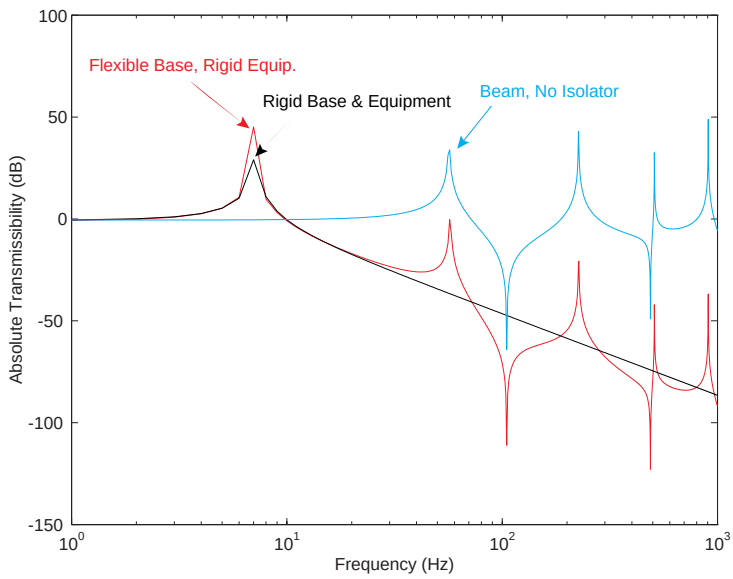


Figure 5.2: Comparison of Effects Due to Isolator at Frequency $f_o = 7.1176$ Hz

The transmissibility for a system when the mount frequency was designed greater than the first mode of the base was also determined. The input and measured response are at the same locations as in the previous case and the mount frequency was chosen at $f_o = 318.3099$ Hz. Figure 5.3 is the transmissibility for the SDOF system, the FBRE system, and a pinned-pinned beam. Unlike the previous case, significant attenuation in this system does not occur until the third mode; this mode directly corresponds to the isolator mount. Therefore, the system does not decrease the transmissibility at 40 dB/decade until after the third mode.

### 5.1.2 Influence of Isolator Damping

It was shown in the previous section that when the mount frequency is designed lower than any of the base modes, the natural frequencies of the FBRE system are a concatenation of the mount frequency and the base frequencies. Since the mount frequency has very little or no effect on the higher-order base modes, the inclusion of isolator damping will have an effect on only the first mode. Remember that the first mode of the FBRE system is due

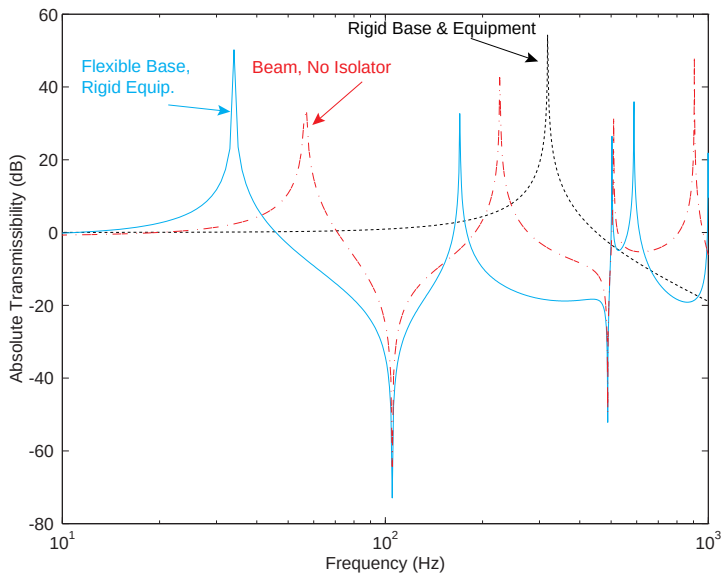


Figure 5.3: Comparison of Effects Due to Isolator at Frequency $f_o = 318.3099$ Hz

to the addition of the isolator and equipment on the base. Figure 5.4 shows the influence of isolator damping for a low-frequency mount designed at $f_o = 7.1176$ Hz. As seen from this figure, the FBRE model with no damping is similar to an undamped SDOF model except for the infinite number of modes present at higher frequencies. The FBRE system decreases at a rate of 40 dB/decade after the first mode, similar to the SDOF system. As the damping is increased in the FBRE system, the transmissibility of the first mode is also attenuated but the transmissibility at the other frequencies is increased.

A different situation occurs when the mount frequency is designed between two of the base modes. It was shown in the previous section that this design will couple the modes depending on the value of the mount frequency. Figure 5.5 shows the influence of this interaction when isolator damping is included for a system having a mid-frequency mount design at $f_o = 71.1762$ Hz. This figure shows that attenuation in the first three modes have occurred. The most significant attenuation occurs in the second mode because this mode is due to the inclusion of the isolator and equipment. The first and third modes are attenuated, but not as significantly as the second mode. One significant drawback in this design is that the transmissibility does not roll-off at 40 dB/decade until the second mode. Therefore, the transmissibility will not be significantly attenuated in the high frequency ranges compared to a low-frequency mount design as shown in Figure 5.4. A low-frequency mount design will also have more attenuation in the first mode than a mid-frequency mount design.

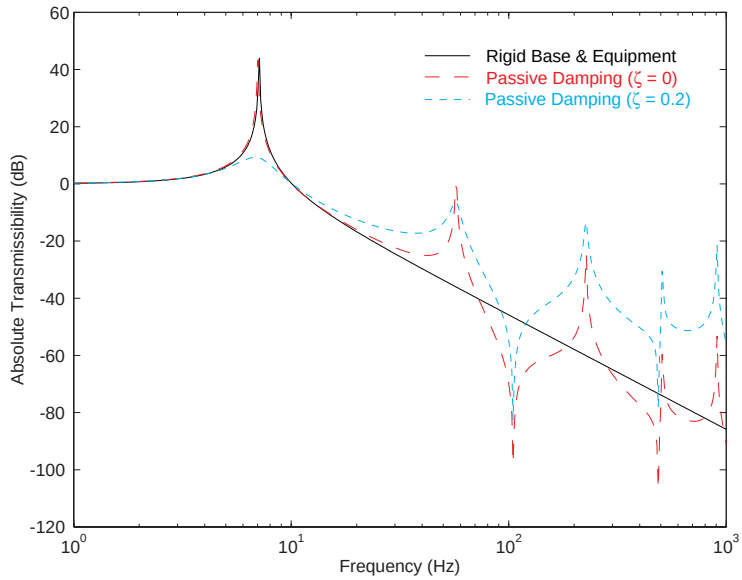


Figure 5.4: FBRE System with Isolator Damping at $f_o = 7.1176$ Hz

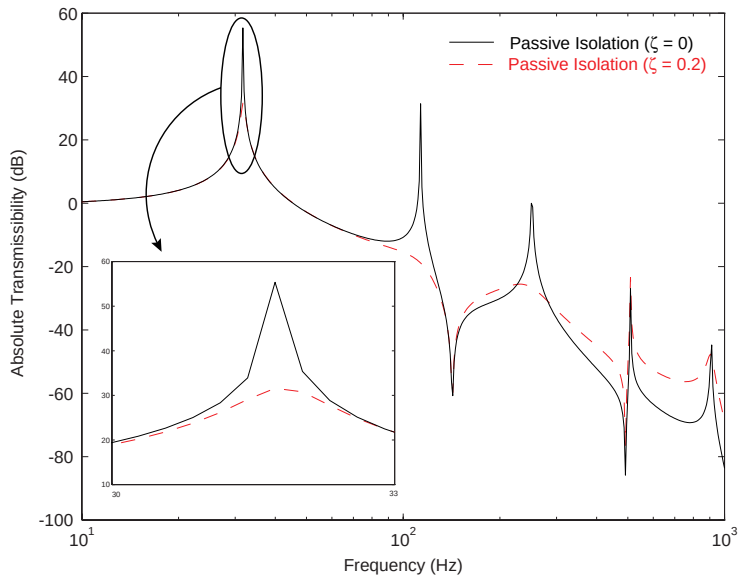


Figure 5.5: FBRE System with Isolator Damping at $f_o = 71.1762$ Hz

### 5.1.3 Comparison of Damping Types

The discussion in the previous paragraphs looked at situations when damping was present in the isolator but no structural damping was present in the beam. In physical systems, some sort of damping will always be present in the beam but this damping is usually small. To determine how beam damping will affect the system response, the following system was considered: an FBRE system with an isolator mount designed at $f_o = 71.1762$ Hz and the isolator placed at $x_i = L/3.125$ from the left end. The stiffness of the isolator and the mass of the equipment are $k = 1\text{x}10^4$ N/m, $m_e = 0.05$ kg, respectively; the key parameters for the base are given in Table 4.1. The system will be excited by a periodic input at the system's first natural frequency located at $x = 0.0406$ m from the left end of the FBRE system. Proportional damping will be used to model the structural damping in the beam and the isolator damping will be modeled as viscous damping.

Figure 5.6 shows the results for various damping types in the FBRE system. The first FBRE system that was examined had no damping in the beam or the isolator. The theoretical response of this system grows without bounds and is shown in Figure 5.6 by the solid lines; the solid lines represent the bounds on the system response. The next case that was examined was a FBRE system that had proportional damping in the base. The response of this system tends to increase until it reaches a steady-state solution at seven seconds; the bounds of the response are represented by the dashed lines. The third case had no beam damping but viscous ($\zeta = 0.1$) damping was present in the isolator. As seen from Figure 5.6, isolator damping has a greater impact on the system response than structural damping. The equipment displacement is much smaller for isolator damping than structural damping and a steady-state response for this system is reached around two seconds. The last case considered the situation when the isolator had viscous damping and the beam had proportional damping. The response reached a steady-state solution at two seconds but its response is slightly less than the isolator damping case.

### 5.1.4 Isolator Performance for Varying Parameters

The above sections were an analysis of isolator performance for mount frequencies at either $f_o = 7.1176$ Hz or $f_o = 71.1762$ Hz while fixing the equipment mass, base mass, and the isolator placement. Therefore, it is worthwhile to determine how the FBRE system will perform for varying equipment mass, base mass, mount frequency, and isolator placement. The analysis is similar to the one used for the two-degree-of-freedom model. The root-mean-square (RMS) value of the absolute transmissibility will be determined because it is an overall indication how well the system is isolated.

It is assumed that the flexible base, rigid equipment (FBRE) system will have no significant amount of isolator or base damping. The amount of damping present in the system was assumed at 0.01%; this level was chosen so that the transmissibility at the resonant modes would be finite. The disturbance source consisted of a periodic function at the left

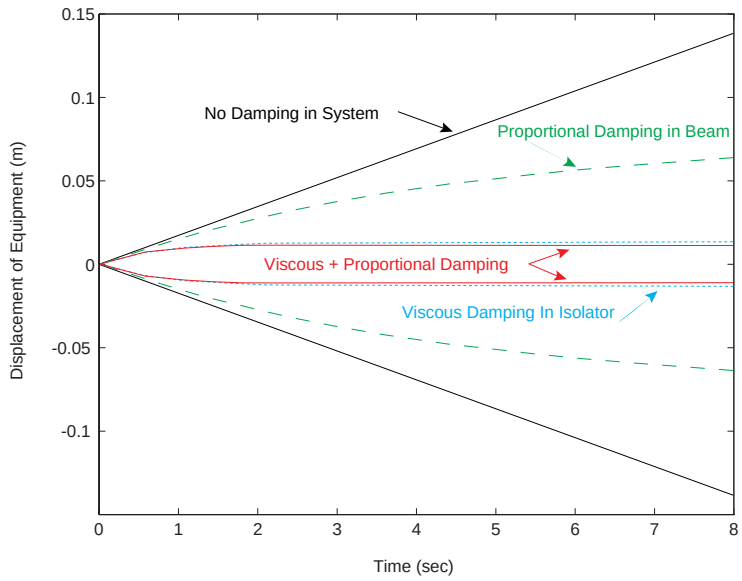


Figure 5.6: Comparison of Damping in FBRE System

end of the base spanning a frequency range from 1 to 2500 Hz. The mount frequency is varied from 7 to 600 Hz, the equipment mass is varied from one-twentieth the mass of the base to twenty times the mass of the base, and the isolator placement varies from the left pinned end to the right pinned end of the base. Once the absolute transmissibility $G(\omega)$ is found for each set of parameters, the RMS level of the transmissibility can be determined by the following equation.

$$RMS = \sqrt{\int_{\omega} |G(\omega)|^2 S_f(\omega) \mathrm{d}\omega} \tag{5.1}$$

The RMS levels are converted to decibels and the results are shown in Figure 5.7 and Figure 5.8 for varying values of mass ratio ($m_e/m_b$), isolator placement, and mount frequency. Figure 5.7 shows the results for three specific mount frequencies: $f_o = 7$ Hz, 225 Hz, and 381 Hz. Figure 5.8 is another perspective of the performance by looking at the different mass ratios while the mount frequency and the isolator placement are varied.

As seen from either Figure 5.7 or Figure 5.8, the best overall isolator design is for a mount frequency chosen at $f_o = 7$ Hz. The RMS levels at this frequency are significantly lower than the RMS levels for the other mount frequencies. This is expected since systems with low-frequency mounts tend to attenuate the high frequency transmissibility at a rate of 40 dB/decade sooner than higher frequency mounts. Therefore, a low-frequency mount design attenuates a higher percentage of the transmissibility for a given frequency range than an isolator mount with a higher frequency. High mass ratios, i.e., equipment mass

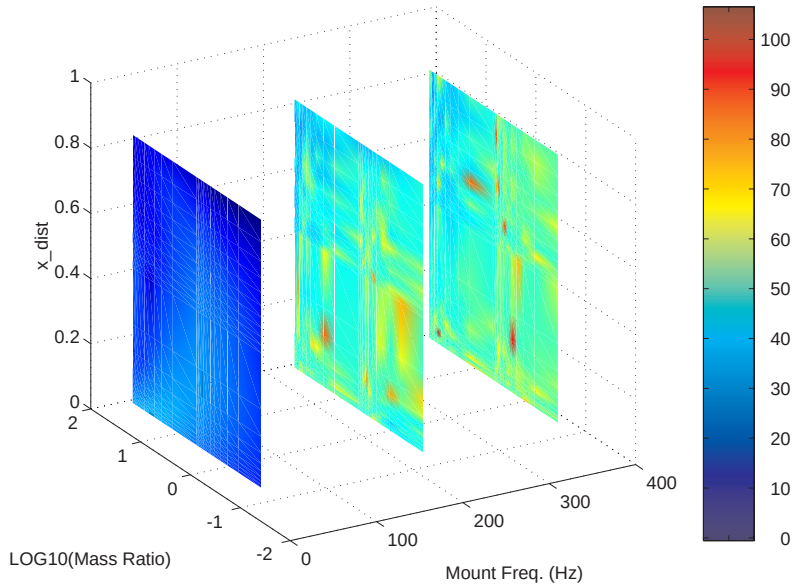


Figure 5.7: RMS Transmissibility of FBRE System for Specific Mount Frequencies

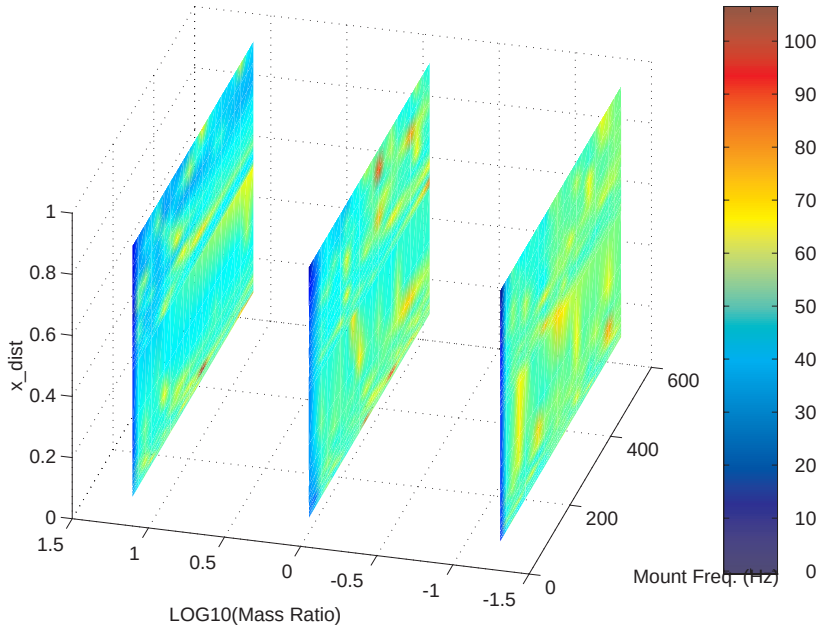


Figure 5.8: RMS Transmissibility of FBRE System for Specific Mass Ratios

greater than base mass, have an overall lower transmissibility than systems with lower mass ratios with all other FBRE parameters equivalent. This can be partially seen in Figure 5.7 but it is much clearer in Figure 5.8. Overall, it is better to have designs with a mount frequency less than 300 Hz and have the equipment mass equal to or greater than the base mass.

It should be noted that this analysis does not include any significant levels of damping in the beam or the isolator. It has been previously shown that isolator damping can attenuate multiple modes with a mid-frequency mount design; that is, an isolator mount designed at a frequency between the base modes. However, it has just been shown that the overall attenuation of the transmissibility is less effective at these higher mount frequencies. Therefore, a trade-off should be performed to determine whether a low-frequency mount design or a mid-frequency mount design should be used.

### 5.1.5 Performance of Dual Isolators

All the results to this point have used a single passive isolator. However, there may be situations when a single isolator may not be feasible to implement. This situation occurs when the isolator is placed at the center-of-gravity of the equipment and the equipment starts to rotate. The single isolator in this instance will not have any effect on the rotational transmissibility. The performance of a single isolator may also be inadequate; therefore, an analysis using dual actuators should be discussed.

The FBRE system with dual isolators is shown in Figure 5.9. The isolators are placed equidistant along the base at a position $x_{cg} = L/3.125$; this position also marks the location of the equipment's center of gravity. The parameter $a_x$ represents the distance from the center of gravity to each isolator's position. It is assumed that the isolator consists of a massless spring and damper with an isolator stiffness of 50 N/m. When damping is present in the isolator, the overall damping ratio will be 10%. It is also assumed that the mass of the equipment is the same order as the mass of the base.

#### 5.1.5.1 Implementation in TFS Method

Since the isolator is no longer attached at a single point on the equipment or the base, the term $\underline{\underline{\mathbf{C}}}_l(s)$ in equation (4.15) must be modified. In this section, the equations of motion for this new system are derived and the forces due to each isolator are calculated. These forces need to be determined as a function of the equipment and base displacement for implementation in the TFS method.

The force of the first isolator from the left end will be denoted by $Q_1$ and its displacement at the base is represented by $u_1$. The force and displacement of the second isolator is $Q_2$ and $u_2$, respectively. The linearized equations of motion for the equipment in the Laplace

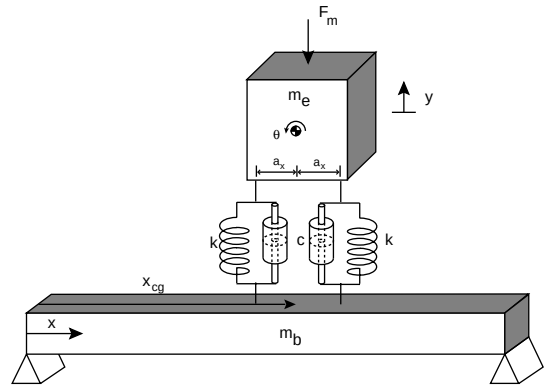


Figure 5.9: FBRE System with Dual Passive Isolators

domain are

$$m_e s^2 Y(s) = -Q_1(s) - Q_2(s) + F_m(s) \tag{5.2a}$$
$$I_g s^2 \Theta(s) = a_x[Q_1(s) - Q_2(s)] \ . \tag{5.2b}$$

The forces $Q_1$ and $Q_2$ are

$$Q_1(s) = k[Y(s) - U_1(s) - a_x\Theta(s)] + cs[X(s) - U_1(s) - a_x\Theta(s)] \tag{5.3a}$$
$$Q_2(s) = k[Y(s) - U_2(s) + a_x\Theta(s)] + cs[Y(s) - U_2(s) + a_x\Theta(s)] \ . \tag{5.3b}$$

and $F_m(s)$ is an arbitrary force located at the equipment's center-of-gravity.

By placing equation (5.3a) and equation (5.3b) into equation (5.2a) and equation (5.2b), the displacement and rotation of the equipment are

$$Y(s) = \frac{F_m + (k + cs)(U_1 + U_2)}{m_e s^2 + 2cs + 2k} \tag{5.4a}$$
$$\Theta(s) = \frac{a_x(k + cs)(U_2 - U_1)}{I_g s^2 + 2a_x^2 cs + 2a_x^2 k} \ . \tag{5.4b}$$

With these parameters, the isolator forces in terms of the base displacements are

$$Q_1 = \frac{(k + cs)[F_m + (k + cs)(U_1 + U_2)]}{m_e s^2 + 2cs + 2k} - (k + cs)U_1 + \frac{a_x^2(k + cs)^2(U_1 - U_2)}{I_g s^2 + 2a_x^2 cs + 2a_x^2 k} \tag{5.5a}$$
$$Q_2 = \frac{(k + cs)[F_m + (k + cs)(U_1 + U_2)]}{m_e s^2 + 2cs + 2k} - (k + cs)U_2 - \frac{a_x^2(k + cs)^2(U_1 - U_2)}{I_g s^2 + 2a_x^2 cs + 2a_x^2 k} \ . \tag{5.5b}$$

These equations can be written in the form

$$\underline{\underline{\mathbf{Q}}}(s) = -\underline{\underline{\mathbf{C}}}(s)\vec{\mathbf{U}}(s) + \vec{\mathbf{F}}_t \tag{5.6}$$

where

$$\vec{\mathbf{Q}}(s) = \begin{Bmatrix} Q_1(s) \\ Q_2(s) \end{Bmatrix}, \quad \underline{\underline{\mathbf{C}}}(s) = \begin{bmatrix} C_{11} & C_{12} \\ C_{21} & C_{22} \end{bmatrix}, \quad \vec{\mathbf{U}}(s) = \begin{Bmatrix} U_1(s) \\ U_2(s) \end{Bmatrix}, \quad \vec{\mathbf{F}}_t = \begin{Bmatrix} f_1(s) \\ f_2(s) \end{Bmatrix} . \tag{5.7}$$

The terms $C_{11}$, $C_{12}$, $C_{21}$, and $C_{22}$ are

$$C_{11} = C_{22} = k + cs - \frac{(k+cs)^2}{m_e s^2 + 2cs + 2k} - \frac{a_x^2 (k+cs)^2}{I_g s^2 + 2a_x^2 cs + 2a_x^2 k} \tag{5.8a}$$

$$C_{12} = C_{21} = -\frac{(k+cs)^2}{m_e s^2 + 2cs + 2k} + \frac{a_x^2 (k+cs)^2}{I_g s^2 + 2a_x^2 cs + 2a_x^2 k} \tag{5.8b}$$

and

$$f_1 = f_2 = \frac{k+cs}{m_e s^2 + 2cs + 2k} F_m \ . \tag{5.9}$$

With this formulation, the dual isolator system may be implemented in the TFS method. Implementation of the dual isolators is similar to a mechanism having a point connection between subsystems. This situation is discussed in Section 4.6.3 and will not be discussed here. In short, each isolator will have an effect on the base displacement at both isolator's location.

#### 5.1.5.2 Dual Isolator Results

The transmissibility comparison between dual and single isolators is shown in Figure 5.10. For each system, it is assumed that there is no isolator damping. One difference in the transmissibility between the two configurations is the extra mode for the dual isolator system. This is to be expected since there are two isolators attached at the base instead of one. Note that the first mode due to the dual isolators is less than the first mode for the single isolator system and the second mode of the dual isolator system occurs at the first mode of the single isolator system. Another difference between the two systems is the overall attenuation of the transmissibility at the higher frequencies. As seen from Figure 5.10, the dual isolator system performs better at higher frequencies than the single isolator system which is due to the choice of the mount frequency. The dual actuator system starts to decrease at a rate of 40 dB/decade at a lower frequency than the single isolator system. The last difference between the two systems are the anti-resonant frequencies. The frequencies of the anti-resonants have increased for the dual isolator system compared to the single isolator system. This is due to the addition of another isolator.

It is also worthwhile to analyze the single and dual isolator systems when each system includes isolator damping. The results are shown in Figure 5.11 and each isolator is assumed to have a total damping ratio of 10%. As seen from this figure, the second mode of the

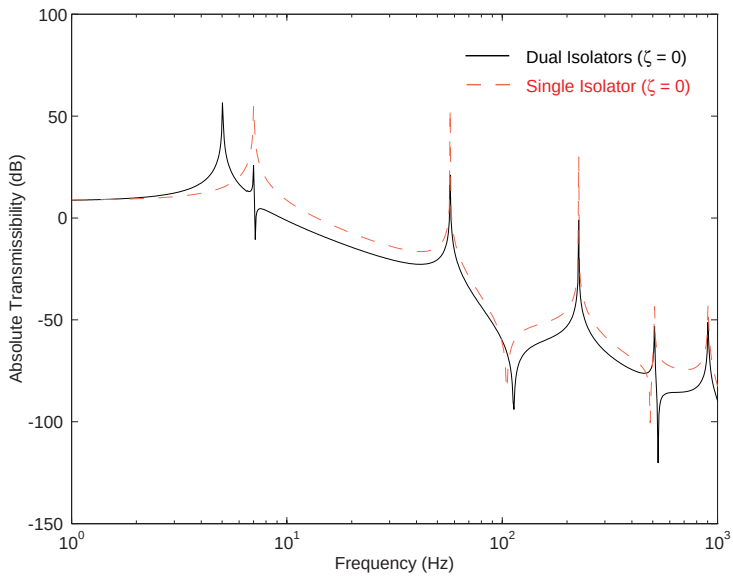


Figure 5.10: Comparison of Single and Dual Actuators of FBRE System

dual isolator system has almost been completely attenuated and the first mode has been significantly attenuated. As in the previous section, the dual isolator system performs better than the single isolator system in the higher frequency ranges. This is due to the first mode of the dual isolator system occurring at a lower frequency than the single isolator system. Note that the high frequency transmissibility of each system starts to increase when isolator damping is present.

The transmissibility for the dual isolator system with and without damping is shown in Figure 5.12 and the dual isolator system has an overall 10% damping in the isolators. As stated previously, the first mode is attenuated and the second mode has almost been completely attenuated. Also, the high frequency transmissibility of the damped system increases with respect to the undamped system's transmissibility.

## 5.2 Active Isolation

Two main objectives in using active isolators are the types of control architectures to use and the placement of the feedback sensor. For the flexible base, rigid equipment (FBRE) system, there are two locations for sensor placement: the base or the equipment. After selecting the sensor placement, three different control methodologies will be implemented: a proportional-plus-integral-plus-derivative ($\mathcal{PID}$) controller, a linear quadratic Gaussian (LQG) regulator, and a positive position feedback (PPF) controller. Table 5.2 is a list of parameters that are used for each control architecture such as the value of the mount

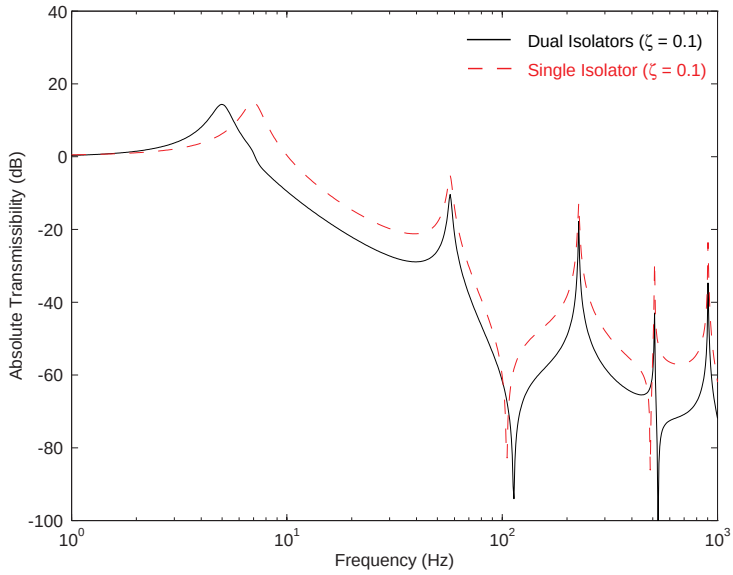


Figure 5.11: Comparison of Single and Dual Isolators Using Damping for the FBRE System

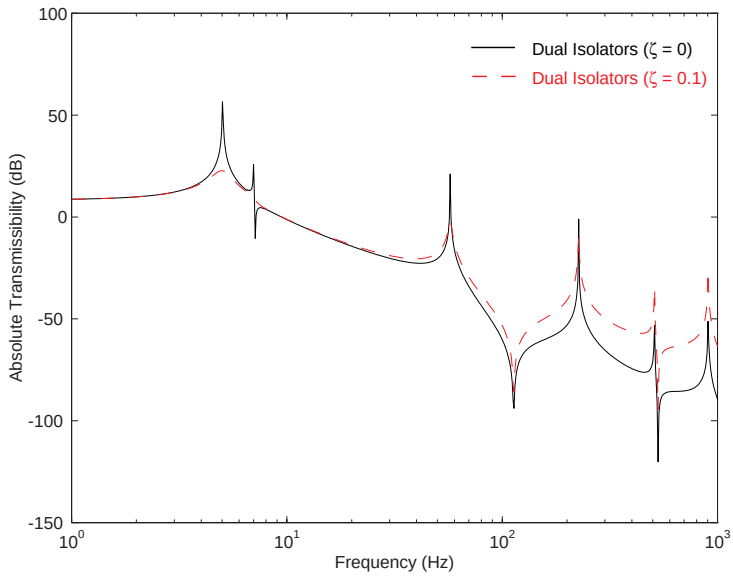


Figure 5.12: Comparison of Dual Isolator System with and without Damping

frequency, the actuator location, etc.

Table 5.2: Parameters for Implementation of Active Isolation

| Parameter | Low Mount System | Mid Mount System |
|---|---|---|
| Mount Frequency | 7.1176 Hz | 71.1762 Hz |
| Isolator Location | 0.08128 m | 0.08128 m |
| Disturbance Location | | |
| Frequency Response | 0.04064 m | 0.04064 m |
| Time Response | 0.04064 m | 0.04064 m |
| Base Damping | Proportional | Proportional |
| Isolator Damping | None | None |

### 5.2.1 Sensor Location

For a SDOF model, velocity feedback will not increase the high frequency transmissibility but does add damping at the resonant condition. Similar results can be obtained for the FBRE system depending on the sensor location. The active controller will implement velocity feedback and the base will have no structural damping. The actuator will add 20% damping to the first mode so a comparison can be made to the results obtained from the previous section on passive damping. A mount design at $f_o = 7.1176$ Hz is used since a design at $f_o = 71.1762$ Hz will give similar results.

Sensor feedback can occur from the equipment or the base. Base feedback is not warranted as seen from Figure 5.13. The first mode of the FBRE system will be lightly damped and the transmissibility at higher frequencies will be increased. This is similar to the situation of a passive isolator with one significant difference being the amount of damping in the first mode. The passive isolator does a significantly better job in attenuating the first mode than the active controller in this case; the active system has a transmissibility of 40 dB (Figure 5.13) at the first mode while the passive system has a transmissibility of about 8 dB (Figure 5.4). Therefore, the passive system dramatically outperforms the active system when feedback occurs from the base.

Different results are obtained when the sensor is located on the equipment. First, the first mode is significantly damped compared to a system using base feedback. Actually, the amount of damping at the first mode is comparable to the system with a passive isolator (Figure 5.4). Notice that the high frequency transmissibility of the active isolator tracks an undamped isolation system. The results of using equipment feedback are similar to a SDOF model with the main difference being the inclusion of an infinite number of modes in the FBRE system.

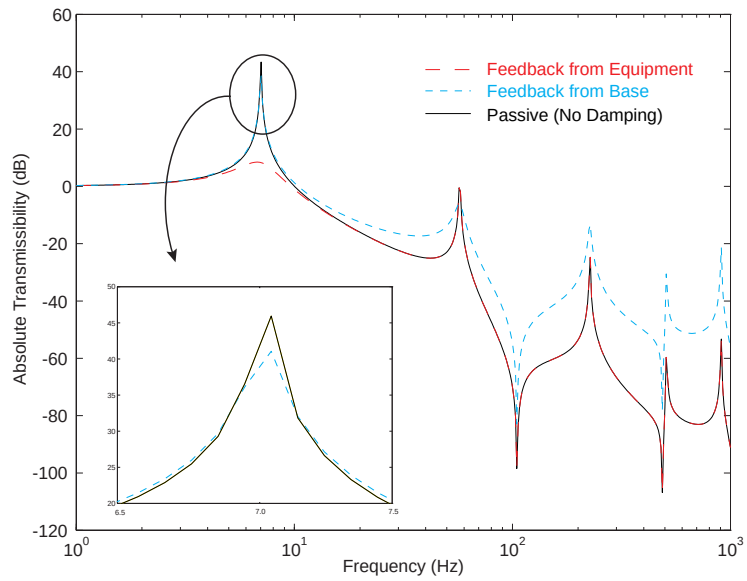


Figure 5.13: Comparison of Feedback Control from Equipment and Base

The choice of sensor placement is consistent with an observability index approach developed by Hughes and Skelton [53]. They developed a procedure to determine observability indices for each system mode; the indices are then ranked according to their magnitudes. This ranking is then used to determine the most beneficial sensor location [54]. For instance, the observability indices of the first FBRE mode for base and equipment feedback are $\mathcal{O}_1^b = 0.1247$ and $\mathcal{O}_1^e = 4.4712$, respectively. Since the observability index for equipment feedback is greater than the observability index for base feedback, the best sensor location is on the equipment.

### 5.2.2 $\mathcal{PID}$ Control

Figure 5.13 shows that velocity feedback can be used to attenuate the first mode of the FBRE system but this type of controller is rarely used because velocity or derivative feedback will increase any high frequency noise present in the system. Therefore, it is very common to use proportional and/or integral feedback with derivative feedback or velocity feedback. Hence the name proportional-plus-integral-plus-derivative ($\mathcal{PID}$) controller. This controller takes on the form

$$f(t) = K_P\ y(t) + K_D \dot{y}(t) + K_I \int y(t)\mathrm{d}t\ .$$

Any basic controls book can show the effects of each gain on the system [42, 43, 55, 56] and they are briefly stated here. Proportional feedback $K_P$ tends to increase the natural

frequency of the system and tends to decrease the damping in the system. Derivative control will add damping to the system and integral control is used to reduce or eliminate steady-state errors but comes at a cost of reduced stability.

Two separate FBRE systems will use $\mathcal{PID}$ control: one system with the mount frequency much less than any of the base modes (low-frequency mount) and the other system with the mount frequency between two modes of the base (mid-frequency mount). The gain selections for the $\mathcal{PID}$ controller are discussed for each system by use of a root-locus plot.

#### 5.2.2.1 Responses for Mount Frequency at $\mathbf{f_o = 7.1176}$ Hz

The first FBRE design is when the mount frequency is much less than any of the flexible base modes. The mount frequency is designed at $f_o = 7.1176$ Hz and the isolator is attached at a distance, $x_i = 0.08128$ m, from the left end of the base. The base was assumed to have no damping and the other pertinent parameters for this system are given in Table 5.2.

The proportional gain $K_P$ tends to modify the frequencies of the system; therefore, a small gain was chosen so that its influence on the system would be minimal. The derivative gain $K_D$ was based on the root-locus design shown in Figure 5.14 where only the first mode is shown. The derivative gain was eventually chosen at $K_D = 3$ to give a fast rise time with as little overshoot as possible.

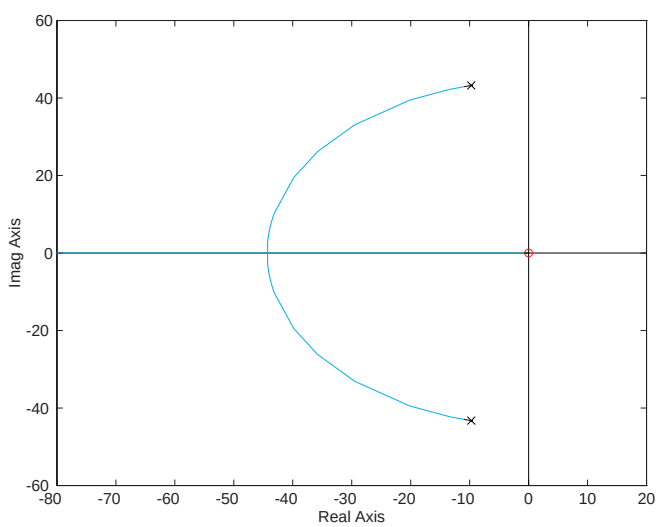


Figure 5.14: Root Locus Design for Derivative Gain when $f_o = 7.1176$ Hz

Unlike derivative control, integral control tends to make a system unstable. Therefore, a root-locus design was performed for the integral gain $K_I$ as well. Figure 5.15 is the root-locus design for the integral gain and a gain of $K_I = 1200$ was eventually chosen to give

good system error and settling time.

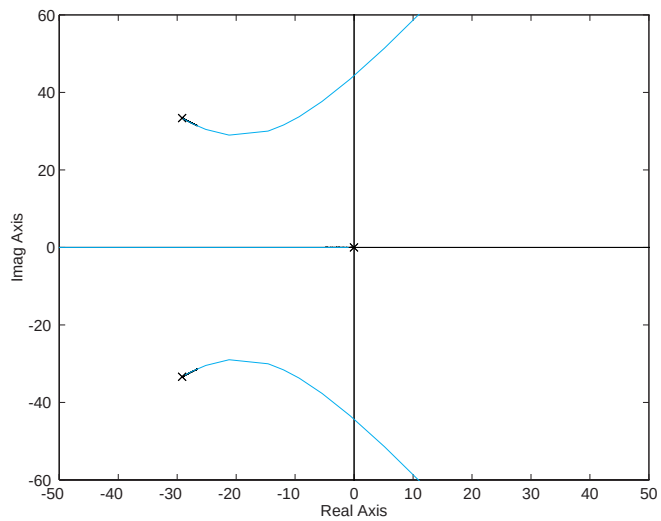


Figure 5.15: Root Locus Design for Integral Gain when $f_o = 7.1176$ Hz

Once the $\mathcal{PID}$ gains have been chosen, the frequency response functions (FRFs) and time responses can be formulated. The FRFs are shown in Figure 5.16 for the undamped system, and the systems using $\mathcal{PD}$ and $\mathcal{PID}$ control. $\mathcal{PD}$ control attenuates the first mode but has little effect on the rest of the transmissibility compared to the undamped system. For this particular system, the interaction between the modes is insignificant; therefore, damping does not "spill" over into the other modes. $\mathcal{PID}$ control is quite similar to $\mathcal{PD}$ control except that it attenuates the low frequency transmissibility. A better comparison between $\mathcal{PD}$ control and $\mathcal{PID}$ control are shown by their time responses.

The transient responses of each system are determined because they will be used to quantify how well the active isolator is performing. Two types of disturbances were used: a step input, and a sinusoidal input at the first natural frequency of the FBRE system. The disturbances were applied along the base at $x = 0.04064$ m from the left end. Figure 5.17 shows the time responses due to a step input. As seen from this figure, with no control (and no passive damping), the FBRE system will oscillate indefinitely at its natural frequencies. The system response will eventually go to zero if proportional damping is modeled in the base. When $\mathcal{PD}$ control is applied to the system, the equipment reaches a steady-state solution in 0.2 seconds. After reaching a steady-state solution, there is a sinusoidal term still present; this is the second and higher modes of the base that are not attenuated. Note that the system response will oscillate at an equilibrium position away from its initial position. With $\mathcal{PID}$ control, the displacement of the equipment reaches a steady-state

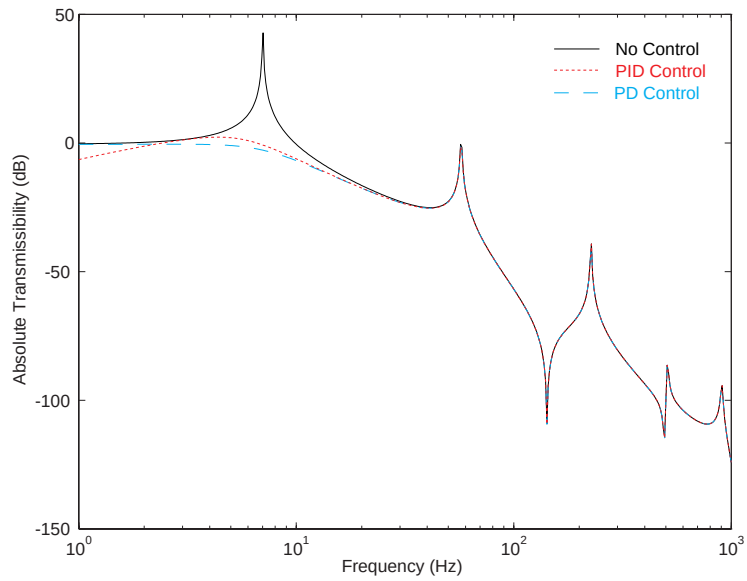


Figure 5.16: FBRE Frequency Response Function using PID for $f_o = 7.1176$ Hz

solution in about 0.3 seconds. Unlike $\mathcal{PD}$ control, the integral term in the $\mathcal{PID}$ controller will make the equipment oscillate around its initial position.

Figure 5.18 shows the controller responses due to a sinusoidal input at the first mode. With no control, the response of the equipment will grow unbounded with time. The theoretical displacement of the equipment will not go to infinity if base damping is present. However, $\mathcal{PID}$ or $\mathcal{PD}$ control will drastically alleviate this growth and the system will eventually settle to a steady-state solution. In this case, $\mathcal{PD}$ control is slightly more effective than $\mathcal{PID}$ control.

#### 5.2.2.2 Responses for Mount Frequency at $\mathbf{f_o = 71.1762}$ Hz

The second FBRE design has a mount frequency that occurs between the first two base modes and the mount frequency is designed at $f_o = 71.1762$ Hz. The pertinent parameters for this system are given in Table 5.2. Similar to the low-frequency mount problem, the proportional gain $K_P$ tends to modify the frequencies of the system; therefore, a small gain was chosen so that its influence would be minimal. The gains for the derivative and integral were chosen in a similar manner to the low-frequency mount problem. The values for these gains are $K_D = 75$ and $K_I = 5.9\text{x}10^5$.

The frequency response functions or the system's transmissibilities for the undamped system and the system using $\mathcal{PD}$ and $\mathcal{PID}$ control are shown in Figure 5.19. $\mathcal{PD}$ control attenuates the first three modes because this system exhibits a strong interaction between the modes. The second mode is attenuated the most because this mode corresponds to the

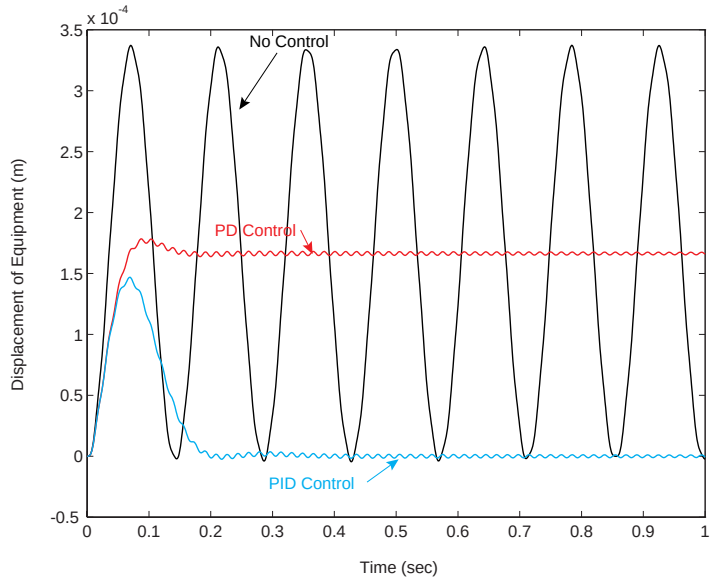


Figure 5.17: FBRE Transient Response to Step Input when $f_o = 7.1176$ Hz

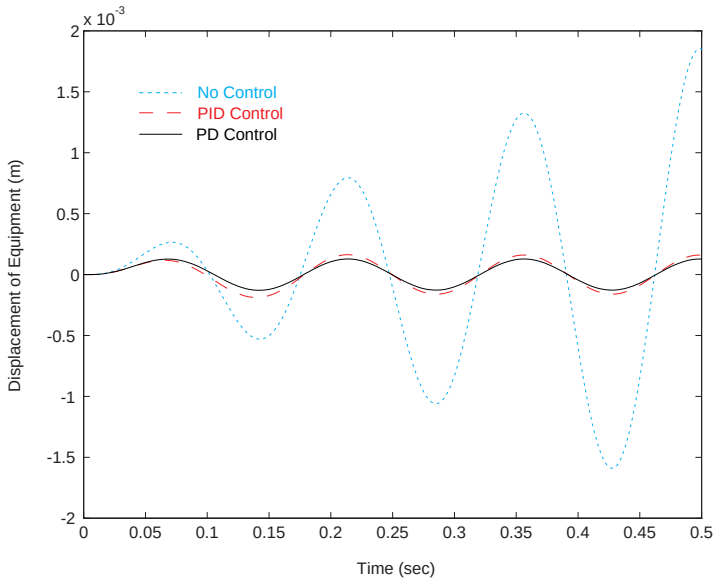


Figure 5.18: FBRE Transient Response to Sine Input when $f_o = 7.1176$ Hz

isolator mount. $\mathcal{PID}$ control has similar results except that it has better attenuation at the lower frequencies. As in the previous example, transient responses will help clarify the major differences between $\mathcal{PID}$ and $\mathcal{PD}$ control.

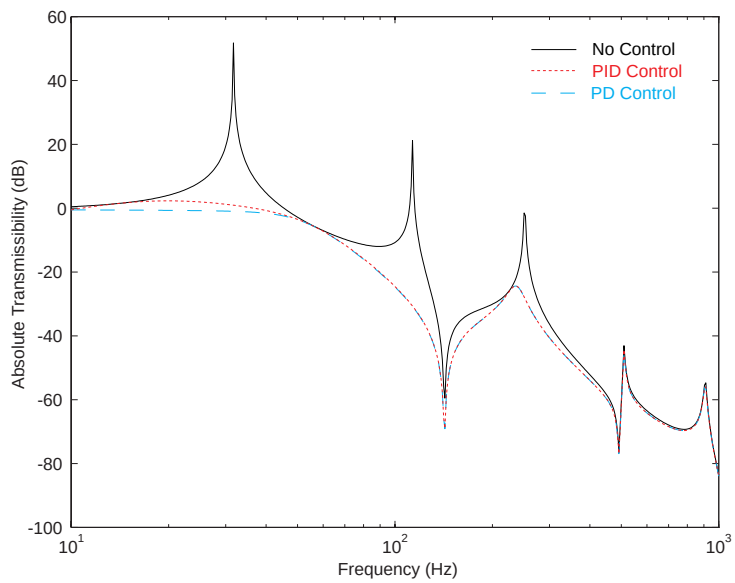


Figure 5.19: FBRE Frequency Response Function using PID for $f_o = 71.1762$ Hz

Figure 5.20 shows the transient responses due to a step input at $x = 0.04064$ m. For the undamped or uncontrolled FBRE system, the system will theoretically oscillate indefinitely at its natural frequencies. The system response will eventually reach a zero steady-state solution if structural damping is modeled in the base. Applying $\mathcal{PD}$ control to the system will make the equipment reach a steady-state solution around 0.04 seconds. Unlike the low-frequency mount problem, there is no oscillation after reaching a steady-state solution. This is attributable to the fact that the first three modes of the system are attenuated. With $\mathcal{PID}$ control, the displacement of the equipment reaches a steady-state solution around its initial position in about 0.07 seconds.

Figure 5.21 shows the equipment response due to a sinusoidal input at the first mode. With no control, the response of the equipment will grow with time. The displacement of the equipment will not go to infinity if damping is included in the base. However, $\mathcal{PID}$ or $\mathcal{PD}$ control will drastically alleviate this growth and the system will eventually settle to a steady-state solution. Once again, $\mathcal{PD}$ control is slightly more effective than $\mathcal{PID}$ control.

### 5.2.3 PPF Control

The previous sections have shown that $\mathcal{PID}$ control can be quite effective, especially at a mount frequency of $f_o = 71.1762$ Hz where multiple modes are attenuated. However,

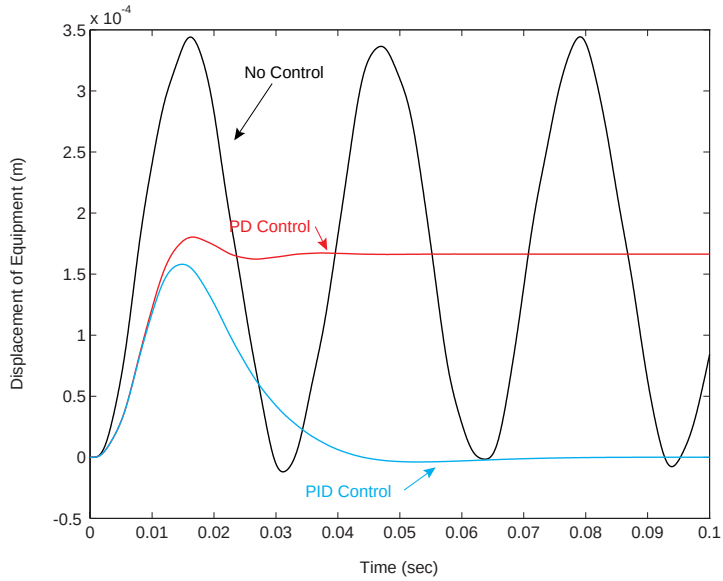


Figure 5.20: FBRE Transient Response to Step Input when $f_o = 71.1762$ Hz

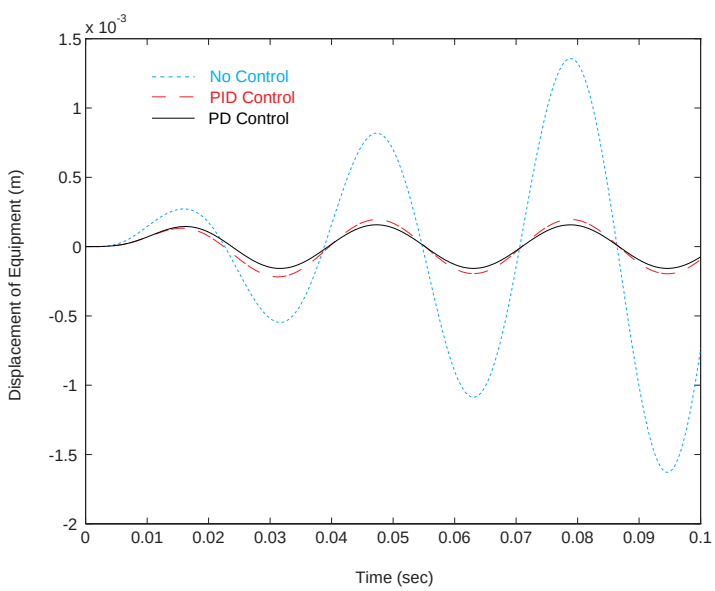


Figure 5.21: FBRE Transient Response to Sine Input when $f_o = 71.1762$ Hz

there may be situations where it is desired to attenuate only one mode. One such control methodology is a positive position feedback (PPF) controller. The PPF controller is a second-order filter in the form

$$\ddot{\eta} + 2\zeta_f \omega_f \dot{\eta} + \omega_f^2 \eta = \omega_f^2 \xi \tag{5.10}$$

where $\xi$ is the structural modal coordinate, $\eta$ is the filter coordinate, $\omega_f$ is the filter frequency, and $\zeta_f$ is the filter damping ratio. The filter coordinate is applied to the structure by the value $g\omega^2\eta$, where $g$ is the gain, and $\omega$ is a mode of the structure. By proper choice of $\zeta_f$ and $\omega_f$, the PPF controller can be used to attenuate any specific mode of the structure. A more detailed discussion on this technique and stability issues are found in the references [50, 51].

#### 5.2.3.1 Responses for Mount Frequency at $f_o = 7.1176$ Hz

For this system, it is desired that the PPF filter attenuates only the first mode. The gain, the frequency, and the damping ratio for the PPF compensator were chosen as $g = 0.005$, $f_f = 7.1176$ Hz, and $\zeta_f = 0.25$. The frequency responses for the undamped and the controlled system are shown in Figure 5.22. As seen from this figure, the PPF filter has effectively added damping to the first mode; almost 30 dB of attenuation has occurred at the first mode. The design parameters for the PPF filter were not optimized and better attenuation of the first mode can be obtained by adjusting these parameters. Other modes can also be attenuated by designing a PPF filter for each mode.

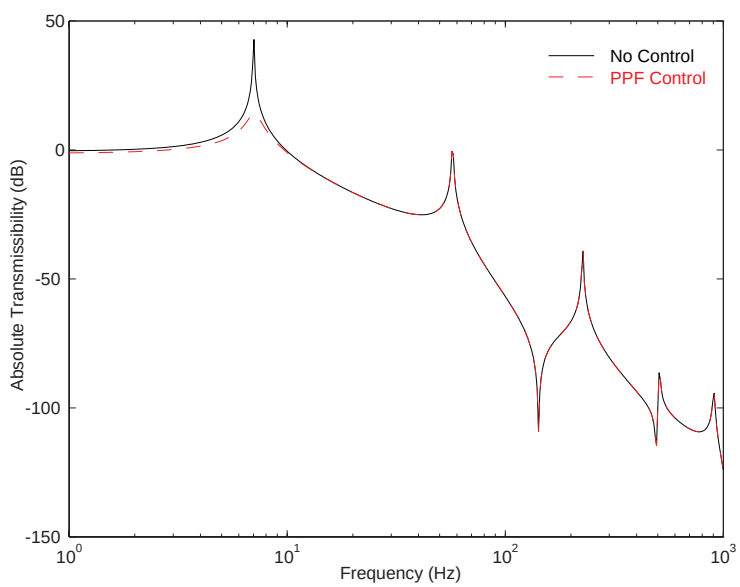


Figure 5.22: FBRE Frequency Response Function using PPF for $f_o = 7.1176$ Hz

The time response using a PPF filter from two disturbance inputs are analyzed; the disturbances include a step input and sinusoidal input. The results for the step input and the sinusoidal input are shown in Figure 5.23 and Figure 5.24, respectively. As seen from Figure 5.23, the step input is attenuated after one second. The PPF filter has also changed the first natural frequency of the system slightly since the structural position is used for feedback. This is somewhat analogous to the proportional gain in the $\mathcal{PID}$ controller.

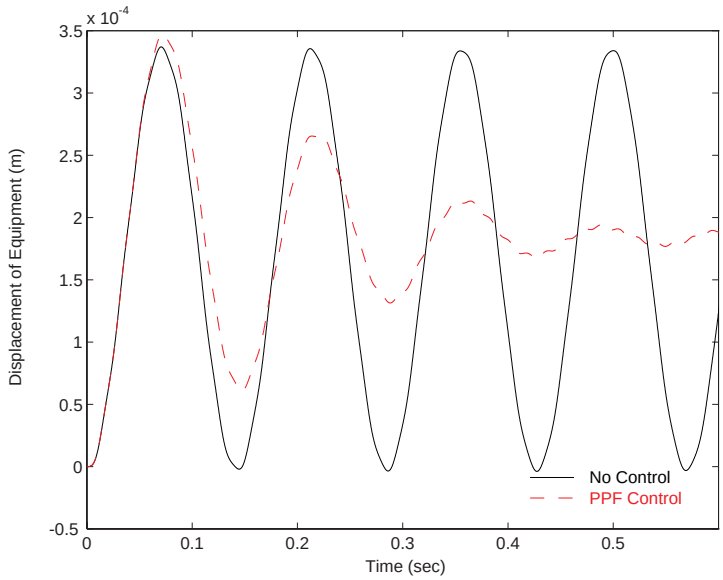


Figure 5.23: FBRE Transient Response to Step Input using PPF when $f_o = 7.1176$ Hz

Figure 5.24 shows the open-loop and closed-loop time response to a sinusoidal input. In the open-loop configuration, the response will grow with time but will be finite for a system that has base damping. The closed-loop response using the PPF filter significantly decreases the amplitude of the sinusoidal signal compared to the open-loop case.

Compared to $\mathcal{PID}$ control, PPF control is not as effective. The attenuation at the first mode is not as great as $\mathcal{PID}$ or $\mathcal{PD}$ control. As a result, the transient response using PPF control is not as good. However, the PPF filter is very useful when a specific mode has to be attenuated.

#### 5.2.3.2 Responses for Mount Frequency at $\mathbf{f_o = 71.1762}$ Hz

Table 5.2 lists the key parameters used to determine the FRF when the mount frequency is designed between two of the base modes. The gain, the filter frequency, and the damping ratio for the PPF compensator were chosen as $g = 0.035$, $f_f = 31.7227$ Hz, and $\zeta_f = 0.45$. The frequency response for the undamped and the controlled system are shown in Figure 5.25. The PPF filter was designed to attenuate the first mode and the first mode

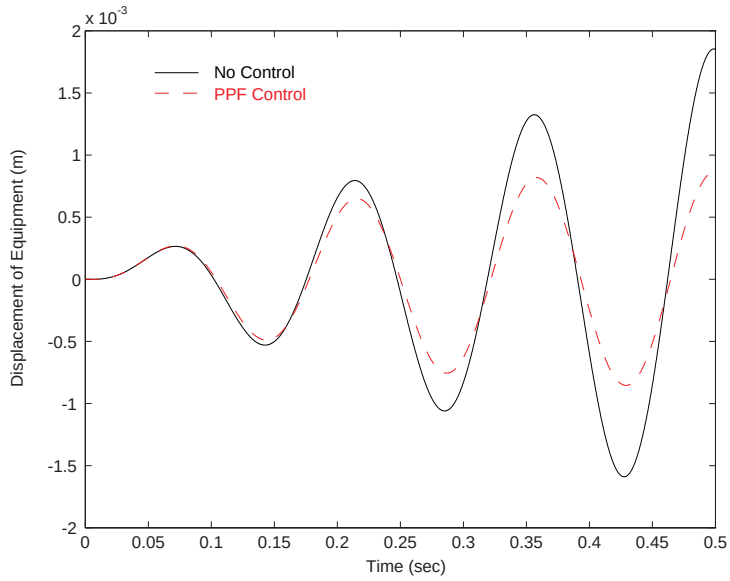


Figure 5.24: FBRE Transient Response to Sine Input using PPF when $f_o = 7.1176$ Hz

was attenuated by 30 dB. Even though multiple modes are attenuated with a $\mathcal{PID}$ or $\mathcal{PD}$ controller for this system, the PPF filter does not affect any of these other modes. This can be attributed to the fact that damping is added through positive position feedback and not velocity feedback for the PPF filter. If positive velocity feedback was used, multiple modes would be attenuated like the $\mathcal{PID}$ controller. Specific system modes can be attenuated by using a PPF filter for each mode that needs to be attenuated.

Similar to the system with a mount frequency at $f_o = 7.1176$ Hz, two disturbance inputs were used: a step input and a sinusoidal input at this system's first natural frequency. The results for these two disturbance inputs are given in Figure 5.26 and Figure 5.27, respectively. As shown in Figure 5.26, the system reaches a steady-state around 0.37 seconds. Unlike the low-frequency mount problem, the PPF filter has not significantly changed the natural frequency.

Figure 5.27 shows the open-loop and closed-loop time response due to a sinusoidal input. As seen from this figure, the open-loop response grows with time but will have a finite amplitude if proportional damping is assumed in the base. The implementation of the PPF filter has significantly decreased the transient response compared to the open-loop response.

### 5.2.4 Linear Quadratic Gaussian Regulator

The previous sections dealt with fairly simple control methodologies; therefore, an optimal controller such as the linear quadratic Gaussian (LQG) regulator will be used in this

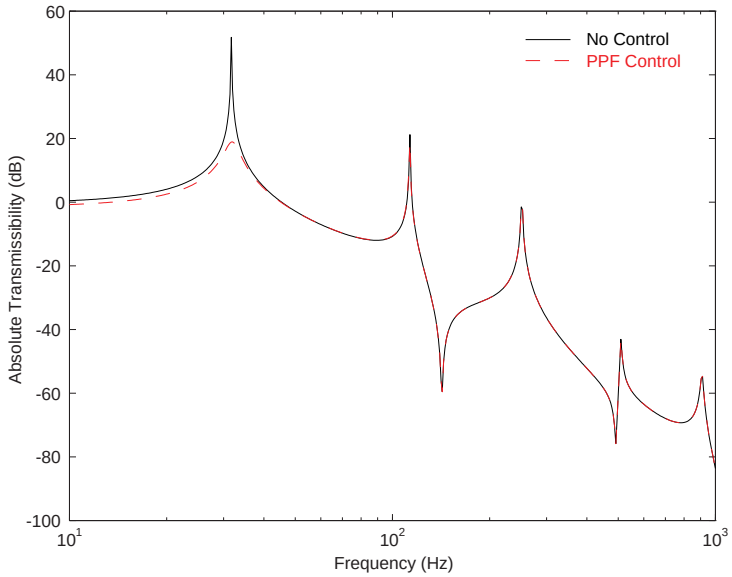


Figure 5.25: FBRE Frequency Response Function using PPF for $f_o = 71.1762$ Hz

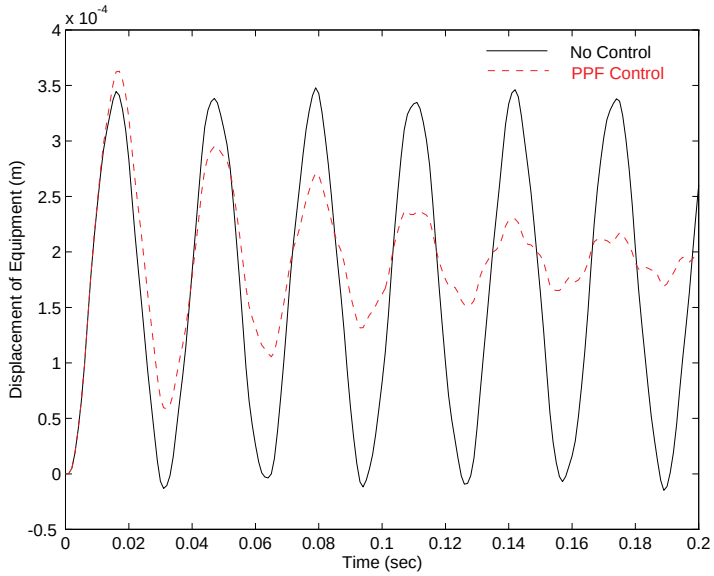


Figure 5.26: FBRE Transient Response to Step Input using PPF when $f_o = 71.1762$ Hz

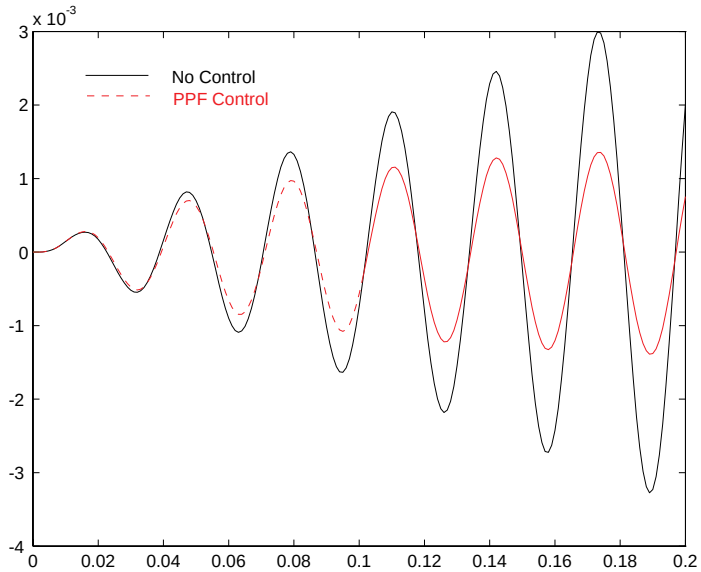


Figure 5.27: FBRE Transient Response to Sine Input using PPF when $f_o = 71.1762$ Hz

section. Detailed discussions on the use or implementation of a LQG regulator are found in Section 2.2.2 for a SDOF model and Section 4.7.4 for the FBRE system. The LQG design will determine the optimal gains for the regulator and the estimator; it is assumed that all of the states are not directly measurable. It is also assumed that a model of the disturbance is attainable and a shaping filter is used to model the disturbance.

Since the LQG regulator cannot be directly implemented using Yang's method, a modal series was used to determine the dynamic matrices $\underline{\underline{\mathbf{A}}}$, $\vec{\mathbf{B}}$, $\vec{\mathbf{C}}$ and $D$. However, unlike other series expansions, the actual eigenfunctions of the FBRE system will be used. By using a series expansion of eigenfunctions, the truncated system will correspond extremely close to the analytical solution. For instance, eight modes are used to model the FBRE system and the truncated system's natural frequencies are within 0.1% of the actual natural frequencies.

#### 5.2.4.1 Responses for Mount Frequency at $\mathbf{f_o = 7.1176}$ Hz

For the system with a mount frequency at $f_o = 7.1176$ Hz, the LQG regulator was designed such that the frequency response function would exhibit some type of notch filter at the first natural frequency. The disturbance source location and other key parameters to determine the FRF are given in Table 5.2. Figure 5.28 shows the response of this particular system using an LQG regulator. The attenuation around the first natural frequency is similar to $\mathcal{PD}$ or $\mathcal{PID}$ control. The significant difference is the beginning of a notch at the first mode. By adjusting the performance index $\vec{\mathbf{z}}$, this notch can be designed to be significantly deeper but will be limited by the performance of the actuator. A design with

a deeper notch was not chosen because the current design gives good overall transient performance as well as adequate performance in the frequency domain. However, if there is concern that a significant disturbance is near the first mode, a redesign may be necessary.

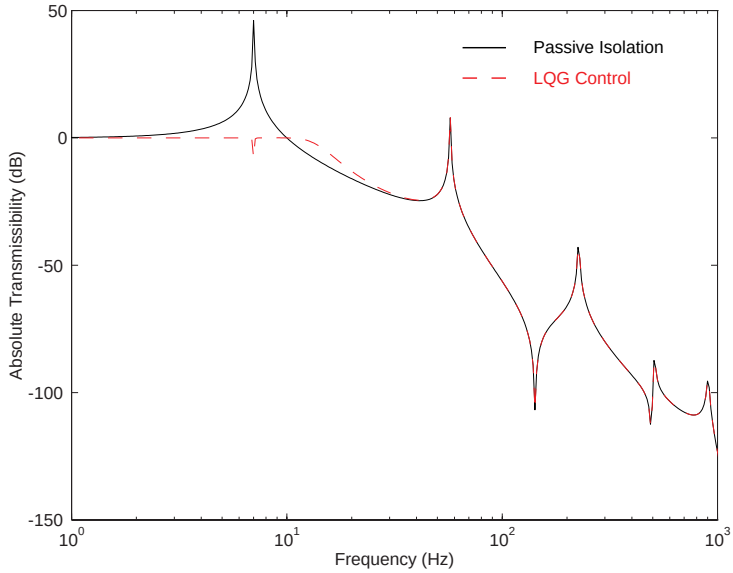


Figure 5.28: FBRE Frequency Response Function using LQG for $f_o = 7.11762$ Hz

Unlike the previous sections, the only transient response to be analyzed is one due to a step input. The performance of the LQG control is somewhat similar to $\mathcal{PD}$ or $\mathcal{PID}$ control and further insight into the LQG control architecture will not be gained by analyzing the time response to a sinusoidal input. The results for a step disturbance is shown in Figure 5.29. As seen from this figure, the $\mathcal{PD}$ controller and LQG controller are very similar. However, the $\mathcal{PD}$ controller was designed to give its best performance while the performance of the LQG controller can be enhanced. This can be accomplished by changing the performance index or the quadratic penalties as outlined in Section 2.2.2. By adjusting the performance index, the LQG controller can be made to look like a $\mathcal{PID}$ controller. Note that the LQG controller has a small oscillation after the first mode is attenuated. This is the second and higher modes of the system which are not affected by the LQG controller.

#### 5.2.4.2 Responses for Mount Frequency at $\mathbf{f_o = 71.1762}$ Hz

The design goal for this system is different than the system with a low-frequency mount. It was discussed in previous sections that this system has a strong interaction between the first three modes. With this realization, the controller was designed to limit the transmissibility of the second mode; in this way, the LQG controller can be compared to the

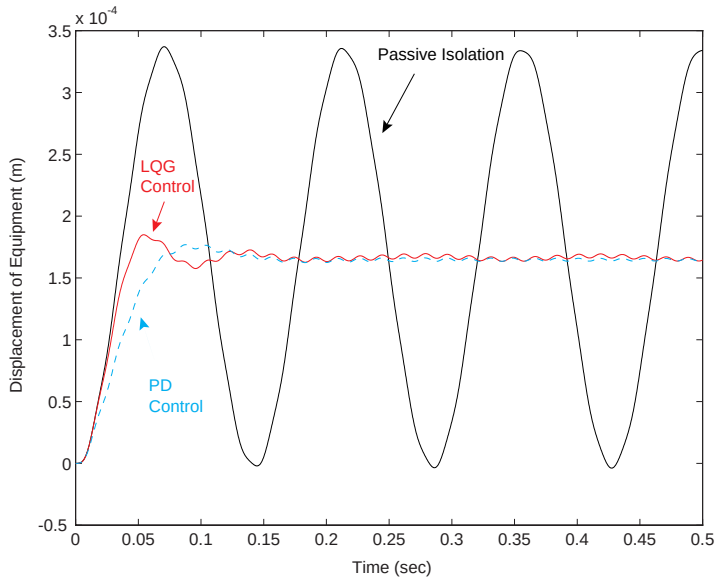


Figure 5.29: FBRE Transient Response to Step Input using LQG when $f_o = 7.1176$ Hz

$\mathcal{PID}$ controller. Figure 5.30 is the frequency response for the LQG controller. A notch was created at the second frequency of the system and due to the high interaction between the first few modes the first and third modes are attenuated as well. The performance of this compensator is similar to the $\mathcal{PID}$ or $\mathcal{PD}$ controller. As shown in Figure 5.19, the attenuation in the first and third modes of the $\mathcal{PID}$ controller is similar to the LQG controller. However, the second mode for the $\mathcal{PID}$ controller has been significantly attenuated while a notch has been created at the second mode for an LQG controller.

Like the low-frequency mount, a comparison of the LQG controller to the $\mathcal{PID}$ controller in the time domain was accomplished. The significant parameters for determining the transient response is given in Table 5.2. Figure 5.31 is the transient response to a step input on the base. This figure shows that the $\mathcal{PD}$ response and LQG response are nearly equivalent with the rise time and settling time being equivalent. The only noticeable difference is where the equipment finally settles for each controller. Even though the performance of each controller is similar, the system with the $\mathcal{PD}$ controller performs near its maximum and the performance of the LQG controller can still be enhanced. This can be accomplished by changing the performance index or by changing how the state and the control input are penalized.

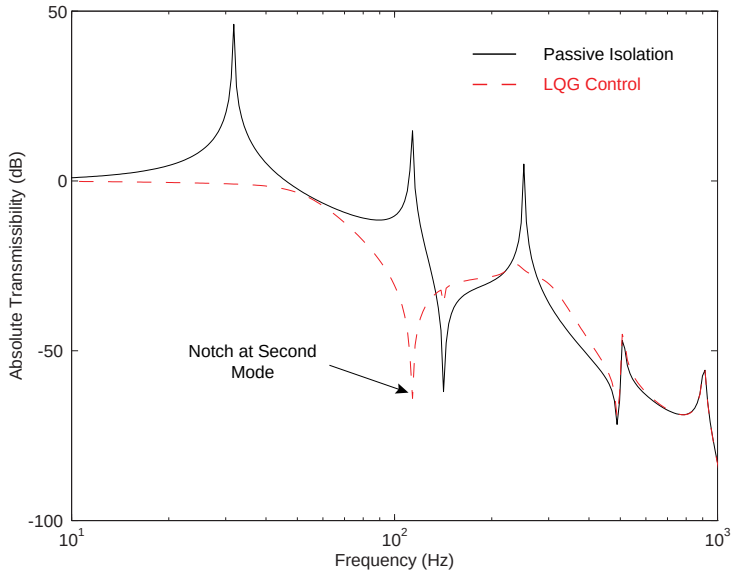


Figure 5.30: FBRE Frequency Response Function using LQG for $f_o = 71.1762$ Hz

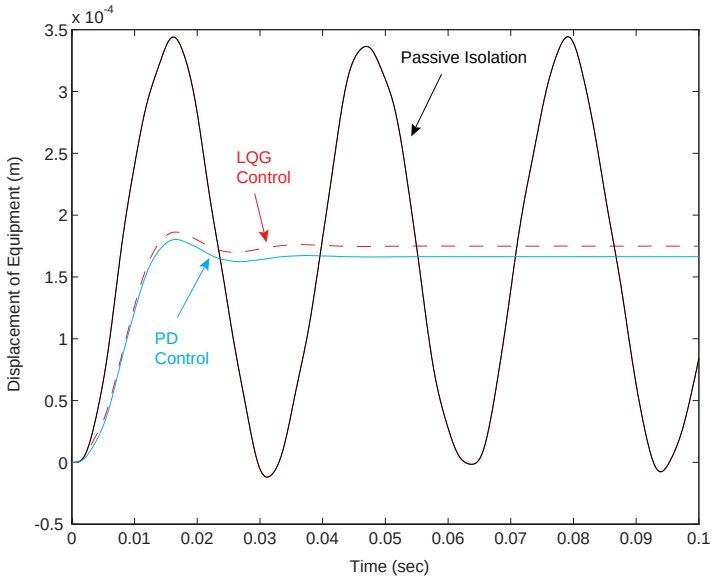


Figure 5.31: FBRE Transient Response to Step Input using LQG when $f_o = 71.1762$ Hz

## 5.3 Summary

The influence of base flexibility on isolation design has been examined and discussed in detail. It has been shown that the choice of the mount frequency will have a significant impact in the isolation design. If the mount frequency is designed between two modes of the base, a strong interaction between the modes will exist. When damping is included in the isolator, this interaction will simultaneously attenuate three modes instead of one mode.

The overall best values for the equipment mass, mount frequency, and isolator placement are also discussed but this discussion does not include the effects of isolator damping. Therefore, trade-offs must be performed to determine the best values for the equipment mass, mount frequency, and isolator placement when damping is present the isolator. A comparison between a single passive isolator and a dual passive isolator is also discussed.

It has also been shown that when an active isolator is used, it is desired to place the sensor on the equipment. If the sensor is placed on the base, the high frequency transmissibility is increased and the amount of attenuation at the first mode is less than a system that uses equipment feedback. Similar to the SDOF model, active isolation adds damping to the system but does not increase the high frequency transmissibility. Control implementations such as $\mathcal{PID}$ control, PPF control, and LQG control are discussed and a comparison between each controller with a passive isolator is made. $\mathcal{PID}$ and LQG were shown to be quite affective especially when modes are coupled through proper choice of the mount frequency. PPF control was shown to attenuate specific modes of the FBRE system without influencing other modes.

Table 5.3 is a summary of the performance for each control methodology. The performances are based on the time responses due to a unit step input; however, the frequency response functions should also be considered when choosing one control methodology over another. For a system with a low-frequency mount, the LQG controller is the best performer in all three performance criteria, that is, smallest rise time, settling time, and overshoot. However, $\mathcal{PID}$ control was the only control design that would bring the equipment back to its initial equilibrium point. When the mount frequency was chosen at $f_o = 71.1762$ Hz, $\mathcal{PD}$ and LQG were the better performers with $\mathcal{PD}$ control being slightly better than the LQG controller.

Table 5.3: Summary of Controller Performances for FBRE System

| Control Method | $f_o = 7.1176$ Hz | | | $f_o = 71.1762$ Hz | | |
|---|---|---|---|---|---|---|
| | $t_s$ | $t_r$ | Overshoot | $t_s$ | $t_r$ | Overshoot |
| | | | | | | |
| Passive (Undamped) | - | - | $1.686\text{x}10^{-4}$ | - | - | $1.7403\text{x}10^{-4}$ |
| $\mathcal{PD}$ | 0.048 | 0.17 | $8.430\text{x}10^{-6}$ | 0.0082 | 0.0404 | $6.495\text{x}10^{-6}$ |
| $\mathcal{PID}$ | - | 0.30 | $1.460\text{x}10^{-4}$ | - | 0.07 | $1.583\text{x}10^{-4}$ |
| PPF | 0.044 | 1.05 | $1.735\text{x}10^{-4}$ | 0.0098 | 0.37 | $1.812\text{x}10^{-4}$ |
| LQG | 0.040 | 0.17 | $2.438\text{x}10^{-6}$ | 0.0092 | 0.040 | $1.144\text{x}10^{-5}$ |

# Chapter 6

# Flexible Base, Flexible Equipment

This chapter is an analysis of a vibration isolation design where the equipment and base are flexible. The chapter follows the same format in Chapter 5, so a direct comparison can be made between the flexible base, rigid equipment (FBRE) and flexible base, flexible equipment (FBFE) system. The chapter is divided into two major sections: one section discussing passive isolation and the other section discussing active isolation.

The section on passive isolation is comprised of four subsections. The first subsection is an analysis of the FBFE natural frequencies for different isolator placements along the base and the equipment, and for various isolator mount designs. The second subsection determines the effect of isolator damping on the system's transmissibility. The third subsection is an analysis of the transmissibility for varying ranges of equipment mass, base mass, mount frequency, and isolator placement. The final subsection looks at dual isolators to increase performance over a single isolator system.

The section on active isolation is comprised of two major subsections. The first subsection determines whether the feedback sensor should be placed on the equipment or the base. The second subsection determines the effectiveness of three different control methodologies on three different flexible base, flexible equipment isolation systems. The control architectures that will be used are classical controllers such as a proportional-plus-integral-plus-derivative ($\mathcal{PID}$) controller and a proportional-plus-derivative ($\mathcal{PD}$) controller, a second-order compensator such as a positive position feedback (PPF) controller and an optimal controller such as a linear quadratic Gaussian (LQG) regulator.

## 6.1 Passive Isolation

It has already been shown in Chapter 5 that the choice of the isolator mount frequency will significantly affect the system transmissibility. Therefore, this section will determine the effect of the isolator mount design when the equipment and the base are flexible. Unlike Chapter 5, the effect of isolator placement along the base and equipment is discussed,

as well as discussing the effect of different base and equipment lengths. The effect of isolator damping is discussed, as well as analyzing the isolation system with varying mount frequencies, mass ratios, and isolator placements. Dual isolators are also considered and its performance is compared to a single isolator system.

### 6.1.1 Mount Effectiveness and Isolator Placement

It was shown in Chapter 5 that the choice of the isolator mount frequency for a flexible system has a significant impact on the overall isolation design. Therefore, it is desired to see if the same type of results will occur for the flexible base, flexible equipment (FBFE) system. Figure 6.1 is a representation of the FBFE system under study; the base or foundation is assumed to have pinned boundary conditions while the equipment is assumed to have free boundary conditions. The base and equipment are attached via a massless isolator; the isolator has a stiffness $k$, and a damping coefficient $c$ or damping ratio $\zeta$. The isolator is attached at a distance $x_j$ from the left end of the base and a distance $x_l$ from the left end of the equipment. The properties of each beam are tabulated in Table 4.1, and the mount or corner frequency is defined as $\omega_o = \sqrt{k/m_e}$. It is also assumed that there is no structural damping present in the equipment and base, and no viscous damping present in the isolator for the systems considered in this section.

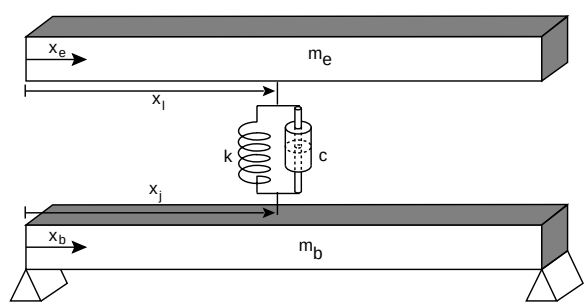


Figure 6.1: Flexible Base, Flexible Equipment System

Table 6.1 lists the FBFE natural frequencies at different isolator locations for an isolation mount designed at $f_o = 7.674$ Hz; the natural frequencies of a pinned-pinned beam and free-free beam are also given. The isolator placement along the base and the equipment are assumed equivalent ($x_j = x_l$) and the base length is equivalent to the equipment length. For a mount frequency designed much less than the first natural frequency of either the base or the equipment, the FBFE system will have natural frequencies that are a concatenation of the mount frequency, pinned-pinned frequencies and free-free frequencies. For instance, consider the situation when the isolator is placed at a distance $x_j = x_l = L/2.561$. The first natural frequency of the FBFE frequency will correspond to the isolator mount and

the rest of the FBFE frequencies will correspond to the pinned-pinned beam and free-free beam frequencies. Unlike the flexible base, rigid equipment (FBRE) system, the first natural frequency is not always less than the mount frequency for a low-frequency mount design; that is, the isolator mount has a lower frequency than any of the base or equipment modes. By modeling the equipment flexibility, the first natural frequency is now dependent on the isolator location. When the isolator is placed at the midpoint of the base and equipment, the first natural frequency of the FBFE system will be less than the mount frequency. As the isolator is placed away from the midpoint of the beams, the first natural frequency of the FBFE system tends to increase. There is a 15.6% difference between the first mode when an isolator is placed at L/2 compared to an isolator placed at L/3.125. The other modes shift as well but not as significantly as the first mode; for example, the second mode shifts by only 0.5%.

Table 6.1: FBFE Frequencies at Mount Frequency $f_o = 7.674$ Hz

| Mode | Pin-Pin | Free-Free | Actuator Placement | | |
|---|---|---|---|---|---|
| | | | L/2 | L/2.561 | L/3.125 |
| | | | | | |
| 1 | 56.580 | 128.261 | 7.512 | 8.053 | 8.904 |
| 2 | 226.320 | 353.555 | 57.622 | 57.508 | 57.332 |
| 3 | 509.220 | 693.109 | 128.603 | 128.495 | 128.363 |
| 4 | 905.282 | 1145.744 | 509.336 | 226.425 | 226.533 |
| 5 | 1414.509 | 1711.544 | 693.195 | 353.644 | 353.701 |
| 6 | 2036.908 | 2390.050 | 1414.541 | 509.250 | 509.222 |
| 7 | 2772.249 | 3182.624 | 1711.579 | 693.121 | 693.121 |

Consider the situation when the mount frequency is placed between two modes of the flexible base, flexible equipment system; this system is referred as a mid-frequency mount design. For example, the mount frequency is designed at $f_o = 76.737$ Hz and this frequency lies between the first modes of the equipment and base. The FBFE frequencies for three different isolator placements are given in Table 6.2 and similar to the FBRE system, the new FBFE frequencies significantly interact with each other at the lower frequencies. For example, consider when the isolator is placed at $x_j = x_l = L/3.125$. Note that the first FBFE frequency corresponds to the first base mode, the second FBFE mode corresponds to the isolator mount and the third FBFE modes corresponds to the first mode of the equipment. The rest of the FBFE modes are a concatenation of the second and higher modes of a pinned-pinned beam and a free-free beam which are given in Table 6.1. The first FBFE modes has moved from 56.58 Hz to 36.828 Hz, the second mode has shifted

from 76.737 Hz to 104.582 Hz and the third mode has shifted from 128.261 Hz to 144.666 Hz. This corresponds to a 34.9%, 26.6% and 11.3% difference in the first three modes, respectively.

Table 6.2: FBFE Frequencies at Mount Frequency $f_o = 76.737$ Hz

| Mode | Isolator Placement | | |
|---|---|---|---|
| | L/2 | L/2.561 | L/3.125 |
| | | | |
| 1 | 29.620 | 32.377 | 36.828 |
| 2 | 98.899 | 100.772 | 104.582 |
| 3 | 181.983 | 162.499 | 144.666 |
| 4 | 520.963 | 240.930 | 249.716 |
| 5 | 702.457 | 364.217 | 371.700 |
| 6 | 1418.694 | 512.629 | 509.436 |
| 7 | 1715.065 | 694.305 | 694.371 |

The previous paragraphs only discussed situations when the isolator was placed at equivalent locations along the equipment and base. However, there can be situations when the isolator is placed at different positions along the base and the equipment. Table 6.3 lists the natural frequencies of the FBFE system for three different isolator placements. Note that the mount frequency was designed at $f_o = 7.674$ Hz. The frequencies for these systems compare very well to each other except that the even modes of the base are not present for the first system since the isolator is placed at the midpoint of the base. Also, the first mode of these systems will greatly depend where the isolator is placed on the equipment. That is, the first FBFE frequency in Table 6.3 will correspond to the systems in Table 6.1 which have similar isolator placements along the equipment. The rest of the FBFE frequencies are dependent on the isolator locations along the base and the equipment. For instance, assume that the isolator is placed at $x_j = L/2.561$ along the base and at $x_l = L/3.125$ along the equipment. The even modes of this system are similar to the even modes in Table 6.1 for an isolator placed at $x_j = x_l = L/2.561$. The odd modes of this system is comparable to the odd modes of the FBFE system in Table 6.1 where the isolator is placed at $x_j = x_l = L/3.125$. Therefore, given the frequencies in Table 6.1, there is an easy way to determine the frequencies for a system having different isolator placements along the base and the equipment. The odd modes of this new system will correspond to the odd modes of Table 6.1 for a given isolator placement along the equipment. The even modes are determined by the even modes in Table 6.1 for a given isolator placement along the base. This does not fully hold for the first system in Table 6.3 since the isolator is placed at the midpoint of the base.

Table 6.3: FBFE Frequencies for Varying Isolator Placements

| Mode | Isolator Placement | | |
|---|---|---|---|
| | $x_b$ = L/2<br>$x_e$ = L/3.125 | $x_b$ = L/2.561<br>$x_e$ = L/3.125 | $x_b$ = L/3.125<br>$x_e$ = L/2.561 |
| | | | |
| 1 | 8.864 | 8.880 | 8.075 |
| 2 | 57.633 | 57.514 | 57.327 |
| 3 | 128.363 | 128.363 | 128.494 |
| 4 | 353.700 | 226.425 | 226.534 |
| 5 | 509.336 | 353.700 | 353.644 |
| 6 | 693.121 | 509.250 | 509.222 |
| 7 | 1145.761 | 693.121 | 693.121 |

Another situation that can occur is when the equipment length is different than the length of the base. For instance, consider the case when the length of the equipment is 85% the length of the base. The frequencies for the equipment are given in Table 6.4 under the heading *Free-Free* and the frequencies of the pinned-pinned base are also given for reference. Similar to the situation with the length of the base and equipment being equivalent, the frequencies of this new FBFE system are a concatenation of the mount frequency, the pinned-pinned frequencies and the free-free frequencies for a low-frequency mount design. Notice that the first natural frequency of the FBFE system has increased since the length of the equipment has decreased. This increase in the first mode is due to the fact that the mass of the equipment has decreased; thereby increasing the mount frequency which is now $f_o = 8.323$ Hz. The other effect of shortening the length of the equipment is to increase the frequencies of the FBFE system that correspond to the equipment. Otherwise, the results discussed for equivalent equipment and base lengths are the same for this system that has different base and equipment lengths.

### 6.1.2 Isolator Damping

Section 6.1.1 assumed that there was no damping present in the isolator; therefore, this section is an analysis of the flexible base, flexible equipment (FBFE) system with isolator damping. Two different FBFE systems will be discussed: a system with a mount frequency designed at $f_o = 7.674$ Hz and the other system designed at $f_o = 76.737$ Hz. The isolator will be placed at equivalent positions along the base and equipment ($x_b = x_e = \mathrm{L}/3.125$).

Figure 6.2 shows the influence of isolator damping when the mount frequency is designed at $f_o = 7.674$ Hz. The first mode of the FBFE system is attenuated and a small portion

Table 6.4: FBFE Frequencies With Equipment Length Different from Base

| Mode | Pin-Pin | Free-Free | Isolator Placement | | |
|---|---|---|---|---|---|
| | | | L/2 | L/2.561 | L/3.125 |
| | | | | | |
| 1 | 56.580 | 177.523 | 8.156 | 8.741 | 9.662 |
| 2 | 226.320 | 489.349 | 57.628 | 57.513 | 57.336 |
| 3 | 509.220 | 959.320 | 177.813 | 177.721 | 177.610 |
| 4 | 905.282 | 1585.805 | 509.336 | 226.426 | 226.534 |
| 5 | 1414.509 | 2368.920 | 959.394 | 489.425 | 489.473 |
| 6 | 2036.908 | 3308.656 | 1414.541 | 509.250 | 509.222 |
| 7 | 2772.249 | 4405.016 | 2368.949 | 905.342 | 905.318 |

of damping is present in the next few modes as well. As in the SDOF model and the FBRE system, viscous damping will cause the transmissibility at frequencies greater than the mount frequency to increase compared to an undamped system.

A different situation occurs when the mount frequency is designed between the first two modes of the base and equipment. Figure 6.3 is the transmissibility when the mount frequency is designed at a value $f_o = 76.737$ Hz. Similar to the FBRE system, a strong interaction exists between the modes; therefore, multiple modes are attenuated. As seen from this figure, the first mode is lightly attenuated while the second, third, fourth and fifth modes are significantly attenuated. As in the low-frequency mount design, the transmissibility at higher frequencies is increased with respect to a system that has no damping.

### 6.1.3 Isolator Performance for Varying Parameters

The first section describes and analyzes various flexible base, flexible equipment (FBFE) systems. This section expands this analysis by analyzing FBFE systems that have wide varying equipment masses, base masses, isolator placements, and mount frequencies. The analysis is equivalent to the one performed on the FBRE system except for two caveats. First, the disturbance source spans a frequency range from 1 to 2000 Hz. The second difference is how the equipment mass is changed. Since the equipment is a distributed member, a change in mass will result in a change in density while holding the length constant or a change in length with the density constant. Both types of systems are equally important; therefore, each type of system will be analyzed.

The first system that will be considered is an FBFE system with a fixed equipment length; therefore, the equipment density is varied. For this system, the mount frequency is

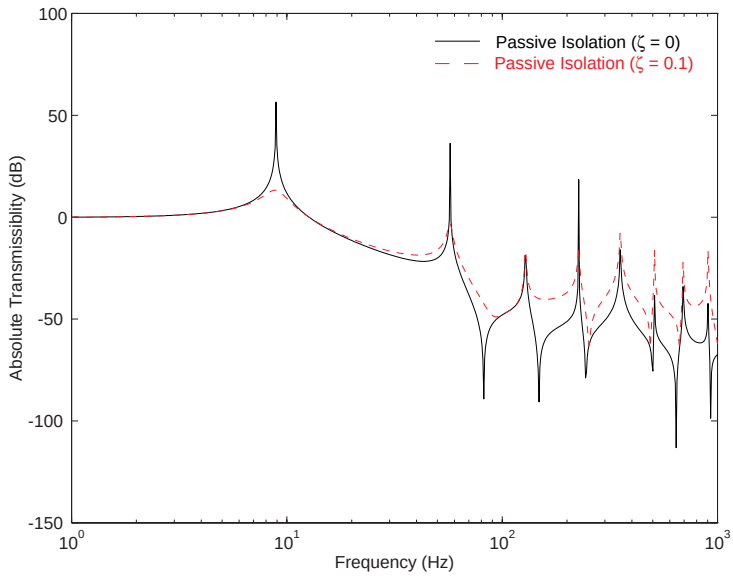


Figure 6.2: Influence of Isolator on FBFE System with $f_o = 7.674$ Hz

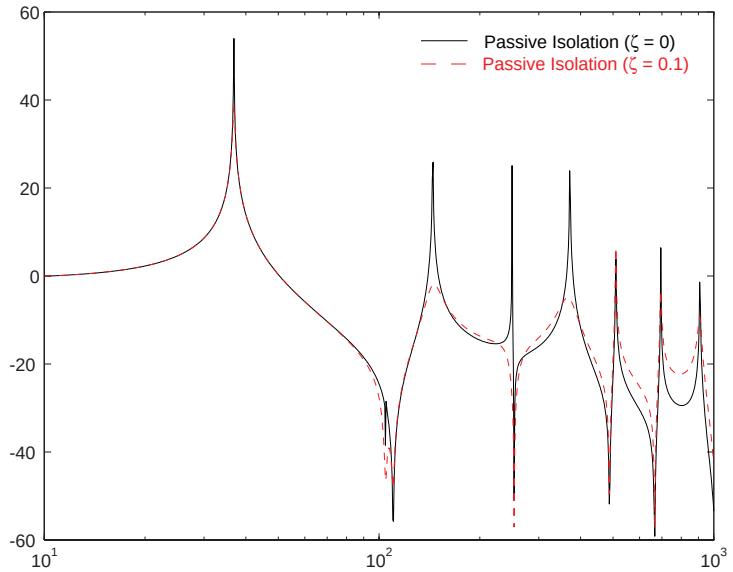


Figure 6.3: Influence of Isolator on FBFE System with $f_o = 76.737$ Hz

varied from 7 Hz to 600 Hz, the equipment density is varied from one-twentieth the density of the base to twenty times the density of the base, and the isolator is placed between the left and right ends of the base and the equipment. After calculating the RMS levels of the transmissibility in decibels, the results are plotted in Figure 6.4 and Figure 6.5. Note that the isolator placement is nondimensional and zero indicates a starting position at the left end of the system and one indicates the isolator position at the right end. Also, the density ratio is actually the log ratio of the equipment density to the base density.

Figure 6.4 shows the RMS transmissibility levels for the FBFE system at three specific mount frequencies: $f_o = 7$ Hz, 225 Hz and 381 Hz. The best overall performance is at extremely low-frequency mounts; however, the inclusion of the equipment flexibility has severely degraded isolator performance which can be seen by comparing Figure 5.7 with Figure 6.4. When the equipment is rigid, almost all isolator placements and mass ratios have a significant effect on the transmissibility at the 7 Hz mount frequency. This is not the case when the equipment is flexible, as seen in Figure 5.7. Also, the best density ratio for the flexible base, flexible equipment system occurs when the equipment density is larger than the base density, similar to the FBRE system. This can be seen much easier in Figure 6.5 where the performance is shown for three different density ratios: equipment density greater than, equal to, and less than the base density. The system with a low density ratio performs much worse than any other density ratio with equivalent mount frequencies and isolator placements.

The second system considered is an FBFE system with the equipment having a fixed density while the length of the equipment varies. Similar to the previous system, the mount frequency is varied from 7 Hz to 600 Hz, the isolator is placed from the left end to the right end of the equipment and the base and the equipment length is varied from one-twentieth the length of the base to twenty time the length of the base. The resulting RMS transmissibility for this system are shown Figure 6.6 and Figure 6.7. Note that the isolator placement is nondimensional and zero indicates a starting position at the left end of the system and one indicates the isolator position at the right end. Also, the length ratio is actually the log ratio of the equipment length to the base length.

Figure 6.6 shows the RMS transmissibility levels for the FBFE system at three specific mount frequencies: $f_o = 7$ Hz, 225 Hz and 381 Hz. The best overall performance for this system is at extremely low-frequency mounts. The transmissibility at higher mount frequencies become severely degraded with respect to the lower mount frequencies. Also, for the higher mount frequencies, the smaller length ratios tend to outperform the systems with larger length ratios. The smaller length ratios are better because as the equipment length gets smaller, a greater portion of the equipment mass is in a smaller volume, and this type of system will start to act more like a rigid system. The performance is better seen in Figure 6.7 where the transmissibility is shown for three separate length ratios: the equipment length greater than, equal to, and less than the base length.

It should be noted that each system does not include any significant amounts of damp-

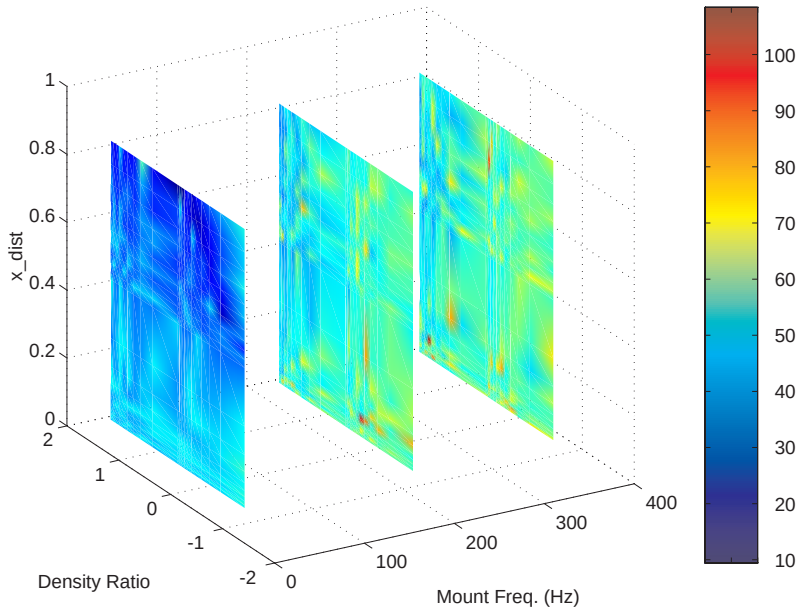


Figure 6.4: FBFE RMS Transmissibility for Varied Equipment Density at Various Mount Frequencies

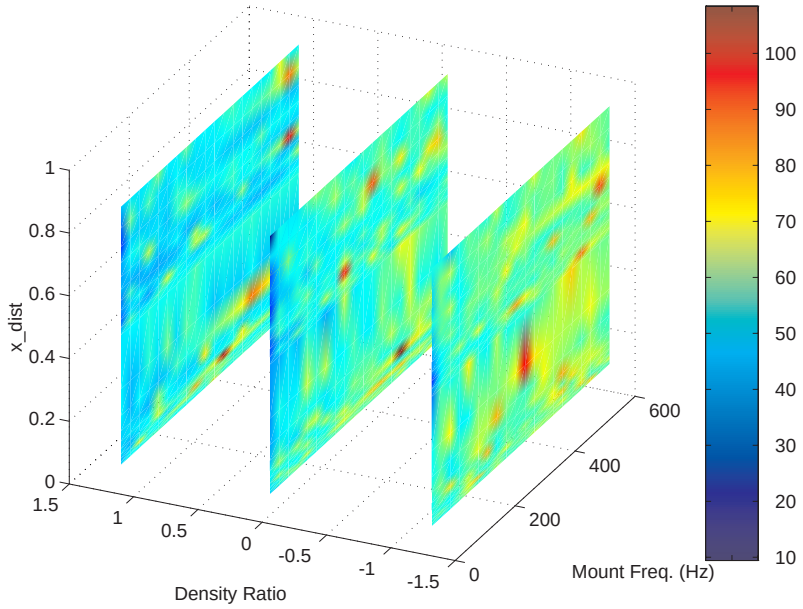


Figure 6.5: FBFE RMS Transmissibility for Varied Equipment Density at Various Density Ratios

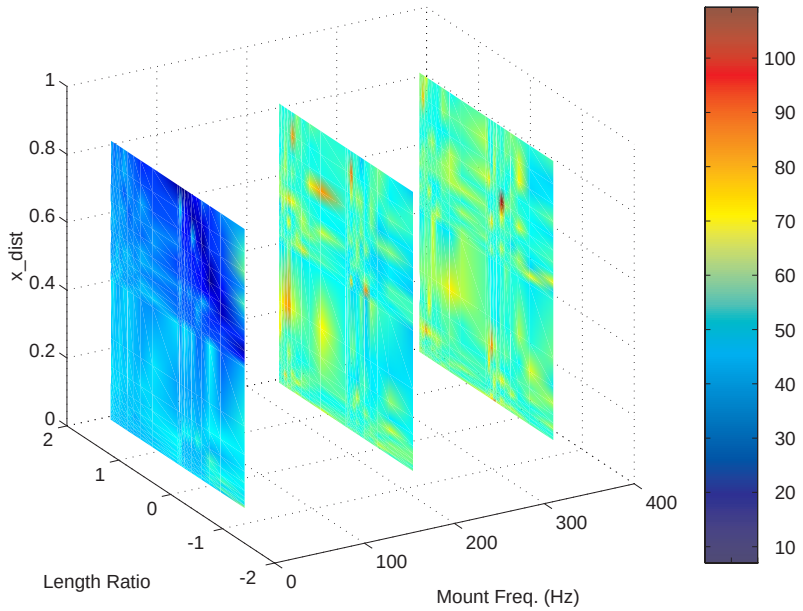


Figure 6.6: FBFE RMS Transmissibility for Varied Equipment Length at Various Mount Frequencies

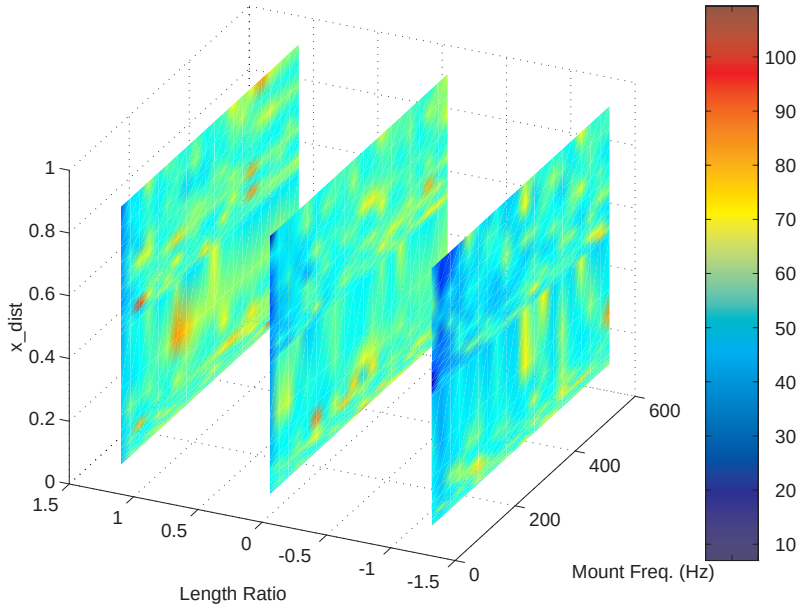


Figure 6.7: FBFE RMS Transmissibility for Varied Equipment Length at Various Density Ratios

ing in the system. System damping at a level of 0.01% was assumed so the resonant modes would be finite. It has already been shown that isolator damping can attenuate multiple modes with proper choice of the mount frequency. However, in an overall sense, the transmissibility is worse at this mid-frequency mount compared to a system with a very low-frequency mount. Therefore, a trade-off must be performed to determine the best combination of the mid-frequency mount and isolator damping.

### 6.1.4 Dual Isolators

The previous sections used a single isolator to perform isolation. However, there may be situations when more than one isolator must be used. For instance, a single isolator may not be used to inhibit the rotational motion of the equipment. Therefore, this section will analyze isolator performance using dual isolators.

The FBFE system using two isolators is shown in Figure 6.8 and each isolator is placed at equal positions along the base and the equipment. The isolators are placed equidistant ($a_x/2$) from the position $x = L/3.125$ on the equipment and base so a comparison to the single isolator system can be made. The isolator components are still assumed massless, and each spring has a stiffness of 50 N/m. When viscous damping is included in the isolator, the system will have an overall damping ratio of 10%.

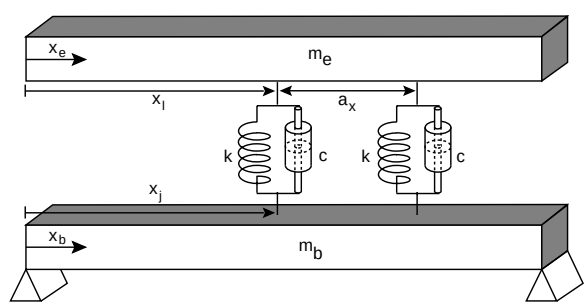


Figure 6.8: FBFE System with Dual Isolators

The results for this new system without any form of damping is shown in Figure 6.9; the single isolator system's transmissibility is also shown. A significant difference between the two systems is the extra mode for the dual isolator system; this is due to the additional isolator. Another difference is the location of the anti-resonant modes where they are slightly shifted with respect to the single isolator system. Unlike the flexible base, rigid equipment (FBRE) system, the performance of the FBFE system using dual isolators has not been significantly increased. Only a minor decrease in the system transmissibility has occurred. However, the use of dual isolators should not be disregarded since they will help mitigate any rotations of the equipment.

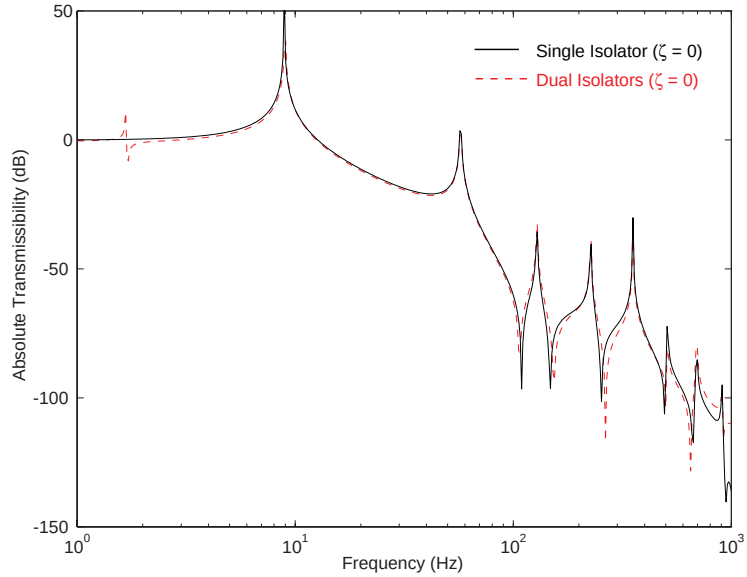


Figure 6.9: FBFE Comparison Between Single and Dual Isolators

It has been shown that a single isolator system that has damping will increase the high frequency transmissibility of the system. This is also the case for the dual isolator system as shown in Figure 6.10. This figure compares the dual isolation system with no damping and one that has an overall damping ratio of 10%. The first two modes of this system are significantly attenuated since these modes correspond to the isolators. The transmissibility in the higher frequency ranges has increased similar to the single isolator system.

## 6.2 Active Isolation

This section describes the use of active isolators for the flexible base, flexible equipment (FBFE) system. Active isolation is divided into two main parts: the first part analyzes the placement of the feedback sensor and the second part uses three different control methodologies to achieve transmissibility reductions. The control strategies used are the same ones used on the flexible base, rigid equipment (FBRE) system. They are a proportional-plus-integral-plus-derivative ($\mathcal{PID}$) controller including a proportional-plus-derivative ($\mathcal{PD}$) controller, a positive position feedback (PPF) controller, and a linear quadratic gaussian (LQG) regulator.

Active isolation will be performed on three separate and unique systems. One system will have a mount frequency designed at $f_o = 7.674$ Hz and another designed at $f_o = 76.737$ Hz. For these two systems the lengths of the beam and the equipment are assumed to

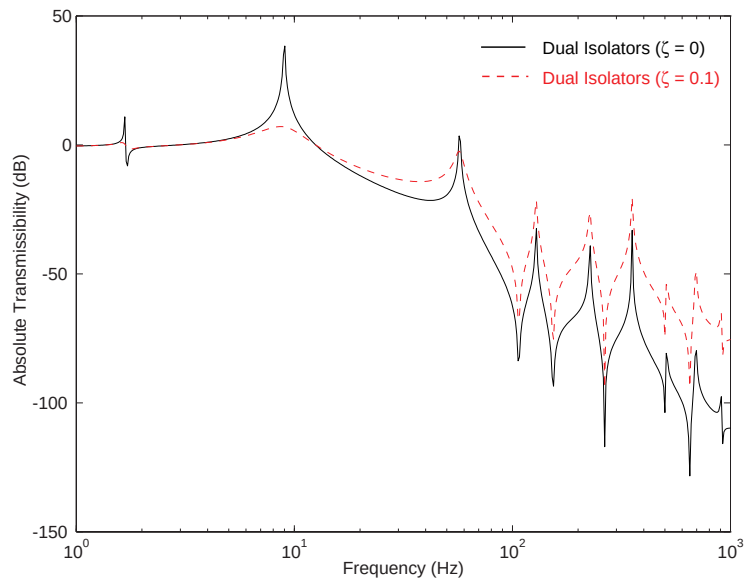


Figure 6.10: FBFE System Using Dual Isolators with and without Isolator Damping

be equivalent. The third system will have different base and equipment lengths while keeping all other base and equipment parameters such as the density the same. The length of the equipment will be 85% the length of the base and the mount frequency will be designed at $f_o = 8.323$ Hz. The measure of performance for each system is determined by the transmissibility which is defined as the ratio of the equipment displacement to the displacement of the base due. The displacement of the equipment is measured at the isolator location while the disturbance source location is given in Table 6.5. A synopsis of other key parameters to perform active isolation on the FBFE systems are given in Table 6.5.

### 6.2.1 Sensor Location

It has already been shown that the optimal placement of the feedback sensor for the FBRE system is on the equipment that will be isolated. With equipment feedback, the transmissibility of the active system will track the transmissibility of an undamped system in the higher frequency ranges. However, when the feedback sensor is placed on the base, the transmissibility of the active system will increase in the higher frequencies. Therefore, sensor placement for the FBFE system has to be analyzed for equipment as well as base feedback. The active controller in this section will use velocity feedback with no structural damping in the base or the equipment. A mount design at $f_o = 7.674$ Hz is used and a mount design at $f_o = 76.737$ Hz will give similar results but are not presented in this

Table 6.5: Parameters for Implementation of Active Isolation on FBFE System

| Parameter | Low-Mount System | Mid-Mount System | Varied Length |
|---|---|---|---|
| Mount Frequency | 7.674 Hz | 76.737 Hz | 8.323 Hz |
| Isolator Location | 0.08128 m | 0.08128 m | 0.08128 m |
| Disturbance Location | | | |
| Frequency Response | 0.06096 m | 0.06096 m | 0.06096 m |
| Time Response | 0.06096 m | 0 06096 m | 0 06096 m |
| Base Damping | Proportional | Proportional | Proportional |
| Isolator Damping | None | None | None |

section.

Figure 6.11 shows the results for the feedback sensor placed on either the equipment and the base. Similar to the FBRE system, the sensor should be placed on the equipment. The transmissibility of the first mode is significantly attenuated for equipment feedback compared to base feedback. Using base feedback, only 15 dB of attenuation is achieved at the first mode while 45 dB of attenuation is achieved with the sensor located on the equipment. When the sensor is placed on the base, the transmissibility at higher frequencies is also increased, similar to using a passive isolator. Equipment feedback does not have that drawback; in fact, the transmissibility at higher frequencies tracks the transmissibility of an undamped system.

Similar to the FBRE system, sensor location for the FBFE system can be verified by analyzing the observability indices. The observability index for the first mode using equipment feedback is $\mathcal{O}_1^e = 2100$ while the index is $\mathcal{O}_1^b = 2\text{x}10^{-4}$ for base feedback. Since the observability index is greater for equipment feedback than base feedback, the best sensor location will be on the equipment.

### 6.2.2 $\mathcal{PID}$ Control

The first active controller to be discussed is the $\mathcal{PID}$ controller. This controller takes on the form

$$f(t) = K_P y + K_D \dot{y} + K_I \int y \mathrm{d}t \tag{6.1}$$

where $K_p$ is the proportional gain, $K_D$ is the derivative gain, $K_I$ is the integral gain, and $y$ is the displacement of the equipment at the isolator location. Three FBFE systems are analyzed as mentioned previously and the selection of the gains for the $\mathcal{PID}$ controller are based on the results in the FBRE section using $\mathcal{PID}$ control.

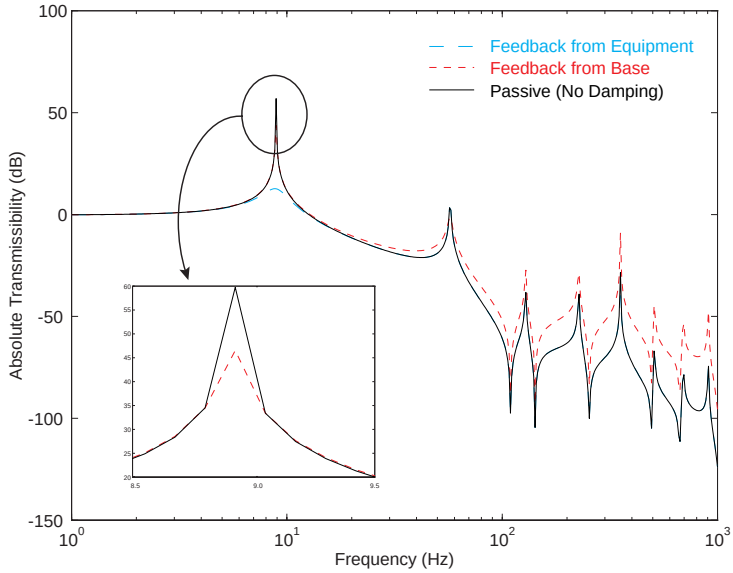


Figure 6.11: Feedback Comparison for the FBFE System

#### 6.2.2.1 Responses for Mount Frequency at $f_o = 7.674$ Hz

The gain selections for the $\mathcal{PID}$ controller are based on the design in the FBRE chapter. The proportional gain was chosen as small as possible since this gain tends to modify the frequencies of the system. The derivative and integral gain were first approximated by the values used for the FBRE system. The gains were then adjusted and the analysis showed that a good parameter set for the gains were equivalent to the ones used on the FBRE system. Therefore, the gains were chosen as $K_D = 3$ and $K_I = 1200$.

With the gains selected, the frequency responses and time responses using $\mathcal{PID}$ and $\mathcal{PD}$ control are determined. The transmissibilities for an undamped system, a system implementing $\mathcal{PD}$ control, and a system implementing $\mathcal{PID}$ control for a mount frequency design at $f_o = 7.674$ Hz are shown in Figure 6.12. $\mathcal{PD}$ control significantly attenuates or damps the first mode but the third and fifth mode are slightly attenuated as well. This is a direct result of modeling the equipment as a flexible member; the third and fifth modes of the FBFE system correspond directly to the modes of the equipment. Therefore, when the active isolator is used to attenuate the first mode, a residual effect is that the modes that correspond to the equipment will be attenuated when using $\mathcal{PD}$ or $\mathcal{PID}$ control. This effect does not occur when the equipment is rigid. Therefore, even though the modes of this system using $\mathcal{PD}$ or $\mathcal{PID}$ control at a first glance do not seem to interact, they actually interact through the equipment flexibility. $\mathcal{PID}$ control has similar results: the main difference is that $\mathcal{PID}$ control will attenuate the lower frequency transmissibility much

better than $\mathcal{PD}$ control.

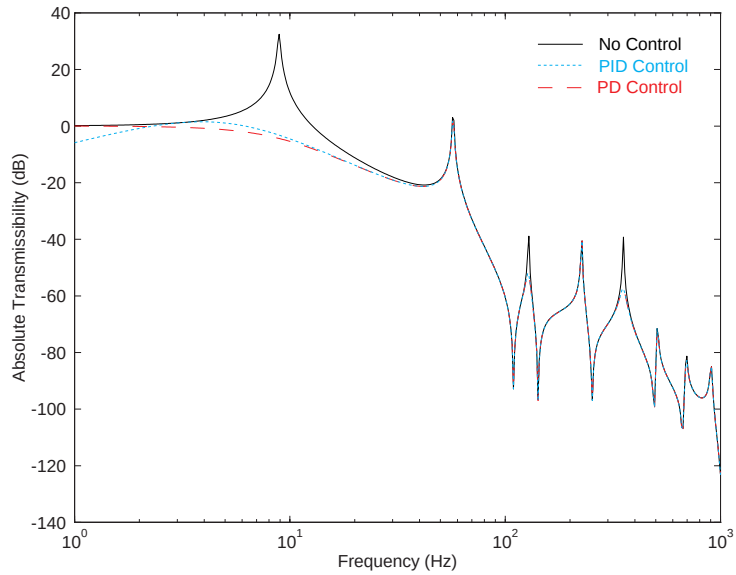


Figure 6.12: FBFE Frequency Response using $\mathcal{PID}$ Control at $f_o = 7.674$ Hz

Another comparison between $\mathcal{PD}$ and $\mathcal{PID}$ control are shown through the system's time response. Unlike the FBRE sections, the only time response that will be given in this section is the response due to a step input. The rationale is that the transient response to a sinusoidal input does not give any additional information on the effectiveness of using $\mathcal{PID}$ or $\mathcal{PD}$ control. The time responses for no isolation and active isolation with $\mathcal{PD}$ and $\mathcal{PID}$ control are shown in Figure 6.13. With an undamped isolator or no control present in the system, the transient response to a step input is an indefinite oscillation of the FBFE modes. Once $\mathcal{PD}$ control is applied, the oscillation is attenuated in 0.15 seconds. However, the system is still oscillating at the second and higher modes of the FBFE system since these modes are not attenuated. Quite different results occur when $\mathcal{PID}$ control is applied. The response is attenuated in 0.26 seconds; however, unlike $\mathcal{PD}$ control the displacement of the equipment will stay near its initial position. Since $\mathcal{PID}$ control does not attenuate the second and higher modes, the system will oscillate at frequencies equivalent to the higher FBFE modes after the system has settled to a steady-state solution.

#### 6.2.2.2 Responses for Mount Frequency at $\mathbf{f_o = 76.737}$ Hz

The gains for this system were chosen in a similar manner to the previous section. The derivative and integral gains were finally selected at $K_D = 88$ and $K_I = 1\text{x}10^6$. The resulting frequency responses for a system with no isolator damping, and a system incorporation $\mathcal{PD}$

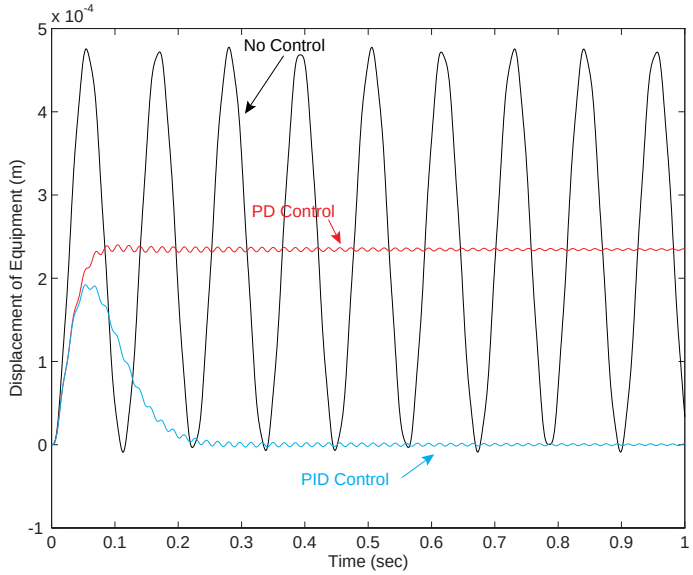


Figure 6.13: FBFE Time Response using $\mathcal{PID}$ Control at $f_o = 7.674$ Hz

and $\mathcal{PID}$ control are shown in Figure 6.14. With a $\mathcal{PD}$ controller, the first seven modes of the FBFE system are attenuated which is due to the strong interaction between the modes. This is very similar to the FBRE system; however, unlike that system, additional interaction in the system modes have occurred due to the equipment flexibility. Notice that the most significant attenuation occurs at the second, third, fifth and seventh modes. The heavy attenuation in the second mode is due to the fact that this mode corresponds to the addition of the isolator mount. The third, fifth and seventh modes are attenuated more than the fourth, sixth and eight mode because they correspond to the modes of the equipment. $\mathcal{PID}$ control has very similar results except that it attenuates the low frequency transmissibility much better than $\mathcal{PD}$ control.

An additional comparison between $\mathcal{PID}$ control and $\mathcal{PD}$ control can be fully realized through their time responses. Similar to the previous section, only the time response due to a step input on the base is analyzed. The transient response for no isolation, and active isolation using $\mathcal{PD}$ and $\mathcal{PID}$ control is shown in Figure 6.15. For an undamped passive isolator, the transient response will be an indefinite oscillation of the equipment at the FBFE's natural frequencies; this assumes there is no base or equipment damping. When $\mathcal{PD}$ control is applied to the system, the transient response settles in 0.05 seconds. Unlike the system with a mount frequency at $f_o = 7.674$ Hz, there is no oscillation of the second and higher modes after the first mode is attenuated. This is a result of $\mathcal{PD}$ control attenuating the first few modes of the FBFE system. $\mathcal{PID}$ control takes a bit longer to attenuate the response (0.06 seconds), but it never lets the system get significantly beyond

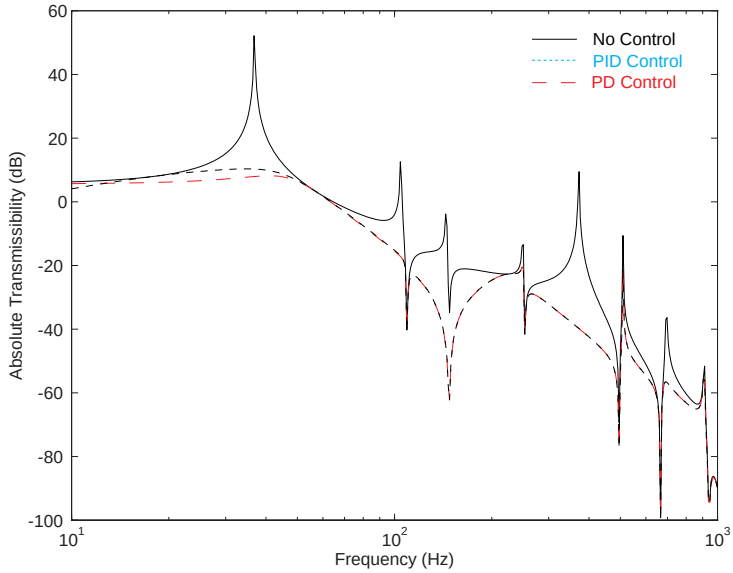


Figure 6.14: FBFE Frequency Response using $\mathcal{PID}$ Control at $f_o = 76.737$ Hz

its initial position. Similar to $\mathcal{PD}$ control, after the first mode is attenuated there is no oscillation after reaching a steady-state solution.

#### 6.2.2.3 System Responses With Varied Base and Equipment Lengths

Since this system is similar to the system with a mount frequency at $f_o = 7.674$ Hz, the initial point for the gains were chosen to be the same. After some analysis it was found that these gains were very adequate for this system, and the transmissibilities for the uncontrolled system, the controlled systems employing $\mathcal{PD}$ and $\mathcal{PID}$ control are shown in Figure 6.16. The $\mathcal{PD}$ control results are quite similar to the system with the mount frequency at $f_o = 7.674$ Hz. The first mode is significantly attenuated with attenuation occurring in the third and fifth modes as well. An enhanced view of the third and fifth modes are shown in this figure to give a better view of the attenuation at these modes. $\mathcal{PID}$ control has identical results except that it attenuates the low frequency transmissibility as well.

Similar to the other systems, the transient response to a step input on the base gives another indication how well $\mathcal{PID}$ and $\mathcal{PD}$ control are performing. The responses for an uncontrolled system, and a system with $\mathcal{PD}$ and $\mathcal{PID}$ control are shown in Figure 6.17. The uncontrolled system oscillates indefinitely at the system's natural frequencies when no isolator or structural damping is present in the system. The system employing $\mathcal{PD}$ control settles to a steady-state solution in 0.12 seconds while the system using $\mathcal{PID}$ control settles

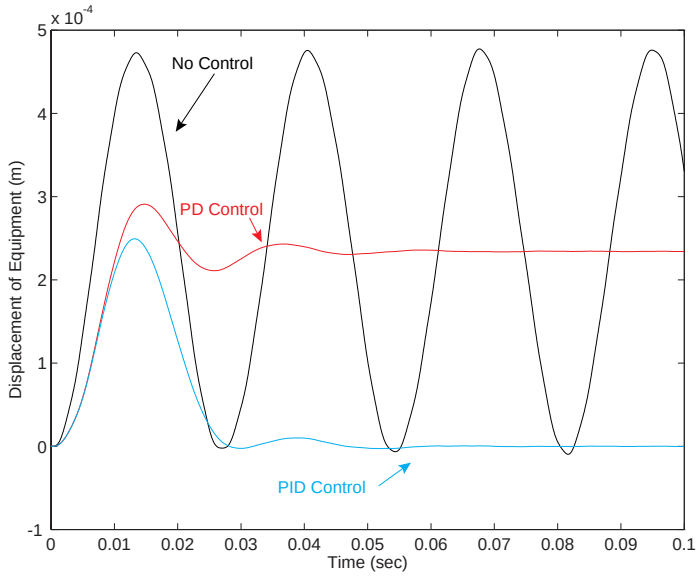


Figure 6.15: FBFE Time Response using $\mathcal{PID}$ Control at $f_o = 76.737$ Hz

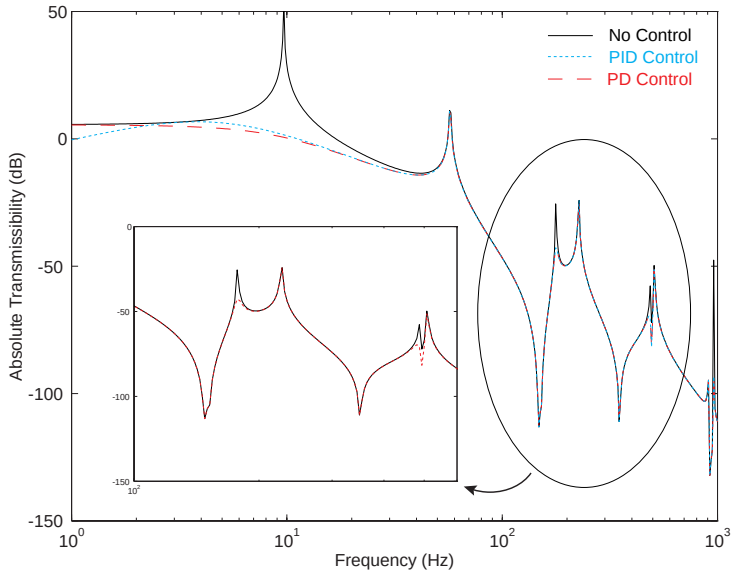


Figure 6.16: FBFE Frequency Response for Different Base and Equipment Lengths

in 0.27 seconds. Similar to the first system discussed, there is a residual oscillation after reaching the steady-state solution due to the second and higher modes of the FBFE system.

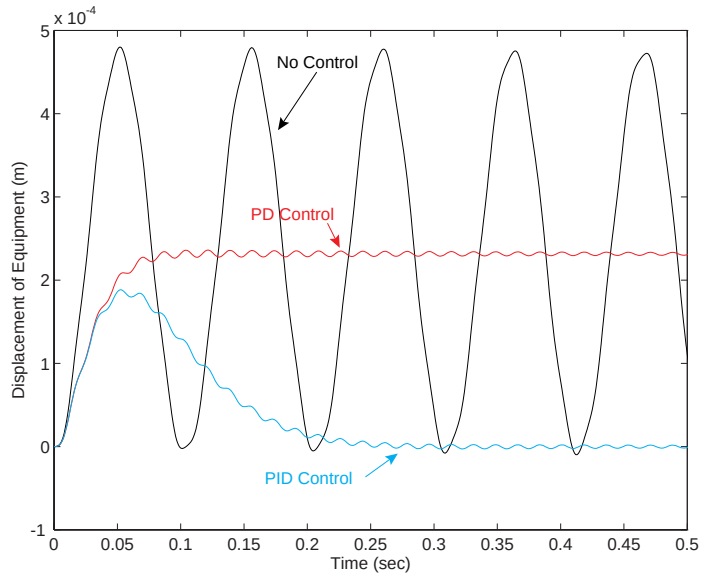


Figure 6.17: FBFE Time Response for Different Base and Equipment Lengths

### 6.2.3 PPF Control

$\mathcal{PD}$ and $\mathcal{PID}$ control is quite effective in attenuating the transmissibility of the flexible base, flexible equipment system. However, these types of controllers are very basic, so a second-order compensator such as the positive position feedback (PPF) controller will be used. The PPF filter is used to attenuate specific modes of a system and in this section the first mode will be targeted. The form of the PPF filter is

$$\ddot{\eta} + 2\zeta_f\omega_f\dot{\eta} + \omega_f^2\eta = \omega_f^2\xi \tag{6.2}$$

where $\xi$ is the structural modal coordinate, $\eta$ is the filter coordinate, $\omega_f$ is the filter frequency, and $\zeta_f$ is the filter damping ratio; the filter coordinate $(g\omega^2\eta)$ is sent back to the structure. For the FBFE system, the structural modal coordinate will be the actual equipment displacement and using the actual structural displacements will not greatly affect the results. As mentioned earlier, the PPF controller can be used to attenuate any specific mode of the structure by proper choice of $\omega_f$ and $\zeta_f$.

#### 6.2.3.1 Responses for Mount Frequency at $f_o = 7.674$ Hz

Similar to the selection of gains for the $\mathcal{PID}$ controller, the filter gain and damping ratio of the PPF filter are based on the FBRE system. The values for the filter gain and damping ratio were chosen as $g = 0.0025$ and $\zeta_f = 0.25$, respectively. The frequency responses for the undamped system and the controlled system are shown an Figure 6.18. As seen from this figure, the first mode has about 30 dB of attenuation. Unlike $\mathcal{PID}$ control where the odd modes are damped, attenuation of these modes is not accomplished. This result is most likely due to the fact that PPF control uses position, not velocity feedback. If the structural velocity coordinate was used as the feedback parameter, more than one mode could possibly be attenuated. If other modes are desired to be attenuated, a PPF filter can be designed for each mode. A byproduct of using the PPF filter is that the first natural frequency of the FBFE system has slightly increased.

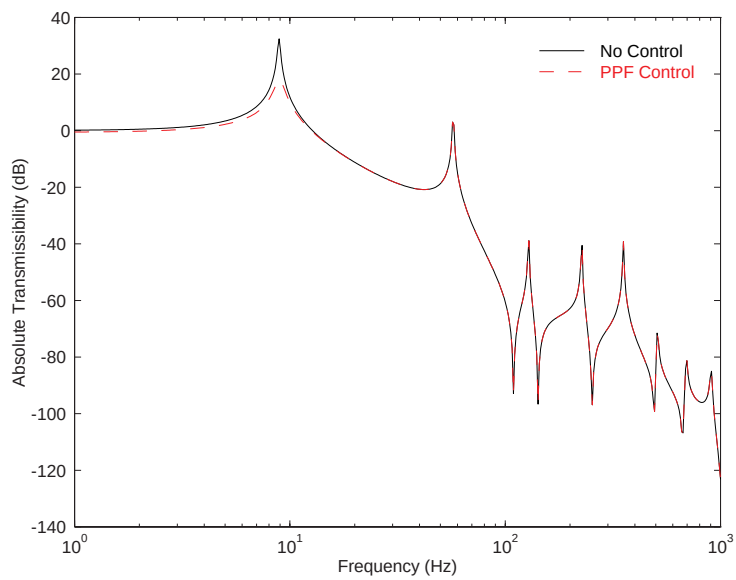


Figure 6.18: FBFE Frequency Response using PPF Control at $f_o = 7.674$ Hz

To see the effect of the PPF controller a little bit more clearly, the time response using a PPF filter is analyzed. Figure 6.19 shows the time response for the uncontrolled system and the system that uses a PPF controller to achieve active isolation. With no controller, the system will oscillate at the system's natural frequencies indefinitely if no base or equipment damping is present. With PPF control, the system reaches a steady-state solution in about 0.85 seconds when the base is disturbed by a step input. Similar to the system incorporating $\mathcal{PID}$ or $\mathcal{PD}$ control, there is a residual oscillation after a steady-state solution is reached. This oscillation is the second and higher modes of the FBFE

system which are not attenuated using PPF control.

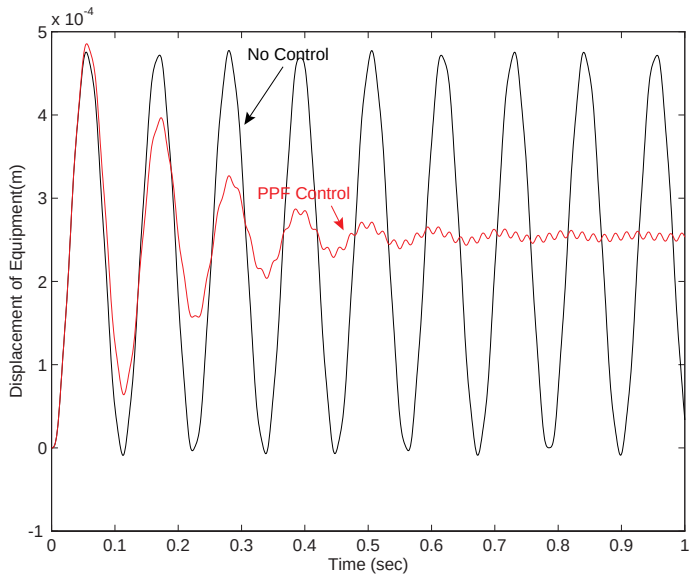


Figure 6.19: FBFE Time Response using PPF Control at $f_o = 7.674$ Hz

A comparison of Figure 6.19 and Figure 6.13 shows that $\mathcal{PD}$ control is a little more effective in attenuating the transmissibility than the PPF controller. However, the usefulness of the PPF controller should not be dismissed since it is very effective in attenuating the transmissibility of any specific structure mode.

#### 6.2.3.2 Responses for Mount Frequency at $\mathbf{f_o = 76.737}$ Hz

The gain for this system was chosen in a similar manner given in the previous paragraph. The final selection of the filter gain and damping ratio were $g = 0.035$ and $\zeta_f = 0.3$, respectively. The frequency responses for the undamped system and the controlled system using a PPF filter are shown in Figure 6.20. The PPF filter was used to specifically attenuate the first mode of this system and about 35 dB of attenuation is achieved. Even though the modes in this system are highly interactive, only one mode is attenuated. This is a basic feature of the PPF filter and if multiple modes are to be attenuated, multiple PPF filters will have to be used.

The effectiveness of using PPF control in the time domain is shown in Figure 6.21. This figure shows the time response of an uncontrolled system and a system using a PPF filter due to a step disturbance on the base. With no controller, the system will oscillate at the FBFE system's natural frequencies indefinitely if no base or equipment damping is present.

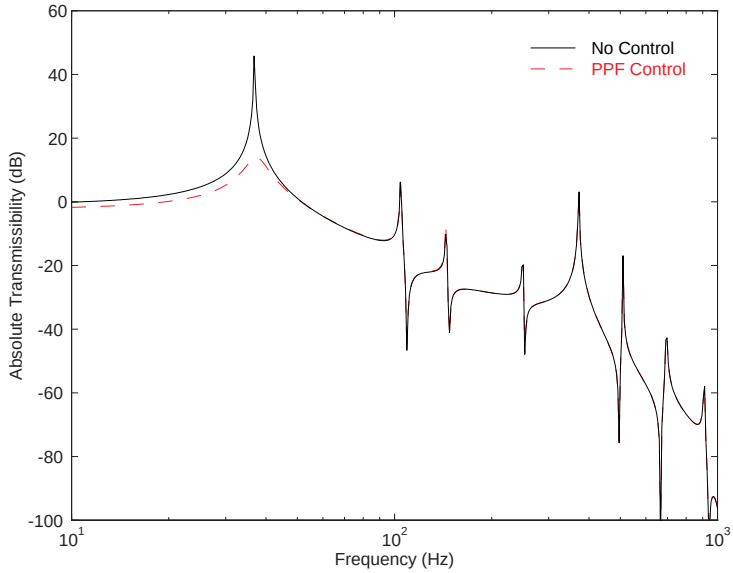


Figure 6.20: FBFE Frequency Response using PPF Control at $f_o = 76.737$ Hz

When the PPF controller is applied to the system, the time response reaches a steady-state solution in 0.18 seconds.

Once again, a comparison between $\mathcal{PD}$ control and PPF control shows that $\mathcal{PD}$ control is more effective in attenuating the equipment's transmissibility than PPF control. As mentioned earlier, the usefulness of the PPF controller should not be dismissed since it is very effective in attenuating any specific mode of a structure.

#### 6.2.3.3 System Responses With Varied Base and Equipment Lengths

The PPF controller parameters were chosen to be the same as the system with the mount frequency at $f_o = 7.674$ Hz. The frequency response for the system with no damping and the system using a PPF controller is shown in Figure 6.22. As seen from this figure, there is about 30 dB attenuation of the first mode. The frequency of the first mode is also slightly higher for the controlled system since position feedback is employed. This is a result that position feedback has a tendency to increase the natural frequency of a system. This PPF filter was used to attenuate the first mode and could have easily been designed to attenuate any of the other modes.

A comparison of the time responses between an uncontrolled system and one using a PPF controller are shown in Figure 6.23. As mentioned previously in the other sections, the uncontrolled system will oscillate at the system's natural frequencies. The time response using PPF control eventually reaches a steady-state solution in 0.75 seconds. Once

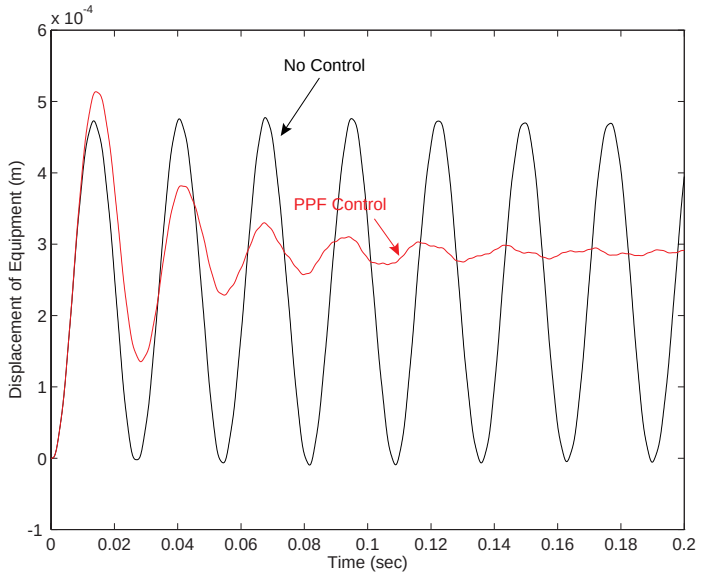


Figure 6.21: FBFE Time Response using PPF Control at $f_o = 76.737$ Hz

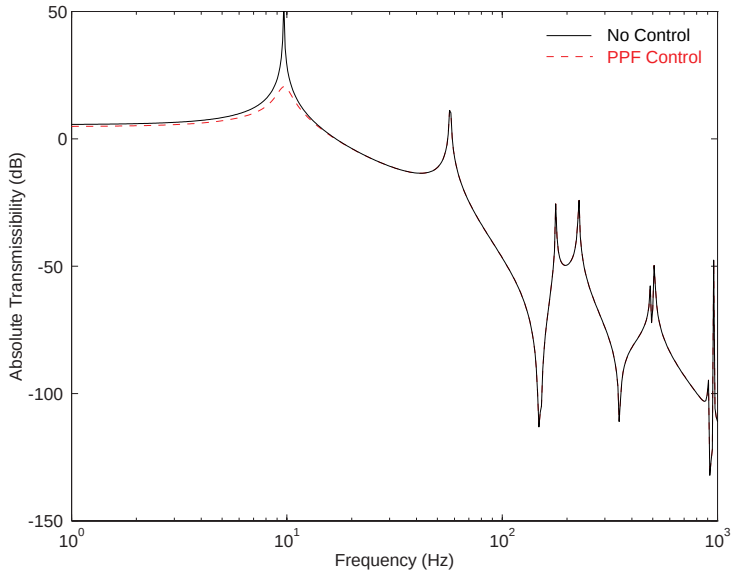


Figure 6.22: FBFE Frequency Response for Different Base and Equipment Lengths

again, since the second and higher modes are not damped, the controlled system will keep oscillating at the second and higher modes after reaching the steady-state solution.

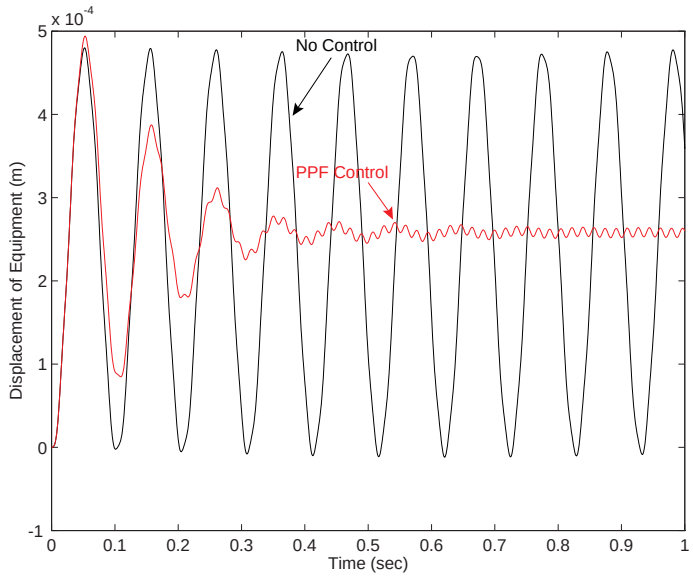


Figure 6.23: FBFE Time Response for Different Base and Equipment Lengths

The $\mathcal{PID}$ and $\mathcal{PD}$ controllers for this system are little more effective in attenuating the transmissibility than the PPF controllers by comparing and contrasting Figure 6.17 and Figure 6.23. Once again, it should be mentioned that the usefulness of the PPF controller is that it can attenuate any specific mode by applying a simple second-order filter that makes use of position feedback.

### 6.2.4 LQG Control

The previous sections looked at relatively simple and low-order compensators. One form of a higher-order controller is an optimal controller such as the linear quadratic Gaussian regulator. A detailed discussion on the use and implementation of the LQG regulator is given in Chapter 2. The LQG controller will find an optimal solution to the regulator problem and an optimal solution for the estimator problem. The estimator is used because every state of the FBFE system will not be directly measurable. It is also assumed that a model of the disturbance is known and the disturbance is modeled with the use of a shaping filter.

As discussed in Chapter 5, an LQG regulator cannot be readily implemented in Yang's transfer function synthesis method. Therefore, a modal expansion method is used to model the FBFE system. However, unlike other expansions, the actual eigenfunctions determined

by the transfer function synthesis method is used. By using the actual eigenfunctions in the modal expansion, the approximated system will behave very near the actual system. For instance, seven modes for the equipment and base are used to model the system and the first dozen or so modes are within 0.1% of the actual values.

#### 6.2.4.1 Responses for Mount Frequency at $f_o = 7.674$ Hz

For this system, it was assumed that the disturbance source oscillated at the first natural frequency of the flexible base, flexible (FBFE) system. The performance index for the LQG controller penalized the equipment velocity states more heavily than the position states and the frequency response is shown in Figure 6.24. The response using an LQG controller is quite similar to a $\mathcal{PD}$ controller except for the beginning of a notch at the system's first natural frequency. The depth of the notch as well as the overall performance of the system is dependent on the performance index, and the index is limited by the actual performance of the actuator.

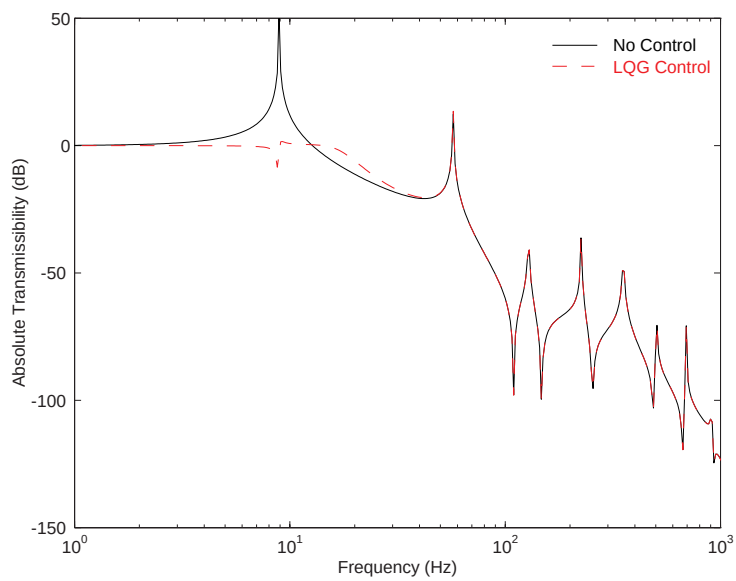


Figure 6.24: FBFE Frequency Response using LQG Control at $f_o = 7.674$ Hz

The time response to a base step input using an LQG controller is shown in Figure 6.25. This figure is also a comparison of the effectiveness between the LQG and $\mathcal{PD}$ controllers. Without any damping, the system will oscillate indefinitely at the system's natural frequencies. This indefinite oscillation does not occur when the LQG or $\mathcal{PD}$ controller is used to suppress the vibrations. These systems perform nearly equivalent with the exception that the $\mathcal{PD}$ controller has a faster settling time while the LQG controller has a faster rise time.

After the system has settled to the steady-state solution, there is a small oscillation still present in the system. This oscillation is the second and higher modes of the FBFE system, and this oscillation will not be present if damping is included in the base or equipment.

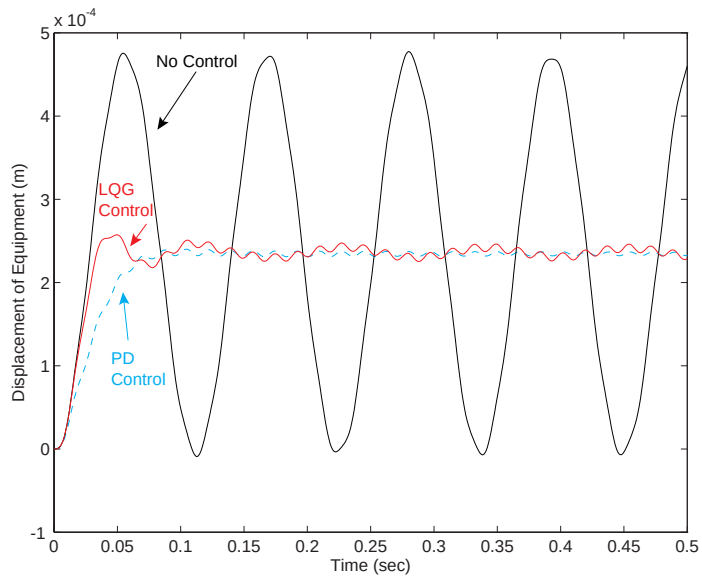


Figure 6.25: FBFE Time Response using LQG Control at $f_o = 7.674$ Hz

#### 6.2.4.2 Responses for Mount Frequency at $\mathbf{f_o = 76.737}$ Hz

For this system it is assumed that the disturbance frequency occurs at the second natural frequency, so a better comparison to $\mathcal{PD}$ control can be made. Similar to the previous system, the performance index for this system penalizes the equipment velocity states more heavily than the equipment position states. The transmissibilities for the undamped system and a system using LQG control are shown in Figure 6.26. This system is somewhat similar to a $\mathcal{PD}$ controller in that the first six modes of the system are attenuated. One difference is that the LQG controller has a notch at the second mode which $\mathcal{PD}$ control does not exhibit. The performance of the LQG controller can be adjusted by changing how the states in the performance index are penalized.

The transient responses to a base step input for the uncontrolled system and the systems using LQG and $\mathcal{PD}$ control are shown in Figure 6.27. The uncontrolled system will oscillate indefinitely at the system's natural frequencies when no isolator or structural damping is present in the system. The LQG controller and $\mathcal{PD}$ controller perform nearly alike with the same rise time and settling time. However, the LQG controller settles at a higher

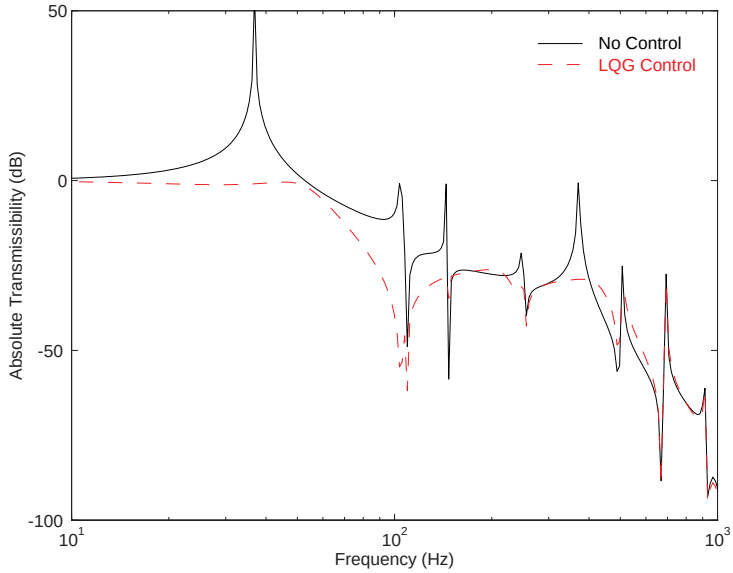


Figure 6.26: FBFE Frequency Response using LQG Control at $f_o = 76.737$ Hz

equipment displacement than the $\mathcal{PD}$ controller. After the system has settled to a steady-state solution, there is no oscillation of any higher frequencies due to the attenuation in the first few modes.

#### 6.2.4.3 System Responses With Varied Base and Equipment Lengths

Unlike the other control strategies, the performance index for the LQG controller cannot be assumed to be the same as the one used in the section for a mount frequency at $f_o = 7.674$ Hz. However, a starting point for the performance index can be assumed equivalent to the system with the base and equipment lengths being the same. Similar to the other systems, the performance index will penalize the velocity states more heavily than the position states. The frequency responses for an uncontrolled system and system using an LQG regulator are given in Figure 6.28. This system performs very close to a system using $\mathcal{PD}$ control except for the occurrence of a notch at the system's first natural frequency. However, unlike $\mathcal{PD}$ control, there is no attenuation at the third or fifth modes.

The transient response to a step input on the base is given in Figure 6.29. This figure is also a comparison between a system using $\mathcal{PD}$ control and LQG control. As seen from this figure, $\mathcal{PD}$ control has a faster settling time than the LQG controller but the LQG controller has a faster rise time. Similar to the first system with a low-frequency mount design, there is a small oscillation present after the time response reaches a steady-state solution. Notice that the magnitude of this oscillation is greater for the LQG controller

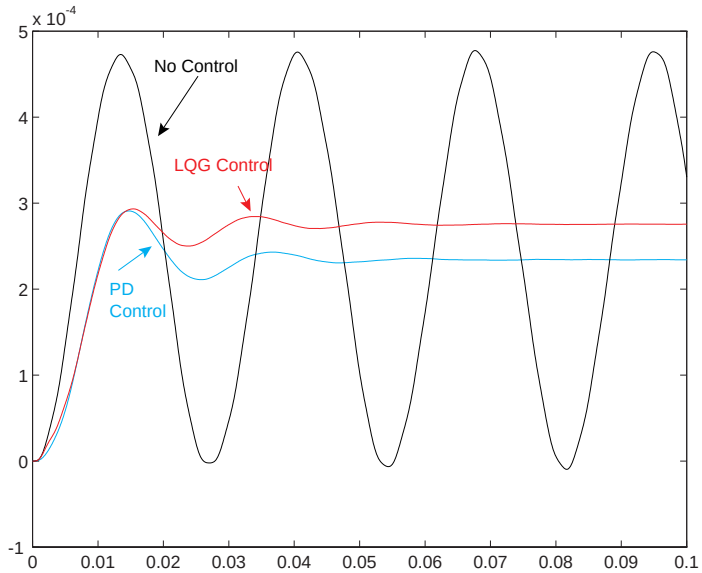


Figure 6.27: FBFE Time Response using LQG Control at $f_o = 76.737$ Hz

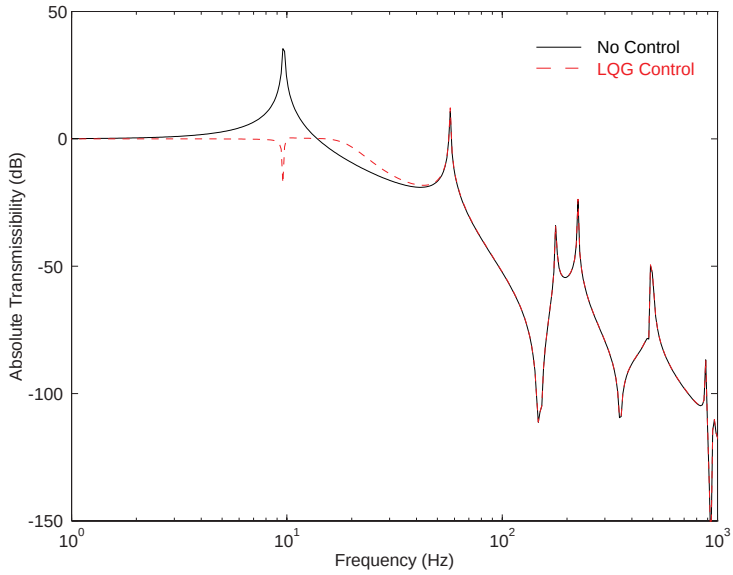


Figure 6.28: FBFE Frequency Response for Different Base and Equipment Lengths

than the $\mathcal{PD}$ controller. This is a direct result that the $\mathcal{PD}$ controller damps the third and fifth mode of this FBFE system while the LQG controller does not.

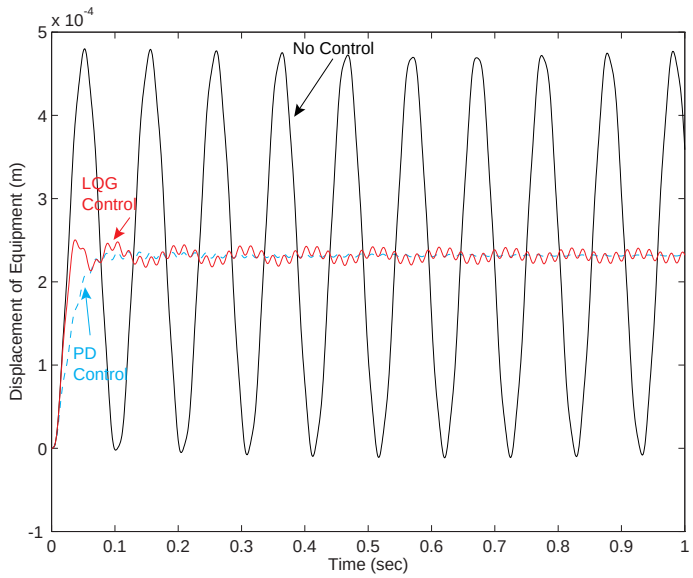


Figure 6.29: FBFE Time Response for Different Base and Equipment Lengths

## 6.3 Summary

Unlike the FBRE system, isolator placement is significant in the FBFE system. By moving the isolator at different locations, errors in the first mode can be around 15%; the errors can go as high as 35% for the first mode. The choice of the isolator mount frequency is also important in the FBFE system. If the mount frequency is designed between the modes of the base and the equipment, a strong interaction between the modes will exist. When isolator damping is present, this mode interaction will result in multiple attenuation of modes.

Before implementing any type of active isolation technique on the flexible base, flexible equipment system, the ideal or optimal placement of the feedback sensor was determined. Similar to the FBRE system, the ideal placement for the feedback sensor is on the equipment. The first mode of the FBFE system is more significantly attenuated using equipment feedback compared to the system using base feedback. Also, base feedback has the tendency to increase the transmissibility at the higher frequencies while equipment feedback does not have this drawback.

Three different control methodologies were used on varying flexible base, flexible equipment (FBFE) systems. Overall, $\mathcal{PID}$ and LQG controllers were very affective in attenuating the FBFE modes while the PPF filter performed adequately in attenuating a specific mode of the FBFE system. The effectiveness of each controller is dependent on the mount frequency, placement of isolator, and physical dimensions of the system. When the mount frequency was designed to be lower than any of the modes of the base and equipment, each controller significantly attenuated the first mode with $\mathcal{PID}$ control adding damping to the third and fifth modes as well. Similar results were obtained when the system had different beam lengths for the equipment and the foundation. Slightly different results were obtained when the mount frequency occurred between the first modes of the base and the equipment. Each controller significantly attenuated the first mode, but the LQG and $\mathcal{PID}$ controllers also attenuated the next five modes.

Table 6.6 is a comparison of each control method's performance in the time domain. When choosing one controller over another, the frequency response of each controller should also be considered. It should be noted that $\mathcal{PID}$ control was the only controller to bring the equipment back to its initial position. The LQG regulator can do this as well by adjusting the performance index, but the regulator was chosen to mimic the $\mathcal{PD}$ controller. Therefore, the $\mathcal{PID}$ controller will have a greater overshoot and longer settling time compared to the $\mathcal{PD}$ controller.

Table 6.6: Summary of Controller Performances for FBFE System

| Control Method | $f_o = 7.674$ Hz | | | $f_o = 76.737$ Hz | | |
|---|---|---|---|---|---|---|
| | $t_s$ | $t_r$ | Overshoot | $t_s$ | $t_r$ | Overshoot |
| | | | | | | |
| Passive (Undamped) | - | - | 2.388x$10^{-4}$ | - | - | 2.387x$10^{-4}$ |
| $\mathcal{PD}$ | 0.0515 | 0.15 | 4.697x$10^{-6}$ | 0.0080 | 0.06 | 5.685x$10^{-6}$ |
| $\mathcal{PID}$ | - | 0.26 | 1.921x$10^{-4}$ | - | 0.06 | 2.493x$10^{-4}$ |
| PPF | 0.034 | 0.85 | 2.407x$10^{-4}$ | 0.0082 | 0.22 | 2.373x$10^{-4}$ |
| LQG | 0.023 | 0.80 | 1.833x$10^{-5}$ | 0.0089 | 0.06 | 1.147844x$10^{-5}$ |
| | | | | | | |
| Control Method | Varied Lengths | | | | | |
| | $t_s$ | $t_r$ | Overshoot | | | |
| Passive (Undamped) | - | - | 2.401x$10^{-4}$ | | | |
| $\mathcal{PD}$ | 0.051 | 0.12 | 4.296x$10^{-6}$ | | | |
| $\mathcal{PID}$ | - | 0.27 | 1.885x$10^{-4}$ | | | |
| PPF | 0.032 | 0.75 | 2.471x$10^{-4}$ | | | |
| LQG | 0.021 | 0.70 | 1.664x$10^{-5}$ | | | |

For the system with a low-frequency mount, none of the controllers drastically outperforms each other. $\mathcal{PD}$ control has the quickest settling time and smallest overshoot but has the largest rise time. The LQG regulator has the fastest rise time, good overshoot but a very long settling time compared to a $\mathcal{PD}$ or a $\mathcal{PID}$ controller. For the mid-frequency mount at $f_o = 76.737$ Hz, $\mathcal{PD}$ and LQG are the better performers. They have similar settling and rise times but the LQG controller has a better overshoot. The last system considered, varied lengths of the base and equipment, has similar results to the low-frequency mount system. None of the controllers dramatically outperforms one another. Again, $\mathcal{PD}$ control has the smallest overshoot and quickest settling time while the LQG regulator has the fastest rise time.

# Chapter 7

# Conclusions, Contributions and Future Work

## 7.1 Conclusions

The concept of vibration isolation has been extensively studied over the last few decades. It was not until the 1960's that the idea of active vibration isolators started to gain acceptance as an alternative to passive isolators. Damped passive isolators are shown to increase the high frequency transmissibility, and this increase does not occur when an active vibration isolator is used. The underlying reason for this situation is that damping in passive systems is proportional to the relative velocity between the isolated member and the disturbance source. Active damping, on the other hand, is based on the "inertial" velocity, and this type of damping is usually referred as a sky-hook damper.

Passive and active isolation systems are most commonly modeled in practice as a single-degree-of-freedom (SDOF) model. As a first thought, it would seem that this model would be severely inaccurate due to its simplicity. However, the SDOF model should not be disregarded since it is very good in quantifying many results for any isolation system. For instance, a SDOF model predicts that the high frequency transmissibility increases when an isolator uses passive damping, although this does not occur for an isolator implementing active control. The SDOF model also predicts that the transmissibility rolls-off at 40 dB/decade after the mount or corner frequency. The main limitation of this model is that it does not account for the flexibility inherent in many systems.

A higher-order model such as a two-degree-of-freedom (2DOF) can be used in place of the SDOF model. This model is a step closer to modeling the flexibility in a system; however, the increase in accuracy does come at a price. The 2DOF model is significantly more complex to analyze than the SDOF model. A unique approach to limit this complexity of analyzing the 2DOF model has been accomplished. This approach uses the RMS transmissibility and visualization software to reduce the number of plots needed for analy-

sis. However, similar to the SDOF model, the 2DOF model does not fully account for the system flexibility, and a higher-order model should be used.

To effectively model the flexibility in a system, distributed not lumped members must be used. One such isolator model is a system that has a flexible (distributed) base and rigid equipment (FBRE) connected via an isolator. This FBRE system has been analyzed in the literature but the flexibility of the base has always been approximated. If the number of terms in the approximation is very large, the approximated system will closely resemble the actual system. Therefore, an approach developed by Yang is used to model any distributed or flexible member. His method models any one-dimensional distributed members analytically; therefore, his approach bypasses standard truncation errors inherent in other methods. Many significant results were obtained using Yang's transfer function synthesis (TFS) approach. First, it has been shown that base flexibility tends to decrease isolator performance. The transmissibility of the FBRE system is similar to the SDOF model except that the FBRE transmissibility has an infinite number of modes due to the flexible base. It has also been shown that when passive damping is incorporated in the isolator, the high frequency transmissibility will increase similar to the SDOF model.

The most significant result for the FBRE system is that the choice of the mount frequency will greatly affect how the system will respond. It is commonly suggested that the mount frequency should be chosen as small as possible. For this particular choice of mount frequency, the FBRE transmissibility is similar to the SDOF model as mentioned above. However, somewhat different results occur when the isolator mount is chosen between two of the base modes. When this situation occurs, an interaction between the modes exist and this interaction becomes quite significant when damping is included in the isolator. The use of isolator damping in this system will attenuate multiple modes while only one mode was targeted for attenuation. This is significant because not only is the equipment mode attenuated but some of the base modes as well. The significance of this result can be better appreciated with the following extension. Let the base represent a spacecraft and the equipment represent a payload on the spacecraft. For this analogy, the interaction of modes states that the payload will be isolated while reducing the vibrations on the spacecraft. Therefore, an addition of another payload to the spacecraft will have a decrease in its vibration levels because the other (isolated) payload has decreased the spacecraft modes. It should be noted that this interaction occurs for systems that use either passive or active damping in the isolator as long as the mount frequency is between two of the base modes.

Active damping is also shown to be more effective than passive damping for the FBRE system because the high frequency transmissibility is not increased. However, the feedback sensor must be placed on the member to be isolated; otherwise, active damping will increase the high frequency transmissibility. For the FBRE system, three separate active control methodologies were used: a proportional-plus-integral-plus-derivative controller ($\mathcal{PID}$), a positive position feedback (PPF) controller, and a linear quadratic Gaussian (LQG) regulator. All controllers were effective in attenuating at least one mode for systems having

low-frequency mounts or mounts designed at higher frequencies. When the mount frequency was chosen between two of the base modes, the LQG and $\mathcal{PID}$ controller attenuated multiple modes similar to a system using viscous damping. The PPF controller did not attenuate multiple modes because this controller is designed to attenuate only a single mode. If multiple modes are to be attenuated, a single PPF filter should be used for each targeted mode.

The flexible base, rigid equipment system is a significant step in understanding the effect of flexibility in isolation systems. However, this isolation system still does not fully explore the effects of flexible systems since the equipment is modeled as a lumped mass. Therefore, a flexible base, flexible equipment (FBFE) system is used to describe a fully flexible isolation system. A majority of the results obtained for the FBFE system are comparable to the FBRE system. These results include that the FBFE transmissibility is similar to the FBRE and SDOF transmissibilities, except that the FBFE transmissibility has extra modes corresponding to the flexibility in the equipment. Also, when passive damping is used in the isolator, the high frequency transmissibility is also increased. This situation does not occur when an active isolator is used in the FBFE system, and the best placement for the feedback sensor is on the equipment as well.

Even the choice of the mount frequency for the FBFE system is similar to the FBRE system. Low-frequency mounts tend to perform the best in an overall sense. However, when the mount frequency is chosen between the modes of the base and equipment, an interaction between the modes exist. Unlike the FBRE system, twice as many modes are coupled due to the equipment being flexible. When damping is included in the isolator, whether done passively or actively, multiple modes are attenuated. Two ways of achieving this attenuation using active control are to use $\mathcal{PID}$ or LQG controllers. Once again, a PPF filter or controller can be used to attenuate a single mode even though the modes are significantly coupled by the choice of the mount frequency design. If multiple modes are desired to be attenuated using PPF control, multiple PPF filters will be needed for each targeted mode.

A major difference between the FBRE and FBFE systems is the effect of isolator placement on each system's natural frequencies. Isolator placement will have no major effect on the FBRE natural frequencies which is not the case for the FBFE system. The first natural frequency of the FBFE system will be least when placed at the midpoint of the base and the equipment. As the isolator mount is placed further away from the midpoint of the beam and equipment, the first FBFE natural frequency will increase. This is true for both low- and high-frequency mount designs, and errors as high as 30% can be found in the first natural frequency.

## 7.2 Contributions

1. A unique method to analyze the transmissibility of an isolation system using a 2DOF model is discussed. Prior literature would analyze the transmissibility of a 2DOF model by making surface plots of the transmissibility. The transmissibility would be plotted versus two nondimensional parameters while the other three nondimensional parameters were fixed. To see the effects due to the other three variables, numerous plots would have to be formulated. The approach used in this dissertation is unique in that it alleviates this problem by calculating the root-mean-square levels of the transmissibility. By doing this, a plot of the transmissibility is made by varying four nondimensional variables while fixing only one nondimensional parameter. Therefore, this methodology minimizes the number of plots needed to determine effective isolation design using a 2DOF system as an isolation model.

   This new method also gives a better indication how well the isolation system is performing because overall trends are much easier to visualize using this new approach. This approach does not give exact results; however, it can be used to pinpoint areas of undesired or desired isolation designs. Once these areas are defined, a detailed analysis around any area can be performed.

2. Previously, the transfer function synthesis (TFS) method developed by Yang has only been proven with respect to a finite element method code. Therefore, a cantilevered-beam experiment is discussed and compared to the results obtained from the TFS method. The TFS method is very accurate in predicting the resonant and anti-resonant modes of the system when the experimental system is properly modeled. That is, the mass and inertia of the sensor has to be modeled since they contribute heavily to the system response. The magnitude of the frequency response at each resonant mode was not accurate until the structural damping was included in the model.

   Another aspect not detailed by Yang but discussed in Chapter 4 is the use of active control. If the controller can be described by a transfer function, the implementation of the controller into the TFS method is done by the use of constraint forces. It should be noted that controllers such as a LQG regulator is described in the state space and cannot be directly implemented into the TFS method. However, the TFS method can still be used to approximately determine the dynamic state-space matrices used by the LQG controller. Unlike other approximate methods, only one approximation is needed for each mode desired. For instance, if the first eight modes of a system are desired, only eight terms in the series expansion are needed to get accurate results for the first eight modes. The underlying reason is that the actual mode shapes of the isolated system are attainable through Yang's method and they can be used in the series expansion.

3. The works by Snowdon, Blackwood, von Flotow and Soliman on system flexibility is extended in this dissertation. It is shown that flexibility will have an affect on the isolation design and for the flexible base, rigid equipment (FBRE) system, the first natural frequency is not dependent on the placement of the isolator. The analysis in this dissertation reveals that this is not the case for the flexible base, flexible equipment (FBFE) system which was previously unknown. If the isolator is placed at the midpoint of the base and equipment, the first natural frequency of the FBFE system will be smaller than the mount frequency. However, as the isolator is placed further away from the base and equipment midpoint, the first natural frequency of the FBFE system increases and eventually exceeds the value of the mount frequency. This increase in the frequency is dependent on the choice of the mount frequency. For a low-frequency mount, a 15.6% error in the first mode was determined. For a mid-frequency mount design, the errors in the first three modes are 34.9%, 26.6% and 11.3%, respectively.

4. The ideal isolator is stiff at very low frequencies to statically hold the isolated system but is compliant at higher frequencies so that disturbances will not affect the motion of the isolated system. This is the major reason why current literature suggest that isolators should be designed with mount frequencies as low as possible. It is shown in this dissertation that low-frequency mounts are the best isolation performers in an overall sense. However, when the mount frequency is designed between modes of the system, a strong interaction between the modes exist. When damping is included in the isolator, whether done actively or passively, this interaction will attenuate multiple modes. This interaction is significant because it shows that a mid-frequency mount design will not only attenuate the equipment's vibrations but the base's vibrations as well. This is quite significant because other systems may be placed on the base without additional isolators since some of the base vibrations are attenuated by the isolator.

## 7.3 Future Work

1. The preceding work assumed that every beam could be modeled as a Bernoulli-Euler beam. This assumption is valid for the beams considered in the dissertation and the theory is equally valid at low frequencies but starts to break down at higher frequencies. Therefore, the Bernoulli-Euler beam theory should be replaced with the Timoshenko beam theory. Timoshenko beam theory is represented by a transverse deflection and angle of rotation at every point along the beam and its inclusion in the TFS method is similar to the section on Formulation for Transverse and Axial Vibrations (Section 4.4). The two governing equations representing the Timoshenko beam are both second order and the total order of this system is four. This is the

same order as an Bernoulli-Euler beam but the main difference is that the Timoshenko beam is defined by two parameters, the deflection and angle of rotation of the beam while the Bernoulli-Euler beam is defined by the deflection of the beam only.

Another important modeling issue is how to quantify the internal damping of the beams. For this body of work, proportional damping was used as the model for the internal damping. The motivation for its use is that the parameters describing proportional damping can be determined experimentally quite easily for beams. Also, proportional damping is easily implemented in the transfer function synthesis method. This does not preclude the use of other damping models for distributed systems. For example, hysteretic damping is easily implemented in the TFS method as well. However, it can be a bit more cumbersome to experimentally determine the damping properties using this model as opposed to proportional damping.

2. The TFS method has been experimentally verified using a cantilevered beam experiment. However, the vibration isolation systems used in this work are more complex than a cantilever beam and they should be experimentally verified as well. Experimental verification of active and passive isolators does pose numerous problems. For instance, one of the main assumptions used in the simulations are that the isolators are massless. This assumption is valid if the mass of the equipment and base are significantly larger than the mass of the isolator. Otherwise, the isolator must include its inertia effects and the isolator transfer functions can be modeled analytically or obtained experimentally. For complex active isolators such as piezoceramic stack actuators, analytical modeling can be very complex and very time consuming. Therefore, experimental transfer functions of the isolators should be used and embedded into the TFS method. Note that the TFS method is a linear method; therefore, all experimental transfer functions for the isolators should be done in the isolator's linear range.

3. The two isolation systems discussed in this dissertation are comparatively simple systems because one-dimensional beams are used to model the base and equipment. However, there are situations where a structure will consist of plates and/or membranes. Plates and membranes are two-dimensional structures and the transfer function synthesis method can still be used with some slight modifications; however, the model will no longer give exact results. In these cases, the terms $G(x, \xi, s)$ and $H(x, s)$ can no longer be exactly determined but they can be approximated. This does not preclude using the TFS method to analyze complex systems because isolation systems can still contain one-dimensional members. Also, if members of the isolation system cannot be modeled analytically, experimental results can be used in lieu of analytical models as mentioned previously.

# Bibliography


[1] Harris, C. M., editor, *Shock & Vibration Handbook*, third edition, M$^{c}$Graw Hill, 1988.

[2] Ungar, E. E., "Equality of Force and Motion Transmissibilities," *Journal of Acoustical Societies of America*, 1991, pp. 596–597.

[3] Nelson, F. C., "Vibration Isolation: A Review, I. Sinusoidal and Random Excitations," *Shock and Vibration*, Vol. 5, 1994, pp. 485–493.

[4] Macinante, J. A., *Seismic Mountings for Vibration Isolation*, first edition, Wiley-Interscience, 1984.

[5] Sciulli, D. and Inman, D. J., "Comparison of Single- and Two-Degree-of-Freedom Models for Passive and Active Vibration Isolation Design," *Smart Structures and Materials 1996: Passive Damping and Isolation*, Vol. 2720, SPIE, San Diego, CA, 1996, pp. 293–304.

[6] Meirovitch, L., *Elements of Vibration Analysis*, second edition, M$^{c}$Graw Hill, 1986.

[7] Inman, D. J., *Engineering Vibration*, first edition, Prentice Hall, 1994.

[8] Watters, B. G., Coleman, R. B., Duckworth, G. L., and Berkman, E. F., "A Perspective of Active Machinery Isolation," *Proceedings of the* $27^{th}$ *Conference on Decision and Control*, Vol. 3, IEEE, Austin, TX, December 1988, pp. 2033–2038.

[9] Rivin, E. I., "Vibration Isolation of Precision Equipment," *Journal of Aerospace Engineering*, Vol. 17, No. 1, January 1995, pp. 41–56.

[10] Ross, C. F., "Active Isolation of Ship Machinery Platforms," *Proceedings of the* $27^{th}$ *Conference on Decision and Control*, Vol. 3, IEEE, Austin, TX, December 1988, pp. 2045–2046.

[11] Jenkins, M. D., Nelson, P. A., and Elliott, S. J., "Active Isolation of Periodic Machinery Vibration From Resonant Substructures," *Journal of Environmental Engineering*, Vol. 4, No. 3, September 1991, pp. 6–11.

[12] Tzou, H. S., "Active Vibration Isolation for Micro-Displacement Feedback Control," *ASME - DE*, Vol. 18, ASME, Montreal, Quebec, Canada, September 1989, pp. 303–309.

[13] Karnopp, D. C., "Active and Semi-Active Vibration Isolation," *Journal of Vibration and Acoustics*, Vol. 117, No. 3b, 1995, pp. 177–185.

[14] Crosby, M. J. and Karnopp, D. C., "The Active Damper - A New Concept for Shock and Vibration Control," *Shock and Vibration Bulletin*, Vol. 43, 1973, pp. 119–133.

[15] Karnopp, D. C., Crosby, M. J., and Harwood, R. A., "Vibration Control Using Semi-Active Force Generators," *Journal of Engineering for Industry*, Vol. 96, May 1974, pp. 619–626.

[16] Miller, L. R., "Tuning Passive, Semi-Active, and Fully Active Suspension Systems," *Proceedings of the* $27^{th}$ *Conference on Decision and Control*, Vol. 3, IEEE, Austin, TX, December 1988, pp. 2047–2048.

[17] Spanos, J., Rahman, Z., and von Flotow, A., "Active Vibration Isolation on an Experimental Flexible Structure," *Proceedings of the SPIE - Smart Structures and Intelligent Systems*, SPIE, Albuquerque, NM, February 1993, pp. 674–680.

[18] Lee-Glauser, G. and Ahmadi, G., "Vibration Isolation of Launch Vehicle Payload and Its Subsystem," *Journal of Aerospace Engineering*, Vol. 8, No. 1, January 1995, pp. 1 – 8.

[19] Wada, B. K., Rahman, Z., Kedikian, R., and Kuo, C. P., "Vibration Isolation, Suppression and Steering (VISS)," *Journal of Intelligent Material Systems and Structures*, Vol. 7, March 1996, pp. 241–245.

[20] von Flotow, A. H., "An Expository Overview of Active Control of Machinery Mounts," *Proceedings of the* $27^{th}$ *Conference on Decision and Control*, Vol. 3, IEEE, Austin, TX, December 1988, pp. 2029–2032.

[21] Hyde, T. T. and Crawley, E. F., "$H_2$ Synthesis for Active Vibration Isolation," *Proceedings of the American control Conference*, Vol. 5, Seattle, WA, June 1995, pp. 3835–3839.

[22] Nagaya, K. and Kanai, H., "Direct Disturbance Cancellation with an Optimal Regulator for a Vibration Isolation System with Friction," *Journal of Sound and Vibration*, Vol. 180, No. 4, 1995, pp. 645–655.

[23] Sievers, L. A. and von Flotow, A. H., "Linear Control Design for Active Vibration Isolation of Narrow Band Disturbances," *Proceedings of the* $27^{th}$ *Conference on Decision and Control*, Vol. 2, IEEE, Austin, TX, December 1988, pp. 1032–1037.

[24] Sievers, L. A., von Flotow, A. H., and Scribner, K. B., "Isolation of a Vibrating Machine Mounted on a Flexible Structure," *Proceedings of the American Control Confernce*, Vol. 2, IEEE, Pittsburgh, PA, June 1989, pp. 1182–1188.

[25] Sievers, L. A. and von Flotow, A. H., "Comparison and Extensions of Control Methods for Narrow-Band Disturbance Rejection," *IEEE Transactions on Signal Processing*, Vol. 40, No. 10, October 1992, pp. 2377–2391.

[26] MacMartin, D. G., "A Feedback Perspective on the LMS Disturbance Feedforward Algorithmn," *Proceedings of the American Control Conference*, Vol. 2, Baltimore, MD, June 1994, pp. 1632–1636.

[27] Sommerfeldt, S. D. and Tichy, J., "Adaptive Control of a Two-Stage Vibration Mount," *Proceedings of the* $27^{th}$ *Conference on Decision and Control*, Vol. 3, IEEE, Austin, TX, December 1988, pp. 2039–2044.

[28] MacMartin, D. G., "Collocated Structural Control: Motivation and Methodology," *Proceedings of the* $4^{th}$ *IEEE Conference on Control and Applications*, Vol. 5, IEEE, Albany, NY, September 1995, pp. 1092–1097.

[29] Beard, A. M., Schubert, D. W., and von Flotow, A. H., "A Practical Product Implementation of an Active/Passive Vibration Isolation System," *Proceedings of SPIE Vibration Monitoring and Control*, Vol. 2264, San Diego, CA, July 1994, pp. 38–49.

[30] Chen, H. M. and Lewis, P., "Adaptive Control for a Vibration Isolation Mount," *Proceedings of Noise and Vibration Control*, ASME, Dallas, TX, November 1990, pp. 121–124.

[31] Blackwood, G. H. and von Flotow, A. H. "Active Vibration Isolation for Controlled Flexible Structures,". Technical Report SERC#13-93, M. I. T. Space Engineering Research Center, Cambridge, MA, October 1993.

[32] Hyland, D. C. and Phillips, D. J., "Advances in Active Vibration Isolation Technology," *Structural Dynamics and Control: Proceedings of* $10^{th}$ $VPI\&SU$ *Symposium*, Blacksburg, VA, May 1995, pp. 367–378.

[33] Snowdon, J. C., *Vibration and Shock in Damped Mechanical Systems*, first edition, John Wiley & Sons, 1968.

[34] Molloy, C. T., "Four-Pole Parameters in Vibration Analysis," *Colloquium on Mechanical Impedence Methods for Mechanical Vibrations*, New York, NY, 1958, pp. 43–68. ASME Annual Meeting.

[35] Snowdon, J. C. "Vibration Isolation: Use and Characteristics,". Technical Report 128, National Bureau of Standards, May 1979.

[36] Sykes, A. O., "Passive Vibration-Cancellation Isolation Mount,"$58^{th}$ *Shock and Vibration Symposium*, National Aeronautics and Space Administration, Huntsville, AL, 1987, pp. 411–439.

[37] Cook, R. D., Malkus, D. S., and Plesha, M. E., *Concepts and Applications of Finite Element Analysis*, third edition, John Wiley & Sons, 1989.

[38] Yang, B. and Tan, C. A., "Transfer Functions of One-Dimensional Distributed Parameter Systems," *Journal of Applied Mechanics*, Vol. 59, December 1992, pp. 1009–1014.

[39] Yang, B., "Distributed Transfer Function Analysis of Complex Distributed Parameter Systems," *Journal of Applied Mechanics*, Vol. 61, March 1994, pp. 84–92.

[40] Snowdon, J. C., "Isolation and Absorption of Machinery Vibration," *Acustica*, Vol. 28, No. 6, 1973, pp. 307–317.

[41] Soliman, J. I. and Hallam, M. G., "Vibration Isolation Between Non-Rigid Machines and Non-Rigid Foundations," *Journal of Sound and Vibration*, Vol. 8, No. 3, 1968, pp. 329–351.

[42] Franklin, G. F., Powell, J. D., and Emami-Naeini, A., *Feedback Control of Dynamic Systems*, second edition, Addison Wesley, 1991.

[43] Kuo, B. C., *Automatic Control Systems*, fifth edition, Prentice Hall, 1987.

[44] Brogan, W. L., *Modern Control Theory*, third edition, Prentice Hall, 1991.

[45] Anderson, B. D. O. and Moore, J. B., *Optimal Control: Linear Quadratic Methods*, first edition, Prentice Hall, 1990.

[46] Kwakernaak, H. and Sivan, R., *Linear Optimal Control Systems*, first edition, Wiley-Interscience, 1972.

[47] Siouris, G. M., *An Engineering Approach to Optimal Control and Estimation Theory*, first edition, Wiley-Interscience, 1996.

[48] Nelson, F. C., "Shock and Vibration Isolation: Breaking the Academic Paradigm," *ASME PVP, Seismic, Shock and Vibration Isolation*, June 1991, pp. 1–6Issue 5.

[49] Application Visualization System, Waltham MA. *Advanced Visual Systems Inc.*, 1994.

[50] Fanson, J. L. and Caughey, T. K., "Positive Position Feedback Control for Large Space Structures," *AIAA Dynamics Specialist Conference*, Monterey, CA, April 1987, pp. 588–317.

[51] Goh, C. J. and Caughey, T. K., "On the Stability Problem Caused by Finite Actuator Dynamics in the Collocated Control of Large Space Structures," *International Journal of Control*, Vol. 41, No. 3, 1985, pp. 787–802.

[52] Atalla, M. J., *Model Updating Using Neural Networks*, Ph.D. dissertation, Virginia Polytechnic Institute and State University, April 1996.

[53] Hughes, P. C. and Skelton, R. E., "Controllability and Observability of Linear Matrix-Second-Order Systems," *Journal of Applied Mechanics*, Vol. 47, 1980, pp. 415–420.

[54] Hughes, P. C. and Skelton, R. E., "Controllability and Observability for Flexible Spacecraft," *Journal of Guidance and Control*, Vol. 3, No. 5, 1980, pp. 452–459.

[55] Ogata, K., *Modern Control Engineering*, first edition, Prentice Hall, 1970.

[56] Bucek, V. J., *Control Systems: Continuous and Discrete*, first edition, Prentice Hall, 1989.

# Vita

Dino Sciulli was born on July 29, 1967 in Pittsburgh, Pennsylvania and is the third of four children of Diodato and Antonia Sciulli. Dino attended the Pennsylvania State University where he graduated from the University Scholars program with a Bachelor of Science degree and received his Aerospace Engineering degree in May, 1989. Fresh out of school, he obtained a position with Rockwell Space Operations Company (RSOC), a subsidiary of Rockwell International. Dino worked as a contractor to NASA Johnson Space Center located in Houston, Texas for slightly over two years. Dino left RSOC to obtain a Masters of Science degree at Stanford University. After graduating with an Aerospace Engineering degree from Stanford University in June 1992, Dino joined the United State Air Force as a civilian employee through the USAF Palace Knight Program. Dino worked on his two year tour at the USAF Phillips Laboratory and then attended graduate school at Virginia Polytechnic Institute & State University under the tutelage of Dr. Daniel J. Inman. Upon receiving his PhD degree from the department of Engineering Science and Mechanics in 1997, he will join the Structures & Controls Division at the Phillips Laboratory located in Albuquerque, NM.

Dino Sciulli